

This thesis is dedicated to the memory of my Grandmother, Chrystal Collins



**THE STRUCTURE, EVOLUTION AND
GEOPHYSICAL EXPRESSION OF MUD
VOLCANO SYSTEMS FROM THE SOUTH
CASPIAN BASIN**

ROBERT JOHN EVANS

**Submitted in partial fulfilment of the requirements for the
degree of Ph.D**

Cardiff University

October 2007

UMI Number: U585295

All rights reserved

INFORMATION TO ALL USERS

The quality of this reproduction is dependent upon the quality of the copy submitted.

In the unlikely event that the author did not send a complete manuscript and there are missing pages, these will be noted. Also, if material had to be removed, a note will indicate the deletion.



UMI U585295

Published by ProQuest LLC 2013. Copyright in the Dissertation held by the Author.
Microform Edition © ProQuest LLC.

All rights reserved. This work is protected against
unauthorized copying under Title 17, United States Code.



ProQuest LLC
789 East Eisenhower Parkway
P.O. Box 1346
Ann Arbor, MI 48106-1346

SUMMARY

This thesis uses a combination of industrially acquired seismic reflection data, well data, topographic data and satellite imagery to investigate the structure, evolution and geophysical expression of extrusive constructions found within large (>500 m diameter) mud volcano systems from the South Caspian Basin. The principal aim is to gain a better understanding the structural architecture of mud volcano systems and the ways in which they are constructed. To this end this thesis includes three core research chapters which present investigations into the internal structure and eruptive history of a large mud volcano system, the geophysical response of seismic data to gassy seabed conditions and the structure and formation of mud volcanic subsidence craters.

In the first core chapter the edifice of the giant Chirag mud volcano system was investigated using three-dimensional (3D) seismic data. Internally, this feature consists of a number of discrete seismic facies units interpreted to represent either wedge-shaped units of erupted mud volcanic sediment or sheet-like units of non-eruptive sediment. Unit stacking patterns indicate the importance of pulsed mud volcanic activity as a control on the internal architecture of large mud volcano edifices and suggest it to be an important mechanism of basinal sediment and fluid expulsion. Analysis of the geometrical relationships of the internal sediment units to an underlying collapse caldera allows for a reconstruction of the system's history of collapse. Together, the details of internal unit type, stacking and relative edifice collapse timing constitute a detailed reconstruction of the volcano system's eruptive history and a record of the structural evolution of a large focussed fluid flow system.

At the seabed a number of volcano systems within the South Caspian Sea study area were found to be imaged by areas of phase-reversed seabed reflection in seismic data. These "seabed phase reversals" are useful for better delimiting and understanding the structure of mud volcano source points and the extent of recent eruptive deposits. At one example kilometre-scale lobate mudflows are seen emerging from two seabed mud pool (salses) emphasizing the importance of both features in shaping the volcano's seabed morphology. Testing the hypothesis that seabed phase reversals are the result of gas within the seabed sediment took the form of a one-dimensional geophysical model of the study area seabed constructed using data from a borehole together with other published data. The results revealed that a phase reversal of the seabed reflection is a geophysical possibility under conditions typical of gassy seabed sediment. There is therefore a high likelihood that seabed phase reversals are the result of gas within seabed sediment. It is therefore suggested that seabed phase reversals can be used alongside other acoustic phenomena that indicate the presence of gas in a sedimentary section.

In the final core chapter circular craters found at the upper terminations of onshore and offshore mud volcano systems are investigated. Using field maps, seismic lines, topographic data and satellite images it has been possible to describe these craters in detail for the first time and compile a generalized model for their structure. This includes a crater rim, an inward dipping crater margin fault, a moat and raised crater pedestal of freshly extruded mud volcanic sediment. The characteristic "moat and pedestal" morphology features at most of the craters featured here as well as at a number of others from elsewhere. Whilst the precise mechanism of crater formation is unclear it is strongly suspected that they form as a result of subsurface evacuation and collapse. They are thus similar to other sedimentary and igneous collapse features for which they may be useful analogues.

A NOTE ON THESIS STRUCTURE

The principal research Chapters of this thesis (3, 4 and 5) have been prepared as scientific papers for publication in three different international journals. The present status of each publication is summarized as follows:

- **Chapter 3** has been published as: *Internal structure and eruptive history of a kilometre-scale mud volcano system, South Caspian Sea*. Robert J. Evans, Richard J. Davies and Simon A. Stewart. Basin Research 19, pp. 53-63.
- **Chapter 4** has been published as: *Phase-reversed seabed reflections in seismic data: examples related to mud volcanoes from the South Caspian Sea*. Robert J. Evans, Simon A. Stewart and Richard J. Davies. Geo-Marine Letters 27, pp. 203-212.
- **Chapter 5** has been published to the Journal of the Geological Society, London as: *The structure and formation of mud volcano summit calderas*. Robert J. Evans, Simon A. Stewart and Richard J. Davies. Journal of the Geological Society, London 165, pp. 169-180.

Although each article is jointly authored with the project supervisors they are the work of the lead author, Robert J. Evans. Project supervisors provided editorial support in accordance with a normal thesis chapter.

ACKNOWLEDGEMENTS

It is with a great sense of pleasure that I now have the task of thanking the numerous people and organizations who have assisted me throughout this project. First I would like to thank my project supervisors Richard Davies and Simon Stewart. Without their continual guidance and support this project would certainly not have been possible. Both inspired me from day one with their enthusiasm for geology and this research. I am grateful to both for providing a constantly open door for me to talk and assuage worries that I often had, for quickly reading my work and continually offering sound advice and commentary which considerably improved the quality of the final work. Simon is also thanked, along with his wife Emma, for the warm hospitality extended to me and field assistants during fieldwork and also for providing invaluable logistical support in Azerbaijan. I must also thank Joe Cartwright for additional support provided to me during this project. I have learnt an enormous amount working in the 3Dlab and owe a great deal of this to Joe's frequent informal technical sessions and thoughtful discussion of technical issues. My geology career started in Pembroke School under the guidance of my geology teacher Chris Evans. Without his inspirational teaching I would not have pursued geology any further and owe a lot to him for setting me on this path.

BP are thanked for providing data for this project and for allowing their use in the presentations and publications. NERC are gratefully acknowledged for providing funding that supported the research. The Tectonic Studies Group also provided funding which helped me attend a conference. Andy Hill and Marie Joly in BP helped me with data provision and technical discussion. Also the reviewers of the papers in this thesis (Sverre Planke, Ben Clennell, Alan Judd) greatly helped to improve their quality. In Cardiff Alun Rogers provided help with GIS software as did Katrien VanLandergan. Elchin Gamidov was our very patient driver in Azerbaijan who is gratefully acknowledged for the many hours he spent in the sun on mud volcanoes so that I could do my fieldwork.

Numerous people in the 3Dlab, past and present, are thanked for their help with this project through technical discussions and friendship. In particular my long standing office mate Mostyn Wall for the many discussions we have had and others. Aggie Georgiopoulou, Katrien VanLandergan, Mike Hohbein, Mairi Nelson and Matt O'Regan. Simon Higgins, Cat Baudon and Päivi Heiniö have also been great friends to me here and often had to listen to me ranting about all things geology and non-geology! Mads Huuse was a great source of technical help and I am grateful to him. Gwen Pettigrew helped me on many occasions with IT issues. All other members of the 3Dlab not mentioned here are also thanked for their friendship and technical advice over the last three years.

Truly invaluable support for me during this project has been provided by my family. I feel like my Mum, Dad and brothers Tom and Jon have done a Ph.D themselves and I cannot thank them all enough for the level of support they have given me during this project. Tom provided great help in the field in Azerbaijan. Finally of course is Suze, my source of endless patient support and inspiration throughout this entire project. Her patience, support and love have been above all else the most important thing to me during this project. She has made finishing possible and the experience of getting there so much more enjoyable.

TABLE OF CONTENTS

Page No.

Summary	i
A note on thesis structure	ii
Acknowledgements	iii
Table of Contents	iv
List of Figures	vii
List of Tables	xviii
List of Enclosures	xix

CHAPTER ONE

1.0 Introduction	1 – 1
1.1 Rationale	1 – 1
1.2 Project aims	1 – 3
1.3 Geographical, tectonic and stratigraphical setting	1 – 4
1.3.1 Study area location and geological history	1 – 4
1.3.2 Regional mud volcanism	1 – 10
1.4 Database and methodology	1 – 16
1.4.1 Seismic reflection data	1 – 17
1.4.2 Other data	1 – 25

CHAPTER TWO

2.0 The geological occurrence of mud volcanism	2 – 1
2.1 Introduction	2 – 1
2.2 Subsurface sediment mobilization and intrusion	2 – 1
2.2.1 The principles of subsurface sediment mobilization	2 – 1
2.2.2 Driving forces for bulk movement	2 – 5
2.2.3 Sedimentary intrusion	2 – 6
2.2.4 Subsurface sediment mobilization structures	2 – 7
2.3 The mud volcano system	2 – 23
2.3.1 The source domain	2 – 23
2.3.2 The intrusive domain	2 – 28
2.3.3 The extrusive domain	2 – 34
2.3.4 The roof domain	2 – 45

CHAPTER THREE

3.0 Internal structure and eruptive history of a kilometre-scale mud volcano system, South Caspian Sea	3 – 1
3.1 Abstract	3 – 1
3.2 Introduction	3 – 2
3.2.1 Background and geological setting	3 – 2
3.2.2 Database and methodology	3 – 5
3.3 Seismic interpretation	3 – 7
3.4 Edifice construction and evolution	3 – 14
3.4.1 Interpretation of seismic facies units	3 – 14

3.4.2 Edifice collapse history	3 – 15
3.5 Discussion	3 – 16
3.5.1 Volcano system eruptive history	3 – 16
3.5.2 Implications for fluid and sediment eruption	3 – 18
3.5.3 Comparison with igneous volcano systems	3 – 19
3.6 Conclusions	3 – 20
3.7 Acknowledgements	3 – 20

CHAPTER FOUR

4.0 Phase-reversed seabed reflections in seismic data: examples related to mud volcanoes from the South Caspian Sea	4 – 1
4.1 Abstract	4 – 1
4.2 Introduction	4 – 2
4.2.1 Mud volcanoes and fluid expulsion	4 – 4
4.2.2 Seismic reflection polarity	4 – 4
4.3 Materials and methods	4 – 6
4.3.1 Seismic reflection data	4 – 7
4.3.2 Seismic reflection polarity	4 – 7
4.4 Seismic interpretation	4 – 10
4.4.1 Azeri mud volcano	4 – 10
4.4.2 Chirag mud volcano	4 – 13
4.5 Results	4 – 13
4.5.1 Synthetic seismograms	4 – 13
4.5.2 Seismic interpretation	4 – 15
4.6 Discussion	4 – 17
4.7 Conclusions	4 – 18
4.8 Acknowledgements	4 – 19

CHAPTER FIVE

5.0 Mud volcano subsidence craters onshore and offshore Azerbaijan	5 – 1
5.1 Abstract	5 – 1
5.2 Introduction	5 – 2
5.3 Geological setting, methods and datasets	5 – 2
5.4 Crater mapping	5 – 5
5.4.1 Onshore example 1	5 – 5
5.4.2 Onshore example 2	5 – 11
5.4.3 Submarine example 1	5 – 13
5.4.4 Submarine example 2	5 – 19
5.5 Crater structure and formation	5 – 21
5.5.1 Crater structure	5 – 21
<i>Rim</i>	5 – 21
<i>Crater margin fault</i>	5 – 21
<i>Moat and pedestal</i>	5 – 23
<i>Gryphons</i>	5 – 24
5.5.2 Crater formation	5 – 24
5.6 Discussion	5 – 28
5.6.1 Other mud volcano craters	5 – 28
5.6.1 Circular collapse structures	5 – 30

5.7 Conclusions	5	31
5.8 Acknowledgements	5	32

CHAPTER SIX

6.0 Summary and discussion	6	1
6.1 Introduction	6	1
6.2 Summary of results: A generalized structural model	6	1
6.2.1 Edifice internal and eruptive history (Chapter 3)	6	1
6.2.2 Seabed phase reversal analysis (Chapter 4)	6	4
6.2.3 Crater mapping and analysis (Chapter 5)	6	6
6.3 Discussion	6	7
6.3.1 Extrusive domain evolution and the record of basinal fluid expulsion	6	7
<i>Pulsed eruptive activity and eruptive unit stacking</i>	6	8
<i>Edifice collapse</i>	6	13
<i>Diversity of eruptive products</i>	6	16
6.3.2 Geophysical expression of the extrusive and roof domains	6	18
6.4 Implications for economic and engineering geology	6	21
6.4.1 Subsurface hazard identification	6	21
6.4.2 Fluid dynamic and structural history	6	22
6.5 Project limitations and suggestions of further work	6	23

CHAPTER SEVEN

7.0 Conclusions	7	1
7.1 General conclusions	7	1
7.2 Mud volcano system structure and evolution	7	1
7.3 Geophysical expression of mud volcano systems and their deposits	7	2
7.4 Structure and origin of mud volcano source points	7	4
7.5 Implications for engineering and economic geology	7	5
7.6 Suggestions for further work	7	6
8.0 References	8	1

Appendices

- I** List of mapped seismic horizons and faults.
- II** Supplementary figures to support the conclusions of Chapter 3.
- III** Supplementary figures to support the conclusions of Chapter 4.
- IV** Supplementary figures to support the conclusions of Chapter 5.
- V** **CD 1-** Thesis in digital format.

LIST OF FIGURES

Chapter One: Introduction

Fig. No.	Figure Caption	Page No.
1.1	Geological setting and study area location: (a) Regional Digital Terrain Model showing the tectonic and topographic setting of the South Caspian Sea and surrounding regions. Modified from Allen et al. (2003). (b) Tectonic map of the South Caspian Basin showing the position of major structural elements and position of the onshore and offshore project study areas (red boxes). Map location is shown as a black box in (a). Modified from Jackson et al. (2002).	1 - 6
1.2	Map showing the position of mud volcano systems within the South Caspian Basin and "mud volcano area" subdivisions. Note the position of the project study areas. From Guliyev and Panahi (2004).	1 - 7
1.3	3D visualization of a seismic section through the Apsheron anticline and a bathymetric seabed map showing the position of large (>500 m diameter) mud volcano systems in its crest, including those investigated in Chapters 3-5. This structure is located within the offshore study area and is imaged by a number of seismic reflection surveys.	1 - 8
1.4	Regional deep seismic line trending approximately N-S through the Caspian Sea showing the deep structure and regional tectonic configuration. At depth northward subduction of South Caspian oceanic crust beneath the middle Caspian has led to the formation of an accretionary prism overlain by an extensive buckle fold system that is detached from the prism by the thick and overpressured Maykop formation (coloured pink). Note the position of the Apsheron anticline (marked AA in black box) which is located within the offshore study area. Approximate position of seismic section is shown in Figure 1.1b. From Stewart and Davies (2006).	1 - 11
1.5	The Apsheron anticline: (a) Seismic depth map of "BMV" horizon showing fold orientation and amplitude. Mud volcano systems marked as white polygons. Horizon location shown in Figure 1.3. (b) RMS (root mean squared) interval amplitude map of the seabed-BMV section showing the position of mud volcano systems (marked as white polygons). Note the radial negative amplitude anomaly associated with the Chirag mud volcano system and other minor anomalies associated with others. (c) Seismic section showing a biconic (two cones placed base to base) mud volcano edifice in the fold crest. Location of this and subsequent Figure parts shown in (a). (d) Seismic section showing a large deep thrust fault. (e) Seismic section showing the extensional fault system present within the anticline crest.	1 - 12
1.6	Seismic profile trending roughly parallel to the strike of the Apsheron anticline transecting four of the structure's principal	1 - 13

	mud volcano systems. Note the vertical zones of poor signal/noise ratio in the centre of each system that probably results from the presence of gas in the section on intense vertical fluid migration. Section location shown in Figure 1.5a.	
1.7	The onshore study area: (a) Geological map showing the position of the Qaraqus Dagi and Gora Kagniza-Dag mud volcano systems along with others. Note their locations in the crests of exhumed anticlines and the variety of fold orientations (red lines). Map location shown in Figure 1.1b. (b) Field photograph taken at the summit of the Lokbatan mud volcano showing a smaller mud volcano edifice in the core of an exhumed anticline. The white line reconstructs the likely pre-exhumation structure. See (a) for photograph location. (c) Field photograph from the Kirmaky Valley showing the exhumed land surface on the flank of a N-S trending anticline. White dashed lines reconstruct the likely pre-exhumation structure. See (a) for photo location.	1 - 14
1.8	Map showing the location of seismic and well data within the offshore study area. Black rectangles denote 3D seismic survey boundaries and surrounding numbers are seismic inlines and crosslines.	1 - 19
1.9	Flow diagram summarizing the processing workflow that was used for the 3D seismic surveys used in this project, chirag and cg4d02. From Robinson et al. (2005).	1 - 21
1.10	3D seismic data phase: Variable area (a) and variable intensity (b) seismic depth section through the seabed from survey chirag showing the near zero-phase character of the seabed reflection. An individual trace is shown in white on both Figure parts to emphasize the waveform of the seabed reflection and other deeper reflections.	1 - 22
1.11	Testing mud volcano push-down: (a) 3D visualisation of seismic depth section and horizon showing the Gunashli 1 mud volcano edifice within a depression at the crest of the anticline. (b) Seismic I.L.N 965 displayed in TWT that was used to model velocity push-down. Note the Gunashli 1 mud volcano edifice in fold crest (shaded yellow). Section is TWT, vertical scale in milliseconds. (c) 2DMove interpretation panel showing the interpretation of I.L.N 965 showing checkshot-derived seismic velocities used in its depth conversion. Note the depression at the base of the edifice. (d) Depth-converted seismic I.L.N 965 showing the restoration of the base-edifice depression. Vertical scale in metres.	1 - 24

Chapter Two: Background

Fig. No.	Figure Caption	Page No.
2.1	Patterns of pressure increase with depth in sedimentary basins: (a) Rates of increase of pressure and stress due to burial. The normal fluid pressure gradient is based on an overlying seawater depth of 250 m and a constant fluid density in the entire column of 1025 kg m ⁻³ . The lithostatic gradient is based on a grain density of 2650 kg	2 - 3

	<p>m^{-3} and a porosity decrease with depth following the average values for sand-silt-clay of Einsele (1989). The hypothetical gradient illustrates the kind of pressure variations that can arise within a sequence of varied sediments. (b) Effective-stress gradient and fluid-potential gradient derived from curves in (a). Note the inverse relationship of fluid-potential and effective stress. Both parts modified from Maltman (1994).</p>	
2.2	<p>Subsurface sediment mobilization and its typical structures: (a) Conceptual view of the range of processes involved in sediment mobilization occurring at different depths beneath the surface. Modified from Maltman and Bolton (2003). (b) Flame structure preserved in sandstones from the Northumberland coast, UK (photo courtesy of S. Bull). (c) Lower Palaeocene-age sandstone injectites of the Panoche sandstone intrusion complex intruding mud rocks of the Moreno shale, California, USA (photo courtesy of W. Vittel). (d) Mud diapir within Carboniferous-age Diamond Rocks south of Kilkee western Ireland. This diapir formed by gravitational slumping of undercompacted muds in the distal portion of a large delta (photo courtesy of S. Bull).</p>	2 - 9
2.3	<p>Sand intrusions. (a)-(d) Selected Seismic sections and 3D visualizations of sand injectites showing their characteristic (v-shaped) architecture. Modified from Huuse (2004).</p>	2 - 11
2.4	<p>Structural styles of mud mobility and mud diapirism: (a) Overview cross section illustrating the key structural elements related to mud mobility and mud diapirism in a deltaic setting based on a section through the Niger delta by (Doust and Omatsola 1990) and Morley and Guerin (1996). (b) The structural characteristics of reactive mud diapirism. Reactive shale bulges can be bounded by regional and counter-regional growth faults. (c) The characteristics of active mud diapirism. Piercing diapirs intrude vertically through the overburden following an early phase of reactive diapirism. Synformal depocentres form in areas of mud withdrawal. Dewatering of the diapir during ascent can lead to shrinkage and the formation of collapse faults at the diapir crest. All parts modified from Van Rensbergen and Morley (2003).</p>	2 - 14
2.5	<p>Seismic line showing the architecture of an interpreted mud diapir and adjacent sediment. The thickness characteristics of the adjacent sediments are used to infer the various stages of diapir growth (reactive, active, passive). The existence of true bulbous mud diapirs such as this example can be questioned. See text for more discussion. From Morley (2003a).</p>	2 - 16
2.6	<p>Comparison of a 2D seismic section (a) with a 3D seismic section (b) over a shale ridge in the footwall of a deltaic growth fault. This typical example of a reactive mud diapir (e.g. Fig. 2.4b) actually appears as a stratified horst block in 3D seismic sections. From Van Rensbergen and Morley (2003).</p>	2 - 17
2.7	<p>Conversion of a slit-like to a pipe like conduit due to uneven flow velocity distribution within the conduit: (a) Flow velocity profiles for a slit-like conduit (top) showing the focus of highest velocities in the centre of the slit. This results in the modification of the slit</p>	2 - 19

	through erosion at its centre and its gradual conversion to a cylindrical pipe (bottom). A feedback loop is created as the central widening leads to an increase in flow velocity and more wall erosion. (b) Cross sections (I and II) through a schematic diatreme (fluid expulsion pipe) showing its slit-like architecture at depth and its pipe-like architecture in the shallower section. This self-organized conduit modification process is one way the hydrofractures at depth may evolve into more pipe-like conduits that are commonly observed in nature. Modified from Novikov and Slobodsky (1985).	
2.8	Narrow gas escape pipes from the Niger delta: (a) 3D visualization of narrow vertical gas escape pipes connecting a gas reservoir at depth to the seabed. (b) Seismic section showing seabed gas escape craters underlain by narrow vertical disturbances in the seismic data (pipes). From Løseth et al. (2001).	2 - 21
2.9	The seismic expression of mud diapirs and pipes: Vertical “fingers” of chaotic seismic data interpreted to represent mud diapirs and mud pipes. Reflections adjacent to the left hand example form synformal depocentres adjacent to the chaotic data suggesting the presence of a diapir. The reflections adjacent to the right hand example are not synformal suggesting this chaotic area of data may represent a mud pipe or gas chimney. From Morley (2003a).	2 - 22
2.10	Summary diagram outlining the basic subsurface configuration and structural domains of a large mud volcano system. The component elements, their field and seismic architecture are listed in the adjoining table.	2 - 24
2.11	Matrix comparing the seismic expression of mud, salt and igneous diapirism: (a) Seismic cross section through the Azeri 2 mud volcano system showing narrow central zone of blanking that may represent the system’s conduit. (b) Horizontal seismic coherence slice through a South Caspian Sea mud volcano system showing large-diameter circular zone of seismic disturbance interpreted as zone of intense deformation within the system’s intrusive domain. From Stewart and Davies (2006). (c) Seismic cross-section of a salt diapir from Brazil. From Stewart (2006). (d) Seismic horizon dip map showing radial faults above a North Sea salt diapir. From Stewart (2006). (e) Seismic section showing the architecture of Middle Jurassic-age volcanic structures from the Outer Moray Firth, UK. (f) Seismic timeslice through similar volcanic features as shown in (e). Both (e) and (f) from Stewart (1999a)	2 - 29
2.12	Effect of methane expansion on the density and porosity of rising “diapiric” material. Note the rapid expansion of methane in the upper 1 km and its dramatic effect on the porosity and density of the sediment. Expansion of methane in this way and the resultant reduction in density is cited by many authors as an important mechanism for driving sediment towards the surface in mud volcano feeder conduits. From Brown (1990).	2 - 33
2.13	Cartoon diagram showing submarine mud volcano systems formed by (a) seafloor-piercing diapir not forming a mud volcano; (b) a	2 - 35

	mud volcano edifice formed on top of a seafloor-piercing diapir; (c) and (d) seepage and mud volcanoes forming as a result of fluid and sediment flow along faults that may or may not be connected to a diapir at depth. From Milkov (2000).	
2.14	Field photograph of an extruded clast of bedded sandstone embedded in mud volcano sediment on the flank of the Garadag mud volcano edifice, Azerbaijan. The width of the clast is approximately 1.5 m. Its occurrence provides a constraint on the diameter of the feeder conduit which must be at least as wide as the clast. Notebook is 20 cm long.	2 - 36
2.15	Structure of the intrusive domain (a) Schematic cross-sectional model of a typical mud volcano system based on the results of geochemical surveys. Fluids and sediments sourced from depth are stored in intermediate level “mud chambers” connected by pipes. From Planke et al (2003). (b) 3D seismic visualization of the intrusive domain of the Chirag mud volcano system showing the seismic architecture of a large central collapse caldera. From Stewart and Davies (2006).	2 - 37
2.16	Extrusive domain structure and terminology: Schematic diagrams of (a) a cone-shaped mud volcano edifice and associated minor extrusive features and (b) a pie-shaped volcano edifice. This simple terminology is useful for describing features within the extrusive domain but the classification based on flank slope angle can only be applied when no tectonic modifications have taken place or collapse of the edifice has not occurred. From Kopf (2002).	2 - 41
2.17	Classification scheme of South Caspian mud volcano systems: A mud volcano system is termed either, (a) concave, (b) convex, (c) flat or (d) buried according to the general seismic architecture of the edifice. From Yusifov and Rabinowitz (2004).	2 - 42
2.18	Sizes and shapes of various terrestrial mud volcano edifices. A = Maghaehu Stream, New Zealand; B = Volcanito near Cartegena, Columbia; C = Moruga Bouff, Trinidad; D = El Totumo, near Cartegena, Columbia; E = Chandragup, Makran Coast, Pakistan; G = Gharniarigh-Tapeh, Gorgan region, northern Iran. From Judd and Hovland (2007).	2 - 43
2.19	Seismic section from the eastern Mediterranean Ridge showing a mud volcano edifice and a dipping backthrust fault thought to be its feeder conduit. Internal layering within the edifice is below the vertical resolution of the seismic data meaning that the edifice appears as a transparent biconic seismic facies unit. The same is true for many other mud volcano edifices and little is known about their internal seismic architecture. Modified from Kopf (1998).	2 - 46
2.20	Dating the cyclic activity of a Christmas tree mud volcano edifice: (a) Seismic line through the edifice without interpretation, (b) same seismic line with identified mud cones and (c) mapped reflectors used to date the various cycles of mud volcanic activity. From Yusifov and Rabinowitz (2004).	2 - 47
2.21	Upward tapering Christmas tree-type mud volcano edifice showing evidence for “secondary” mud volcano edifices within	2 - 50

the system's roof domain. From Stewart and Davies (2006).

Chapter Three: Mud volcano eruptive history

Fig. No.	Figure Caption	Page No.
3.1	(a) Tectonic map of the South Caspian Basin showing the location of the study area. Inset map of the Caspian region shows map location as black box. Modified from Jackson et al. (2002). (b) 3D bathymetric map of the study area seabed showing position of Chirag and other mud volcanoes at the shelf-break.	3 – 3
3.2	3D schematic diagram showing the sub-surface architecture of a typical South Caspian Sea mud volcano system. Vertical scale can be 100s of metres to 5 km. This study is focussed on the internal architecture of the edifice. Modified from Stewart and Davies (2006).	3 – 4
3.3	Uninterrupted and interpreted seismic section U-U' through the Chirag edifice showing the 5 seismic facies units that make up the edifice and the internal reflection geometries and reflection terminations that have been used to define and map them. TMV= Top Mud Volcano reflection, BMV= Base Mud Volcano reflection on this and subsequent figures. BMV inset depth map for section location.	3 – 6
3.4	Uninterrupted and interpreted seismic section V-V' through the Chirag edifice showing the stacking arrangement of the interpreted seismic facies units. Note the position of the mud cone crater (marked Z) within Unit 1. BMV inset depth map for section location.	3 – 8
3.5	(a) Acoustic amplitude map of a selected horizon within the onlapping unit that overlies the Chirag edifice showing the pattern of mud flows radiating from the central area of edifice. (b) Representative seismic section showing the cross-sectional seismic character of mud flows within the onlapping unit. See Fig. 3.5a for section location and position of features 1 and 2. (c) Field photograph of a gryphon on the Doruvdag mud volcano, Eastern Azerbaijan. Note the similarities between small-scale flow patterns on the gryphon and large-scale flow patterns in the amplitude map of Fig. 3.5a.	3 – 9
3.6	Isopach maps of seismic facies Units 1-5 showing their shape and lateral extent. Note position of mud cone crater in Unit 1 (marked Z). Colourbars of unit thickness are in metres. White circular area denotes the blanked area within the caldera centre. Seismic facies units have not been mapped within this zone.	3 – 12
3.7	(a) Uninterpreted seismic section through the edifice and caldera of the Chirag mud volcano system. In (b) this section is coloured to reflect the interpreted stages of caldera growth. See text for discussion and Fig. 3.7c for section location. (c) 3D visualisation of the BMV surface showing the position of the hangingwall synform (marked Y) adjacent to the caldera margin. (d) Seismic section through synform Y showing the structural concordance of	3 – 13

	reflection X to the BMV surface. See text for discussion, Fig. 3.7b for key to colours and Fig. 3.7c for section location.	
3.8	Schematic diagram showing a 5 stage model for the evolution and eruptive history of large mud volcano systems, based on the analysis of Chirag. See text for discussion.	3 - 17

Chapter Four: Seabed phase reversals

Fig. No.	Figure Caption	Page No.
4.1	(a) Tectonic map of the South Caspian Basin and surrounding area showing position of study area within South Caspian Sea. Modified from Jackson et al. (2002). (b) 3D seabed depth map of the study area seabed showing the position of major mud volcanoes at the shelf break.	4 - 3
4.2	Evidence for gas expulsion during mud volcanic extrusion: (a) Photograph of a bursting gas bubble within a gryphon (small mud cone) at the summit of an Azerbaijan mud volcano. (b) Hand specimen-scale evidence for gas release from mud volcano deposits. Photograph of a vertical slice through a recent Azerbaijan volcano mud flow showing gas vesicles within the sediment. Coin for scale.	4 - 5
4.3	Composite depth profile curves showing geophysical model input data: (a) Composite sonic and density profiles for physical properties of normal non-gassy seabed conditions. (b) Composite sonic and density profiles for physical properties of gassy seabed conditions. Line styles indicate the data source for both figure parts. See text for further discussion. TVDSS = true vertical distance sub-sea. *Data source Hamilton and Bachman (1982).	4 - 9
4.4	The Azeri mud volcano: (a) 3D bathymetric map of the seabed at the site of the Azeri mud volcano. Note the conical shape of the volcano's summit and the area of phase-reversed seabed reflection at the volcano summit. The phase-reversed section is coloured according to its acoustic amplitude; see Fig. 4.4b for further details. (b) Acoustic amplitude map of the phase-reversed section of seafloor at the Azeri mud volcano summit. U= Linear negative amplitude anomalies interpreted as seafloor mudflows, V= Circular amplitude anomalies of relatively low reflection amplitude interpreted as seafloor salses, W= "halo" of reduced positive reflection amplitude surrounding phase-reversed section of seafloor reflection; this is interpreted to be the result of the progressive de-gassing of gas-bearing sediment within the phase-reversed area. Map location shown on Fig. 4.4a. (c) Representative seismic section through the Azeri volcano showing the character of the phase reversal. The seabed phase reversal occurs in the area between the vertical arrows. See Fig. 4.4b for section location (d) "High-resolution" seismic profile through the Azeri volcano showing the character of the phase reversal, which occurs between the vertical arrows. X= The convex-downward positive polarity reflection interpreted as the base of a seafloor salse. See Fig. 4.4b	4 - 11

	for section location.	
4.5	Seafloor salse and mudflows of the Azeri mud volcano: (a) 3D seabed depth map showing the relationship between the seafloor salse and mud flows. The phase-reversed area of seafloor is coloured according to acoustic amplitude. Y= Circular amplitude anomaly that corresponds to flat summit area of volcano; interpreted as seafloor salse. Z= Linear and lobate amplitude anomaly radiating from the seafloor salse; this is interpreted as a mudflow. Location of phase-reversed area is shown on Fig. 4.4a. (b) Photograph of the Garadag mud volcano, Azerbaijan showing mud flows originating from a salse similar to that observed at Azeri mud volcano in seismic data. Circled rucksack for scale.	4 - 12
4.6	The Chirag mud volcano: (a) 3D seabed bathymetric map showing morphology of the volcano at the seabed. An area of phase-reversed seabed reflection is marked by the blue dashed line. (b) "High-resolution" seismic profile through the Chirag volcano showing the character of the phase reversal. See Figure 6a for section location. Vertical arrows indicate the position of the blue line shown in Figure 4.6a.	4 - 14
4.7	Results of synthetic seismic modelling: SynTool synthetic seismogram panel showing (a) Results of non-gassy geological model convolved with a 50 Hz zero-phase Ricker wavelet. (b) Results of gassy seabed geological model convolved with a 50 Hz zero-phase Ricker wavelet. AI = acoustic impedance, SB = seabed.	4 - 16

Chapter Five: Mud volcano subsidence craters

Fig. No.	Figure Caption	Page No.
5.1	(a) Map of the Caspian Sea and surrounding countries showing the position of study area indicated as the black box. (b) Map of eastern Azerbaijan and the South Caspian Sea showing the position of the onshore and submarine crater examples described in this study. Location of map shown in (a).	5 - 3
5.2	The Qaraqus–Dagi mud volcano (QD in this and subsequent Figures). (a) Topographic map of the QD volcano edifice derived from 15 m resolution Digital Elevation Model. Note position of topographic profiles. (b) Slope map showing the position and morphology of the summit crater. (c) Transverse topographic profile showing the position of laterally confining ridges. (d) Longitudinal topographic profile showing the position of the crater rim and open southeastern crater margin. (e) Zoom-in transverse topographic profile showing characteristic "moat and pedestal" morphology of the QD crater. Note the difference in scale to profiles (c) and (d).	5 - 7
5.3	Colour IKONOS satellite image draped over the 15 m resolution DEM showing the structure and morphology of the QD volcano edifice and crater.	5 - 8
5.4	(a) Uninterpreted and (b) interpreted colour IKONOS satellite image of the QD mud volcano crater labelled to show the key	5 - 9

	structural and geomorphological elements that constitute the crater. Shaded grey areas signify mud breccia deposits.	
5.5	(a) Field photograph illustrating the crater rim, crater margin fault line, moat and fill of the QD mud volcano crater. Note the sharp break of slope at the outer edge of the moat taken to indicate the position of the crater margin fault line. Maximum rim height is approximately 15 m. (b) Field photograph showing the relationship of concentric stacked mud breccia units within the crater's pedestal. Note the increased level of weathering and vegetation of the outermost (older) units of mud breccia.	5 - 10
5.6	The Gora Kagniza–Dag mud volcano system (GKD). (a) Field photograph showing the large scale morphology of the volcano system's kilometre-scale edifice. The edifice width at its base is approximately 4 km and it is approximately 400 m high. Note the distinctive flat top of the edifice. (b) Simplified geological map of the volcano crater labelled to show its main structural and geomorphological features. (c) Field photograph of the crater margin labelled to show its rim, crater margin fault scarp and fill. Note the absence of the moat. Scarp is 2 m high. (e) Field photograph showing the curved crater rim and crater margin fault scarp surrounding a single domed unit of mud volcanic breccia. Note the position of the crater margin fault relay zone. Horizontal crater width is approximately 325 m.	5 - 12
5.7	(a) 3D seismic reflection profile showing the subsurface seismic architecture of the mud volcano system, including onlapping sediments, the buried volcano edifice and ring-like downward tapering feeder system faults. TMV= top volcano edifice reflection, BMV= base mud volcano reflection. Section location shown in (b) a 3D seismic depth map of the BMV seismic reflection showing the position of the circular feeder system faults and the location of the crater margin fault at the seabed (dashed line).	5 - 14
5.8	(a) 3D bathymetric map of the Apsheron anticline seabed area showing the position of Chirag and other large mud volcano systems at the shelf break. (b) 3D bathymetric map interpreted to show the main structural elements of the Chirag mud volcano crater.	5 - 16
5.9	(a) Uninterpreted “high-resolution” 2D seismic profile through the Chirag crater. Location section is shown in Fig. 5.8b. (b) Line drawing of seismic section in (a) showing the key structural features used to assist in the interpretation of the crater structure. Note the position of the crater margin faults (A) and their spatial coincidence with the outer edge of the moat (B). Truncation of the crater margin fault blocks beneath an inward dipping reflection (C) suggests that a period of crater edge degradation occurred after the formation of the crater prior to its continued filling.	5 - 17
5.10	(a) Seabed acoustic amplitude map of the Chirag mud volcano crater showing the position and extent of the phase-reversed raised central area of crater fill. The phase-reversed area corresponds exactly to the edges of the pedestal. (b) High-resolution seismic	5 - 18

	profile through the eastern margin of the Chirag mud volcano crater displayed at approximately $V = 3 \times H$ the show the truncation of crater margin fault tips against the inward and inward dipping reflection overlying them. Note the position of the reflection-free wedge shaped seismic facies unit beneath the lower fault tips interpreted as a buried unit of mud volcano sediment. Location of section is shown in Fig. 5.9b.	
5.11	(a) Bathymetric map of a selected area of seafloor from submarine example 2 area seabed coloured according to the angle of seabed slope. Note the position of six circular mud volcano craters and the cone shaped mud volcano edifice to the north. (b) Zoom in slope bathymetric map labelled to show the structural and geomorphological elements of one of the area's craters. Slope direction is to the south. Map location is shown in (a). (c) Bathymetric profile through the largest mud volcano crater showing the characteristic "moat and pedestal" morphology of the largest crater in the area. Profile location is shown in (a).	5 - 20
5.12	Schematic block diagram illustrating the principal structural and morphological elements of a typical circular mud volcano crater identified in this study. Dashed lines indicate areas of tentative interpretation. See text for discussion.	5 - 22
5.13	Schematic depiction of the formation of mud volcano craters as collapse features induced by subsurface volume changes occurring during and eruption. (a) Evacuation and deflation of subsurface source region during eruption inducing crater formation. Degradation of the crater rim by small slope movements creates the erosional truncation observed at the crater margin. (b) Further crater fill leads to onlapping of the degraded crater margins. (c) Final crater fill is deposited as the pedestal and central gryphons. In this example mud breccia does not reach the rim and the moat is preserved. This may not be the case for all mud volcano craters.	5 - 27

Chapter Six: Summary and discussion

Fig. No.	Figure Caption	Page No.
6.1	A generalized structural model for a typical South Caspian Sea mud volcano system drawn and annotated to highlight the most significant findings of this project. See text for further discussion and explanation of letter annotations.	6 - 2
6.2	Varied styles of mud volcano sediment unit stacking within edifices as evidence for waning, sustained and increasing pressure drive with time. (a) Idealized mud volcano edifice structure based on the modelling of Murton and Biggs (2003) which is thought to represent a decreasing pressure drive with time. (b) 3D seismic image of a South Caspian Sea mud volcano edifice showing a progressive decrease in the volume of eruptive units with time (from Stewart and Davies 2006). (c) Field photograph of the Qaraqus-Dagi mud volcano crater pedestal showing the progressive decrease in eruptive unit diameter and volume with	6 - 12

	<p>time. Each of these examples depicts a situation whereby the earliest eruptive pulses are the largest and the most recent are the smallest. (d) 2D seismic image through a South Caspian Sea mud volcano edifice showing a series of stacked mud cone each with a similar volume indicating a sustained pressure drive with time (from Yusifov and Rabinowitz 2004). (e) 3D seismic image through the Chirag mud volcano edifice showing a series of stacked eruptive units that progressively increase in volume through time. This pattern may be evidence for progressively increasing pressure drive with time.</p>	
6.3	<p>The significance of mud volcano edifice collapse: (a) Schematic depiction of a simple mud volcano system during its constructive phase. Pressure at the base of the conduit due to the weight of mud in it is not high enough to balance the pressure drive from the parent bed and the mud column and edifice grow in height. The maximum column height is reached when pressure at the base of the conduit balances the pressure drive from the parent bed as in (b). Collapse of the edifice as depicted in (c) has the effect of reducing the mud column height and reducing the pressure at its base. This may act as a stimulus for renewed eruption and the continuation of the system's activity after it has reached its theoretical maximum height.</p>	6 - 15

LIST OF TABLES

Chapter One: Introduction

Table No.	Table caption	Page No.
1.1	Summary table showing the principal attributes of the seismic reflection data used in this project.	1 - 20

Chapter Three: Mud volcano eruptive history

Table No.	Table caption	Page No.
3.1	Summary table showing the 3D external form, dimensions, internal reflection configuration and defining reflection terminations of the five seismic facies units that make up the Chirag edifice. BMV = Base Mud Volcano.	3 – 11

Chapter Five: Mud volcano subsidence craters

Table No.	Table caption	Page No.
5.1	Summary table of the principal dimensions, geomorphological and structural characteristics of each crater described in this study. Slope = angle of slope crater is located on; W/L = crater width/length ratio.	5 - 6

LIST OF ENCLOSURES

Published papers:

Evans R. J., Davies, R. J. & Stewart S. A. 2007. *Internal structure and eruptive history of a kilometre-scale mud volcano system, South Caspian Sea*. Basin Research 19 pp. 53-63.

Evans R. J., Stewart S. A. & Davies, R. J. 2007. *Phase-reversed seabed reflections in seismic data: examples related to mud volcanoes from the South Caspian Sea*. Geomarine Letters 27 pp. 203-212.

Evans R. J., Stewart S. A. & Davies R. J. 2008. The structure and formation of mud volcano summit calderas. Journal of the Geological Society, London. 165, pp. 169-180.

Davies, R. J., Swarbrick, R. E., **Evans, R. J.** & Huuse, M. 2007. *Birth of a mud volcano: East Java, 29 May 2006*. GSA Today 17, pp. 4-9.

CHAPTER ONE

1.0 Introduction

1.1 Rationale

Subsurface sediment mobilization and fluid flow are important geological phenomena that occur in all of the world's sedimentary basins. Numerous studies have demonstrated that the burial regimes, tectonic stresses and other dynamic processes commonly occurring in sedimentary basins can cause fluids, and indeed sediments, within them to become displaced from their original locations and, in some cases, expelled to the surface (Judd and Hovland 2007; Maltman and Bolton 2003). Since it is very difficult to observe this occurring in "real-time" a common approach has been to examine the geological structures that form as a result of subsurface sediment mobilization and fluid flow within modern and ancient sediments. For many years the description and interpretation of bed- to kilometre-scale subsurface sediment mobilization structures has been of key importance to developing the understanding of the way fluids move within a basin and are expelled from it (Cartwright 2007).

Of these structures mud volcano systems are some of the largest, most dynamic and spectacular. They occur in sedimentary basins worldwide often in genetic association with the rapid burial of sediments, hydrocarbon maturation and tectonic compression (Milkov 2000). Like other subsurface sediment mobilization structures such as sand injectites, fluidization pipes and diapirs they are initiated when weak sediments intrude other non-mobilized sediments (Cartwright et al. 2007; Maltman and Bolton 2003). However, mud volcano systems differ from most other subsurface sediment mobilization structures in that they consist of both kilometre-scale intrusive and extrusive structural and sedimentary constructions. Large intrusive sedimentary features are common but extrusive ones are not. Pockmarks and craters for instance are formed when intrusive structures terminate at the surface but they preserve little or no large-scale sedimentary record of their activity. Little can be done to establish the history of fluid and sediment expulsion or the ways in which the structure has formed and evolved without sampling the seabed directly. Where other extrusive sedimentary constructions are formed and preserved, such as sand volcanoes within injectite complexes, they are often too small for significant insights to be

gained into how and when the system formed and evolved (Samaila et al. 2006). Unlike these and other structures the extrusive edifices of mud volcano systems are large and numerous. The aggradational nature of their construction together with the widely documented link between sediment and fluid extrusion makes these features a compact and easily accessible sedimentary record of basinal fluid and sediment expulsion. Their close spatial and genetic association with hydrocarbons means that many are frequently imaged by seismic reflection and other data acquired to assist with oil and gas extraction. There therefore exists a vast global database that documents the structure and geophysical expression of mud volcano edifices that has the potential to help reconstruct the history of mud volcano system activity and basinal fluid and sediment expulsion.

This PhD project uses commercial two-dimensional (2D) and three-dimensional (3D) seismic reflection data alongside field mapping and other data to investigate the extrusive constructions of mud volcano systems from Azerbaijan and the South Caspian Sea. This area is ideal for the study of mud volcanoes since there are a large number offshore that are well-imaged by seismic data and many are easily accessible in Azerbaijan. The high quality of the seismic data together with the large size of some mud volcano edifices in the area means that their internal architecture and geophysical expression can be observed and interpreted leading to a reconstruction of the system's eruptive history and a better understanding of the ways in which these important fluid expulsion conduits evolve structurally. Onshore mud volcano edifices of Azerbaijan are of comparable size to those offshore and some are covered by high quality topographic data and satellite imagery. Therefore it is possible to compare the structures observed offshore with those seen onshore.

Whilst multi-disciplinary studies of mud volcanoes from this and other regions have recently increased in number, none have focussed solely on the large-scale extrusive constructions of the mud volcano system. There are none that have attempted to thoroughly assess the potential of extrusive mud volcanic features for better understanding the eruptive history of the system or the subsurface processes that control the architecture and evolution of the system. The present chapter now introduces the aims of the project, the geographical and geological setting of the study area, the project dataset and methods of investigation.

1.2 Project aims

The research presented in this thesis is focussed on the seismic and field architecture, geophysical expression and structuration of extrusive sedimentary features of the mud volcano system. These features are favoured for study for two principal reasons: 1) The quality of seismic reflection data at the typical depth of extrusive features is good and is better there than at deeper levels where intrusive structures are located; 2) The extrusive features of the mud volcano systems of Azerbaijan are well exposed and easily accessed. No exposures of deeper structural elements are currently known to exist in this region. To this end and considering the data available to this project, specific project aims are identified below.

(1) Document the seismic and structural architecture of the extrusive constructions found within large mud volcano systems and assess their potential use as records of basinal sediment and fluid expulsion.

- 1.1. Define a methodology for mapping the internal architecture of large mud volcanic edifices using 3D seismic reflection data.
- 1.2. Analyse the way extrusive edifices are constructed and determine the controls on their internal structure.
- 1.3. Reconstruct the eruptive history of a large mud volcano system using seismic reflection analysis of the internal structure of its extrusive edifice.

(2) Document and account for the geophysical expression of the extrusive features of large mud volcano systems.

- 2.1. Investigate the response of seismic reflection data to gassy seabed conditions.
- 2.2. Investigate the geophysical expression of subsurface mud volcanic deposits in seismic data within the extrusive edifice and sediments overlying it.

(3) Characterize the structure and origin of mud volcano source points.

- 3.1. Identify seismic-scale structures that characterize the morphology and structure of areas at the upper terminations of mud volcano systems.
- 3.2. Describe their structure and identify their mechanism of origin and significance.

3.3 Assess the potential of detailed analysis of volcano source points for constraining eruptive histories and structural evolution of mud volcano systems.

1.3 Geographical, tectonic and stratigraphical setting

The mud volcano systems investigated in this project are all located in either eastern Azerbaijan or the northwestern area of the South Caspian Sea (Fig. 1.1a, b). These areas fall within the South Caspian Basin (SCB), an area heavily influenced by Tertiary to Holocene age compression associated with the collision of the Arabian and Eurasian plates (Jackson et al. 2002). The Basin is one of the oldest oil producing regions on Earth with the first activity dating back to the 4th Century (Devlin et al. 1999). It is also an area of prolific mud volcanism (Fig. 1.2, Yusifov and Rabinowitz 2004). The accessible nature of well-exposed onshore mud volcano systems together with the high quality seismic imaging of offshore examples makes it an ideal region to conduct a multi-disciplinary study of mud volcanism.

This section introduces the location of the project study area, summarizes the sequence of events that have influenced its geological history and provides a brief discussion of the distribution and causes of mud volcanism in the area.

1.3.1 Study area location and geological history

Mud volcano systems from two principal areas of the South Caspian Basin are investigated in this thesis. One area is located onshore eastern Azerbaijan, the second is offshore within the northern part of the South Caspian Sea (Fig. 1.1b). The offshore area is located along a section of the Apsheron sill, a linear fold train that marks the northern limit of the SCB (Fig. 1.1b). This fold train divides the South Caspian from the Middle Caspian and is both an important tectonic and bathymetric lineament (Jackson et al. 2002; Kuprin 2002). Seismic reflection data from this offshore study area image the Apsheron anticline, the trapping structure for the multi-billion barrel Azeri-Chirag-Gunashli oilfield (Fig. 1.3). The onshore study area is located in a section of the SCB situated near the south eastern edge of the Greater Caucasus Mountains and the Kura Basin, which is the onshore continuation of the SCB (Fig. 1.1b, Nadirov et al. 1997). Mud volcano systems within the onshore study area are

located within the Shamakha Gobustan “mud volcano area” of Guliyev and Panahi (2004) (Fig. 1.2). Offshore they are located within the Precaspian area (Fig. 1.2). The geological history of the South Caspian Basin is complex and has been principally influenced by periods of Mesozoic age extension followed by later phases of compression that continue up until the present day. The Basin’s pre-Oligocene geological history is poorly constrained owing to sparse exposure and a lack of deep boreholes in the Basin’s interior. However, various origins for the basin have been suggested including a Cretaceous to Palaeogene age strike-slip-related pull-apart basin, a trapped remnant of early Mesozoic age oceanic crust and a Middle to Late Jurassic age back-arc marginal basin (Apol'skiy 1974; Berberian 1983; Zonenshain and LePinchon 1986). A general consensus seems to now prevail and the latter is considered by most authors to be the most likely.

Following some early phases of compression relating to widespread Eocimmerian orogeny, back-arc spreading and the opening of the SCB is thought to have taken place no earlier than the Middle Jurassic (Brunet et al. 2003). Spreading continued behind a long volcanic arc until the Palaeogene. The extension opened an extensive seaway, termed the Great Caucasus Trough that spanned an area from the Black Sea in the west to Turkmenistan in the east (Brunet et al. 2003). Approximately 8-10 km of sediment accumulated within the seaway during this time (Devlin et al. 1999). By the late Palaeogene the Arabian and Eurasian plates had started to collide and this led to regional uplift and episodic periods of marine restriction within parts of the seaway (Brunet et al. 2003; Devlin et al. 1999; Dewey et al. 1986; Hempton 1987). Deposition of thick organic-rich shales of the Oligocene-lower Miocene age Maykop Formation and other fine-grained sediments took place at this time within half-graben. The Maykop Formation constitutes both the principal hydrocarbon source rock of the SCB and is the widely accepted parent bed for all the region’s mud volcano systems (Dadashev et al. 1995; Nadirov et al. 1997).

Renewed tectonism in the Miocene led to uplift of some portions of the seaway and the isolation of the deeper South Caspian and Black Seas. The South Caspian Sea became a freshwater lake which was rapidly filled by fluvio-deltaic clastic sediment shed from the surrounding Caucasus, Kopet Dag and Alborz mountain ranges that were uplifted as a result of the collision (Allen et al. 2006; Morton et al. 2003).

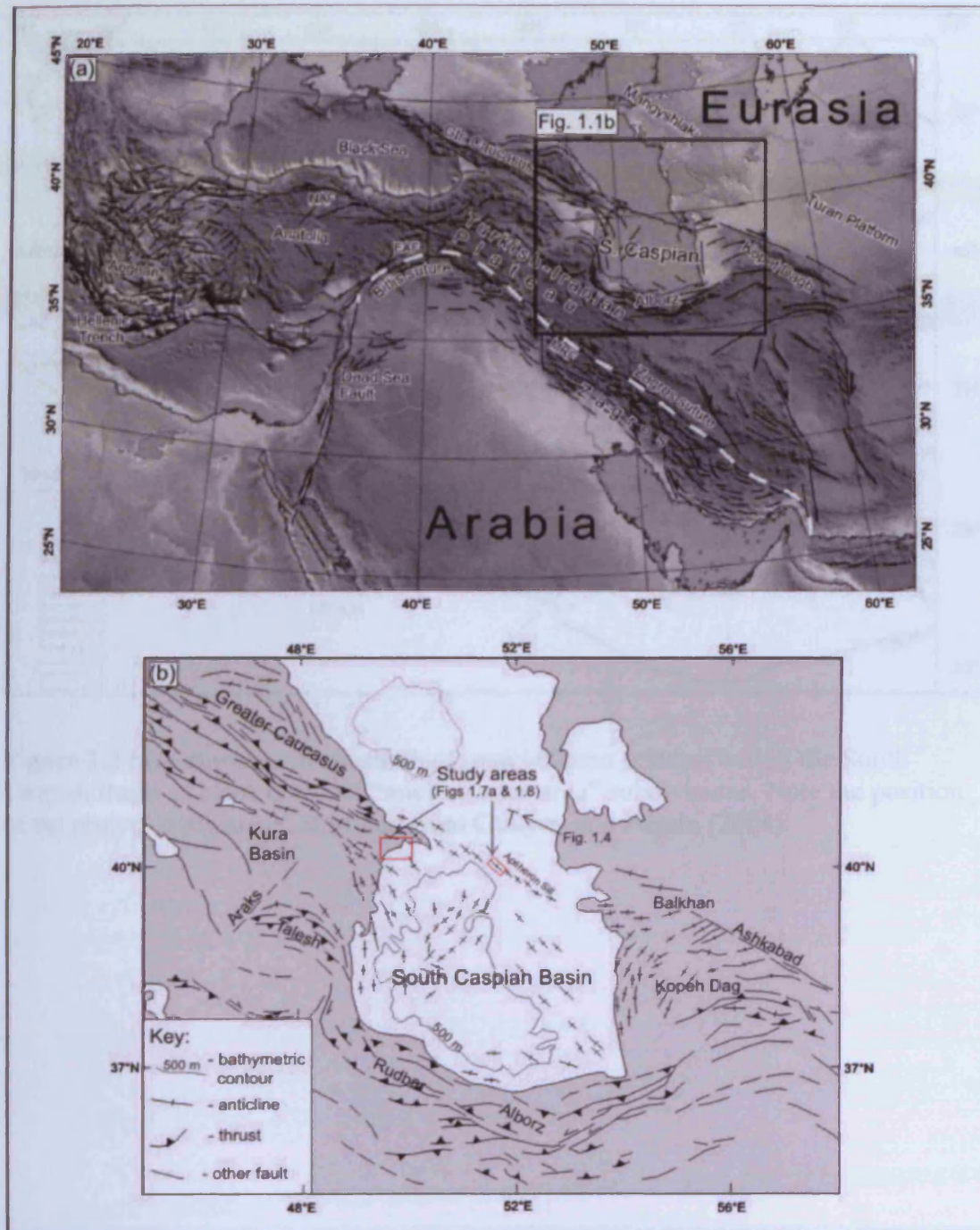


Figure 1.1 Geological setting and study area location: (a) Regional Digital Terrain Model showing the tectonic and topographic setting of the South Caspian Sea and surrounding regions. Modified from Allen et al. (2003). (b) Tectonic map of the South Caspian Basin showing the position of major structural elements and position of the onshore and offshore project study areas (red boxes). Map location is shown as a black box in (a). Modified from Jackson et al. (2002).

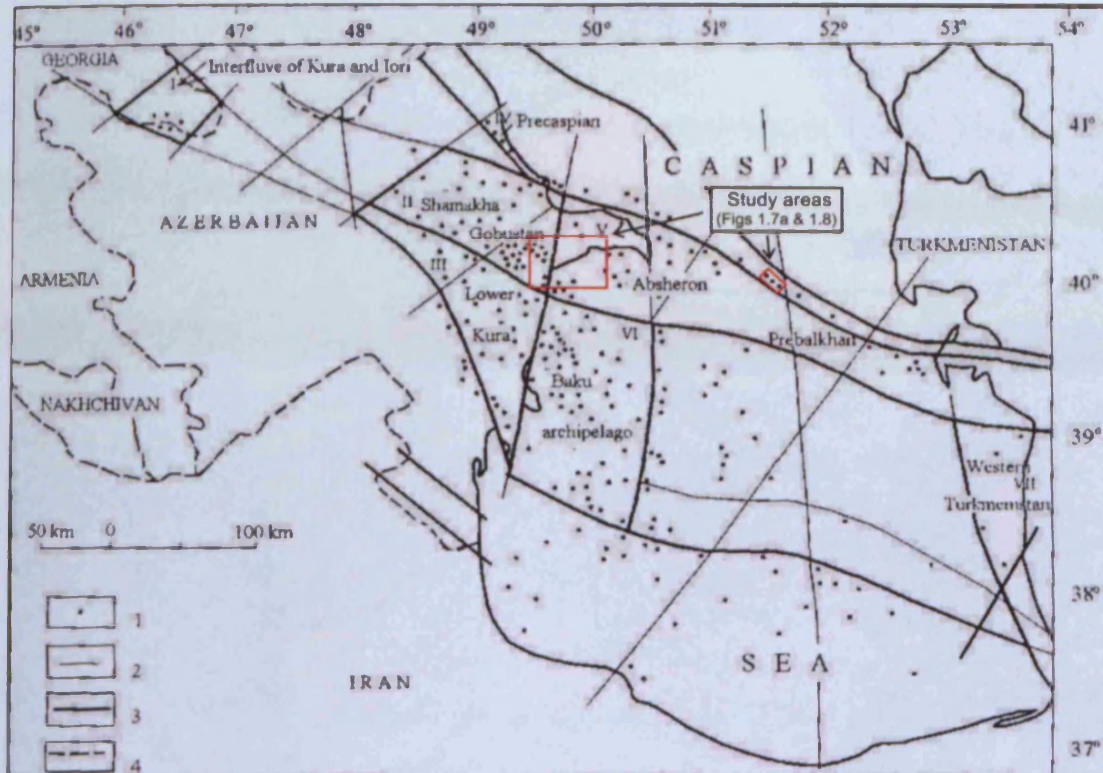


Figure 1.2 Map showing the position of mud volcano systems within the South Caspian Basin as black dots and “mud volcano area” subdivisions. Note the position of the project study areas. Modified from Guliyev and Panahi (2004).

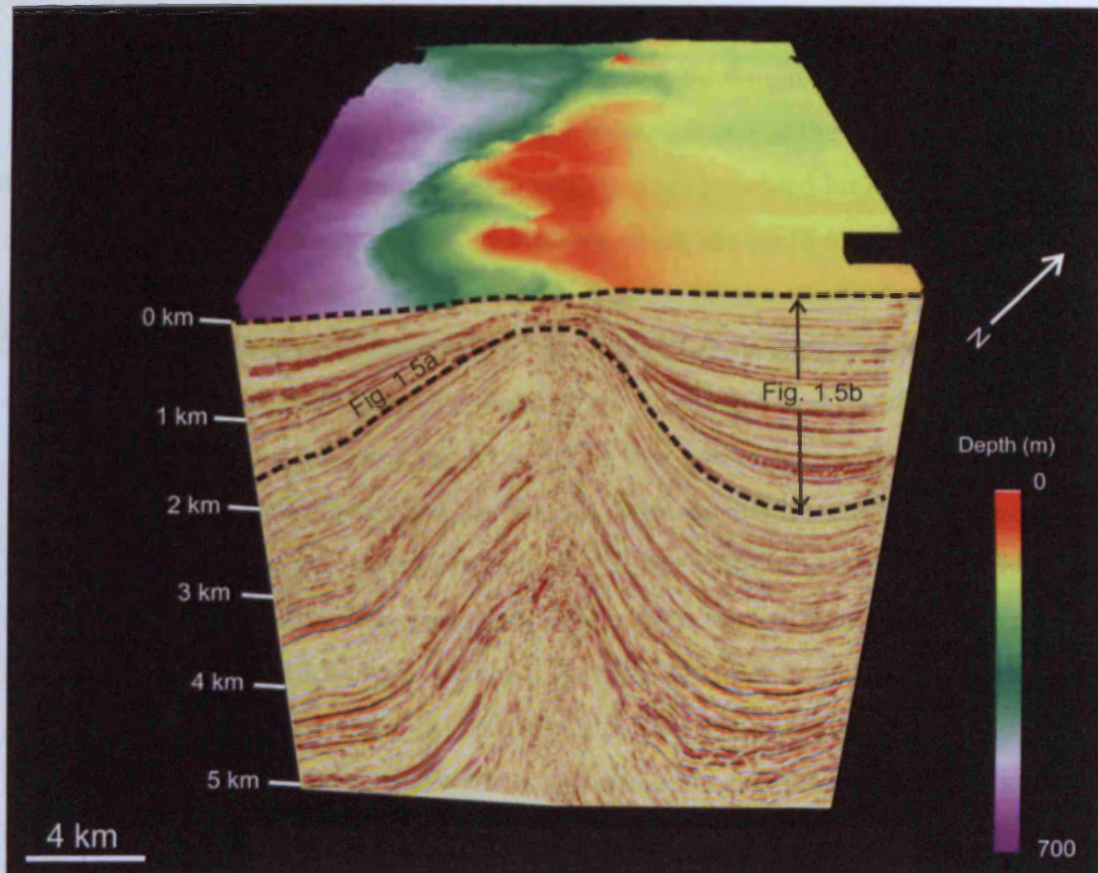


Figure 1.3 3D visualization of a seismic section through the Apsheron anticline and a bathymetric seabed map showing the position of large (>500 m diameter) mud volcano systems in its crest, including those investigated in chapters 3-5. This structure is located within the offshore study area and is imaged by a number of seismic reflection surveys.

The depth at approximately 10-12 km depth beneath the surface and appears to be linked to any deep structural lineaments associated with the underlying subduction zone (Duxin et al. 1999; Knapp et al. 2004; Wall and Wang 2005). This depth corresponds to the location of the Maykop Formation across much of the region and suggests that it is responsible for decoupling the Pliocene folds from the underlying subduction complex (Fig. 1.4).

Onshore and offshore the folds are of great significance to this project as mud volcanoes are the dominant feature and majority of the region's mud volcano systems (Gardner and Rubinowicz 2004). Offshore the mud volcano systems are located in the Apsheron anticline, the largest of the mud volcano systems located within the Apsheron anticline. This structure measures approximately 30 km long and is located 60 km north-northeast above the underlying subduction zone (Fig. 1.4 & 1.5a). The structural significance of this structure cannot be overstated by a series of seismic reflection surveys. Seismic mapping and analysis projects conducted during this

Most sediment was supplied by the palaeo-Volga river system to the north (Allen et al. 2002). Subduction of the South Caspian basement beneath the middle Caspian initiated at this time and invoked rapid subsidence of the northwest area of the basin (Allen et al. 2002; Jackson et al. 2002). This provided large amounts of accommodation space for the deltaic sediments which are up to 6 km thick in places (Allen et al. 2002). They are widely referred to as the Productive Series and are important hydrocarbon reservoirs and the host rocks for the intrusive elements of the region's mud volcano systems (Hinds et al. 2004; Reynolds et al. 1998).

Approximately 2.1 Ma after the onset of Productive Series deposition, continued tectonic compression and subduction became manifest as widespread folding of the Productive Series (Devlin et al. 1999). Within the basin the folds trend in various directions which are thought to reflect the complex tectonic regime and relationships to surrounding microplates (Fig. 1.1b, Nadirov et al. 1997). Along the Apsheron sill the folds are arranged into a NNW-SSE trending en-echelon array that may indicate an element of right-lateral transpression in this location or a stress influence coming from the west (Fig. 1.1b, Nadirov et al. 1997). Within the onshore study area and in other areas of Azerbaijan folds trend grossly parallel to the Apsheron sill but local variations are common and curved fold axes are often observed (Fig. 1.1b, Allen et al. 2003). The symmetrical shapes of many folds together with details from deep seismic lines and structural restorations have been cited as evidence that the folds detach at approximately 10-12 km depth beneath the surface and are not directly linked to any deep structural lineaments associated with the underlying subduction zone (Devlin et al. 1999; Knapp et al. 2004; Wall and Wiener 1998). This depth corresponds to the location of the Maykop Formation across much of the region and suggests that it is responsible for decoupling the Pliocene age folds from the underlying subduction complex (Fig. 1.4).

Both onshore and offshore the folds are of great significance to this project as anticlinal crests are the locations for the vast majority of the region's mud volcano systems (Yusifov and Rabinowitz 2004). Offshore the mud volcano systems investigated in the core research chapters of this project are located within the Apsheron anticline. This structure measures approximately 50 km long and is located at a point almost directly above the underlying subduction zone (Figs 1.4 & 1.5a). The commercial significance of this structure means it is imaged by a series of seismic reflection surveys. Seismic mapping and attribute analysis conducted during this

project has identified seven mud volcano systems within the anticline crest (Fig. 1.5a-c & Fig. 1.6). Of these, the Chirag and Azeri mud volcano systems are investigated in detail in chapters 3-5 (Fig. 1.6). Deep within the fold a number of thrust faults can be identified dipping either to the north or south along various sections of the fold (Fig. 1.5d). Although others studies have found folds within the SCB to be symmetrical and therefore characteristic of buckle folding, it does appear that some of these deep thrusts have an influence on fold vergence (Fig. 1.5d). In the crest of the anticline are developed a well-imaged series of extensional faults which are likely to have formed by a combination of outer-arc extension and gravitational collapse (Fig. 1.5e, Morley 2007). Cross-cutting relationships indicate that these have developed, at least in part, after the deposition of some large mud volcanic edifices (see chapter 3).

Mud volcano systems investigated within the onshore study area are also located within the crests of anticlines (Fig. 1.7a). These structures are directly analogous to the folds imaged offshore although they may have been initiated up to 2 Ma years earlier (Aliyev 1960). Unlike the offshore structures the onshore folds have been subjected to a period of uplift during Pleistocene age exhumation of the Azeri land surface. Folds crest are eroded to an undetermined depth and currently active mud volcano edifices sit unconformably on Productive Series strata (Fig. 1.7b, c).

1.3.2 Regional mud volcanism

Mud volcanism in the South Caspian Basin is prolific and the area is thought to host approximately 30% of the world's known population of mud volcano systems (Fig. 1.2, Guliyev and Feizullayev 1995). Numerous examples are present within the South Caspian Sea and in eastern Azerbaijan (Fig. 1.2). Onshore, most are clustered in the onshore Lower Kura and Shamakha Gobustan "mud volcano areas" of Guliyev and Panahi (2004). Offshore, most examples are clustered into the Absheron and Baku Archipelago (Fig. 1.2). Fewer examples are located in more distal parts of the Basin. The distribution of mud volcano systems is thought to be principally controlled by the presence of its regional parent bed, the Oligocene to Miocene age Maykop Formation. Pinch-out of this Formation in the west against the NNW-SSE trending Talysh-Vandam structural high restricts the mud volcanism to areas east of the high (Cooper 2001). In the north mud volcanism is restricted by the absence of the Maykop Formation north of the Apsheron sill.

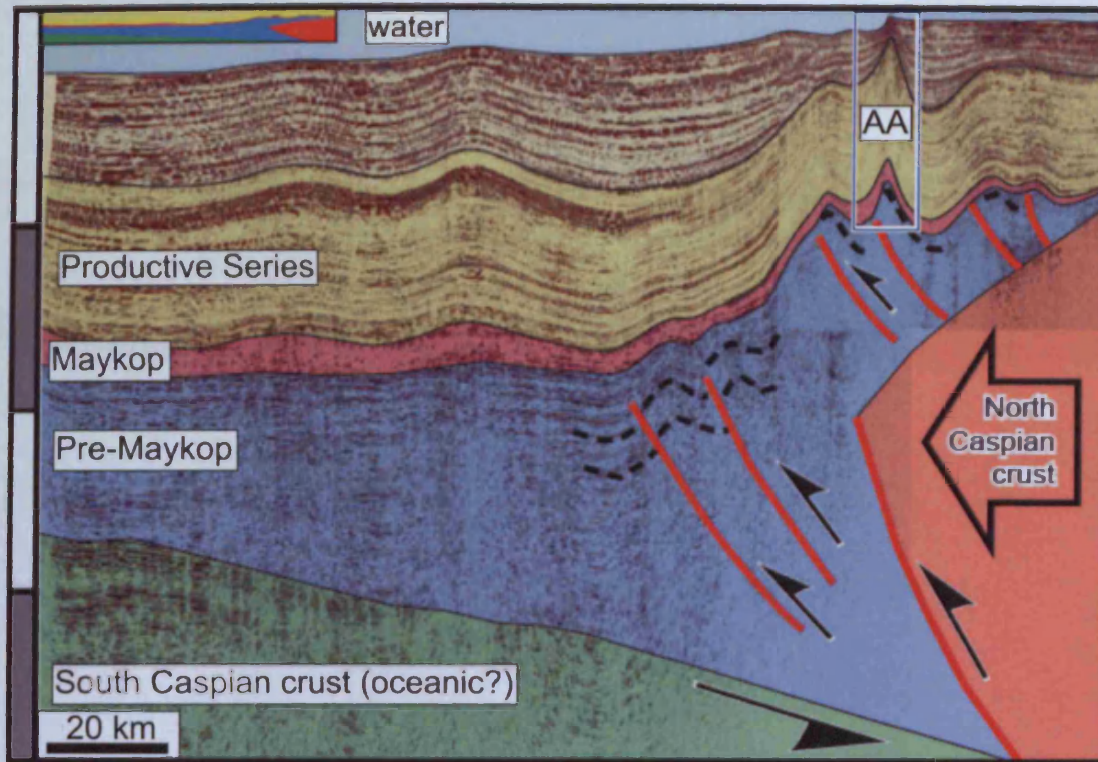


Figure 1.4 Regional deep seismic line trending approximately N-S through the Caspian Sea showing the deep structure and regional tectonic configuration. At depth northward subduction of South Caspian oceanic crust beneath the middle Caspian has led to the formation of an accretionary prism overlain by an extensive buckle fold system that is detached from the prism by the thick and overpressured Maykop formation (coloured pink). Note the position of the Apsheron anticline (marked AA in black box) which is located within the offshore study area. Approximate position of seismic section is shown in Figure 1.1b. From Stewart and Davies (2006).

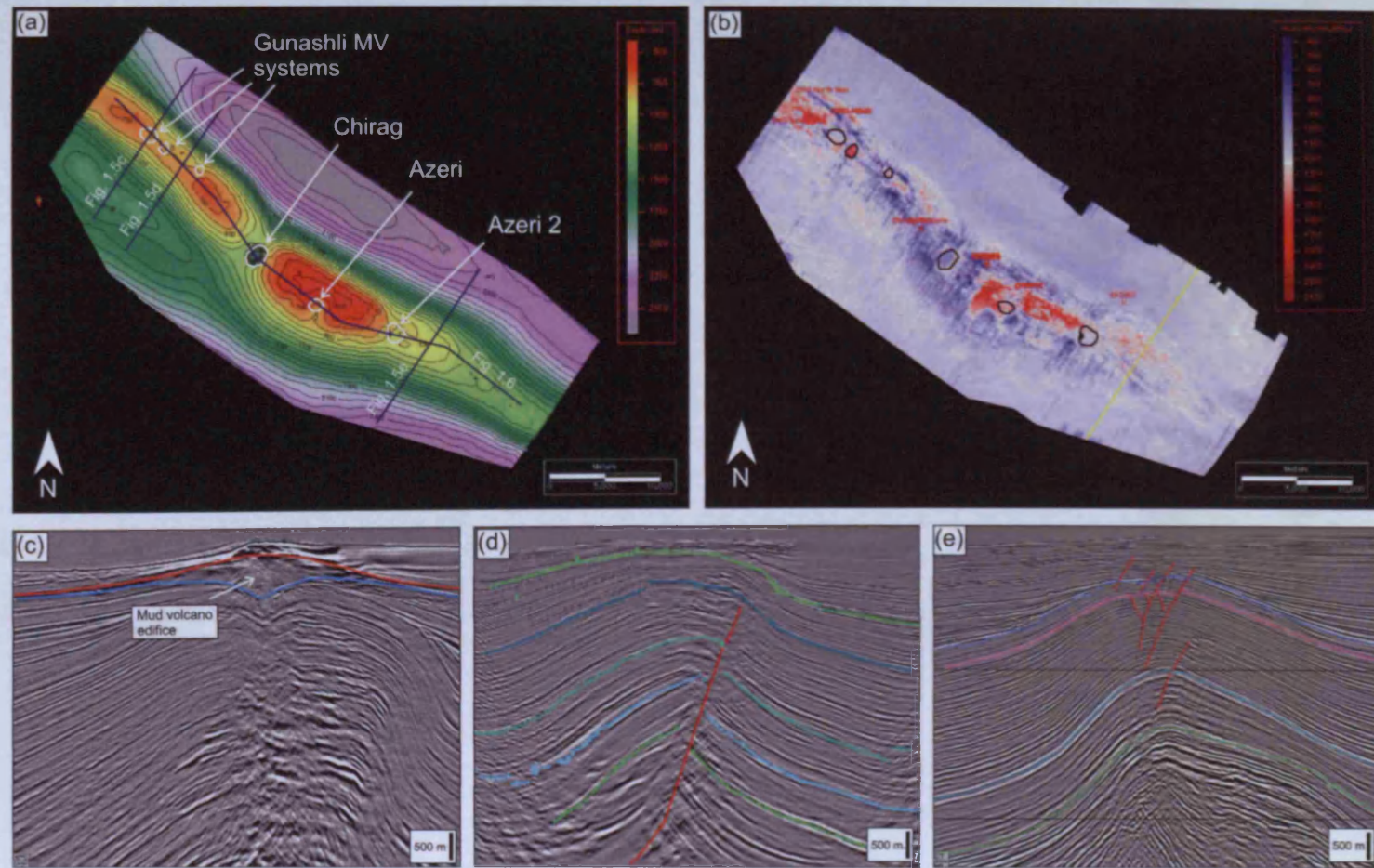


Figure 1.5 The Apsheron anticline: (a) Seismic depth map of “BMV” horizon showing fold orientation and amplitude. Mud volcano systems marked as white polygons. Horizon location shown in Figure 1.3. (b) RMS (root mean squared) interval amplitude map of the seabed-BMV section showing the position of mud volcano systems (marked as white polygons). Note the radial negative amplitude anomaly associated with the Chirag mud volcano system and other minor anomalies associated with others. Interval location is shown in Fig. 1.3. (c) Seismic section showing a biconic (two cones placed base to base) mud volcano edifice in the fold crest. Location of this and subsequent Figure parts shown in (a). (d) Seismic section showing a large deep thrust fault. (e) Seismic section showing the extensional fault system present within the anticline crest.

1-13

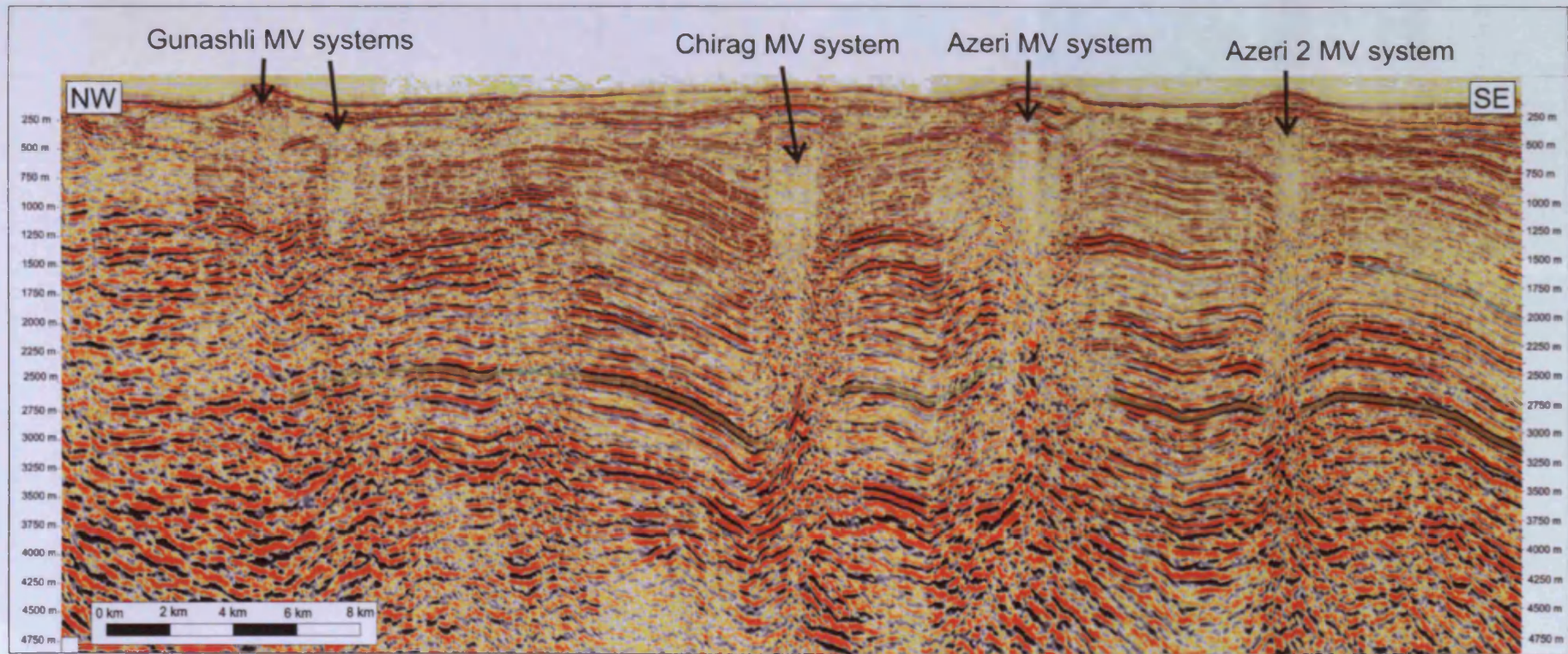


Figure 1.6 Seismic profile trending roughly parallel to the strike of the Apsheron anticline transecting four of the structure's principal mud volcano systems. Note the vertical zones of poor signal/noise ratio in the centre of each system that probably results from the presence of gas in the section or intense vertical fluid migration. Section location shown in Figure 1.5a.

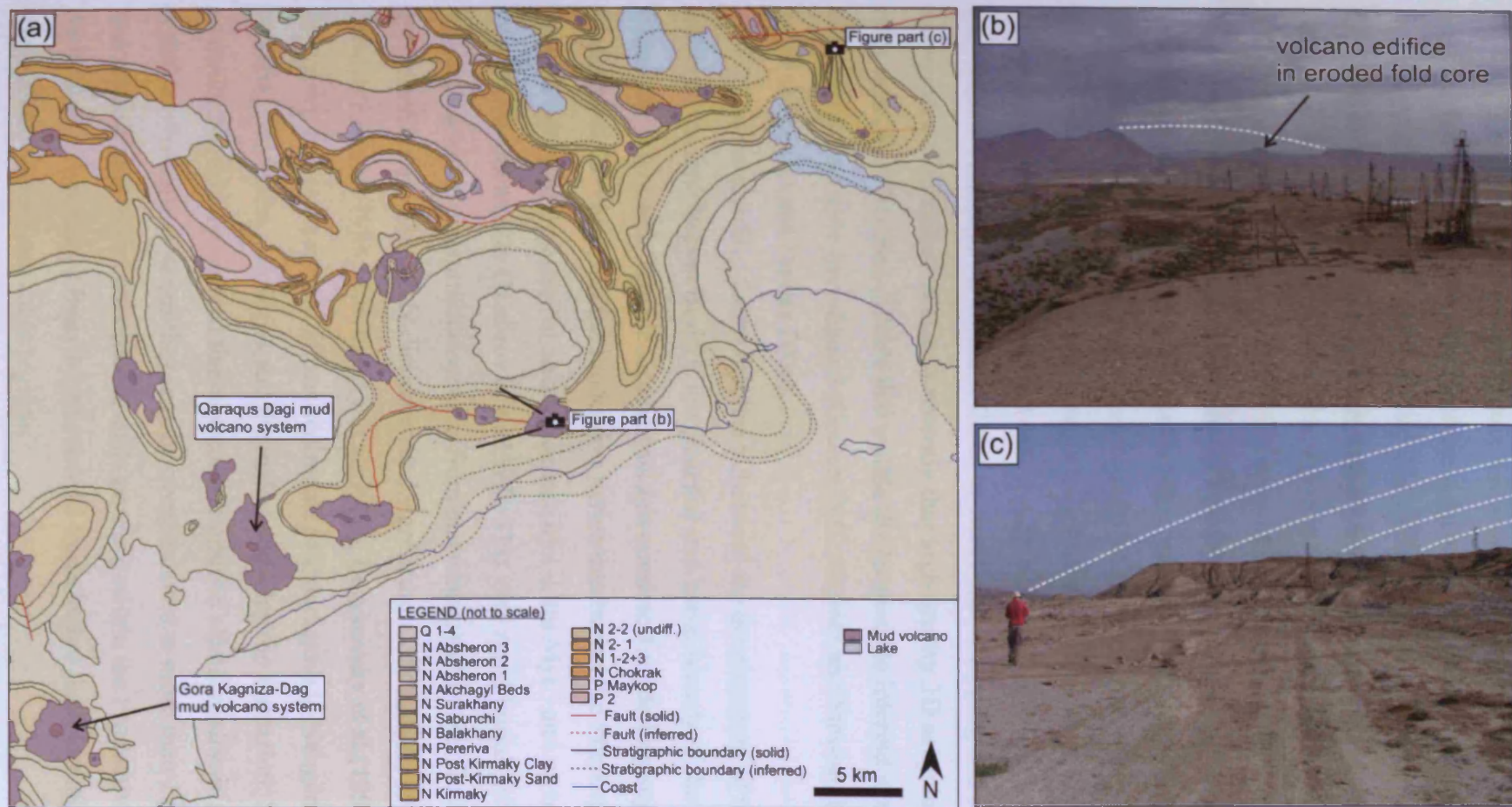


Figure 1.7 The onshore study area: (a) Geological map showing the position of the Qaraqus Dagi and Gora Kagniza-Dag mud volcano systems along with others. Note their locations in the crests of exhumed anticlines and the variety of fold orientations (red lines). Map location shown in Figure 1.1b. (b) Field photograph taken at the summit of the Lokbatan mud volcano showing a smaller mud volcano edifice in the core of an exhumed anticline. The white line reconstructs the likely pre-exhumation structure. See (a) for photograph location. (c) Field photograph from the Kirmaky Valley showing the exhumed land surface on the flank of a N-S trending anticline. White dashed lines reconstruct the likely pre-exhumation structure. See (a) for photo location.

A total of 76 onshore mud volcano systems are known in Azerbaijan and these have erupted approximately 300 times since records began (Aliyev et al. 2002). Each example is manifest as a conical edifice that can be up to 6 km wide and 400 m high. Offshore, as many as 99 mud volcano systems have been recorded in the northwestern portion of the South Caspian Sea and many more are known to exist elsewhere within it. Approximately 75% are located in the crest of anticlines with the remainder located on the flanks of anticlines or in synclines (Yusifov and Rabinowitz 2004). Large submarine mud volcano systems occasionally erupt to form islands or promontories and are frequently detected by remote geophysical surveys. The study of onshore and offshore mud volcanism in the SCB has a long history (Aliyev et al. 2002; Guliyev and Feizullayev 1995; Huseynov and Guliyev 2004). Much of it was focussed on geochemical studies of the expelled fluids or small-scale mapping and description of minor extrusive features. It is only recently that high quality 3D seismic reflection and other data have become available that enable the large-scale internal structure of mud volcano systems to be investigated (Cooper 2001; Davies and Stewart 2005; Fowler et al. 2000; Stewart and Davies 2006).

The most critical factor that has influenced the development of mud volcanism within the South Caspian Basin is the presence and burial history of the Maykop Formation parent bed. Subsidence analysis and numerical modelling suggest that the fluvio-deltaic sediments of the Productive Series that buried the Maykop muds during the Pliocene were deposited at an average rate of 1.4 km Myr^{-1} and up to 2.4 km Myr^{-1} during the Quaternary (Nadirov et al. 1997). This very rapid burial, which approaches values for turbidite systems from elsewhere, meant that fluids within the mud could not be adequately dissipated and significant overpressure developed (Bredehoeft et al. 1988; Burykovsky et al. 1995). Burykovsky et al. (1995) have shown that this overpressure affects sediments of Palaeogene to Neogene-age including the Productive Series and the underlying Maykop formation. Shales are generally more overpressured than the coarser grained clastic reservoir facies and within the Productive Series they may be overpressured to more than 1.8 times the hydrostatic value. As a consequence shale porosity within the Productive Series at a depth of 4-5.5 km ranges from 3-20%, several times higher than normally consolidated shales from other regions.

In addition to shales within the Productive Series, the rapid burial and overpressuring of the Maykop Formation parent bed was crucial to the development



of widespread mud volcanism. Maykop pore pressure gradients of 0.020-0.023 MPa m⁻¹ developed in response to the rapid burial. Effective stress reduction and mechanical weakening of the sediment as result of this is suggested by Burykovsky et al. (1995) to be key to the development of mud volcanism through allowing subsurface sediment mobilization. In the particular case of the Maykop Formation, which is also the regional hydrocarbon source rock, the maturation of hydrocarbons within it and the addition of other fluids injected from below is highly likely to have contributed to the development of overpressure. Maturation of the Maykop and expulsion of oil and gas is thought to have taken place in the last 1 to 3.5 Ma (Abrams and Narimanov 1997; Lerche and Bagirov 1999; Lerche et al. 1997). Oil, and particularly gas, maturation from source rocks in general is known to be accompanied by a large volumetric expansion and therefore is likely to have enhanced the burial-induced overpressure developed within the Maykop (Osborne and Swarbrick 1997).

A final additional factor influencing overpressure build up in the Maykop and the establishment of mud volcanism in the South Caspian Basin is the continued tectonic compression resulting from the regional tectonic regime. In general active compressive regions such as the SCB are the sites of subsurface fluid flow and dynamic tectonism which are considered to be favourable conditions for mud volcanism. Indeed, the predominant location of mud volcano systems within anticlines is thought to reflect the importance of regional compression through the increase of lateral stress on the parent bed at depth. Little is known however about the specific ways in which compression influences the Maykop parent bed at depth and exactly why mud volcanoes are mostly located within anticline crests.

1.4 Database and methodology

Submarine mud volcanoes within the offshore study area are investigated using two-dimensional (2D) and three-dimensional (3D) seismic reflection data supplemented by data from a site-survey borehole (marked BH1 in Fig. 1.8). Mud volcanoes on land are investigated by field mapping using other remote data. South of the main offshore study area some additional mud volcano systems are imaged by a bathymetric survey derived from the seabed reflection pick of a 3D seismic survey. This section provides details of the data and methods used in this project and in the case of the seismic data,

highlights some potential problems that may arise when they are used to image and correctly interpret large mud volcano systems.

1.4.1 Seismic reflection data

All seismic reflection data used in this project were acquired within a rectangular shaped NW-SE trending area measuring approximately 1300 km² located approximately 100 km offshore Azerbaijan in the South Caspian Sea (Fig. 1.1b). This area represents the limits of a large 3D seismic reflection survey acquired in 1995 for the purposes of commercial petroleum exploration of the Apsheron anticline (Fig. 1.8). Since then a number of other 3D and 2D seismic reflection surveys have been acquired within this survey area. Seven 3D seismic surveys were available to this project, although only two have been extensively interpreted and used in this thesis (Fig. 1.8 and Table 1.1). The remaining five have not been extensively used due to either their non-optimal location or poor quality. In addition a 2D seismic reflection line was available to the project. This was acquired in 1995 during site surveys that were designed to maximise the resolution of the seismic image in the shallow section. Table 1.1 summarizes the main attributes and acquisition parameters of each survey. The processing sequence used for both the 3D surveys is summarized in Figure 1.9.

All surveys are near zero-phase at the seabed meaning that the geophysical interface that has produced the reflection is located at the positive amplitude peak or negative amplitude trough of the wavelet (Fig. 1.10, Simm and White 2002). Each one has been carefully interpreted first for large-scale structure and then in detail within and around the area's mud volcano systems. Depth, isopach and attribute maps were created for key horizons and intervals (dip, acoustic and RMS interval and horizon amplitude).

In general the quality of all three seismic surveys used in this project is considered to be high. In some areas however, the quality of the 3D seismic data is dramatically reduced. This mainly occurs in the central areas of mud volcanoes (Fig. 1.6) and in other areas within the crest of the anticline. Acoustic phenomena that may have influenced this deterioration in quality include the effect of gas in the sediment pore spaces, the effect of intense extensional faulting in the anticline crest and attenuation of seismic energy by gassy patches of seafloor (Judd and Hovland 1992; Parnell and Schwab 2003; Schroot et al. 2005).

As Table 1.1 shows, both the 3D surveys were processed using prestack depth-migration (Robinson et al. 2005) and spatially varying velocity cubes (R. Johnson 2006 *pers. comm.*). As such the positional accuracy is likely to be high and any seismic artefacts resulting from the presence of anomalously high or low seismic velocity units are likely to be minimised. However, during depth migration it is not clear whether the position or size of mud volcano edifices in the anticline was specifically considered as a potential acquisition problem. As mud volcano edifices are likely to consist of large volumes of, possibly gassy, low seismic velocity sediment they represent lithological units capable of influencing the correct 3D position of underlying seismic reflections through the velocity push-down effect (Brown 1999). In order to investigate the potential problem this may cause during the rest of the project I conducted a short investigation using time-migrated and depth-migrated seismic lines. First I selected a good quality time migrated seismic line that imaged the central section of a mud volcano system; a potential location for velocity push down effects (Fig. 1.11a). Interpretation of this line shows a seismically transparent biconic (two cones base to base) unit that I interpret as a buried mud volcanic edifice (Fig. 1.11a, b, see also chapter 3). The lower apex of the edifice bicone is located within a focussed depression of approximately 150 ms structural relief. My aim was to test whether this depression is a genuine downwarping of the edifice base or a result of velocity push-down. By depth-converting the seismic line in the Midland Valley software program 2DMove the seismic velocity (V_p) of the central part of the edifice that is required to restore the sagged base and remove the depression can be determined. If this velocity is realistic for buried mud volcano deposits it would suggest that sags and depressions beneath buried mud volcano edifices could be the result of velocity push-down. Velocities for the area outside the central zone of the mud volcano edifice were constrained using a shallow checkshot survey from BH1.

After substituting a range of different velocities into the central area of the mud cone and the section overlying it (grey and yellow areas of Fig. 1.11c) it was established that the maximum velocity at which the depression was restored is 1200 m/s (Fig. 1.11d). This is considerably lower than that of typical seafloor sediments (1400-1550 m/s, Hamilton and Bachman 1982) or indeed typical seawater (approximately 1500 m/s).

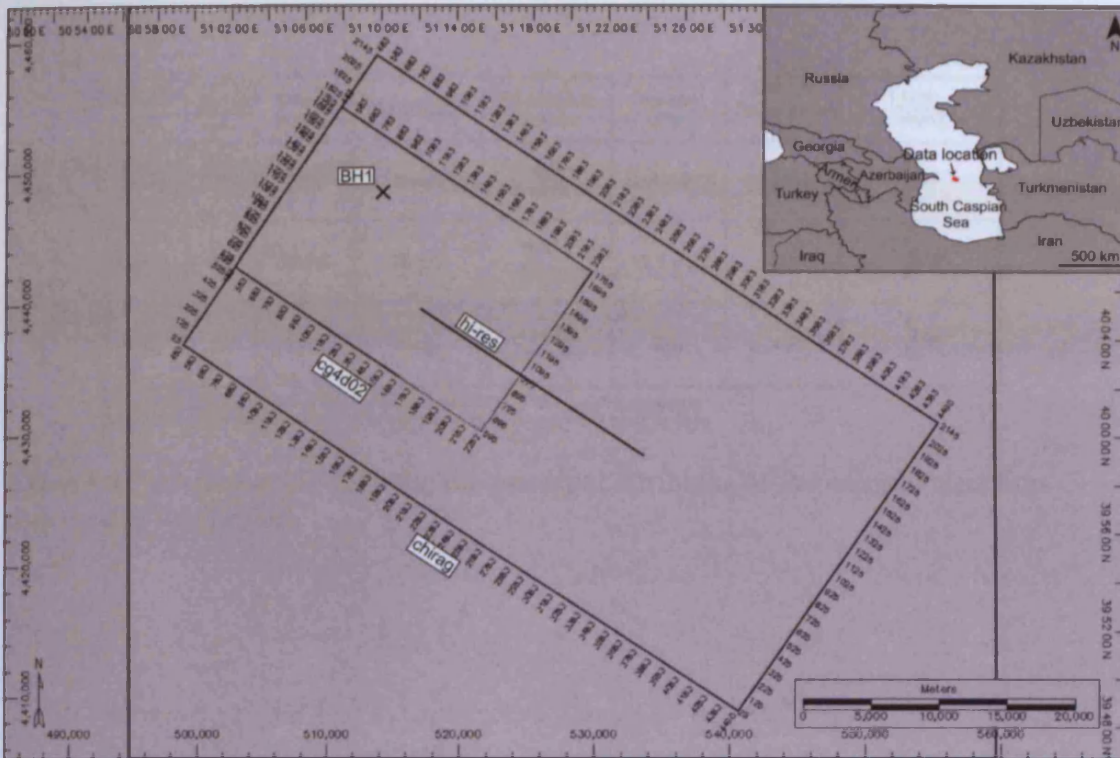





Figure 1.8 Map showing the location of seismic and well data within the offshore study area. Black rectangles denote 3D seismic survey boundaries and surrounding numbers are seismic inlines and crosslines.

Survey name	2D/3D	Year of Acquis.	Time/Depth	Acquisition method	Bin size ¹ (m)	Vert./Lat. Resolution ² (m)	LOW HIGH
chirag	3D	1995	Depth	Towed streamer	12.5 x 37.5	12/24	
cg4d02	3D	2002	Depth	Towed streamer	12.5 x 25	12/24	
hi-res	2D	1995	Time	Towed streamer	N/A	4/8	

¹Survey bin sizes interpolated to a final interpretation grid of 12.5 x 12.5 m during processing
²Resolution measurements for chirag and cg4d02 survey at 1 km depth, hi-res at 100 m depth

Table 1.1 Summary table showing the principal attributes of the seismic reflection data used in this project.

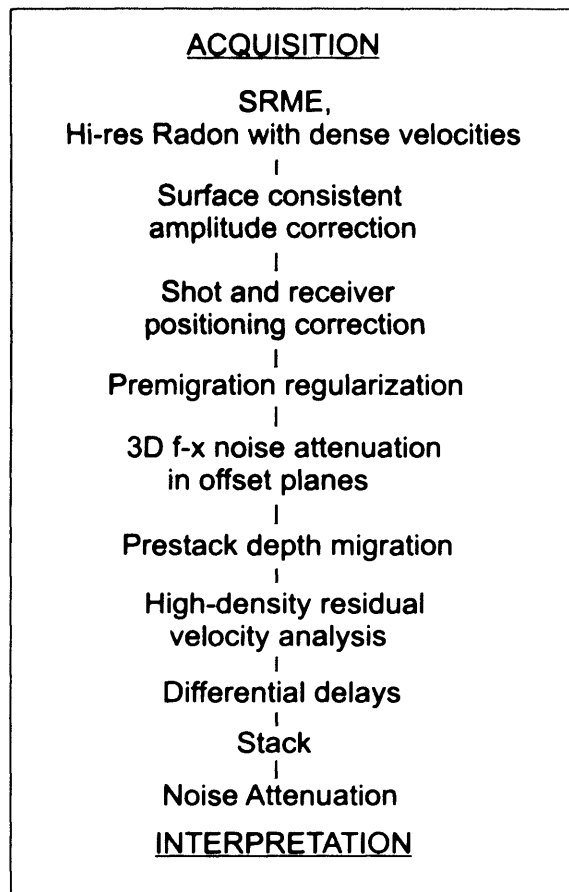


Figure 1.9 Flow diagram summarizing the processing workflow that was used for the 3D seismic surveys used in this project, chirag and cg4d02. From Robinson et al. (2005)

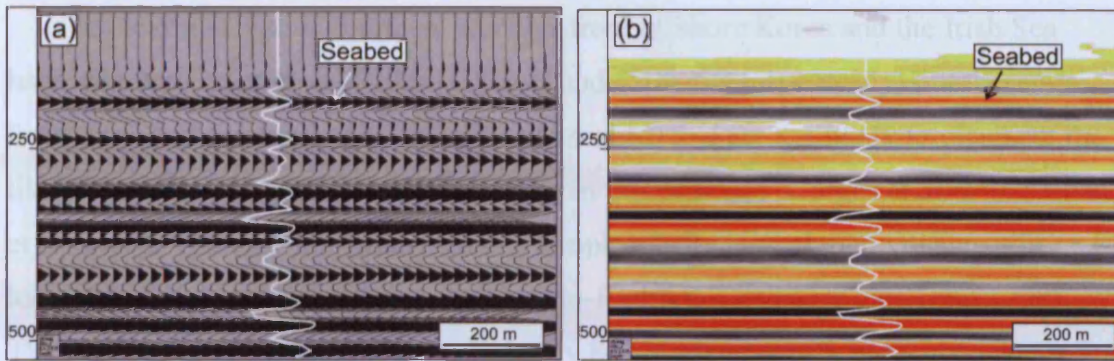


Figure 1.10 3D seismic data phase: Variable area (a) and variable intensity (b) seismic depth section through the seabed from survey chirag showing the near zero-phase character of the seabed reflection. An individual trace is shown in white on both Figure parts to emphasize the waveform of the seabed and other deeper reflections.

However, the effect of a gas bubble in sediment may be to cause a push-down of the trace with depth, and needs to be considered here. For example, the effect of air bubbles reducing sediment density, velocity and producing significant velocity fluctuations (Frost, 1980; Judd and Oldham 1992; Schreier et al. 2005). Andreasen et al. (2007) have used the equations of Gregory (1976) to suggest that 1% of sediment with similar properties to that in this example ($\rho = 1850$ kg/m³, porosity = 40%) will be reduced to approximately 1200 kg/m³ when saturated with 4% gas. Values as low as 1000 kg/m³ are possible when gas concentration is increased. This suggests that under conditions of fairly low gas saturation (4%) a velocity push-down could occur beneath a mud volcano edifice. It is not confirmed whether the example well with here contains any gas in the sediment. It does not have a significantly blanked central section like others in the suite, indicating that the section may not be highly gas-rich (e.g. Fig. 1.6). Considering that only small amounts of gas is required to produce significant signal disruption in seismic data (<1%, Farnley 1983) the continuity of seismic reflections beneath the edifice may suggest that it is not gas saturated at all. However, a small degree of acoustic turbidity can be observed in the central portion of the edifice indicating that very small amounts of gas may be present within the section.

The conclusion of this short investigation is therefore that mud volcano sediment alone is unlikely to be of a low enough ρ to induce a velocity push-down beneath a mud volcano edifice. The effect of gas is likely to be more significant and may well lower sediment ρ enough to induce a push-down. Physical properties of buried mud volcano sediments when saturated with gas are not well constrained meaning that I

Gas-bearing shallow sediment samples from offshore Korea and the Irish Sea have very low seismic velocities (800 m/s and 1200 m/s respectively) but these are from very shallow depths (<5 m below the seabed) and are not likely to represent the likely conditions at the depth of the edifice in this example (Gorgas et al. 2003; Yuan et al. 1992). The only known drilled and geophysically logged mud volcano edifice is located in the eastern Mediterranean (Jurado-Rodriguez and Martinez-Ruiz 1998). The logged section is located approximately 80 – 190 m beneath the seabed and is therefore at a similar depth to the edifice in this example. Seismic velocities within the logged edifice section are no lower than 1604 m/s, the average value is approximately 1766 m/s. This evidence suggests that a V_p of 1200 m/s is not likely to occur within a mud volcano edifice.

However, the effect that gas within the sediment pore spaces may have on the V_p of the mud volcanic sediment needs to be considered here since gas, even in small amounts, has the effect of dramatically reducing sediment seismic velocity and producing numerous acoustic phenomena (Fannin 1980; Judd and Hovland 1992; Schroot et al. 2005). Andreassen et al. (2007) have used the equations of Gregory (1976) to suggest that V_p of sediment with similar properties to that in this example ($V_p = 1900$ m/s, porosity = 40%) will be reduced to approximately 1200 m/s when saturated with 4% gas. Values as low as 1000 m/s are possible when gas concentration is increased. This suggests that under conditions of fairly low gas saturation (4%) a velocity push-down could occur beneath a mud volcano edifice. It is not confirmed whether the example dealt with here contains any gas in the sediment. It does not have a significantly blanked central section like others in the anticline indicating that the section may not be highly gas-rich (e.g. Fig. 1.6). Considering that only small amounts of gas is required to produce significant signal disruption in seismic data (<1%; Fannin 1980) the continuity of seismic reflections beneath the edifice may suggest that it is not gas saturated at all. However, a small degree of acoustic turbidity can be observed in the central section of the edifice indicating that very small amounts of gas may be present within the section.

The conclusion of this short investigation is therefore that mud volcano sediment alone is unlikely to be of a low enough V_p to induce a velocity push-down beneath a mud volcano edifice. The effect of gas is likely to be more significant and may well lower sediment V_p enough to induce a push-down. Physical properties of buried mud volcano sediment when saturated with gas are not well constrained meaning that I

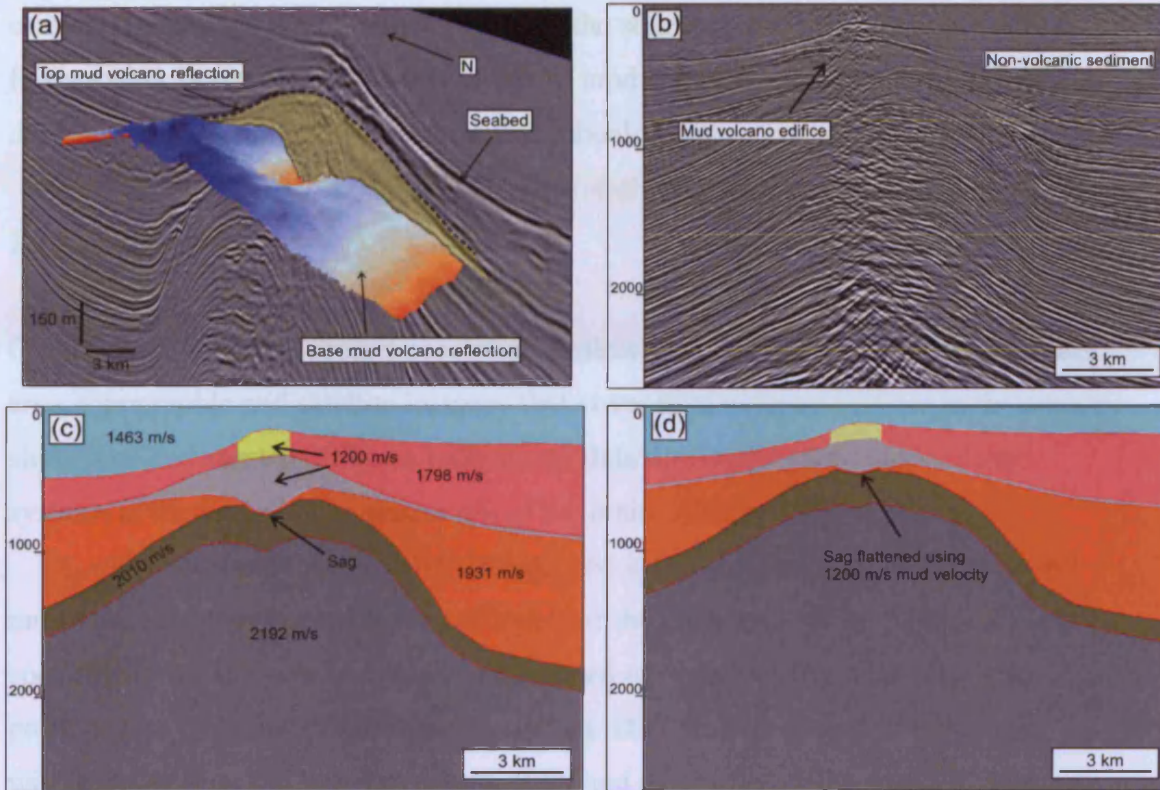


Figure 1.11 Testing mud volcano push-down: (a) 3D visualisation of seismic depth section and horizon showing the Gunashli 1 mud volcano edifice within a depression at the crest of the anticline. (b) Seismic ILN 965 displayed in two-way-time that was used to model velocity push-down. Note the Gunashli 1 mud volcano edifice in fold crest (shaded yellow). Section is TWT, vertical scale in milliseconds. (c) 2DMove interpretation panel showing the interpretation of ILN 965 showing checkshot-derived seismic velocities used in its depth conversion. Vertical scale in milliseconds TWT. Note the depression at the base of the edifice. (d) Depth-converted seismic ILN 965 showing the restoration of the base-edifice depression. Vertical scale is in metres.

cannot conclude on the influence of gas on the seismic data in this example. Until further work better constrains this aspect of mud volcanic seismic interpretation depressions beneath mud volcano edifices should be interpreted with caution.

1.4.2 Other data

Other data used in this project consist of shallow well data within the offshore study area, topographic and satellite imagery that cover mud volcano edifices in the onshore study area and some multibeam bathymetry data that image some mud volcano systems at the seabed in an area south of the main offshore study area.

The borehole (marked BH1 in Fig. 1.8) is located northeast of the Gunashli mud volcano system towards the northwest of the study area. It was acquired specifically for site survey purposes and aimed to better constrain the physical properties of the shallow sedimentary section. Data from it consist of a shallow wireline sonic log run between depths of 88 and 412 m below the seafloor, a density profile from the seabed to a depth of 428 m and a checkshot survey between depths of 9 and 980 m below the seabed. Other data from within the South Caspian Sea consist of a 3D seismic-derived bathymetric survey that images some mud volcano systems in an area south of the main study area. These data are used in chapter 5 and are displayed so that one pixel represents an area of seabed measuring 25 x 25 m.

Onshore a digital elevation model (DEM) and an IKONOS satellite image was available for one example described in chapter 5 (Doyle 1984). The IKONOS image is full colour and has a horizontal resolution of 4 m. The DEM is displayed so that one pixel represents an area of land measuring 15 x 15 m.

CHAPTER TWO

2.0 The geological occurrence of mud volcanism

2.1 Introduction

The principal aim of this chapter is to constrain the scope of this project by providing a review of the current state of knowledge on the geological occurrence of mud volcanism. Subsequent sections will address this aim by:

- (1) Identifying the context of mud volcanism within the wider topic of subsurface sediment mobilization in sedimentary basins.
- (2) Reviewing the concept of the “mud volcano system” summarizing the processes and mechanisms occurring within each “structural domain”.
- (3) Reviewing the literature that deals with the specific aspects of mud volcanic geology that are dealt with in this project.

Later in this chapter sub-sections 2.3.3 and 2.3.4 are of particular significance since these are the areas of the mud volcano system that are focussed on in the core research chapters of this project (3-5).

2.2 Subsurface sediment mobilization and intrusion

Mud volcanism is a widespread and well-documented expression of subsurface sediment and fluid mobilization, intrusion and extrusion. However, it merely forms part of a spectrum of geological phenomena that all relate their occurrence to subsurface sediment mobilization. This section reviews the conditions necessary for subsurface sediment mobilization and intrusion to occur and introduces some of the typical structures that are formed by it.

2.2.1 The principles of subsurface sediment mobilization

In general, as sediments undergo burial the expulsion of fluids and the onset of diagenesis leads to a progressive increase in the sediments' strength until they become

lithified. In some cases this increase in strength is temporarily reversed meaning that the sediments become capable of mobilization (sometimes termed remobilization). Mobilization involves both rendering the sediment capable of motion and the bulk movement that commonly results (Maltman and Bolton 2003). Most explanations of sediment mobilization involve its weakening due to the overpressuring of the sediment pore fluids. A sediment is said to be overpressured if its pressure of the fluid in its pore spaces exceeds the hydrostatic (normal) pressure for a given depth (Osborne and Swarbrick 1997). The degree to which a fluid is overpressured can be described as the fluid potential or head (Fig. 2.1a).

Under normal conditions, a sediment undergoing loading by overlying sediments progressively expels fluids in response to the increasing load (Maltman 1994). The pressure within the remaining pore fluid due to the load imparted by the overlying fluid column is termed the normal or hydrostatic fluid pressure (P_f , Fig. 2.1a). Any additional load sustained by the particles is termed the effective stress (σ' , Eq. 2.1, Fig. 2.1a, b).

$$\sigma' = \sigma - P_f \quad (\text{Equation 2.1})$$

where σ is the total stress. The relationship of fluid pressure to effective stress means that increases in fluid pressure lead to decreases in effective stress (Fig. 2.1b).

The origins of loading that can bring about overpressuring can be considered “dynamic” (arising from a source external to the sediment), or “static” (arising from processes within an evolving sediment, Maltman 1994). In sedimentary basins the most common form of dynamic loading arises from the weight additions due to progressive deposition of overlying sediments (the lithostatic load Owen 1987). Typical static loading processes include aquathermal pressuring, hydrocarbon generation, expansion of gases (such as methane) and mineral dehydration (Osborne and Swarbrick 1997). Overpressuring arises when the sediment becomes loaded but is unable to drain adequately in response to the increasing load. This inability to drain is primarily a function of permeability meaning that low permeability sediments, such as clays, are particularly prone to overpressuring (Burykovsky et al. 1995). Other mechanisms such as encasement within low permeability sediment or the effect of

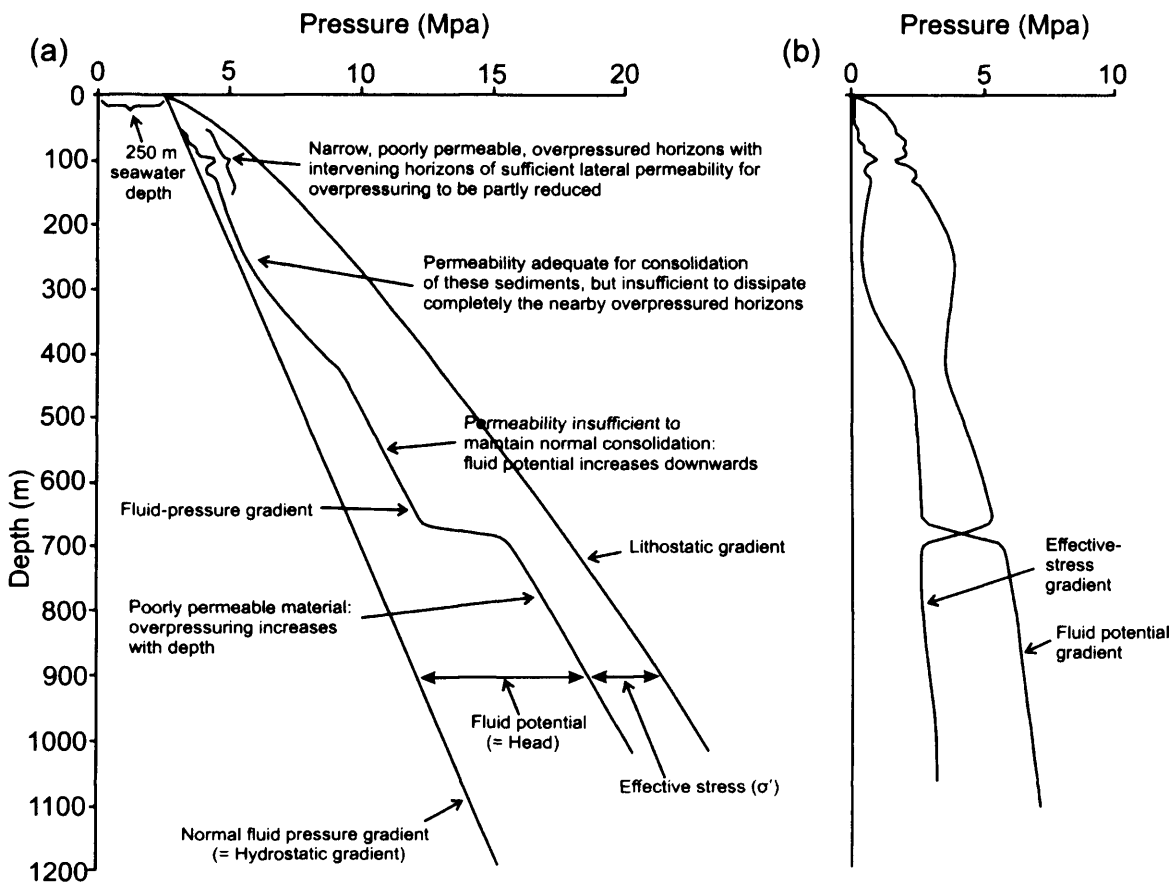


Figure 2.1 Patterns of pressure increase with depth in sedimentary basins: (a) Rates of increase of pressure and stress due to burial. The normal fluid pressure gradient is based on an overlying seawater depth of 250 m and a constant fluid density in the entire column of 1025 kg m^{-3} . The lithostatic gradient is based on a grain density of 2650 kg m^{-3} and a porosity decrease with depth following the average values for sand-silt-clay of Einsele (1989). The hypothetical gradient illustrates the kind of pressure variations that can arise within a sequence of varied sediments. (b) Effective-stress gradient and fluid-potential gradient derived from curves in (a). Note the inverse relationship of fluid-potential and effective stress. Both parts modified from Maltman (1994).

sealing faults can similarly retard drainage of coarser grained sediments. In either instance, loading and inadequate drainage will progressively impose a greater proportion of the load onto the pore fluids and lower the effective stress (Eq. 2.1). Crucial to the process of sediment mobilization, the reduction in effective stress leads to a reduction in inter-grain contact (frictional strength) and inhibits diagenetic processes such as cementation and pressure solution, both of which act to lithify and strengthen the sediment. In cases where the entire load is borne by the pore fluids (effective stress = zero) the sediment loses all its strength and, assuming the grain cohesion is negligible, the sediment behaves like a fluid. This is a mechanical state known as “liquefaction”. “Fluidization” is a similar mechanical state to liquefaction but arises when the sediment loses its strength through moving interstitial fluids buoying the particles. In addition to reducing the sediment strength fluidization can drive deformation through the upward transport of particles (Owen 2003). Both liquefaction and fluidization are forms of liquidization and are both important mechanical states which facilitate subsurface sediment mobilization (Maltman 1994). Other forms of liquidization including thixotropy and quick clay failure relate to collapse of the packing arrangement of sediment grains and are not discussed in detail here (Torrance 1983).

Since any tendency towards liquidization leads to a reduction in sediment strength complete liquidization is not required for sediment to become mobilized. Under conditions of moderate overpressure or when a large proportion of cohesive clay minerals are present the sediment will retain a degree of strength and behave plastically rather than as a fluid (Collinson 1994). Sediments in this mechanical state can be termed “hydroplastic” (Maltman and Bolton 2003). Similarly, a mechanical state important to subsurface sediment mobilization that occurs before the onset of liquidization is deformation at the sediment’s critical state. This is a state where the sediment can undergo very large amounts of shear even at low deforming stress due to a particular combination of porosity, fluid-pressure and stress (Maltman and Bolton 2003). The sediment behaves in a weak, ductile manner rather than as a fluid. In any one instance of subsurface sediment mobilization liquefaction, fluidization, hydroplastic and critical state deformation are likely to work together (Barber et al. 1986; Maltman and Bolton 2003).

2.2.2 Driving forces for bulk movement

Although the mechanical states described above make sediment capable of mobilization, in themselves they are not sufficient to bring about bulk movement. A driving force is required. Principally this force originates from the mobilized sediment's tendency to move along fluid pressure or density gradients.

Firstly, liquidized sediments, by definition, behave as fluids and as such will be subject to fluid pressure gradients. For example, the fluid potential within an overpressured sediment layer is no longer balanced by the elevation head meaning that the fluid will attempt to move to lower values of the fluid pressure gradient (i.e. move from high pressure areas to lower pressure areas, Brown 1994). The sediment will undergo bulk movement if the pressure gradient is high enough to trigger movement. Movement will continue as long as the pressure gradient is maintained and the sediment remains in a mechanical state capable of mobilization. In most sedimentary basins pressure decreases upwards as it is usually the lithostatic load that imparts the majority of the loading force on the sediment. This means that most liquidized sediments will have a tendency to move upwards. Locally however, the fluid potential gradient can decrease in any direction making it possible for mobilized sediment to move in any direction, even downwards.

A second driving force for mobilized sediment (both liquidized and hydroplastic) is created by the fact that overpressured sediments are often less dense and less viscous than normally pressured sediments overlying them. This sets up a reversed density gradient which can be highly unstable (Anketell et al. 1970). In an attempt to restore a downwards-increasing density gradient low density sediments will have a tendency to rise due to buoyancy whereas the higher density overburden will have a tendency to sink. This effect may be enhanced by the action of expanding gas within the pore spaces of the mobilized sediment (Brown 1990). Movement of sediment across the boundary between the two layers can be triggered by tectonic shocks or minor irregularities in the relief of their interface which trigger Rayleigh-Taylor instability (Anketell et al. 1970). Complex structures can evolve as part of a spectrum that is controlled by the kinematic viscosities of the sediments involved. If given sufficient time, the two layers may become totally repositioned in the section and the normal downward-increasing density gradient can be restored.

2.2.3 Sedimentary intrusion

It is clear from the above discussion that for various reasons liquidized or hydroplastic sediments can be driven to undergo bulk movement away from their present location in the subsurface. Unless the bulk movement is restricted to areas within the mobilized sediment unit, some form of rupturing of the unit's boundaries is required for bulk movement to occur. When the boundaries of the unit are ruptured the relevant fluid or density potential gradients drive the mobilized sediment into the rupture forming a sedimentary intrusion. Assuming that the sediment surrounding the liquidized unit has a mechanical strength sufficient to allow brittle failure, we can consider two principal rupturing mechanisms that commonly occur in sedimentary basins. These are hydrofracturing and tectonic fracturing.

A hydrofracture will form if the pressure in the sediment pore fluid (P_f) is high enough to exceed the minimum principal stress (σ_{min}) plus the tensile strength of the overburden (T ; Eq. 2.2).

$$P_f > \sigma_{min} + T \quad \text{(Equation 2.2)}$$

Hydrofracture orientation will be principally determined by the direction of the minimum compressive stress (Boehm and Moore 2002; Jolly and Lonergan 2002). An additional factor is anisotropy in the host sediment (such as bedding) that influences the magnitude of the tensile strength in different directions (Jolly and Lonergan 2002). For example in a horizontally layered sedimentary sequence the vertical tensile strength (T_v) is likely to be less than the horizontal tensile strength (T_h). These differences can be particularly important in situations where differences in the three principal stresses are small (Boehm and Moore 2002). In tectonically relaxed sedimentary basins the minimum compressive stress direction is typically horizontal because the main source of compressive stress is the lithostatic load (Cosgrove 2001). Therefore, the conditions in most sedimentary basins favour the development of sub-vertical hydrofractures and the development of sedimentary dykes (Eq. 2.3).

$$P_f > \sigma_h + T_h \quad \text{(Equation 2.3)}$$

In cases where the minimum compressive stress direction is vertical (e.g. in shallow sections of a basin undergoing tectonic compression) the conditions favour the formation of horizontal hydrofractures leading to the development of sedimentary sills (Eq. 2.4; Jolly and Lonergan 2002).

$$P_f > \sigma_v + T_v \quad (\text{Equation 2.4})$$

Further modifications to these simple mechanical principles can occur when considering the changes in the differential stress ($\sigma_v - \sigma_h$). For example, Cosgrove (2001) suggests that when the differential stress is less than four times the tensile strength of the overburden ($4T$) extensional fractures form that open against the direction of minimum compressive stress. Where the differential stress exceeds $4T$, typically in the deeper parts of a sedimentary basin, shear fractures form that dip at around 60° .

Other fractures can provide important pathways for the expulsion of fluids from overpressured units and can strongly influence the orientation of sedimentary intrusions (e.g. Hurst et al. 2003b). For example when there are faults within the host sediment that each have little or no tensile strength, the pore fluid pressure needs only to exceed the resolved normal stress (σ_n) across the fracture for it to become dilated (Eq. 2.5; Jolly and Lonergan, 2002).

$$P_f > \sigma_n \quad (\text{Equation 2.5})$$

As the fluid pressure increases a wider range of fracture orientations can become dilated and intruded (Delaney et al. 1986).

2.2.4 Subsurface sediment mobilization structures

Evidence for subsurface sediment mobilization principally takes the form of structures formed when mobilized sediment deforms or breaches internal layering within the mobilized unit or the interface between itself and the surrounding sediment. The wide range of variables controlling the form of mobilization structures, some of which are discussed above, means that the spectrum of structures is very broad.

A useful method of subdividing sediment mobilization structures is the depth at which they occur (Fig. 2.2, Van Rensbergen et al. 2003). Shallow mobilization structures are those that generally form above depths of approximately 500-1000 m beneath the surface; deep structures occur below this depth (Fig. 2.2a). A depth of 1000 m marks the onset of significant sand lithification, the lower limit of shallow fluid generation processes and the common transition depth to regional-scale overpressure (Van Rensbergen et al. 2003). As such, shallow and deep mobilization processes and structures can vary considerably. The boundaries between these processes though are unclear and it is not uncommon to see structures typical of shallow sediment mobilization occurring in deep sections of sedimentary basins and vice-versa. As large mud volcano systems can vertically span many kilometres from their deep root zones to the surface, both deep and shallow sediment mobilization structures are worthy of further discussion here.

In the shallow subsurface the mechanical strength of sediment is generally low owing to the high porosity of unconsolidated sediment, low sediment cohesion and inter-granular contact. This section of sedimentary basins is the zone of maximum compactional strain where the rate of porosity change is greatest (Bjorlykke 1993; Karig and Morgan 1994). Compaction and fluid expulsion are likely to be dominant aspects of the phase of early burial of sediments (Cartwright and Huuse 2005). Under these conditions liquefaction, fluidization and plastic flow are common (Fig. 2.2a). At very shallow depths (10's of metres or less below the surface) pressure- and density-potential gradients can easily be established if drainage of sediment in its early stages of burial is not sufficient (Fig. 2.1a). These gradients provide the driving forces for bulk movement and account for numerous centimetre- to metre-scale mobilization structures. Examples include fluidization pipes, dish-and-pillar, and sheet dewatering structures, which are all formed by the rapid expulsion of fluids (Collinson 1994). Density contrasts or the action of shear stress leads to the development of load casts, flame structures and load balls (Fig. 2.2b, Anketell et al. 1970; Collinson 1994; Owen 2003). Larger (i.e. seismic-scale) structures formed by sediment mobilization in the shallow subsurface are rare but have been observed in seismic reflection profiles. For example, Davies (2003) described a series of giant fluidization structures from the Niger Delta interpreted to be due to differential loading and seal failure during the early stages of burial.

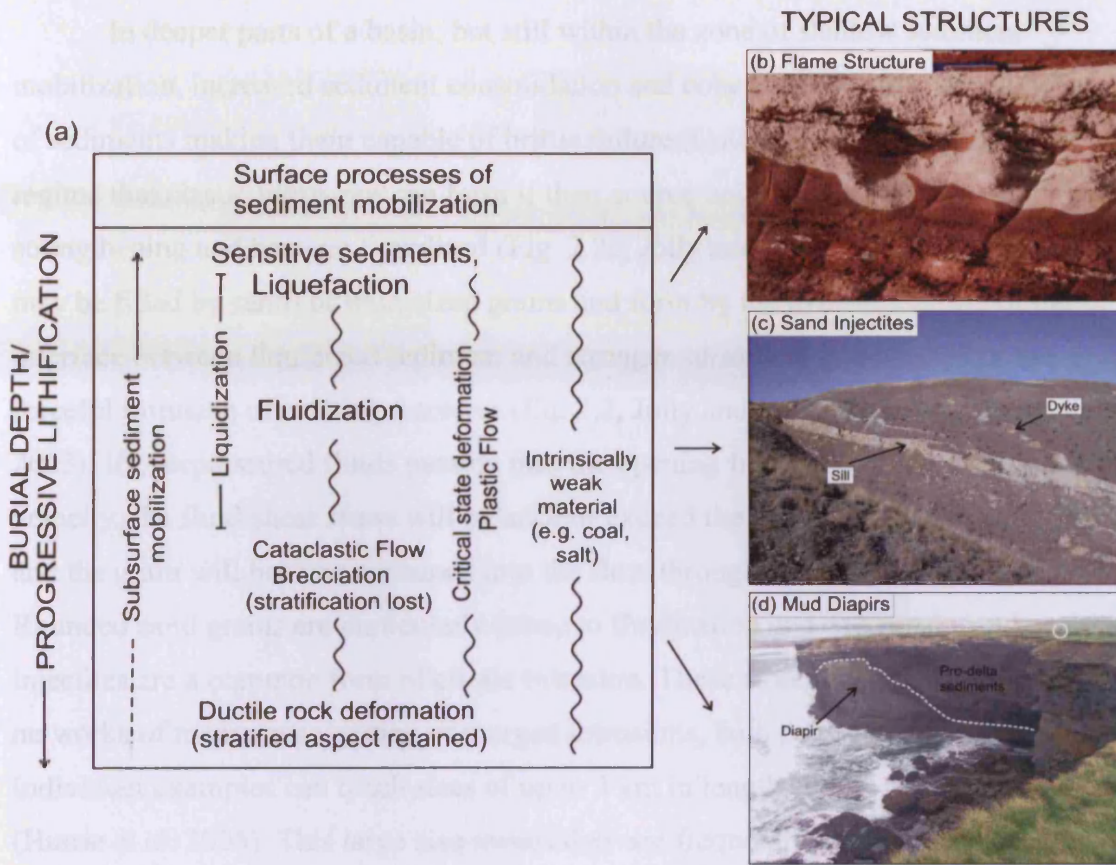


Figure 2.2 Subsurface sediment mobilization and its typical structures: (a) Conceptual view of the range of processes involved in sediment mobilization occurring at different depths beneath the surface. Modified from Maltman and Bolton (2003). (b) Flame structure preserved in sandstones from the Northumberland coast, UK (photo courtesy of S. Bull). Pen for scale. (c) Lower Palaeocene-age sandstone injectites of the Panoche sandstone intrusion complex intruding mud rocks of the Moreno shale, California, USA. Sand sill is approximately 3 m thick. (photo courtesy of W. Vittel). (d) Mud diapir within Carboniferous-age Diamond Rocks south of Kilkee western Ireland. This diapir formed by gravitational slumping of undercompacted muds in the distal portion of a large delta. Person circled for scale. (photograph courtesy of S. Bull).

In deeper parts of a basin, but still within the zone of shallow sediment mobilization, increased sediment consolidation and cohesion leads to a strengthening of sediments making them capable of brittle failure (Collinson 1994). It is in this regime that clastic intrusions can form if their source units have resisted this strengthening and become liquidized (Fig. 2.2c; Jolly and Lonergan 2002). Intrusions may be filled by sand- or mud-sized grains and form by the hydrofracturing of the interface between liquidized sediment and stronger surrounding sediments or the forceful intrusion of existing fractures (Eq. 2.2, Jolly and Lonergan 2002; Hurst et al. 2003). If overpressured fluids passing into the opening fracture do so at a sufficient velocity, the fluid shear stress will balance or exceed the weight of a sediment grain and the grain will become entrained into the flow through fluidization (Leeder 1999). Rounded sand grains are particularly prone to fluidization and as a result sand injectites are a common form of clastic intrusion. These structures can develop large networks of many cross-cutting or merged intrusions, both dykes and sills (Fig. 2.2c). Individual examples can reach sizes of up to 3 km in length and 20 m thickness (Huuse et al. 2005). This large size means they are frequently observed on seismic reflection profiles, typically as v- or w-shaped amplitude anomalies in cross-section (Fig. 2.3a-d, Hurst et al. 2003a). Intrusion orientation is controlled by the orientation of the principal stresses and the tensile strength of the surrounding sediments (Eq. 2.3 and 2.4). As such sand injectites can be useful palaeostress indicators when pre-existing fractures are not involved (Boehm and Moore 2002). The intrusion size and fill is controlled by volume and type of sediment within the source body and the duration of sufficient pressure drive. Although generally considered as shallow sediment mobilization structures (<800 m depth) sand injectites can form at any depth provided there is a source of uncemented sand that can be fluidized (Jolly and Lonergan 2002).

Mud is also capable of filling fractures to form clastic intrusions through mobilization in the shallow subsurface. For example, Morley (2003b) has described a network of mud filled dykes, sills and a laccolith-like unit from the Jerudong anticline in Brunei, which show gross similarities to sand injectites and igneous intrusions (Pickering et al. 1988). Consolidated clay particles however, have a greater degree of cohesion than sand grains and are not as readily fluidized (Brown 1990). A combination of liquidization, plastic flow and critical state deformation may therefore be important in the formation of shallow mud injectites (Brown and Orange 1993).

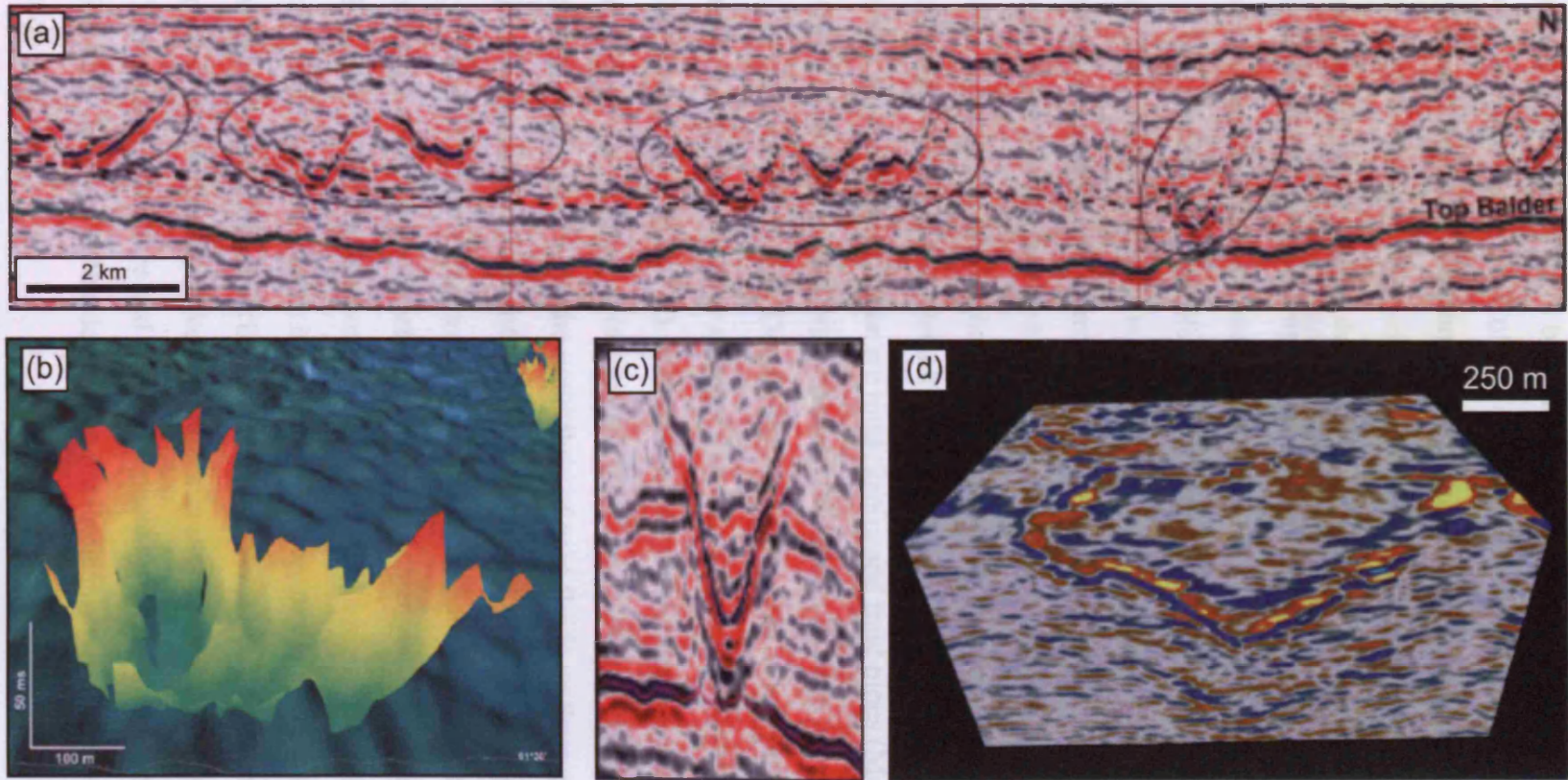


Figure 2.3 Sand intrusions. (a)-(d) Selected Seismic sections and 3D visualizations of sand injectites showing their characteristic (v-shaped) architecture. Modified from Huuse and Mickelson (2004).

With increasing depth in sedimentary basins (>1000 m) sediment pore water is progressively expelled, sediment becomes more consolidated and lithified and its mechanical strength increases (Collinson 1994). The conditions required for liquefaction and fluidization become more difficult to preserve and their occurrence is more uncommon. Whilst under certain conditions (e.g. very rapid burial) these processes can still occur at great depths, it is plastic flow and critical state deformation that become more important as sediment mobilization mechanisms in the deeper sections of sedimentary basins (Fig. 2.2a).

A well-documented manifestation of deep subsurface sediment mobilization that is of relevance to this thesis is the bulk movement of mobilized mud (a phenomenon sometimes termed mud or shale tectonics). This process occurs when large thicknesses of overpressured fine-grained sediment become mobilized as a result of uneven or density loading or the fluidization and entrainment of particles (Van Rensbergen and Morley 2003). Broadly speaking two types of mud mobilization structure can be recognized. These are mud diapirs and mud pipes (Morley 2003a). Brown (1990) referring to mud pipes as diatremes, distinguishes between the two on the basis of their genetic origin. Diapirs form when a more or less intact mass of plastic mud is driven upwards by its internal overpressure and buoyancy (Brown 1990; Hovland 1990; Kopf 2002). Essentially the mud deforms as a plastic layer behaving rather like viscous salt or magma (Clemens 1998; Jackson et al. 1994). Mud pipes are formed in response to the rapid flow of pore fluids up through a sedimentary mass which becomes fluidized and entrained into the flow (Brown 1990; Morley 2003a). In terms of morphology a mud diapir is distinguished from a mud pipe by its wider and more bulbous cross sectional shape and larger plan view diameter of a few tens to hundreds of metres (Brown and Orange 1993). In many cases these differences can be difficult to observe due to incomplete exposure or the poor quality of seismic data that images mud intrusions (Brown 1990; Morley 2003a). Both mud diapirs and mud pipes have been directly linked to the occurrence of mud volcanism (Milkov 2000). Their general structure and causative mechanisms are thus worthy of further discussion here. Their specific relevance to mud volcanism is discussed further in sub-section 2.3.2.

Mud diapirs have been described at outcrop (Barber et al. 1986; Brown and Orange 1993; Clari et al. 2004) and from seismic data worldwide including areas of the Niger Delta, the North Sea and the Alboran Sea (Fig. 2.4, Hovland 1990; Morley

2003a; Morley and Guerin 1996; Talukder et al. 2003). Within a mud diapir sediments can undergo deformation in a variety of mechanical states (Maltman and Bolton 2003). Plastic flow and critical state deformation are most pervasive and generally a diapir is seen as evidence for the bulk movement of a semi-intact plastic unit of sediment with some degree of mechanical strength rather than as a completely liquidized mass. Where suspected mud diapirs are exposed at the surface evidence for this type of deformation is often observed as shear fabrics and marginal “scaly clays” formed by deformation at the sediment’s critical state (Brown 1990; Brown and Orange 1993; Clari et al. 2004; Maltman and Bolton 2003). However, Maltman and Bolton (2003) have suggested that with decreasing burial depth (i.e. during diapir ascent) liquidization becomes more pervasive as the confining stress reduces (see also Talukder et al. 2003). Furthermore, Brown (1990) has suggested that methane exsolution at depths of 2 km or less can locally induce liquidization within parts of a diapir and lead to the formation of mud pipes rooted in the upper parts of diapirs. Therefore, although principally a result of ductile sediment deformation the internal areas of diapirs can show evidence for a range of deformation styles (Brown and Orange 1993).

Suspected mud diapirs are often observed in deltaic settings (Figs 2.2d and 2.4). Rapid loading of fluid-rich pro-delta muds by prograding delta front sediments makes these favourable settings for the build up of significant overpressure within mud layers (Harrison and Summa 1991; McClay et al. 2003; Morley 2003a; Morley and Guerin 1996). Large parabolic disturbances in seismic data are often interpreted as the mud diapirs due to their columnar shape and lack of internal reflectivity (Fig. 2.5). The deformation and thickness distribution of surrounding sediments is then analysed to interpret the various phases of diapir growth (Fig. 2.5). Reactive diapirism involves the flowage of mobile shale into a higher region without piercement of the overburden. In deltaic settings this can lead to the development of “shale bulges” bounded on their oceanward and landward flanks respectively by regional and counter-regional growth faults (Fig. 2.4b). Thickening of surrounding sediments towards the diapir is therefore seen as evidence for a phase of reactive diapir growth (Fig. 2.5). Active mud diapirism occurs when a diapir pierces and rises through the overburden due to pressure drive and/or buoyancy forces (Fig. 2.4c). Thinning of sediment onto the crest of the diapir is characteristic of this phase as is the presence of

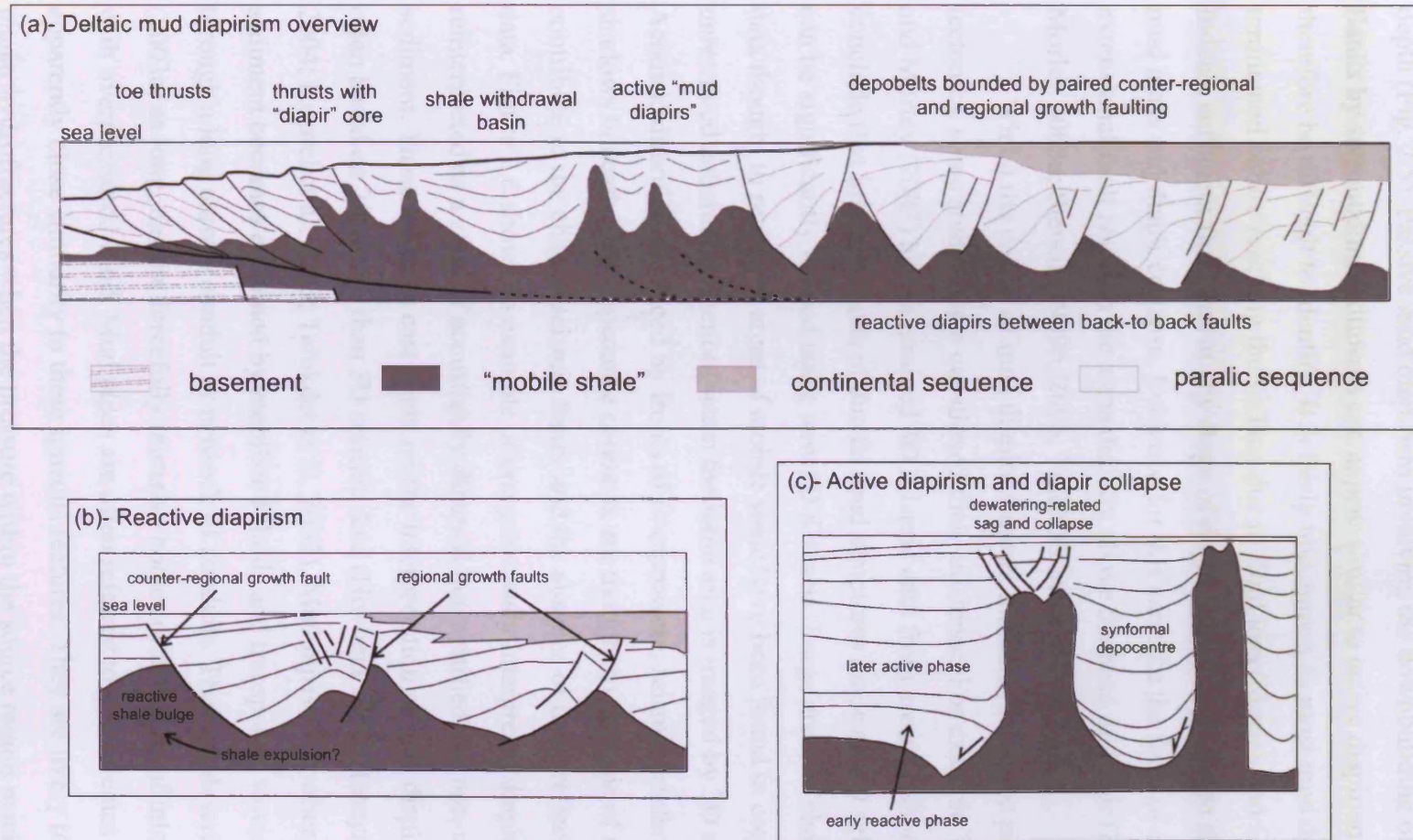


Figure 2.4 Structural styles of mud mobility and mud diapirism: (a) Overview cross section illustrating the key structural elements related to mud mobility and mud diapirism in a deltaic setting based on a section through the Niger delta by Doust and Omatsola (1990) and Morley and Guerin (1996). (b) The structural characteristics of reactive mud diapirism. Reactive shale bulges can be bounded by regional and counter-regional growth faults. (c) The characteristics of active mud diapirism. Piercing diapirs intrude vertically through the overburden following an early phase of reactive diapirism. Synformal depocentres form in areas of mud withdrawal. Dewatering of the diapir during ascent can lead to shrinkage and the formation of collapse faults at the diapir crest. All parts modified from Van Rensbergen and Morley (2003).

laterally adjacent synformal basins that form as a result of mud withdrawal from depth (Fig. 2.5). Passive mud diapirism involving the downbuilding of the diapir flanks by surrounding sediments can appear similar to active diapirism and can therefore be difficult to identify. It is fairly uncommon as most mud diapirs are terminated before reaching the surface due to fluid loss (Morley and Guerin 1996). Indeed, sufficient fluid loss at any stage of diapir growth can lead to shrinkage of the mud mass and diapir collapse. Evidence for this can take the form of circular or radial extensional fault zones in the areas directly above the head of diapir (Fig. 2.4c, Morley 2003a; Stewart 1999b, 2006; Talukder et al. 2003).

Whilst the notion of mud diapirs appears fundamental to the processes of mud tectonics, some studies have questioned their existence. For example Van Rensbergen and Morley (2003) have examined 3D seismic data from areas offshore Brunei and conclude that interpretations of ductile mud structures made on 2D seismic images can be significantly revised using new 3D datasets. Large areas of chaotic 2D seismic data thought to represent areas of mobile shale have been found to contain previously unresolved coherent reflections when the same area is imaged by 3D seismic data. Acoustic dimming produced by fronts of overpressure, seismic artefacts or acoustic shadows beneath high impedance contrasts are thought to be some of the factors that contribute to the chaotic seismic facies and the absence of these reflections in the 2D data. Figure 2.6 shows an example of one previously interpreted diapir that is now reinterpreted as a zone of acoustically dimmed but stratified and non-mobilized sediment. These findings cast doubt on the interpretation of mud diapirs, which are often based on 2D rather than 3D seismic data (Hovland 1990; Huseynov and Guliyev 2004; Krastel et al. 2003; Talukder et al. 2003). Mud pipes form when liquidized sediment becomes entrained by mobilized fluids and transported towards the surface through a long narrow conduit or network of conduits. They are described by Morley (2003a) as long, narrow forcefully intrusive bodies or networks of intrusions filled with overpressured fluid. Mud pipes are often referred to as diatremes due to their apparently close similarity to these igneous features. They are likely to initiate as planar hydrofractures when the pressure within the source region reaches a sufficient level to breach the overburden (see sub-section 2.2.3; Eq. 2.2). This sets up somewhat of a paradox when considering the cylindrical rather than planar architecture of mud pipes.

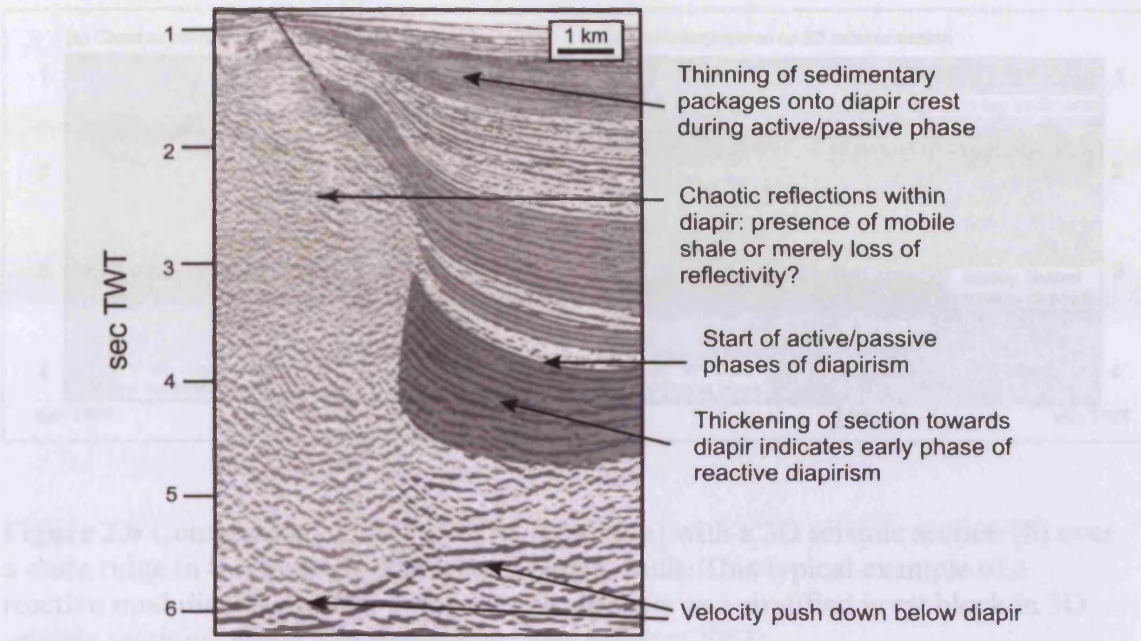


Figure 2.5 Seismic line showing the architecture of an interpreted mud diapir and adjacent sediment. The thickness characteristics of the adjacent sediments are used to infer the various stages of diapir growth (reactive, active, passive). The existence of true bulbous mud diapirs such as this example can be questioned. See text for more discussion. From Morley (2003a).

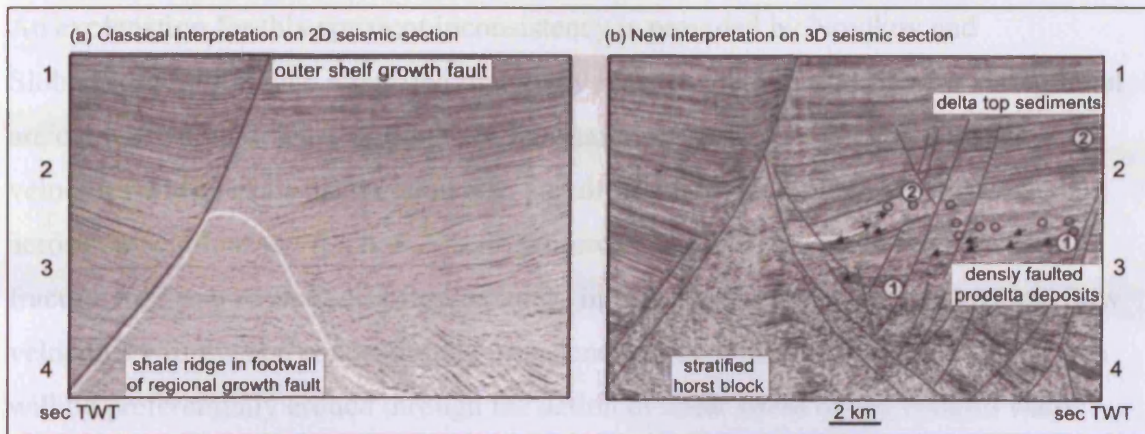


Figure 2.6 Comparison of a 2D seismic section (a) with a 3D seismic section (b) over a shale ridge in the footwall of a deltaic growth fault. This typical example of a reactive mud diapir (e.g. Fig. 2.4b) actually appears as a stratified horst block in 3D seismic sections. From Van Rensbergen and Morley (2003).

and the impact of sand particles (Macdonald et al., 1994). The driving force of pipe formation and the fluidization of the particulate fill is predominantly the fluid pressure within the source, and any tectonic forces resulting from the passage of growth faults from the margin. Fluids (Brown, 1990; Macdonald et al., 2003). If the velocity of fluid movement and fluid drag forces is high enough to overcome the weight of the grain plus any grain-grain cohesive forces, the grain will be entrained in the flow and fluidized. The minimum fluid velocity required to fluidize a grain is dependent on the grain size and shape (Lowe, 1975). Unconsolidated clay particles require the lowest fluid velocities to become fluidized (0.07 cm/s). Coarse sand and gravel require fluidization velocities much higher than fluid velocities (approximately 10 cm/s). In a consolidated soil, the cohesive bonds between clay particles increase the minimum fluid velocity required for fluidization (approximately 3 cm/s). It is important to note that during formation of sedimentary intrusions (both pipes and diapirs) fluid velocities can greatly exceed these minimum values by being forced by the presence of melt-seals blocks embedded within ancient intrusive structures with sand and mud filled (House et al., 2005; Pickering et al., 1988). Indeed it is likely that fluid velocities in some sediment pipes are great enough to significantly erode the host rock in a similar manner postulated for igneous conduit systems (House et al., 2005; Macdonald et al., 1994; Pickering et al., 1988).

An explanation for this apparent inconsistency is provided by Novikov and Slobodskoy (1985) who identified that many igneous diatremes are planar at depth but are cylindrical, or at least elliptical, in the shallower section. It is argued that flow velocities within a slit-like conduit (i.e. a hydrofracture) are not evenly distributed across the width of the fracture. Frictional forces near the peripheral sectors of the fracture lead to a reduction of flow velocity in these areas (Fig. 2.7). The greatest flow velocities will thus be concentrated in the centre of the conduit meaning that this area will be preferentially eroded through the action of shear stress on the conduit walls and the impact of solid particles (Macedonio et al. 1994). The central part of the conduit will therefore become enlarged whereas the narrower peripheral areas will become sealed. The original planar conduit is converted to a cylindrical one (Fig. 2.7)

Unlike diapirs the sediment within a mud pipe at the time of its activity is thought to have little or no mechanical strength (effective stress = zero) and behaves effectively as a fluid (i.e. liquidized). The driving force of pipe formation and the fluidization of the particulate fill is predominantly the fluid pressure within the source unit and any frictional forces resulting from the passage of gas exsolved from the mobilized fluids (Brown 1990; Mazzini et al. 2003). If the velocity of fluid movement and fluid drag forces is high enough to overcome the weight of the grain, plus any grain-grain cohesive forces, the grain will be entrained into the flow and fluidized. The minimum fluid velocity required to fluidize a particle depends on the grain type and size (Lowe 1975). Unconsolidated clay particles require the lowest fluid velocities to become fluidized (0.07 cm/s). Coarse sand and gravel grain fluidization requires much higher fluid velocities (approximately 10 cm/s or higher). When consolidated, the cohesive bonds between clay particles increase the minimum fluid velocity required for fluidization (approximately 5 cm/s). It is likely however that during formation of sedimentary intrusions (both pipes and tabular intrusions) fluid velocities can greatly exceed these minimum values evidenced by the presence of metre-scale blocks embedded within ancient intrusive structures, both sand and mud filled (Huuse et al. 2005; Pickering et al. 1988). Indeed it is likely that fluid velocities in some sediment pipes are great enough to significantly erode the wall rock in a similar manner postulated for igneous conduit systems (Huuse et al. 2005; Macedonio et al. 1994; Pickering et al. 1988).

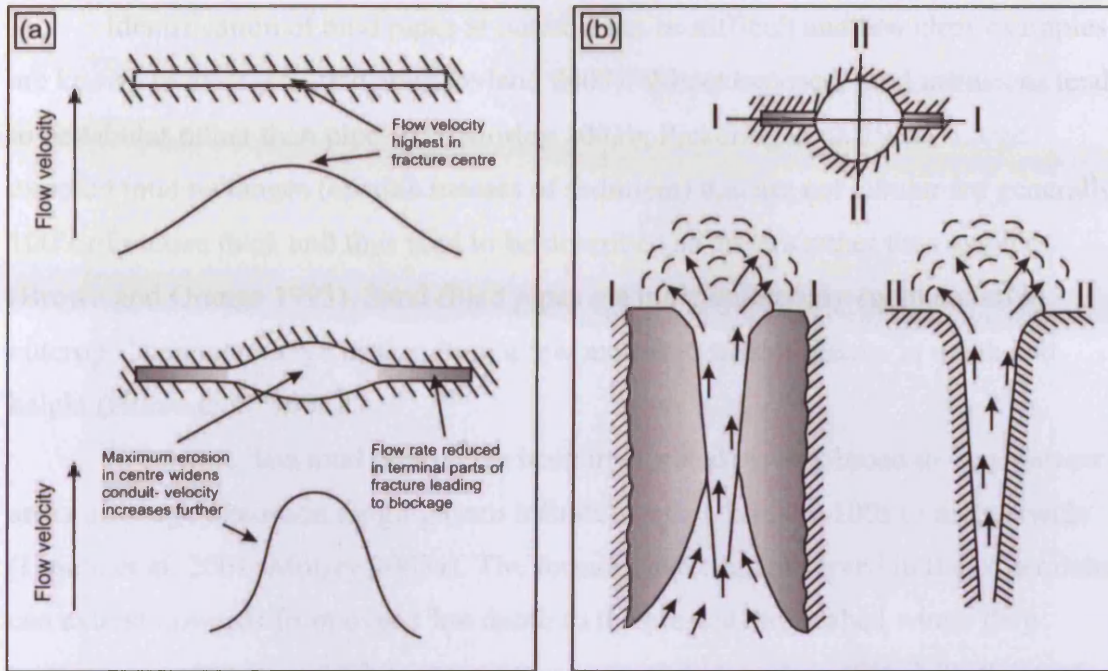


Figure 2.7 Conversion of a slit-like to a pipe like conduit due to uneven flow velocity distribution within the conduit: (a) Flow velocity profiles for a slit-like conduit (top) showing the focus of highest velocities in the centre of the slit. This results in the modification of the slit through erosion at its centre and its gradual conversion to a cylindrical pipe (bottom). A feedback loop is created as the central widening leads to an increase in flow velocity and more wall erosion. (b) Cross sections (I and II) through a schematic diatreme (fluid expulsion pipe) showing its slit-like architecture at depth and its pipe-like architecture in the shallower section. This self-organized conduit modification process is one way the hydrofractures at depth may evolve into more pipe-like conduits that are commonly observed in nature. Modified from Novikov and Slobodskoy (1985).

Identification of mud pipes at outcrop can be difficult and few clear examples are known to exist (cf. Judd and Hovland 2007). Where exposed, mud intrusions tend to be tabular rather than pipe-like (Morley 2003b; Pickering et al. 1988). Large exposed mud mélanges (chaotic masses of sediment) that are not tabular are generally 100's of metres thick and thus tend to be described as diapirs rather than as pipes (Brown and Orange 1993). Sand filled pipes are more commonly encountered at outcrop. These can range in size from a few metres to tens of metres in width and height (Huuse et al. 2005).

In seismic data mud pipes have been interpreted as very broad to very narrow areas of image distortion ranging from infinitely small to many 100s of metres wide (Løseth et al. 2001; Morley 2003a). The former have been observed in the Niger delta can extend upwards from over 1 km depth to the present day seabed where they terminate as craters measuring up to 300 m wide and 60 m deep (Fig. 2.8). Pipes of this nature are believed to be formed by the blow out of high pressured gas from a hydrocarbon reservoir at depth and may not extrude large volumes of sediment at the surface. Wider diameter zones of seismic image distortion have also been interpreted as mud pipes (Morley 2003a). This is principally due to the absence of surrounding syn-kinematic basins or deformation of laterally adjacent units (Fig. 2.9). The increased width is thought to be the result of the presence of numerous, possibly interconnected, mud pipes that collectively act to disrupt layering and lower the signal/noise ratio of the seismic data over a broader area. Networks of mud pipes can therefore look very much like diapirs in seismic data (Fig. 2.9). This raises the possibility that mud pipe networks may have been misinterpreted in the past as diapirs and casts further doubt on the true existence of mud diapirs.

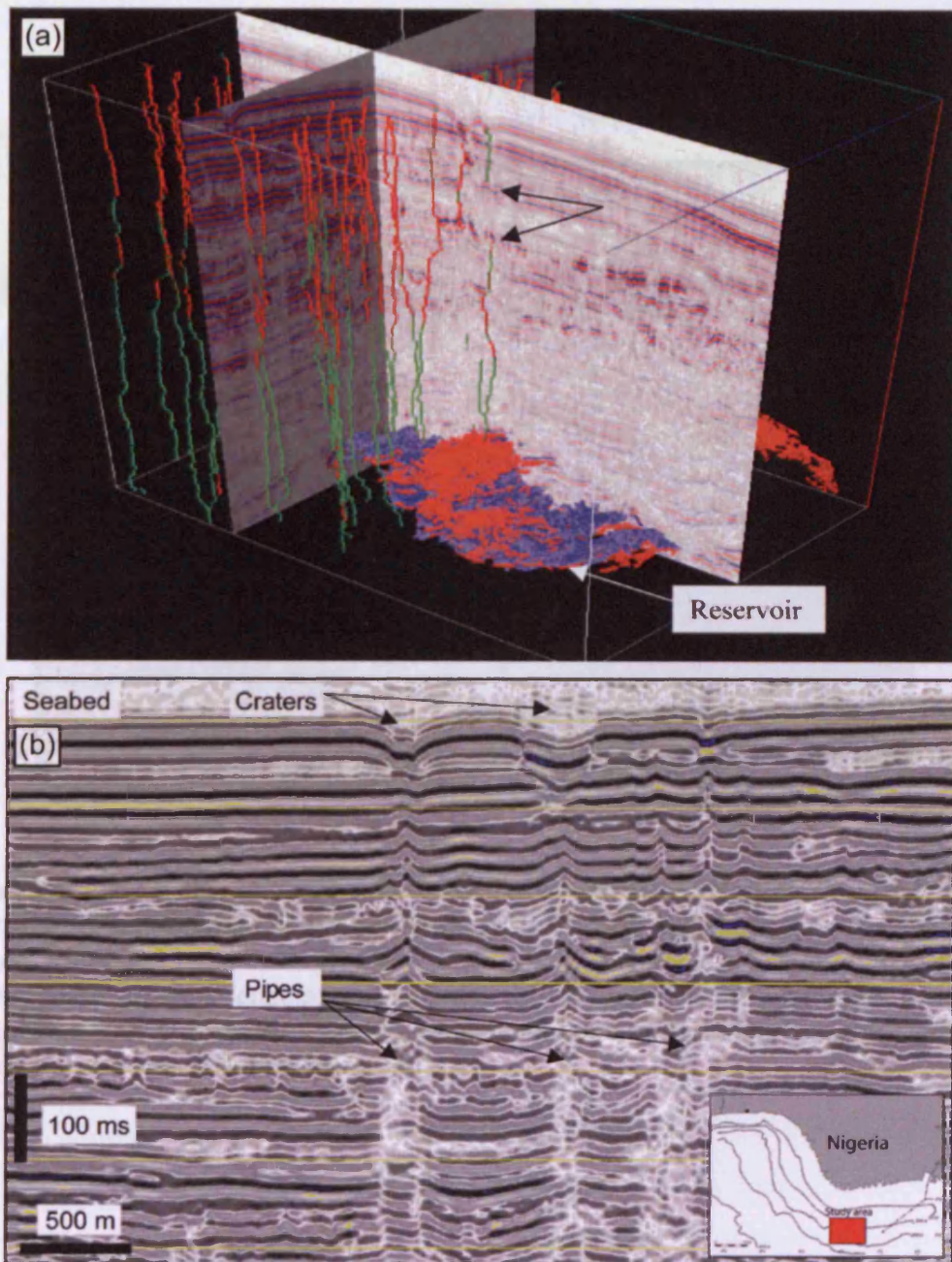


Figure 2.8 Narrow gas escape pipes from the Niger delta: (a) 3D visualization of narrow vertical gas escape pipes connecting a gas reservoir at depth to the seabed. Pipe height can exceed 1000 m. (b) Seismic section showing seabed gas escape craters underlain by narrow vertical disturbances in the seismic data (pipes). From Løseth et al. (2001).

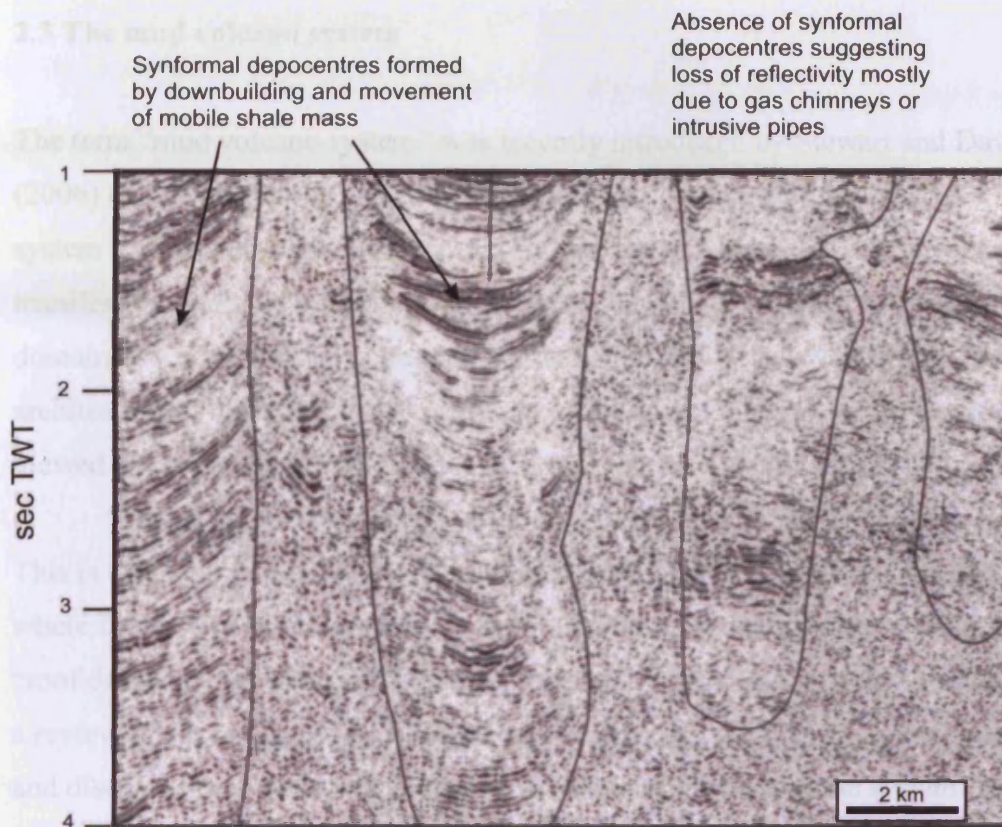


Figure 2.9 The seismic expression of mud diapirs and pipes: Vertical “fingers” of chaotic seismic data interpreted to represent mud diapirs and mud pipes. Reflections adjacent to the left hand example form synformal depocentres adjacent to the chaotic data suggesting the presence of a diapir. The reflections adjacent to the right hand example are not synformal suggesting this chaotic area of data may represent a mud pipe or gas chimney. From Morley (2003a).

The source domain comprises the focused structural domain of the gas charge system. It can be regarded as including: 1) the system's parent bed(s) that supply a large fraction of the charge; 2) other zones beneath the parent bed(s) that have contributed little to the system (Fig. 2.10). As such the source domain in total is perpendicular to axial directions. The upper boundary of the source domain is defined by the first unconformable unit that has been eroded and invaded by allochthonous fluids and structures. In many cases this boundary is likely to be represented by the lithological contrast between the parent bed and an overlying sequence that has not been subjected to any subsurface modification. Determining the depth and location of the parent bed is a fairly straightforward task given distances. Sedimentological and palaeontological characteristics of “marker particles” collected at the surface can be compared to levels of the known regional stratigraphy (Devilla et al. 2001; Devilla et al. 2002; Kopf 2003). Geochemical analysis of expelled pore

2.3 The mud volcano system

The term “mud volcano system” was recently introduced by Stewart and Davies (2006) to describe an integrated system including the volcanic edifice and a feeder system that connects the edifice to the source region. Under this scheme a single manifestation of mud volcanism can be subdivided into a number of “structural domains”, within which a characteristic set of processes occur that control the architecture of that part of the system. At a basic level the mud volcano system can be viewed as consisting of three principal structural domains (Fig. 2.10).

Deepest within the section at the root of the system is the “source domain”. This is overlain by the “intrusive domain” and finally the “extrusive domain”. In cases where the system becomes buried a fourth structural domain can be considered the “roof domain” overlying the extrusive domain. The remainder of this section provides a review of the processes and mechanisms occurring within each structural domain and discusses how these influence the resultant architecture of the system. We begin with the lowermost source domain and work upwards. The discussion is illustrated with reference to Figure 2.10 which shows some of the seismic and outcrop characteristics of typical mud volcano systems.

2.3.1 The source domain

The source domain comprises the deepest structural domain of the mud volcano system. It can be regarded as including; 1) The system’s parent bed(s) that supply a large fraction of the extruded sediment to the surface and; 2) Other zones beneath the parent bed(s) that have contributed fluids to the system (Fig. 2.10). As such the source domain in total is potentially of great thickness. The upper boundary of the source domain is defined by the deepest stratigraphic unit that has been intruded and invaded by allochthonous fluids and sediment. In many cases this boundary is likely to be represented by the lithological contact between the parent bed and an overlying sequence that has not been subjected to any subsurface mobilization. Determining the depth and location of the parent bed is a fairly straightforward task in most instances. Sedimentological and palaeontological characteristics of “marker particles” collected at the surface can be compared to details of the known regional stratigraphy (Delisle et al. 2001; Deville et al. 2003; Kopf 2002). Geochemical analysis of expelled pore

2 - 24

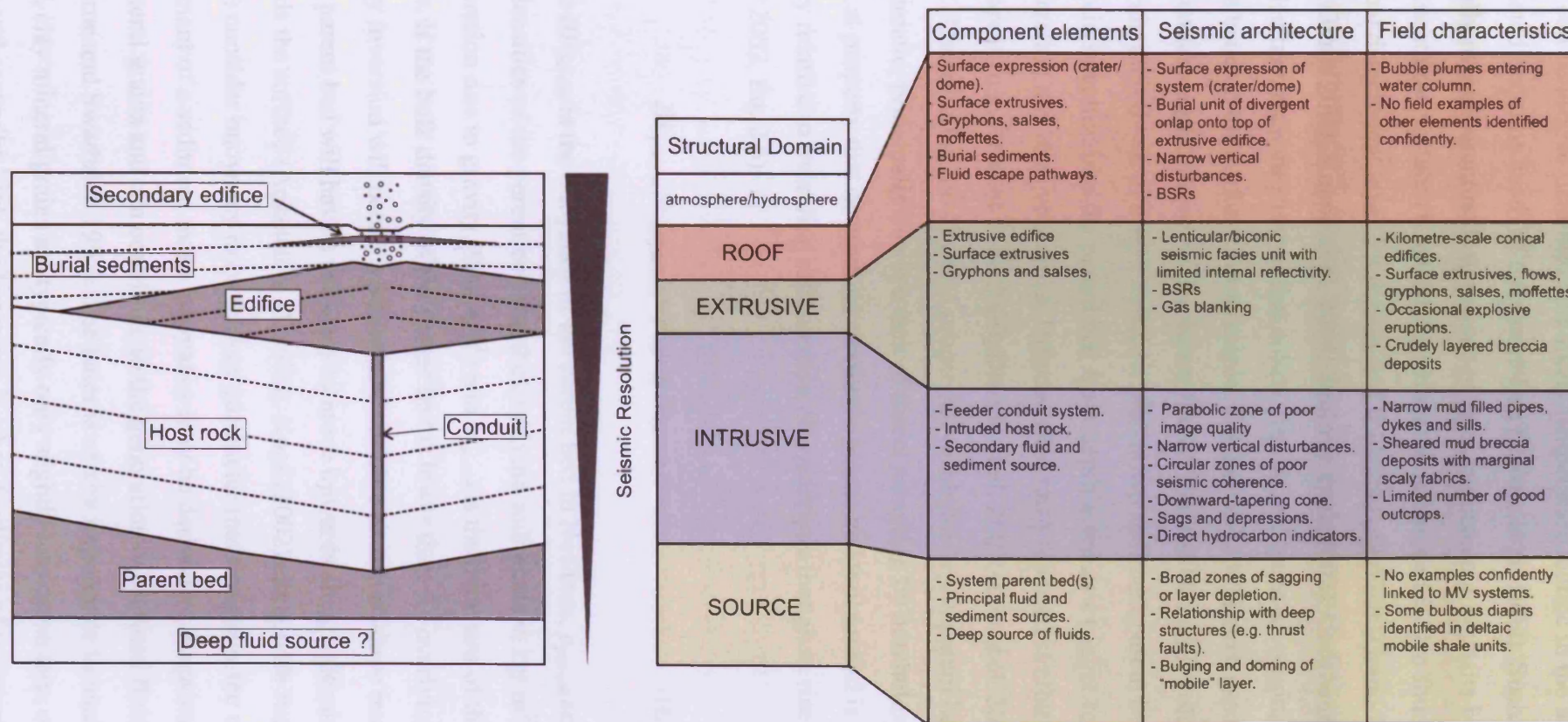


Figure 2.10 Summary diagram outlining the basic subsurface configuration and structural domains of a large mud volcano system. The component elements, their field and seismic architecture are listed in the adjoining table.

fluids can be used to determine the likely temperature regime in the area the fluids originated and thus depth of the parent bed (Martin et al. 1996). Such analyses typically reveal parent beds to consist of thick argillaceous deposits buried up to 12 km beneath the surface (Kopf 2002). Often the parent bed is also found to act as a regional detachment layer for thrusts and folds that overlie it (Grando and McClay 2007; Graue 2000; Knapp et al. 2004; Schluter et al. 2002). Geochemical analysis of expelled materials may reveal that solids, liquids and gases all originate from different depths beneath the surface. For example, Kopf et al. (2003) have used the geochemical signatures of mud volcano fluids from the Caucasus collision zone to constrain their depth of origin as below the known sediment parent bed. They suggest that fluid injection into the parent bed from depth acted as a trigger for parent bed mobilization and mud volcanism. Other studies have reported similar findings from other areas (e.g. Bristow et al. 2000; Deville et al. 2003; You et al. 2004)

Determining the physical properties within an *in situ* parent bed is problematic, principally due to a lack of direct sampling by boreholes. One key physical property that determines whether a parent bed will ascend is its low bulk density relative to overlying sediments, a characteristic that gives rise to buoyancy (Kopf 2002, Eq. 2.6).

$$BF_{parent} = (\rho_{parent} - \rho_{os}) \cdot g \cdot h_{parent} \quad (\text{Equation 2.6})$$

Where BF_{parent} is the buoyancy of the parent bed in Newtons, ρ_{parent} and ρ_{os} are the bulk densities of the parent bed and the overlying sediments in kg/m^3 , g is the acceleration due to gravity ($9.81 \text{ m}/\text{s}^2$) and h_{parent} is the thickness of the parent bed in metres. If the bulk density of the parent bed is lower than the overlying sediments a density inversion will occur, a potentially unstable situation where buoyant sediments in the parent bed will have a tendency to move upwards along a density gradient towards the surface (Anketell et al. 1970). Kopf (2002) along with Judd and Hovland (2007) consider buoyancy to be the key parameter that facilitates the upward movement of a sediment mass. Buoyancy may be derived by the primary low density of mineral grains and can contribute to the generation of elevated fluid pressures (Osborne and Swarbrick 1997). The latter is of key importance to mud volcanism as firstly, clay mineral grains are typically only slightly less dense than other clastic grains and secondly, high fluid pressure is a key facilitator of sediment mobilization

through the reduction of effective stress (Maltman and Bolton 2003, see also sub-section 2.1.1). Rapid burial of low permeability sediments, the volume increase resulting from hydrocarbon generation and diagenetic reactions such as the transformation of illite to smectite have all been suggested as directly influencing the generation of overpressure in mud volcano parent beds (Kopf 2002; Milkov 2000; Osborne and Swarbrick 1997). Indeed the majority of mud volcano provinces are likely to feature areas that have undergone rapid burial, many are petroliferous and a large fraction of the low permeability parent beds are likely to be smectite rich (Loncke et al. 2004; Milkov 2000; Reed et al. 1990). Many are located in zones of tectonic compression which may play an additional role through lateral sediment loading (Aslan et al. 2001; Milkov 2000). Pore fluid type also plays a significant role in lowering the bulk density of a parent bed. Gas in particular is significant since it has a density far lower than other pore fluids such as water or oil (Judd and Hovland 2007). Whether derived from the maturation of organic matter within the parent bed or injected from areas below, gas in the pore space of a sediment mass will significantly lower its bulk density and contribute to its buoyancy (Gregory 1976).

According to Judd and Hovland (2007) there are two possible outcomes of density inversion. Either the underlying sediment will push through the overburden as a coherent sediment mass or excess pore fluids will lead to fluidization and escape from the parent bed, entraining particles as it does so (see sub-section 2.2.1). This suggestion presents two potential end member scenarios when considering the physical properties of mud volcano parent beds. At one end of the spectrum we have a buoyant hydroplastic parent body that remains largely intact during mobilization. Analogies may be drawn between this scenario and mobile salt or igneous systems where there exists a mass of buoyant salt or magma that is capable of large-scale ductile deformation and flow. In certain cases we see evidence for this kind of deformation in thick overpressured mud units. For example, mud lumps and diapirs of many hundreds of metres size can be observed within the slope areas of large sedimentary deltas such as the Mississippi or Niger (Morley and Guerin 1996). Indeed, seismic images from areas such as the Niger delta show evidence for ductile deformation within thick units of argillaceous sediment (Fig. 2.4, Morley 2003a). In further support of the presence of such systems there are seismic data that image mud volcano systems from the South Caspian Sea that show evidence for broad sagging of areas around the mud system interpreted as being caused by mud evacuation from

depth (Stewart and Davies 2006). The fact that these depressions can be larger than the diameter of the system's edifice suggests there may be some form of ductile deformation and flow within the parent bed.

At the other end of the spectrum is a mud layer that, in terms of the material's physical properties, shows little similarity to mobile salt or igneous systems; it is more rigid and less prone to large-scale ductile deformation. In this scenario the parent bed, although potentially overpressured, is less extensively mobilized. Mobilization responsible for mud volcanism is caused primarily through fluidization by allochthonous fluid injection (Kopf et al. 2003). As fluids invade the mud layer they act to buoy particles and thus lead to localized zones of fluidization beneath the eventual site of the mud volcano system. Once the seal of the system is breached fluids are able to escape and carry grains towards the surface. As this process continues the zone of mobilization will become more and more depleted of sediment. As the parent bed is not extensively mobilized lateral sediment flow towards the depleted zone will be minimal. Localized collapse of the overburden forming a focussed collapse structure above the zone of sediment removal would therefore be expected. Evidence to support the occurrence of these processes within a parent bed is twofold. Firstly, there are a number of geochemical studies from the South Caspian Basin indicating that a large proportion of the fluids expelled from mud volcanoes originate from below the mud parent bed (Kopf et al. 2003; Planke et al. 2003). Secondly, seismic reflection images from the South Caspian Sea show the presence of highly focussed collapse structures at the centre of large mud volcano systems possibly indicating the focussed evacuation of sediment from the parent bed (Davies and Stewart 2005; Stewart and Davies 2006). Furthermore, it seems counter-intuitive to assume that an overpressured parent bed will flow once its seal is breached when it is its low permeability and tendency not to flow that have led to its overpressuring in the first place (cf. Mazzini et al. 2007).

Determining where typical mud volcano system parent beds lie within the suggested spectrum of possibilities is difficult. This is illustrated by the conclusions of (Deville et al. 2006) who suggest that large sedimentary uplifts and mud volcanoes from the Barbados accretionary prism could be linked either to large up-welling masses of semi-intact mobile shale or narrow pipes and chambers filled by fluidized mud. It is likely that in any one parent bed example a combination of liquidization and ductile flow may play a role. Estimating the extent to which each of these is effective

in any one mud volcano province may be possible to some extent by mapping the deformation of the parent bed and overlying strata using seismic data or assessing the nature of any subsidence or collapse associated with mud volcano systems.

2.3.2 The intrusive domain

The intrusive domain of the mud volcano system connects the extrusive and source domains (Fig. 2.10). Included is the conduit system responsible for transporting fluids and sediment from the source domain to the surface and the host rock that is intruded by it. The lower boundary of this domain is the upper surface of the source domain and its upper boundary is the surface or seabed and the base of any overlying extrusive edifice (Fig. 2.10). Close parallels can be drawn between the intrusive domain of mud volcano systems and intrusive salt or igneous systems. All consist of some form of through-going intrusive body or conduit network that is laterally bounded by intrusive contacts with the surrounding host rock (Fig. 2.11). All three can produce geometrically similar structures and can appear similar in seismic reflection profiles (Stewart 1999b, Fig. 2.11).

The precise nature of feeder systems and the forces driving flow through them are poorly understood aspects of mud volcanic geology because: 1) Few modern or ancient volcano systems are eroded to a sufficient depth to allow examination of conduit systems at outcrop (Brown and Orange 1993; Clari et al. 2004); 2) Seismic reflection data that image the intrusive domains of mud volcano systems are often poor quality due to inherent difficulties imaging steep or vertical conduits and blanking caused by gas (Judd and Hovland 1992); 3) Physical properties of the material within the conduit and the timescales over which mud volcanoes are constructed are poorly constrained making numerical estimates of conduit shape and diameter difficult (Kopf and Behrmann 2000).

At a basic level, the simple observation that mud volcanoes expel sediments and clasts along with fluids necessitates the presence of some form of sub-vertical dilatational rupture being located within the system's intrusive domain. Diffuse percolation networks that are thought to feed some fluid-only seepage features such as bubble streams or pockmarks can not be considered as viable conduits for mud volcano systems (Judd and Hovland 2007; Matthews 1996). The potential energy contained within overpressured fluids is an important driving force for the initiation of

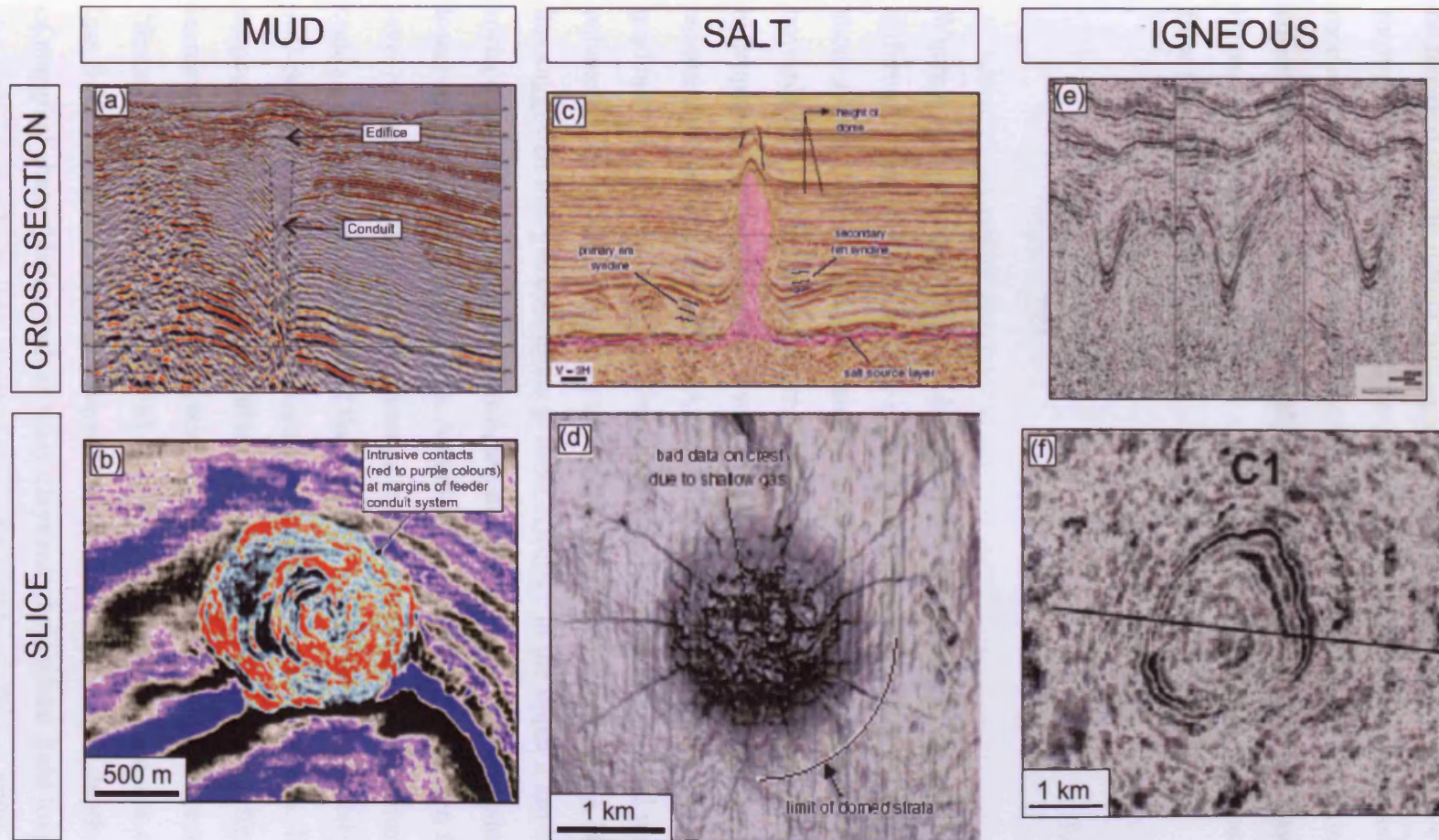


Figure 2.11 Matrix comparing the seismic expression of mud, salt and igneous diapirism: (a) Seismic cross section through the Azeri 2 mud volcano system showing narrow central zone of blanking that may represent the system's conduit. (b) Horizontal seismic coherence slice through a South Caspian Sea mud volcano system showing large-diameter circular zone of seismic disturbance interpreted as zone of intense deformation within the system's intrusive domain. From Stewart and Davies (2006). (c) Seismic cross-section of a salt diapir from Brazil. From Stewart (2006). (d) Seismic horizon dip map showing radial faults above a North Sea salt diapir. From Stewart (2006). (e) Seismic section showing the architecture of Middle Jurassic-age volcanic structures from the Outer Moray Firth, UK. (f) Seismic timeslice through similar volcanic features as shown in (e). Both (e) and (f) from Stewart (1999a)

this rupture and drive of a mud volcano system once it is established. When the contact between the source and intrusive domain is breached this potential energy will be released driving further propagation of the conduit system and, eventually, the flow through the conduit to the surface. Hydrofracturing provides one possible breaching mechanism, tectonic faults or other vertical discontinuities provide alternatives (see sub-section 2.1.3). Once the initial conduit is established the fluid flow rate (Q) out of the source domain into the newly created intrusive domain is described by Pouseille's flow (Eq. 2.7).

$$Q = \frac{\pi \cdot r^4 \cdot \Delta p}{8\eta l} \quad (\text{Equation 2.7})$$

Where r and l are the radius and length of the migration pathway; Δp is the pressure differential and η is the viscosity of the flowing fluid. As flow proceeds, the fluid shear stress acting on sediment grains fluidize and entrain particles that are carried upwards into the fracture (Leeder 1999). If the parent bed is liquefied or in a hydroplastic mechanical state it will flow *en masse* into the fracture creating what is essentially a sedimentary dyke. As depth decreases any gas that is in solution will gradually become exsolved, adding buoyancy to the sediment-fluid mixture and enhancing the ability of the flow to remain mobilized (Graue 2000). Brown (1990) has suggested that gas exsolution is most effective in the upper 2 km beneath the surface and that it provides a significant driving force for mud intrusions through lowering their density (Fig. 2.12). An analogy can be drawn between this increased level of gas exsolution and fragmentation of rising magmas in igneous volcanic conduit (Cashman et al. 2000). If the host rock is sufficiently permeable some fluid will be lost to the host rock by seepage through the conduit margins. Too much seepage and the fluid pressure within the conduit will be reduced, effective stress will increase to a point at which the sediment is no longer mobile and the system will "freeze" (Morley and Guerin 1996). If this is to be prevented the rate of lateral fluid loss from the conduit must be slower than the fluid supply from depth. Development of marginal shear fabrics such as scaly clays may help retard fluid loss in a manner similar to mud cake build up at the edges of a well bore (Brown 1990; Brown and Orange 1993; Pickering et al. 1988).

During conduit activity frictional forces together with the destructive action of clasts entrained into it will act to erode the conduit walls, laterally enlarging it and modifying its shape. This process is evidenced by the large number of angular clasts extruded with the mud in nearly all mud volcano examples and the presence of angular clasts within exposed mud intrusions (Deville et al. 2006; Kopf 1998, 2002). The exact process by which this occurs in the subsurface is not well understood but it is likely to bear some similarity to the erosional processes that occur in igneous volcanic conduits (Macedonio et al. 1994).

Historically, models for the architecture of feeder conduits have centred on the concept of a rising cylindrical mud diapir (see sub-section 2.2.4). “Primary” low density of clay grains in the diapir, the buoyancy produced by exsolving gas and the pressure drive from depth are cited as ways in which diapirs are driven to rise. Analogies are often drawn between bulbous mud and salt or igneous diapirs that have been widely documented in many areas (Clemens 1998; Jackson et al. 1994). As discussed in sub-section 2.1.4, little evidence exists to support the existence of bulbous mud diapirs. In many cases it is likely that the interpretation of a diapir is driven by the observation of large parabolic zones of blanking in seismic reflection data that mimic the expected shape of a large diapir beneath a mud volcano edifice at the surface (Krautel et al. 2003). Like igneous or salt diapirs, it is not clear how the rising mass of sediment is accommodated in the host strata (e.g. Paterson and Fowler 1993). The ways in which gas within it influences its buoyancy and why this gas does not quickly dissipate during diapir ascent, particularly when rapidly exsolving, are not understood. Further constraints are suggested by Kopf (2002) who points out that if diapirs are indeed as wide as suggested by some authors (e.g. up to 6 km, Griboulard et al. 1998) the flow rates to the surface would be many orders of magnitude larger than have ever been observed. This is the case even when it is a simple grain density contrast and no other factor, such as overpressure or gas buoyancy, that provides the driving force. It would seem then that a classic diapiric model is problematic and this has led some authors to cite narrower mud pipes (diatremes) or a combination of diapirs, mud pipes and pre-existing fractures as the feeder conduits for mud volcano systems (Fig. 2.13, Brown 1990; Graue 2000; Milkov 2000).

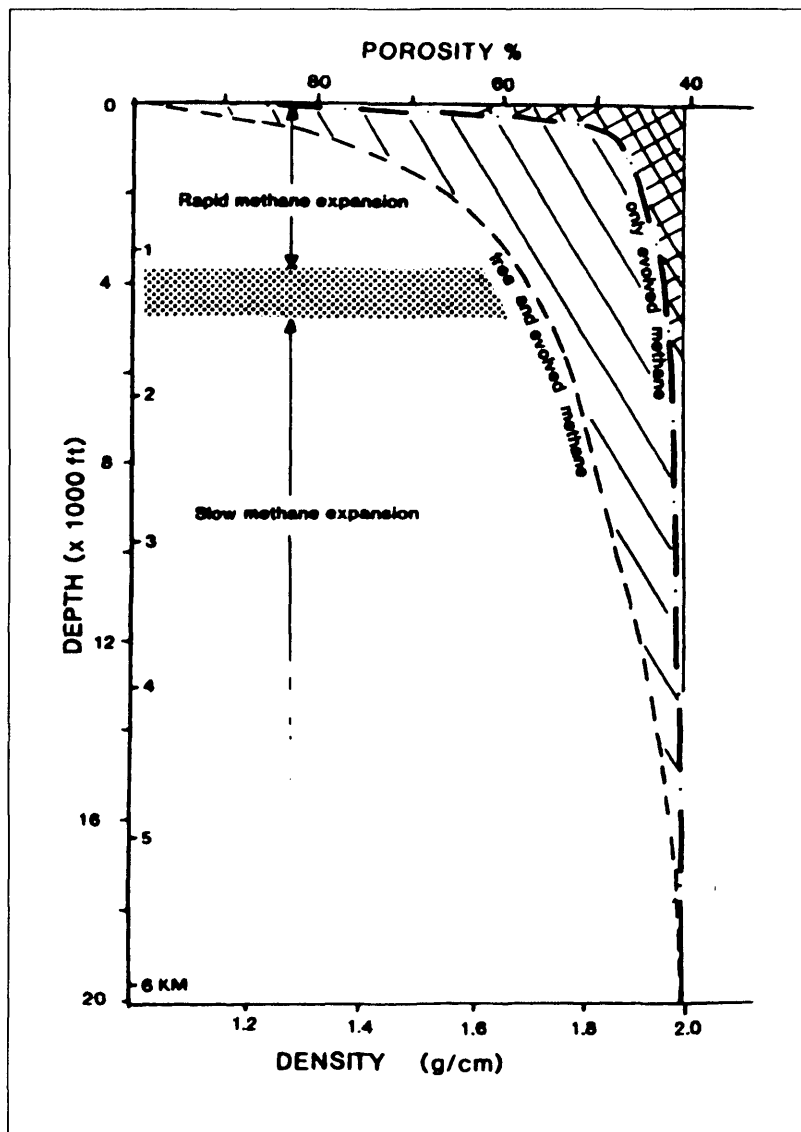


Figure 2.12 Effect of methane expansion on the density and porosity of rising “diapiric” material. Note the rapid expansion of methane in the upper 2 km and its dramatic effect on the porosity and density of the sediment. Expansion of methane in this way and the resultant reduction in density is cited by many authors as an important mechanism for driving sediment towards the surface in mud volcano feeder conduits. From Brown (1990).

In principle, these ideas seem more plausible as the narrowing of the conduit near the surface would restrict flow rates to more like what is observed in nature. How narrow conduits can be is a point that can be constrained by noting the maximum size of clasts extruded during mud volcanic eruptions. Clasts are commonly interpreted to be the product of wall rock erosion by the through-going sediment-fluid mixture. Judd and Hovland (2007) have reported clasts as large as 1.5 m across and clasts observed during fieldwork for this project were of a similar size (Fig. 2.14). A more complex method of estimating minimum conduit diameter that utilised the physical properties of the eruptive products was taken by Kopf and Behrman (2000) who used adaptations of Stoke's Law to estimate the diameter of conduits from the Mediterranean Ridge mud volcanoes. Their results suggest that conduits even for large volcanoes can be as narrow as 2-3 m across. Modelling such as this though is difficult as the properties of conduit fill are very poorly constrained and are often obtained from measurements of mud volcanic sediment at the surface. It is not known how key parameters such as mud density or viscosity would differ when in the conduit.

Recently, increasingly complex models have been suggested for mud volcano feeder systems involving mud chambers linked by narrow pipes (Cooper 2001; Deville et al. 2006; Planke et al. 2003), or complex networks of interconnected fractures and pipes within circular fault-bound feeder systems (Davies and Stewart 2005). These have been invoked either due to the apparent architecture of the systems as seen in seismic reflection data (Cooper 2001; Davies and Stewart 2005), or by geochemical evidence that suggests the presence of some form of intermediate depth mud and fluid store within the intrusive domain (Fig. 2.15a, Planke et al. 2003). Collapse of feeder conduit systems during mud volcano evolution has been a recent idea of Davies and Stewart (2005) who have suggested that large mud volcano feeder systems bear some resemblance to igneous calderas (Fig. 2.15b).

2.3.3 The extrusive domain

The extrusive domain of the mud volcano system is the location of eruptive activity and extrusion of fluids and sediment at the surface (Fig. 2.10). Its lower boundary is the top of the intrusive domain and any extrusive edifice that has developed. Its upper boundary is either the surface or the top of the extrusive edifice. Within this structural

domain the eruptive products of the mud volcano system are extruded at the land surface or seabed. These include mud volcanic sediment, gas, oil and water.

Mud volcanic sediment is remarkably similar in character all over the world and typically consists of a fine-grained grey coloured matrix embedded with millimetre- to metre-scale clasts of other rock. Stratigraphic analysis shows that in the vast majority of cases the fine-grained matrix is the parent bed of the system and the clasts originate as fragments of conduit wall rock broken off by the action of the sediment flowing towards the surface (Dadashev et al. 1995). Numerous authors have termed this eruptive product mud volcano breccia or conglomerate depending on the degree of clast rounding (Kopf 2002).

Fluids are a second important eruptive product expelled within the extrusive domain. Of the gas fraction, methane is usually the most abundant (>90%) and is found in association with virtually all known mud volcano examples (Etiope and Milkov 2004; Judd 2005). It is strongly suspected that this is a result of its critical role in enhancing the potential of the parent bed to mobilize, enhance parent bed buoyancy and add drive to the upward flow of sediment through the feeder system (Brown 1990; Hedberg 1974; Judd and Hovland 2007). It can be both bacterial and thermogenic in origin and is generally evidenced by direct measurement at the surface or acoustic phenomena in remote geophysical data (Judd and Hovland 1992). Recently the problem of accurately measuring the amount of gas expelled to the atmosphere from mud volcanoes has received much attention, not least because of the important role of methane as a greenhouse gas (Judd 2005; Kopf 2003). According to the most recent estimates mud volcanoes emit as much as 6.15×10^{13} g year⁻¹ of methane to the atmosphere per year (Kopf 2003). Other gases, more minor in volume than methane (<10% of the total), include carbon dioxide, sulphur, nitrogen, higher hydrocarbons and other noble gases (Lavrushin et al. 1996). Other fluids such as water and occasionally oil are additional products of mud volcanic eruptions. Geochemical analysis of both these fluids can provide the basis for constraining the depth of their origin.

In terms of structural elements, the extrusive domain principally consists of sedimentary constructions formed by the deposition of erupted sediments at the surface or seabed. These include the principal extrusive edifice, mud flows, small mud pools (salses), mud cones (gryphons) and moffettes (small gas vents). Generally it is only the larger structural elements such as the edifice and mud flows that are

domain the eruptive products of the mud volcano system are extruded at the land surface or seabed. These include mud volcanic sediment, gas, oil and water.

Mud volcanic sediment is remarkably similar in character all over the world and typically consists of a fine-grained grey coloured matrix embedded with millimetre- to metre-scale clasts of other rock. Stratigraphic analysis shows that in the vast majority of cases the fine-grained matrix is the parent bed of the system and the clasts originate as fragments of conduit wall rock broken off by the action of the sediment flowing towards the surface (Dadashev et al. 1995). Numerous authors have termed this eruptive product mud volcano breccia or conglomerate depending on the degree of clast rounding (Kopf 2002).

Fluids are a second important eruptive product expelled within the extrusive domain. Of the gas fraction, methane is usually the most abundant (>90%) and is found in association with virtually all known mud volcano examples (Etiope and Milkov 2004; Judd 2005). It is strongly suspected that this is a result of its critical role in enhancing the potential of the parent bed to mobilize, enhance parent bed buoyancy and add drive to the upward flow of sediment through the feeder system (Brown 1990; Hedberg 1974; Judd and Hovland 2007). It can be both bacterial and thermogenic in origin and is generally evidenced by direct measurement at the surface or acoustic phenomena in remote geophysical data (Judd and Hovland 1992). Recently the problem of accurately measuring the amount of gas expelled to the atmosphere from mud volcanoes has received much attention, not least because of the important role of methane as a greenhouse gas (Judd 2005; Kopf 2003). According to the most recent estimates mud volcanoes emit as much as 6.15×10^{13} g year⁻¹ of methane to the atmosphere per year (Kopf 2003). Other gases, more minor in volume than methane (<10% of the total), include carbon dioxide, sulphur, nitrogen, higher hydrocarbons and other noble gases (Lavrushin et al. 1996). Other fluids such as water and occasionally oil are additional products of mud volcanic eruptions. Geochemical analysis of both these fluids can provide the basis for constraining the depth of their origin.

In terms of structural elements, the extrusive domain principally consists of sedimentary constructions formed by the deposition of erupted sediments at the surface or seabed. These include the principal extrusive edifice, mud flows, small mud pools (salses), mud cones (gryphons) and moffettes (small gas vents). Generally it is only the larger structural elements such as the edifice and mud flows that are

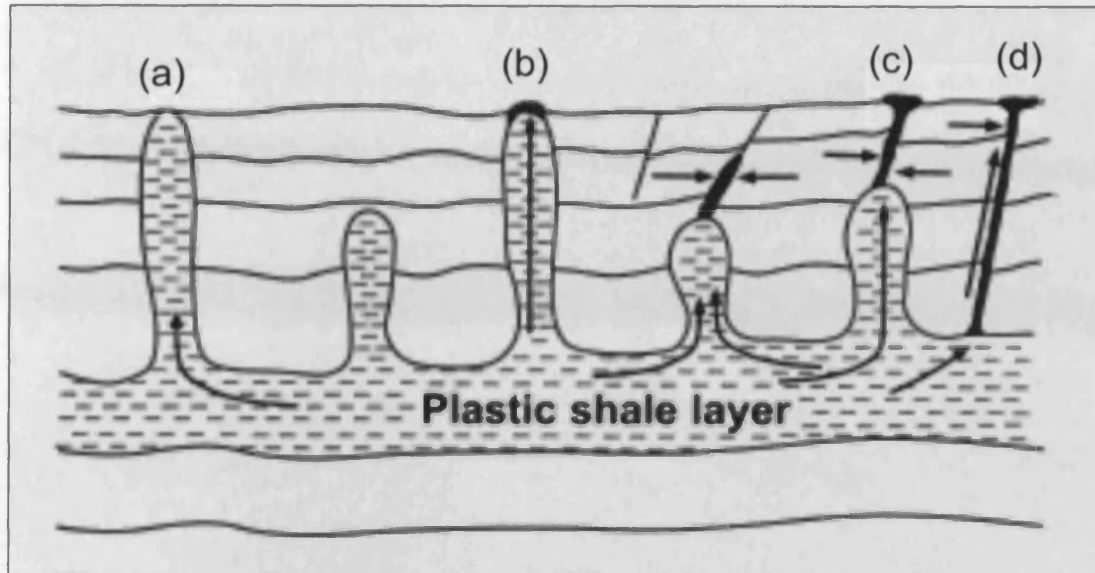


Figure 2.13 Cartoon diagram showing submarine mud volcano systems formed by (a) seafloor-piercing diapir not forming a mud volcano; (b) a mud volcano edifice formed on top of a seafloor-piercing diapir; (c) and (d) seepage and mud volcanoes forming as a result of fluid and sediment flow along faults that may or may not be connected to a diapir at depth. From Milkov (2000).

Figure 2.14 Field photograph of an eroded clay-rich mud volcano (centered in image) mud volcano situated on the flank of the G. A. long and narrow ridge, Azerbaijan. The width of the crest is approximately 1.5 m. The eroded mudflow contained on the dip slope of the volcano which may be as high as 10 m. The notebook is 20 cm long.

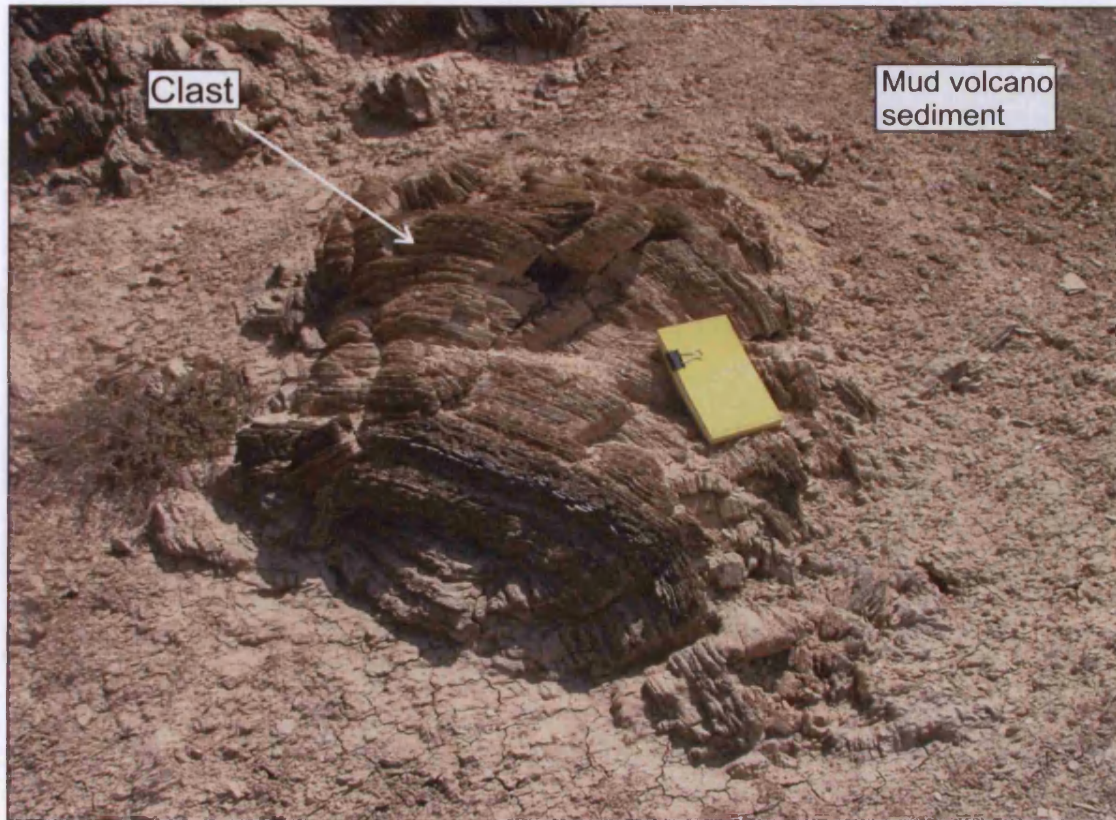


Figure 2.14 Field photograph of an extruded clast of bedded sandstone embedded in erupted mud volcano sediment on the flank of the Garadag mud volcano edifice, Azerbaijan. The width of the clast is approximately 1.5 m. Its occurrence provides a constraint on the diameter of the feeder conduit which must be at least as wide as the clast. Notebook is 20 cm long.

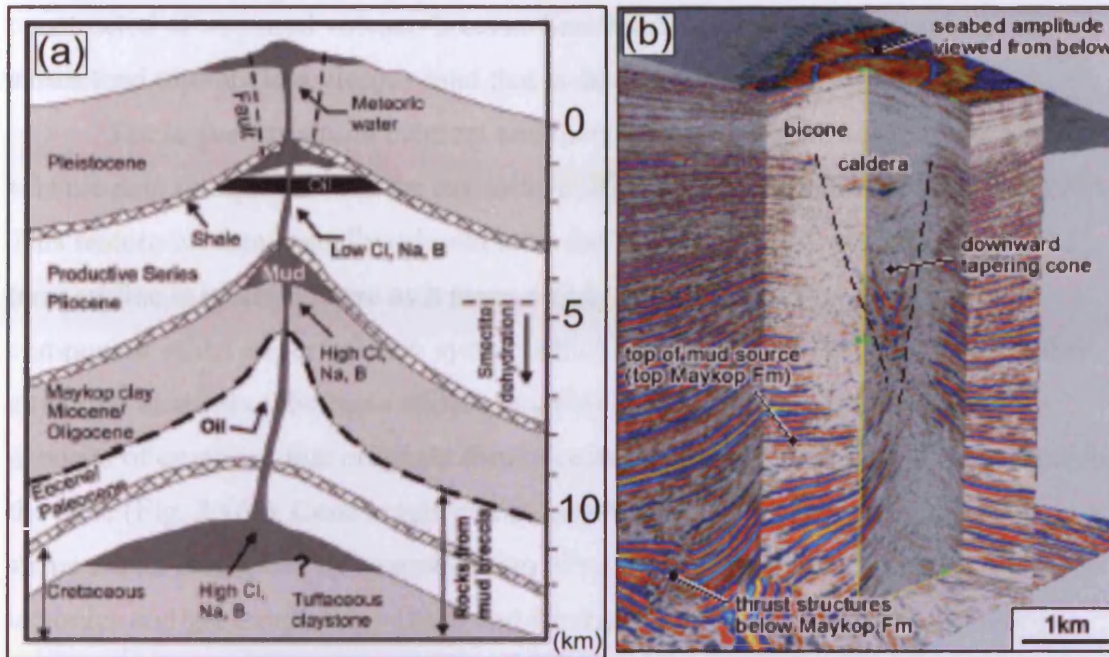


Figure 2.15 Structure of the intrusive domain (a) Schematic cross-sectional model of a typical mud volcano system based on the results of geochemical surveys. Fluids and sediments sourced from depth are stored in intermediate level “mud chambers” connected by pipes. From Planke et al. (2003). (b) 3D seismic visualization of the intrusive domain of the Chirag mud volcano system showing the seismic architecture of a large central collapse caldera. The total height of the system is approximately 5 km. From Stewart and Davies (2006).

constructed of true mud volcano breccia. Smaller structures such as gryphons or salses tend to erupt less viscous mud that is devoid of any large clasts.

The largest structural element and therefore most significant in terms of seismic data interpretation is the extrusive edifice (referred to here as the edifice). This feature is often casually referred to as the “mud volcano” in the literature. The term edifice is preferred here as it more clearly distinguishes this feature as a component of the larger volcano system which in total consists of a number of other structural elements. The basic edifice model is that of a cone constructed by the deposits of eruptions that originate from a central feeder conduit located at the apex of the cone (Fig. 2.16a). Cone height and diameter, flank slope angle and plan view shape are all controlled by a combination of mud properties, eruptive style, local tectonics and geomorphology (Judd and Hovland 2007; Murton and Biggs 2003). Once extruded at the cone’s apex mud will be arranged into flows that progressively aggrade to build the edifice cone. Flow shape and length is controlled by factors that influence the behaviour of gravity-driven viscous currents including gravity, flow inertia, viscosity and yield strength (Lance et al. 1998; Murton and Biggs 2003; Van Rensbergen et al. 2005b). These properties are influenced by the flow’s sediment type, gas and water contents. They play an important role in determining the edifice slope angle, a characteristic that Kopf (2002) has used as a basis for a simple classification of mud volcano systems. Edifice cones with shallow slope angles ($<5^\circ$) are termed mud pies (Fig. 2.16b) and those with steeper cone flank slope angles ($>5^\circ$) are termed cones or domes (Fig. 2.16a, see also Loncke et al. 2004). Yusifov and Rabinowitz (2004) build on this simple nomenclature and suggest that large (>500 m diameter) mud volcano systems from the South Caspian Sea can be classified using the basic cross-sectional architecture of the edifice and any associated seabed bathymetry observed in seismic reflection profiles (Fig. 2.17). Their classification of concave, convex, flat and buried edifice types may act as a good “first-pass” method of describing the general architecture of an edifice, but it does little to convey the role of any processes involved in edifice construction or the reasons for the morphological differences. Other classification systems have elaborated further to include aspects of the volcano system’s eruptive style alongside the morphology of the edifice. Kalinko (1964) and later Dimitrov (2002) have suggested that mud volcano systems in general be grouped into three types based on these criteria (see Judd and Hovland, 2007 for a more detailed review). Lokbatan-type systems are characterised by short periods of

explosive activity separated by periods of dormancy. Mud breccia is stiff and the resultant edifice is steep-sided. Chikishlyar-type systems are characterised by more or less continuous gentle emission of gassy mud and water building flatter, more plate-like edifices. Schugin-type systems are most common and represent an intermediate type between Lokbatan- and Chikishlyar-types. They are characterized by repeated phases of relatively weak activity resulting in the construction of a variety of edifice styles.

Conical mud edifices are commonly observed at the seabed and on land (Holland et al. 2003; Somoza et al. 2003; Van Rensbergen et al. 2005a; Wiedicke et al. 2001). The largest may measure up to 400 m in height and approximately 4 km diameter (Fig. 2.19, Hovland and Judd 1988). Cones typically feature a summit depression which can be termed a crater, caldera, pingo or cauldron (2.17a). If the depression is filled with liquid mud it is termed a salse, tassik or mud lake (Delisle et al. 2001; Kopf 2002). Little is known about the origin of these depressions. Judd and Hovland (2007) state that “explosive venting” or “summit collapse” are two possible mechanisms of origin. Metre-scale gryphons and salses are frequently observed near the edifice summit areas within or outside the summit depressions (Aslan et al. 2001). Often they are clustered into discrete areas of the edifice surface (Hovland et al. 1997). Evidence for gas extrusion from these features is frequently observed in the form of bubbles bursting at the surface of soupy mud pools or hissing sounds emitting from otherwise dormant gryphons. Gas ignition can occur due to the high speed and violent action of some volcanic eruptions (Ivanov and Guliyev 1988). Metre-scale mounds of red thermally metamorphosed mud, termed “sinter”, are formed by this process and many are observed on the surface of large mud volcano edifices (Hovland et al. 1997).

To date the main methods of investigating the extrusive domain of the mud volcano system have been through field mapping, interpretation of seismic reflection or bathymetry data and the collection of seabed cores or other samples. Through the former Hovland et al. (1997) and Planke et al (2003) have identified some architectural elements of the summit areas of the Dashgil and Lokbatan mud volcano edifices from Azerbaijan and mapped the distribution and eruptive style of gryphons, salses and sinter cones on their surface. A focus of many field-based studies has been the estimation of the quantities of gas extruded during mud volcanic eruptions (Dimitrov 2002; Etiope et al. 2002; Etiope et al. 2004; Etiope and Klusman 2002;

Etiope and Milkov 2004; Hovland et al. 1997; Kopf et al. 2001). Methods vary from counting and measuring bubbles bursting within gryphons and salses to the use of methane sensitive detectors and sampling devices. Other studies focus in detail on the geochemical signature of expelled liquids and gases with a view to better constraining their source regions and the subsurface architecture of the system (Kopf et al. 2003; Planke et al. 2003). No field-based studies have attempted to characterize the structural elements of mud volcano edifices at more one example at a time. Only a limited number have attempted to use details of small-scale edifice geomorphology to gain insights into the temporal evolution of mud volcano edifices and the eruptive histories that have led to their present day structure (Hovland et al. 1997). There has been no attempt to integrate field observations with other data types such as seismic reflection images or bathymetric maps.

In recent years the growing global archive of seismic reflection data has led to an increase in the number of seismic-based studies of mud volcano systems (Cooper 2001; Davies and Stewart 2005; Fowler et al. 2000; Graue 2000; Stewart and Davies 2006; Yusifov and Rabinowitz 2004). The aggradational nature of edifice construction means that the cross sectional architecture of the extrusive domain has the potential to provide a detailed seismic stratigraphic record of fluid and sediment expulsion from the subsurface (Murton and Biggs 2003). In theory the extrusive domain should be one of the better imaged components of the mud volcano system since seismic resolution is highest at shallow depths (Fig. 2.10). However, with both 2D and 3D seismic data, imaging problems are common and often acoustic blanking due to gas prevents a detailed interpretation of the architecture of the extrusive domain or any of its component elements (Judd and Hovland 1992; Krastel et al. 2003; Somoza et al. 2003; Wiedicke et al. 2001). Where imaging is more complete it is often the size of the edifice that limits the amount of internal detail that can be observed and mapped (Fig. 2.19 Hansen et al. 2005). Often an edifice is seen as a lenticular shaped transparent seismic facies unit with little internal reflectivity (Fig. 2.20, Kopf 1998). Exceptions to this include some well-imaged mud volcano systems from the South Caspian Sea and offshore Trinidad which show a series of vertically stacked conical seismic facies units separated by units of onlapping non-eruptive sediments (Fig. 2.20, Deville et al. 2003; Yusifov and Rabinowitz 2004)

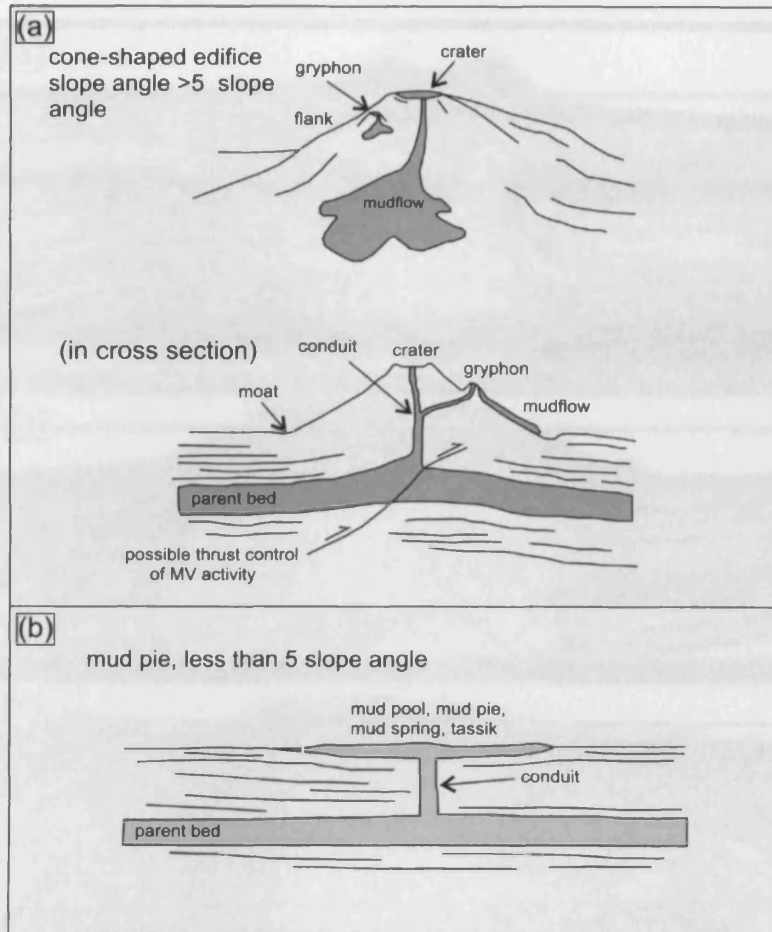


Figure 2.16 Extrusive domain structure and terminology: Schematic diagrams of (a) a cone-shaped mud volcano edifice and associated minor extrusive features and (b) a pie-shaped volcano edifice. This simple terminology is useful for describing features within the extrusive domain but the classification based on flank slope angle can only be applied when no tectonic modifications have taken place or collapse of the edifice has not occurred. Re-drawn from Kopf (2002).

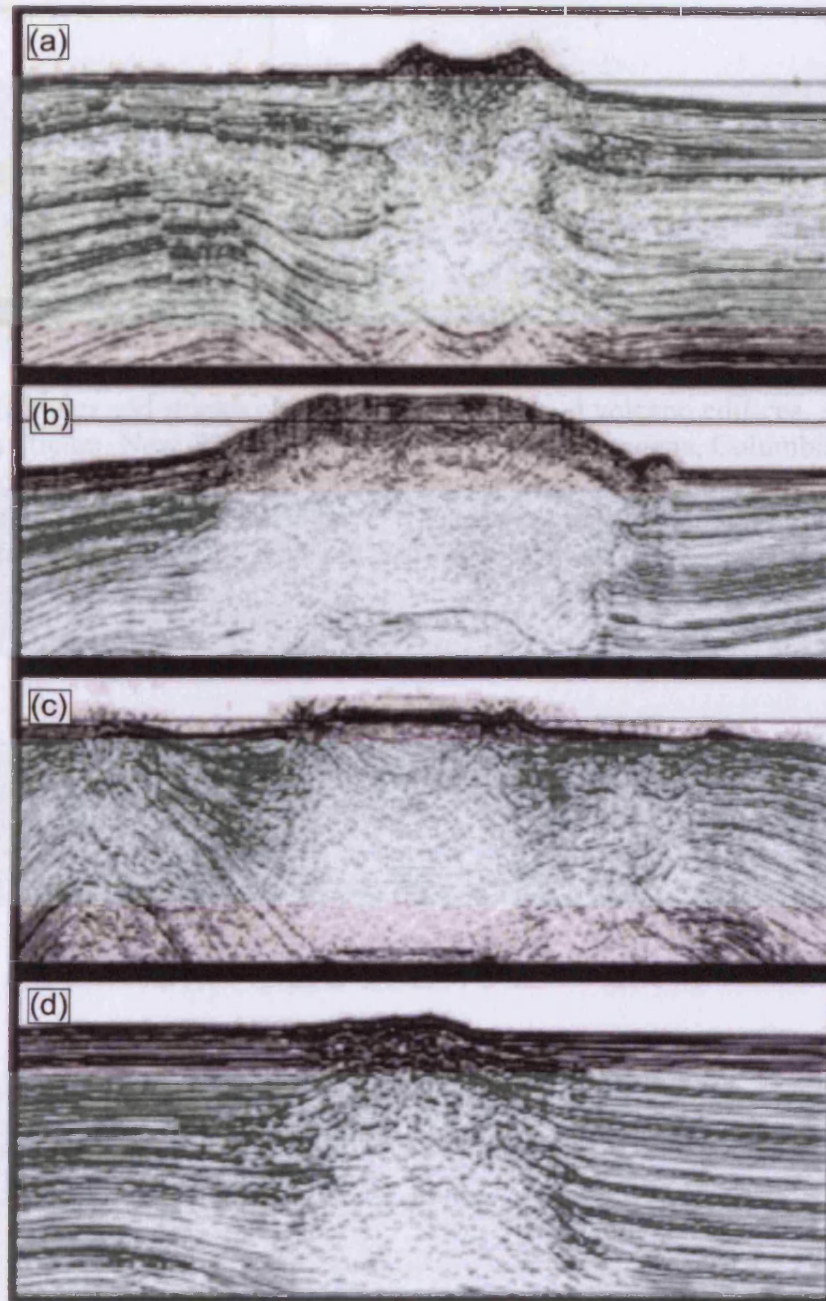


Figure 2.17 Classification scheme of South Caspian mud volcano systems: A mud volcano system is termed either, (a) concave, (b) convex, (c) flat or (d) buried according to the general seismic architecture of the edifice. From Yusifov and Rabinowitz (2004).

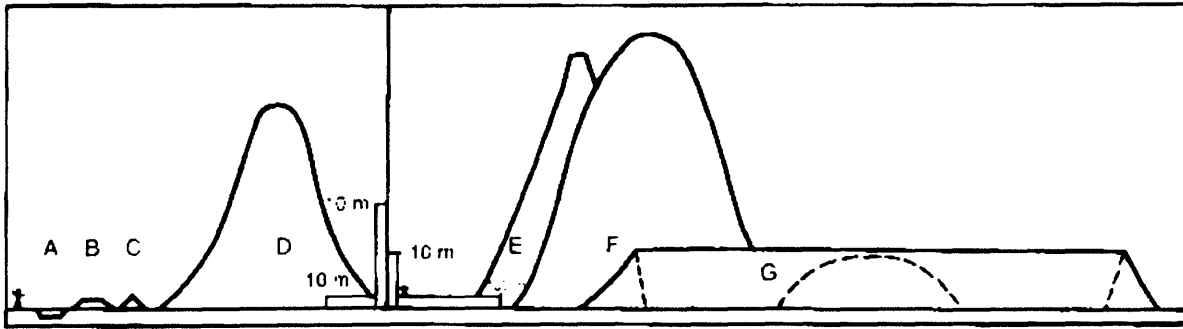


Figure 2.18 Sizes and shapes of various terrestrial mud volcano edifices. A = Maghaehu Stream, New Zealand; B = Volcanito near Cartagena, Columbia; C = Moruga Bouff, Trinidad; D = El Totumo, near Cartagena, Colombia; E = Chandragup, Makran Coast, Pakistan; G = Gharniarigh-Tapeh, Gorgan region, northern Iran. From Judd and Hovland 2007 (2007).

An additional limitation faced by seismic-based mud volcano studies is that most use two-dimensional (2D) seismic data meaning that only a limited assessment of the systems cross sectional architecture can be carried out (Kopf 1998). Detailed mapping of internal reflections throughout the entire area of the extrusive domain, measuring volumes of erupted material and constraining the three-dimensional relationship of the edifice to its feeder system is not possible. Three-dimensional (3D) seismic reflection data provide a method that can overcome these shortcomings. To date however, only a limited number of studies have used 3D seismic data to investigate mud volcano systems. None of these have provided a detailed assessment of the internal structure of the extrusive domain or any of its component elements. There are no studies that have used high-quality 3D seismic data to reconstruct the eruptive history of a mud volcano system from the architecture of its extrusive domain.

Bathymetry data (e.g. swath, sidescan sonar, single- and multi-beam) have been used in many examples to document the seafloor morphology of mud volcanoes. Whilst individual gryphons and salses are still beyond the resolution limits of these methods, recent studies have been able to gain some insights into the processes occurring during edifice construction. For example Van Rensbergen et al. (2005a) have used bathymetric images from the Gulf of Cadiz to interpret various styles of mud flow, constrain the morphology of summit craters and infer post-depositional sedimentary “diapirism” and intrusion within mud volcanic edifices. Somoza et al. (2003) have used bathymetric images of mud volcanoes from the same region to characterise their general bathymetric expression and aspects of their evolution. These and other studies indicate that analysis of high quality bathymetric images is a potentially useful method of characterizing the seabed morphology of mud volcano edifices and other elements within the extrusive domain. Seismic data and field mapping are other potentially powerful methods of investigation. As yet no studies have integrated these three methods to help build a more complete picture of the extrusive domain or attempt to gain insight into the evolutionary stages involved in the growth and development of the mud volcano system.

2.3.4 The roof domain

The roof domain is the shallowest structural domain of the mud volcano system. Its base is defined by the top of the extrusive domain and any extrusive edifice that has formed. Its top is defined by the surface of any sediment that has buried the system and covered the extrusive edifice or other eruptive constructions. The roof domain therefore is only present in systems that have undergone burial and it can only be identified if a cross-section through the system is available (i.e. a seismic profile). It is not possible to determine whether a system has a roof domain through surface analysis alone. Principally the roof domain consists of sediments that bury the system, any through-going minor intrusive systems that connect the buried portion of the system to the surface and any surface expression that results. The positive topographic relief of cone shaped extrusive edifices means that the contact between the buried extrusive domain and the roof domain is observed in seismic data as an onlap surface. Identification of this surface is important in identifying the boundary between the extrusive and roof domains. Onlap demonstrates that a buried extrusive edifice was a positive topographic feature and rules out the possibility that it may represent a mud intrusion such as an intermediate level chamber. This is important as previous studies have apparently identified intrusive mud chambers using 3D seismic data are probably actually more likely to be buried and overlapped extrusive edifices (Cooper 2001). Systems that have undergone significant collapse or subsidence or have undergone periods of erosion may not feature onlap at the top of the extrusive-roof domain boundary. Indeed, in severe cases where uplift and erosion have removed the extrusive edifice, roof domain sediments may be found vertically adjacent to the intrusive domain. In some cases only a very thin veneer of non-eruptive sediment is found to be covering the extrusive edifice. At only approximately 1 m thick sediment layers identified overlying edifices in the eastern Mediterranean are sub seismic and therefore are only identifiable through bottom sampling (Kopf 1998; Robertson 1996). Whilst these thin sediment layers do not have a great impact on the seismic architecture of the system they are important in determining whether the system is active and constraining the duration of any breaks in eruptive activity.

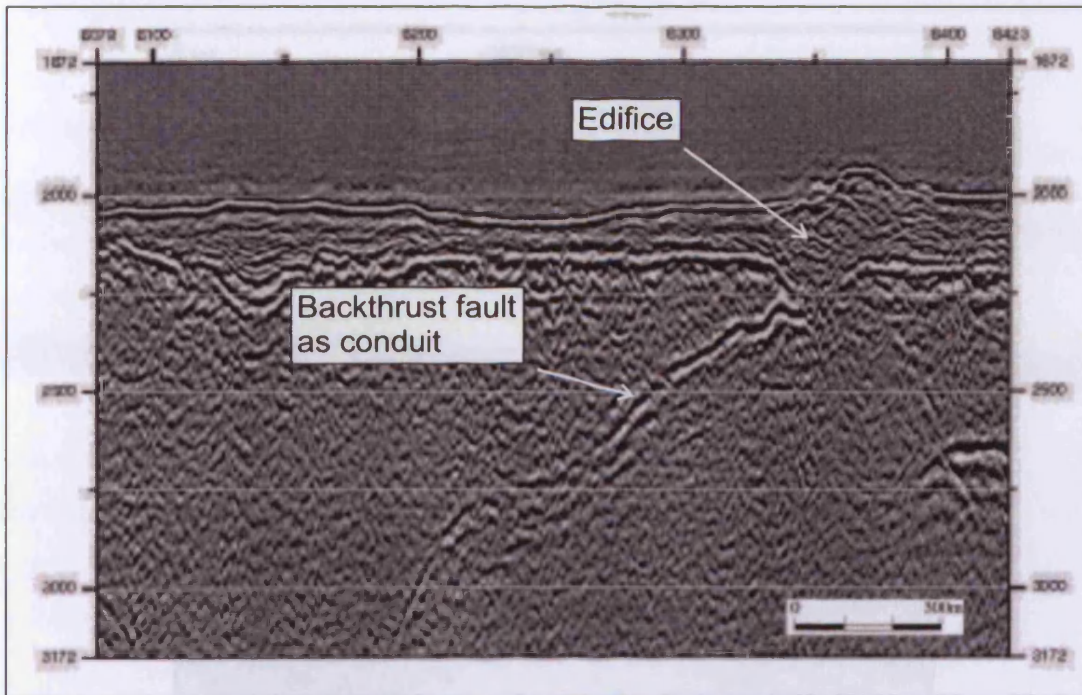


Figure 2.19 Seismic section from the eastern Mediterranean Ridge showing a mud volcano edifice and a dipping backthrust fault thought to be its feeder conduit. Internal layering within the edifice is below the vertical resolution of the seismic data meaning that the edifice appears as a transparent biconic seismic facies unit. The same is true for many other mud volcano edifices and little is known about their internal seismic architecture. Modified from Kopf (1998).

Figure 2.19 Data from the seismicity of a Chiriqui mud volcano edifice. (a) Seismic line through the edifice showing the backthrust fault, some internal layering with identified mud cones, and the fault structure along the various cycles of mud volcanic activity. From Koppe et al. (1998).

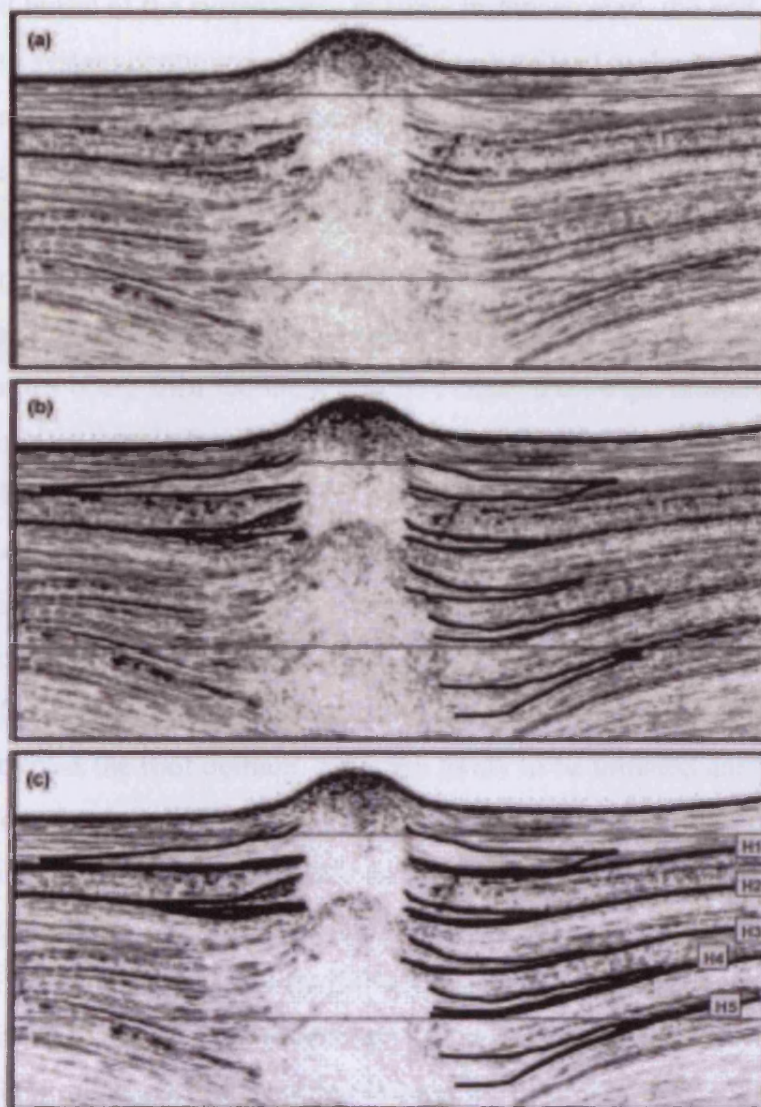


Figure 2.20 Dating the cyclic activity of a Christmas tree mud volcano edifice: (a) Seismic line through the edifice without interpretation, (b) same seismic line with identified mud cones and (c) mapped reflectors used to date the various cycles of mud volcanic activity. From Yusifov and Rabinowitz (2004).

Whilst burial of the system may in some instances mark the end of activity of a mud volcano system continued pressure build up can lead to the breaching of the roof domain and further fluid and sediment extrusion. Reactivation of the system during or after burial may occur through: 1) Renewed pressure drive from depth leading to the upward propagation of the intrusive domain to the surface (Stewart and Davies 2006); 2) Compaction and dewatering of already extruded sediment due to differential loading or density re-equilibration (Van Rensbergen et al. 2005a). If any of these scenarios occur then sediment will be extruded onto the non-eruptive sediment forming a “secondary” extrusive edifice within the roof domain (Fig. 2.10). Further burial of this edifice followed by periods of further extrusion may result in the formation of a stacked series of secondary edifices separated by units of non-eruptive sediments (Fig. 2.20). This architecture has been observed in seismic profiles and systems that exhibit it termed Christmas tree volcanoes (Deville et al. 2006; Stewart and Davies 2006). Current seismic data has so far been unable to resolve the conduit systems that bypass the roof domain. They are likely to be initiated and controlled by the same factors that influence the breach of the source domain deeper in the system (see sub-sections 2.2.1-2.2.3). Once they do breach the surface sediment and fluid will be expelled forming similar structures to those found within the extrusive domain. On a small scale, gryphons, salses and moffettes may form. If flow is more voluminous large extrusive edifices may be constructed. So far seismic data has shown the volume of the stacked extrusive edifices to either remain fairly similar in size with time (Fig. 2.20) or progressively reduce producing an upward-tapering Christmas tree architecture (Fig. 2.21; e.g. Stewart and Davies 2006).

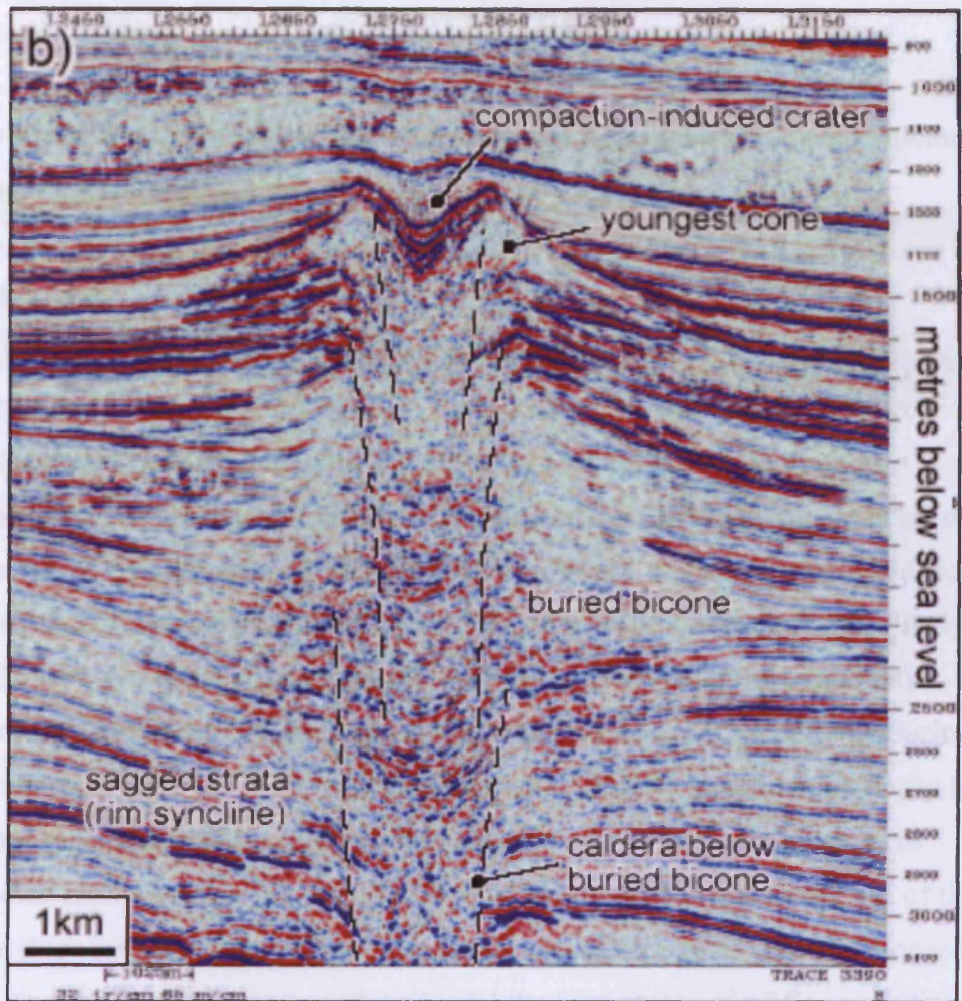


Figure 2.21 Upward tapering Christmas tree-type mud volcano edifice showing evidence for “secondary” mud volcano edifices within the system’s roof domain. From Stewart and Davies (2006).

CHAPTER THREE

3.0 Internal structure and eruptive history of a kilometre-scale mud volcano system, South Caspian Sea¹

3.1 Abstract

We describe the internal structure of a multi-kilometre scale mud volcano edifice from the South Caspian Sea using 3D seismic reflection data leading to a reconstruction of the volcano system's eruptive history. By adapting elements of classic seismic stratigraphy to the study of this volcano we have found its edifice to consist of a series of stacked mud cones. This internal architecture is most likely to have formed as a result of repeated episodes of expulsion of a fluid-mud mix. Underlying the stack of cones is an asymmetric fault-bounded caldera measuring approximately 2 km in diameter. This caldera shows close structural similarity to the trapdoor type of magmatic caldera. Based on the geometrical relationships of individual mud cones to this caldera we conclude that caldera-like collapse of the edifice floor initiated following the deposition of the first mud cone (the pioneer cone). Growth of the caldera continued until the later stages of edifice evolution when it eventually abated. This eruptive history shows strong similarities to recent models for magmatic caldera eruption cycles. The study therefore highlights the potential analogue value of mud volcano systems to the study of igneous volcanism. Furthermore it identifies three-dimensional (3D) seismic data as a potentially useful tool in reconstructing the history of mud volcanic eruption and fluid and sediment expulsion from sedimentary basins.

¹Published as:

Evans R.J. et al. 2007. Internal structure and eruptive history of a kilometre-scale mud volcano system, South Caspian Sea. *Basin Research*, 19, pp. 153-163.

3.2 Introduction

The internal structure of mud volcano edifices provides an important record of the volcano system's eruptive history as well as a sedimentary record of fluid and sediment subsurface remobilization and extrusion. However, describing the internal architecture of mud volcanic edifices has been problematic in the past due to a lack of good three-dimensional exposure on land (cf. Clari et al. 2004) and the typically poor quality of seismic data that images mud volcanoes (Judd and Hovland 1992).

Consequently the eruptive histories of many large mud volcano systems can only be speculated upon using historical data of observed eruptions (Aliyev et al. 2002).

In this paper we use high quality 3D seismic reflection data to: (1) map and describe the internal seismic architecture of a multi-kilometre scale mud volcanic edifice and, (2) use characteristics of its internal structure to reconstruct the system's eruptive history. For many years this has been an aim of igneous geologists who have used lithological and structural characteristics of edifices to reconstruct magmatic eruptive histories (Sigurdsson 1999). Here we demonstrate what may be possible for any edifice using a high-quality seismic reflection dataset.

Our analysis focuses on one large mud volcano system located in the South Caspian Basin herein termed Chirag. It is located approximately 100 km east-south-east of the Apsheron Peninsula (Fig. 3.1a and b).

3.2.1 Background and geological setting

The term "mud volcano system" was recently introduced by Stewart and Davies (2006) to describe an integrated system including the volcanic edifice and a feeder system that connects the edifice to the source domain. Recent seismic images of South Caspian mud volcano systems have provided insights into the seismic architecture of these features (Davies and Stewart 2005; Stewart and Davies 2006). These are summarized in Fig. 3.2, which schematically depicts the subsurface architecture of a typical South Caspian Sea mud volcano system and the extrusive edifice, upon which we focus.

Previous studies aimed at accurately describing the architectures of mud volcanic edifices have mainly been conducted using geophysical surveying techniques (Cooper 2001; Evans et al. 2007b; Kopf 1998; Somoza et al. 2003) or field mapping

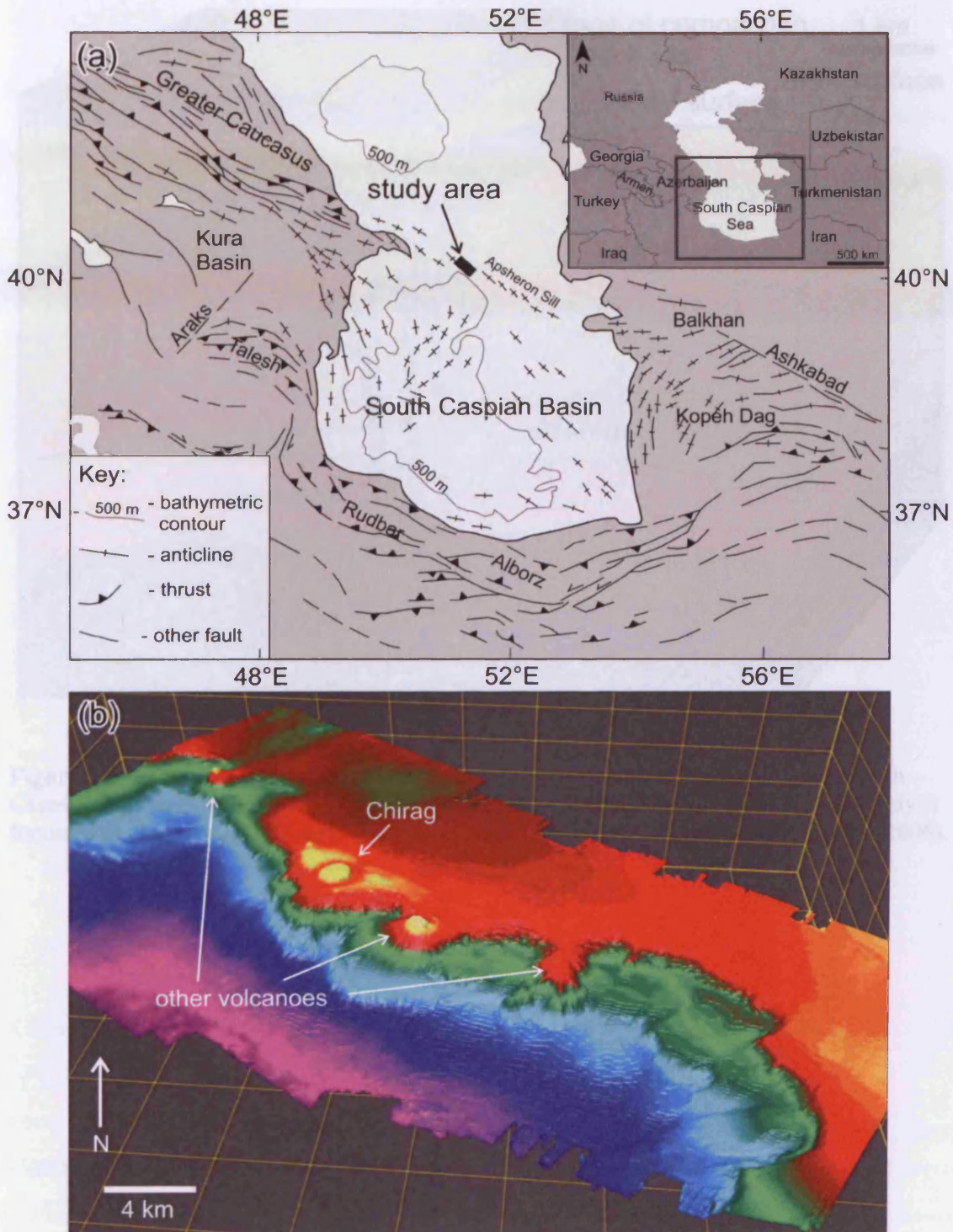


Figure 3.1 (a) Tectonic map of the South Caspian Basin showing the location of the study area. Inset map of the Caspian region shows map location as black box. Modified from Jackson et al. (2002). (b) 3D bathymetric map of the study area seabed showing position of Chirag and other mud volcanoes at the shelf-break.

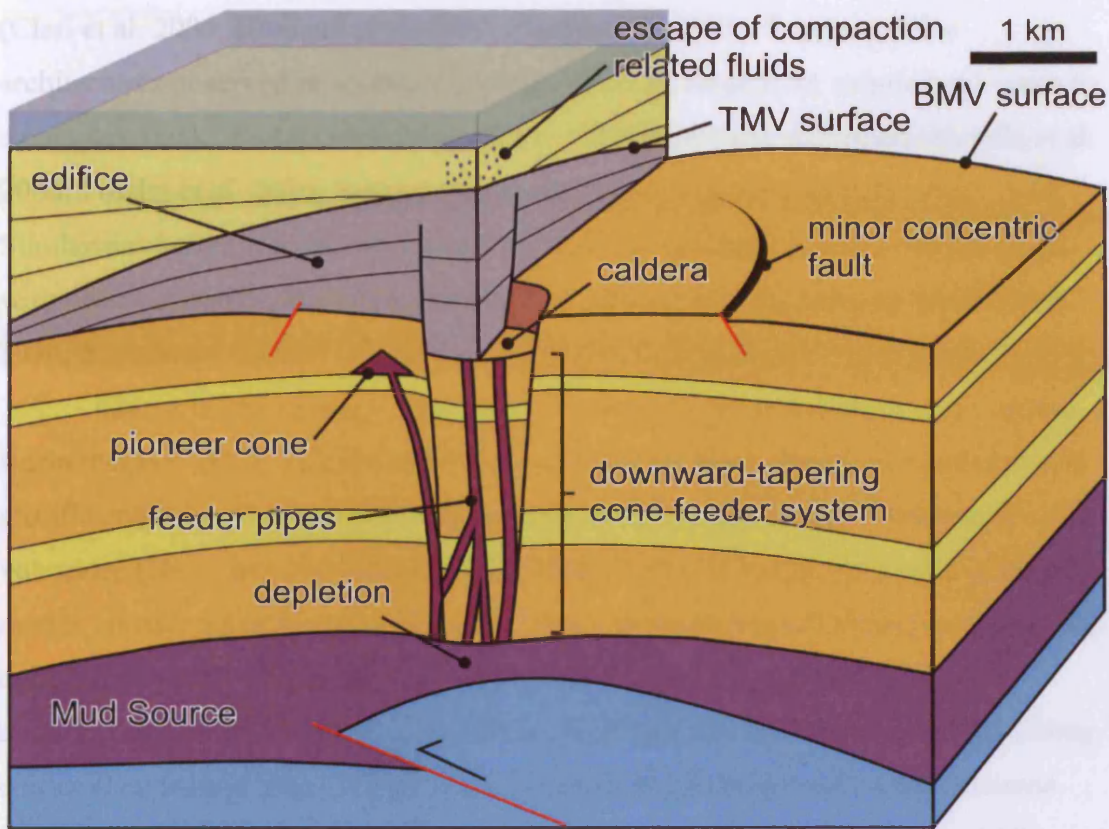


Figure 3.2 3D schematic diagram showing the sub-surface architecture of a typical South Caspian Sea mud volcano system. Vertical scale can be 100s of metres to 5 km. This study is focussed on the internal architecture of the edifice. Modified from Stewart and Davies (2006).

1.2.2 Database and methodology

Ching and other nearby volcanoes were interpreted using reflection data acquired in 2005 using land-based seismic reflection data. This data image the crust of the Azov-Bing-Sourbye basin. The seismic data shows a clear reflection at edifice level in approximately 0.4 s, which is interpreted as an increase in acoustic impedance due to further compaction and a polarity reflection negative as a decrease in acoustic impedance (Brown 1999).

The analysis of the Ching well is presented in Figure 3.2. The well is a number of discrete seismic layers units, to which the seismic data have been adapted elements of classic seismic interpretation.

(Clari et al. 2004; Hovland et al. 1997; Planke et al. 2003). Typical edifice architectures observed in seismic reflection data can range from simple mud cones to a complex stack of mud cones interbedded with background sediments (Deville et al. 2003; Fowler et al. 2000; Stewart and Davies 2006; Yusifov and Rabinowitz 2004). Similarities between mud and igneous edifices can include a broadly conical shape with positive topographic relief and outward dipping internal layering (Gatliff et al. 1984; Sigurdsson 2000).

Chirag is one of many large mud volcanoes found within the South Caspian Basin (Milkov 2000; Yusifov and Rabinowitz 2004). Mud volcanism in this basin is prolific and it is estimated that it contains up to 25% of the worlds known mud volcanoes (Huseynov and Guliyev 2004; Kopf 2002). The regional source of erupted mud is considered to be the argillaceous Maykop Formation of Oligocene to Miocene age (Abrams and Narimanov 1997; Kopf et al. 2003). This Formation is approximately 1 km thick and is buried to a depth of almost 5 km beneath the Chirag edifice (Davies and Stewart 2005). A compressional tectonic regime has persisted since the Late Pliocene (Allen et al. 2002; Allen et al. 2003; Jackson et al. 2002) resulting in the formation of a large number of anticlines within the basin. The anticlinal crests are both the sites of large hydrocarbon accumulations and many large mud volcanoes (Devlin et al. 1999).

3.2.2 Database and methodology

Chirag and other nearby volcanoes are imaged by prestack depth-migrated 3D seismic reflection data acquired in 2002 using towed streamer cable technology. These data image the extent of the Azeri-Chirag-Gunashli hydrocarbon field located within the Apsheron anticline (Fig. 3.1b). The line spacing is 12.5 m and the vertical resolution ($\lambda/4$) at edifice level is approximately 12 m. A positive polarity reflection represents an increase in acoustic impedance across an interface and is coloured red. A negative polarity reflection represents a decrease in acoustic impedance and is coloured black (Brown 1999).

The analysis of the Chirag edifice principally involves its subdivision into a number of discrete seismic facies units. In order to identify and map these units we have adapted elements of classic seismic stratigraphy to the study of mud volcanism

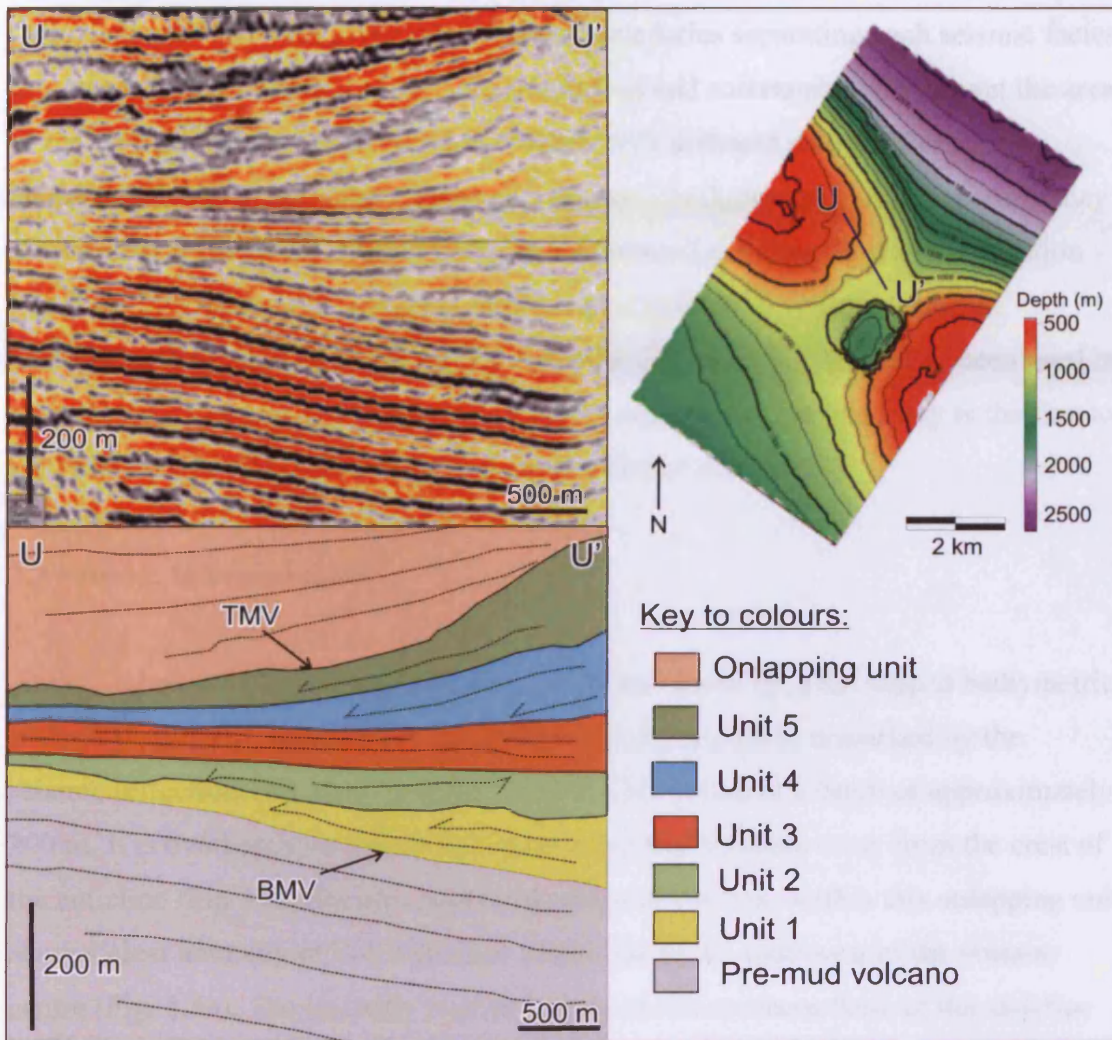


Figure 3.3 Uninterpreted interpreted seismic section U-U' through the Chirag edifice showing the 5 seismic facies units that make up the edifice and the internal reflection geometries and reflection terminations that have been used to define and map them. TMV= Top Mud Volcano reflection, BMV= Base Mud Volcano reflection on this and subsequent figures. BMV inset depth map for section location.

Volcano reflection (BMV) is the prominent reflection of the underlying mudstone reflection (Fig. 3.4). The section U-U' (Fig. 3.3) shows a complex internal reflection geometry that has to be interpreted as a series of mudstone units. The implementation of the mapping method described above has enabled us to identify five seismic facies units within the edifice that have been mapped in Fig. 3.3 and 3.4. The dimensions of each unit, their internal reflection terminations, internal reflection geometries and reflection terminations are summarized in Table 3.1. In each case, showing the depth and reflection terminations are shown in Fig. 3.6. Of note is a U-shaped depression, 100m wide and 150m deep, located within a thick section of Unit 1 (Fig. 3.3 and 3.4).

(Mitchum and Vail 1977). For example, the boundaries separating each seismic facies unit were chosen because (a) they are continuous and correlatable throughout the area of the edifice, (b) they divide sections of data with different seismic facies characteristics (e.g. amplitude, internal reflection configuration), and, (c) locally they are surfaces upon which other reflections terminate (i.e. onlap, downlap, truncation – Fig. 3.3). The latter is the principal method used to identify seismic sequence boundaries (Mitchum and Vail 1977). A similar approach has previously been used in the analysis of large-volume basaltic extrusive complexes, but this study is the first to apply this method to sedimentary volcanism (Planke et al. 2000).

3.3 Seismic interpretation

At the seabed the Chirag volcano system is characterised by a flat topped bathymetric summit (Fig. 3.1b). Beneath the seabed, the top of the edifice is marked by the seismic reflection Top Mud Volcano (TMV). This occurs at a depth of approximately 200 m. It is overlain by a unit of divergent onlap that thickens away from the crest of the anticline (Fig. 3.4). Seismic amplitude maps of horizons within this onlapping unit show a clear anomaly of low reflection amplitude to the southwest of the volcano centre (Fig. 3.5a). The anomaly is present only on the southern flank of the anticline and has a radial pattern centred on the volcano centre. The best images of the anomaly show it to consist of a number of lobate and linear features which originate from the volcano centre (marked 1 and 2 in Fig. 3.5a). In seismic sections these features can be identified as very subtle changes in reflection amplitude (Fig. 3.5b).

Deeper in the section, the base of the main edifice is termed the Base Mud Volcano reflection (BMV) and is the uppermost extent of the underlying concordant reflections (Fig. 3.4). The section BMV-TMV defines a lenticular to biconic (two cones placed base to base) section of variable seismic facies up to 1.4 km thick. Implementation of the mapping methodology described above has enabled us to identify five seismic facies units within this interval; each one has been mapped in 3D (Figs 3.3 and 3.4). The dimensions of each unit, their 3D external form, internal reflection configurations and defining reflection terminations are summarized in Table 3.1. Isopach maps showing their shape and lateral extent are shown in Fig. 3.6. Of note is a u-shaped depression measuring 570 m wide and 150 m deep positioned within a thick section of Unit 1 (marked Z in Figs 3.4 and 3.6).

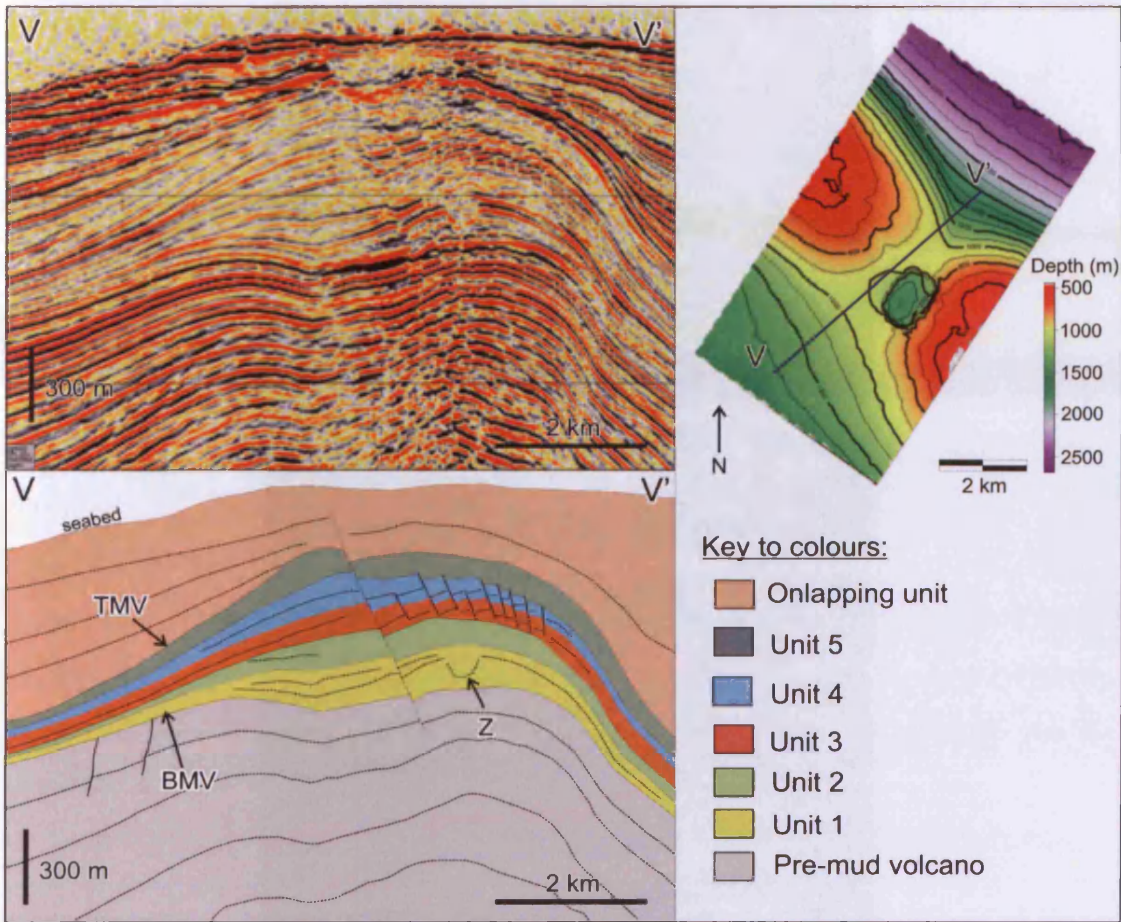


Figure 3.4 Uninterpreted and interpreted seismic section V-V' through the Chirag edifice showing the stacking arrangement of the interpreted seismic facies units. Note the position of the mud cone crater (marked Z) within Unit 1. BMV inset depth map for section location.

Figure 3.5(a) is an amplitude map of a seismic section through the Chirag edifice showing the position of the mud cone crater (marked Z) within Unit 1. The mud cone crater is located within the onlapping unit. See Fig. 3.4 for the interpreted seismic section. Figure 3.5(b) is a field photograph of a mud volcano in the Chirag edifice. Note the similarity between mud cones and mud volcanoes in the amplitude map of Fig. 3.4.

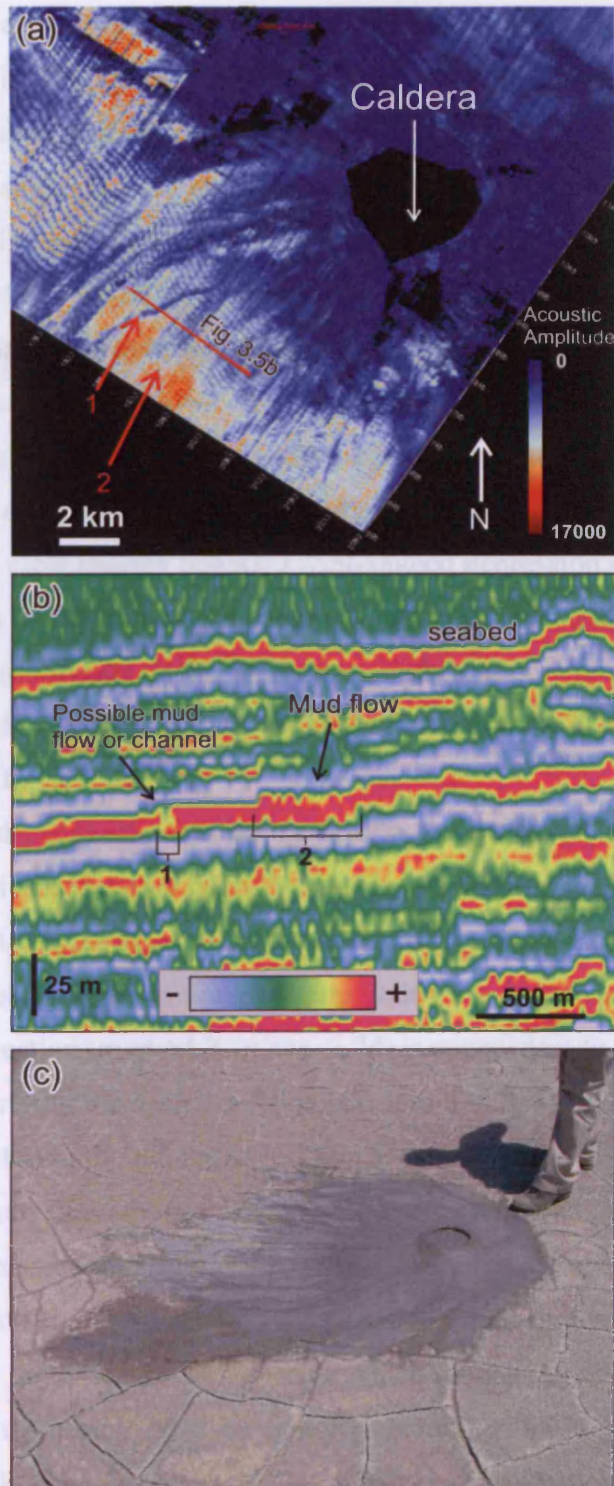


Figure 3.5 (a) Acoustic amplitude map of a selected horizon within the onlapping unit that overlies the Chirag edifice showing the pattern of mud flows radiating from the central area of edifice. (b) Representative seismic section showing the cross-sectional seismic character of mud flows within the onlapping unit. See Fig. 3.5a for section location and position of features 1 and 2. (c) Field photograph of a gryphon on the Doruvdag mud volcano, Eastern Azerbaijan. Note the similarities between small-scale flow patterns on the gryphon and large-scale flow patterns in the amplitude map of Fig. 3.5a.

At the centre of the edifice is a roughly vertically oriented zone of poor seismic image quality (Fig. 3.7a). The lack of coherent reflectivity in this zone is likely to be the result of blanking due to the presence of gas in the section. Blanking occurs through the scattering and absorption of acoustic energy within the gas charged sediment resulting in vertical zones of poor signal-noise ratio on the display (Judd and Hovland 1992). BMV is the only reflection that can be traced into this blanked zone where it can be observed in multiple seismic surveys (Fig. 3.7a and b). Within this zone it has an unusual convex-down geometry and lower frequency than areas surrounding it. This may result from a combination of poor seismic migration, high-frequency filtering and pushdown. Mapping it as part of the surrounding BMV reflection reveals a clear sharply bounded oval-shaped depression (Fig. 3.7c). Offset around the margins of this depression reaches a maximum value of approximately 480 m along the southeastern side of the depression. Offset reduces progressively around the edge of depression until there is no resolvable offset on the depressions northwest side (Fig. 3.7a and b).

Outside of the depression, to the northwest, the BMV reflection is synformal in an area that adjoins and passes laterally into the depression (marked Y in Fig. 3.7c). This synform directly faces the section of greatest offset of the BMV reflection. Discontinuous reflections within the overlying Unit 1 are deformed by this synform. The lowermost reflection (marked X in Fig. 3.7d) is concordant to the BMV reflection. The overlying top-Unit 1 reflection is less tightly folded and shows an onlapping relationship to the reflection marked X (Fig. 3.7d).

Strike sections through the edifice show that its total thickness decreases across the southeastern margin of the depression where the offset of the BMV reflection is greatest (Fig. 3.7a and b). The most significant decrease in thickness occurs in the lower three seismic facies units, which in total are approximately 400 m thick in the area to the northwest of the depression and 200 m thick on its southeastern side (Fig. 3.7a and b). The thickness of Unit 4 reduces by a lesser extent and the thickness of Unit 5 does not change. These thickness changes, together with the clear offset of BMV and other deeper reflections outside the blanked zone, have led us to reconstruct the likely architecture of the edifice within the depression by projecting the seismic facies unit boundaries into the zone of blanking (dotted interpretation lines in Fig. 3.7b).

Seismic Facies Unit	3D External Form	Volume (km ³)	Diameter (km)	Max. Thickness (m)	Internal Reflection Configuration
1	Wedge	2.6	6.5	185	Discontinuous reflections downlapping BMV.
2	Wedge	1.7	5.5	165	Reflection-free with occasional erosional truncation
3	Sheet	N/A	N/A	150	Parallel and continuous internal reflections.
4	Wedge	2.2	6.0	215	Discontinuous downlapping reflections.
5	Wedge	4.1	11.2	195	Upper surface onlapped by overlying unit. Largely reflection-free.

Table 3.1 Summary table showing the 3D external form, dimensions, internal reflection configuration and defining reflection terminations of the five seismic facies units that make up the Chirag edifice. BMV = Base Mud Volcano.

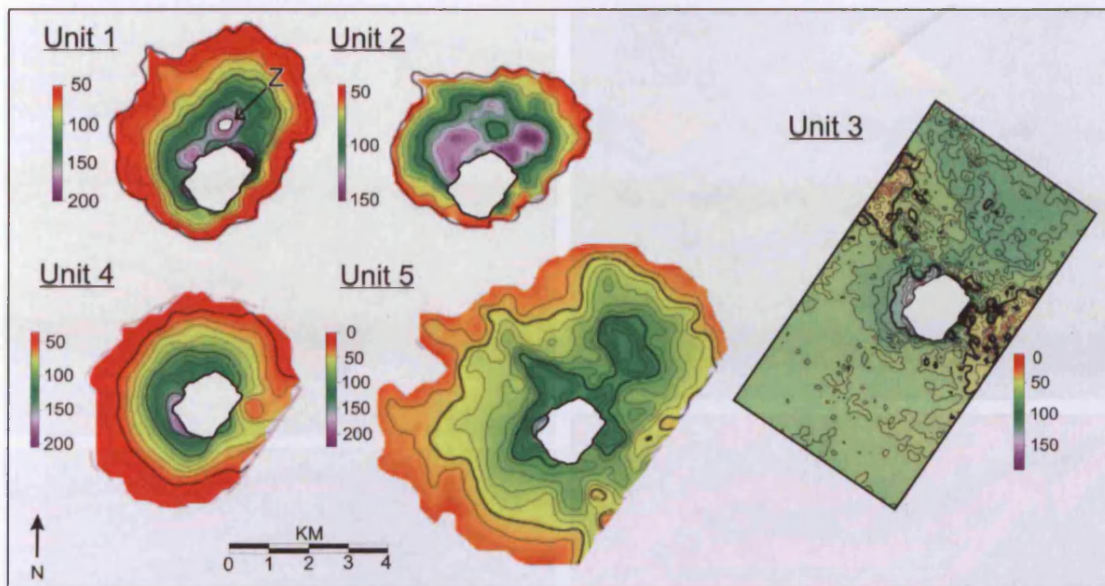


Figure 3.6 Isopach maps of seismic facies Units 1-5 showing their shape and lateral extent. Note position of mud cone crater in Unit 1 (marked Z). Colourbars of unit thickness are in metres. White circular area denotes the blanked area within the caldera centre. Seismic facies units have not been mapped within this zone in 3D.

Figure 3.7 (a) Unit 1 profile seismic section through the caldera and caldera rim of the stratigraphic volcano system. In (b) this section is enhanced to reflect the increased stage of post-eruptive growth. See text for discussion and Fig. 3.7c for section location. (c) 3D visualization of the BMV surface showing the position of the hangingwall synclines (marked Y) adjacent to the caldera margin. (d) Seismic section through system Y showing the structural concordance of reflection X to the BMV surface. See text for discussion, Fig. 3.7b for key to colours and Fig. 3.7c for section location.

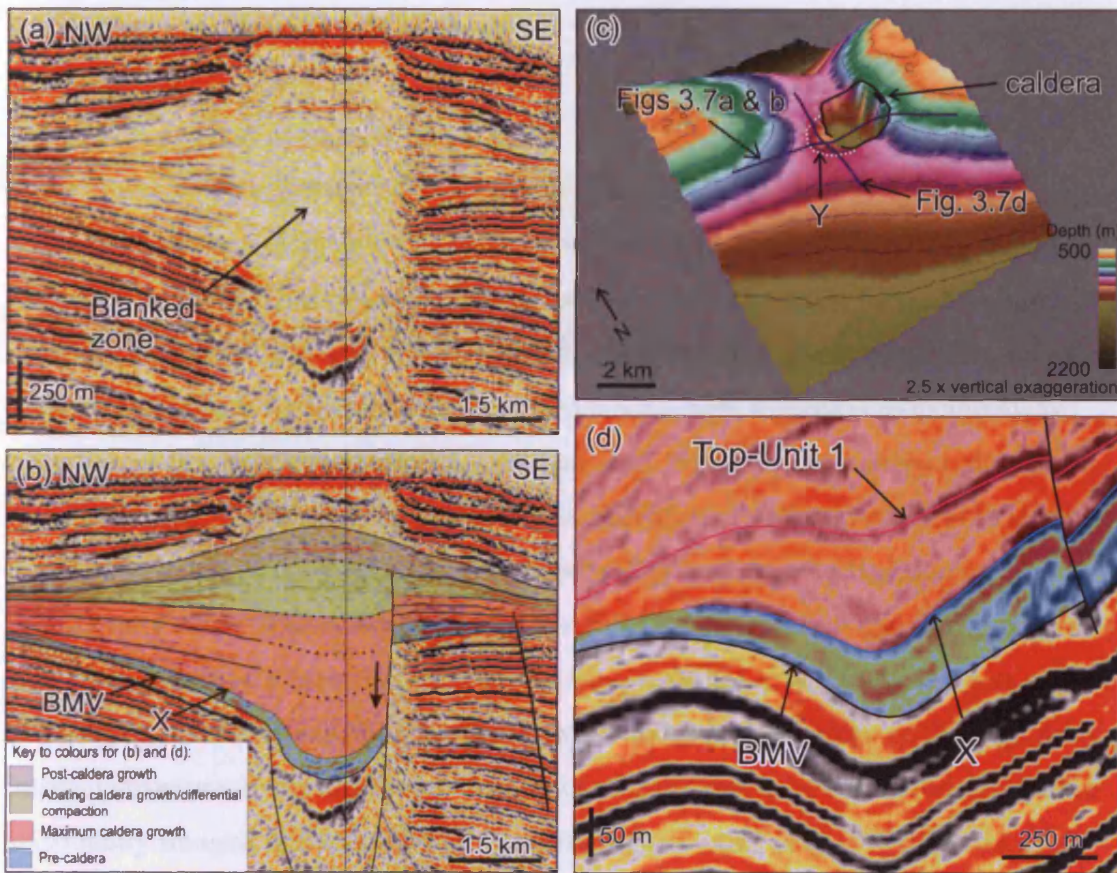


Figure 3.7 (a) Uninterpreted seismic section through the edifice and caldera of the Chirag mud volcano system. In (b) this section is coloured to reflect the interpreted stages of caldera growth. See text for discussion and Fig. 3.7c for section location. (c) 3D visualisation of the BMV surface showing the position of the hangingwall synform (marked Y) adjacent to the caldera margin. (d) Seismic section through synform Y showing the structural concordance of reflection X to the BMV surface. See text for discussion, Fig. 3.7b for key to colours and Fig. 3.7c for section location.

Overlying the edifice within the capping unit, is further evidence for activity of the mud volcano system that occurred following abandonment of the main edifice. The position and shape of the amplitude anomaly observed within this unit is consistent with an interpretation as a series of mud flows. The fact that each mud flow was a stratigraphically ordered flow is a tectonically reasonable expectation and indicates that its thickness is below the limit of vertical seismic resolution (200 m) which in this case is approximately 1.2 m. The radial stratigraphy of these Miocene-scale mud flows bears a clear resemblance to the centrifugally-flow patterns observed at active mud and gas flow vents (200-500 m) that exist in numerous currently active offshore mud volcanoes (Fig. 3.5c). This observation highlights the multi-scale nature of mud volcano depositional components. It also provides an

3.4 Edifice construction and evolution

3.4.1 Interpretation of seismic facies units

As with conventional seismic facies analysis, the internal reflection configuration, external form and 3D associations of each seismic facies unit can be used to interpret its origin (Mitchum and Vail 1977). Table 3.1 shows that four out of the five seismic facies Units have a wedge-shaped 3D external form with thickness reducing away from the edifice centre (see also Figs 3.3 and 3.4). Similar wedge-shaped units have previously been identified and interpreted as buried mud volcanic cones both in the South Caspian Basin (Yusifov and Rabinowitz 2004), and in the Barbados accretionary prism (Deville et al. 2003). We follow this approach and interpret Units 1, 2, 4 and 5 as buried mud cones. Downlapping reflections within these Units are likely to represent the outward dipping internal layering that makes up the finer scale internal structure of the mud cone. Similar configurations have been observed within seismically imaged igneous volcanic constructions (Gatliff et al. 1984; Planke et al. 2000). Examples where the internal reflection configuration is chaotic or reflection-free are likely to result from cases where no internal layering has developed, or it has not been imaged. The sheet-like external form and parallel and continuous internal reflection configuration of Unit 3 is not consistent with its interpretation as a mud cone. Instead we interpret this seismic facies unit as tabular sheet of non-eruptive sediment deposited during a break in the volcanic activity.

Overlying the edifice, within the onlapping unit, is further evidence for activity of the mud volcano system that occurred following construction of the main edifice. The position and shape of the amplitude anomaly observed within this unit is consistent with its interpretation as a series of mud flows. The fact that each mud flow occurs as an amplitude anomaly rather than as a seismically resolvable top and base indicates that its thickness is below the limit of vertical seismic resolution ($\lambda/4$), which in this case is approximately 12 m. The radial arrangement of these kilometre-scale mud flows bears a close resemblance to the centimetre-scale flow patterns observed at metre-scale mud and fluid vents (gryphons) that occur on numerous currently active onshore mud volcanoes (Fig. 3.5c). This observation highlights the multi-scale nature of mud volcanic depositional components. It also provides an

insight into the likely pattern of mud flows that stack to form the wedge-shaped seismic facies units identified within the main edifice.

3.4.2 Edifice collapse history

The sub-circular depression in the BMV reflection located at the centre of the edifice has been an important structural element throughout the volcano system's evolution. The extensional offset of the BMV reflection around this depression leads us to interpret this feature as a circular fault system that has formed by the focussed gravitational collapse of the BMV surface. The feature has previously been termed the "caldera" of the mud volcano system by Davies and Stewart (2005) due to its structural similarity to igneous calderas. We refer the reader to this study for a detailed description of the caldera's deeper structure (see also Fig. 3.2).

The uneven displacement distribution around the caldera's bounding fault system indicates that collapse has been asymmetric; similar to the "trapdoor" type of igneous caldera (Cole et al. 2004). As the thickness of the internal mud cones will be affected by the development of this caldera, our 3D analysis of the internal structure of the edifice provides a useful framework for assessing the temporal evolution of the caldera fault system. The following discussion of this evolution is illustrated with reference to Fig. 3.7b where we have coloured internal sections of the edifice to reflect the perceived level of caldera growth during the volcano system's evolution.

Seismic facies Units 1, 2 and 3 thicken towards the centre of the caldera and thin significantly across the margin with greatest displacement. This pattern suggests that the centre and hinged side of the caldera was a zone of greater accommodation space during the deposition of these Units. It is therefore likely that the caldera was actively subsiding during construction of the lower part of the edifice (coloured red in Fig. 3.7b). Within this growth section, the reflection "X" is deformed by the synform that faces the area of greatest caldera fault displacement (marked Y in Fig. 3.7c). The position and extent of this synform suggests a genetic link with the largest displacement section of the caldera fault. We interpret it as a hangingwall basin to the section of the caldera fault that it faces (Fig. 3.7c, Childs et al. 2003). It can therefore be used as an "indicator" of caldera fault activity. The structural concordance observed between BMV and reflection X in Unit 1 indicates that reflection X was present prior to the development of the synform (Fig. 3.7d). The lowermost part of

Unit 1 (below reflection X) therefore must have been erupted before the formation of the synform and thus prior to the initiation of the caldera fault. The section can therefore be considered as pre-caldera and has been coloured blue in Fig. 3.7b and d. The small u-shaped depression present within the Unit 1 mud cone is part of this pre-caldera section (Fig. 3.4). The shape of this feature and position near a thick section of the cone suggests that it is likely to represent an eruptive crater. This has previously been termed ‘the pioneer cone’ by Davies and Stewart (2005). We consider it likely to have been the source of the pre-caldera erupted mud.

Overlying the growth section, the smaller thickness reduction of Unit 4 across the caldera fault may also suggest that the caldera was actively subsiding during its deposition. However, by this stage in the edifice’s evolution a thick pile of recently erupted sediment had accumulated above the hinged side of the caldera meaning that this change in thickness could also be the effect of differential compaction (coloured yellow in Fig. 3.7b). No thickness reduction of Unit 5 indicates that and no further caldera collapse was occurring at the time of its deposition (coloured grey in Fig. 3.7b).

3.5 Discussion

3.5.1 Volcano system eruptive history

Our analysis reveals a complex eruptive history involving construction and collapse of a large edifice followed by extrusion of minor eruptive deposits during its burial. We have summarized the key stages of this history in a schematic model for the evolution of large mud volcanoes based on the analysis of Chirag (Fig. 3.8).

Stage I involves the deposition of the “pioneer cone” which was sourced by a narrow (<10 m diameter) feeder conduit terminating at the surface as a volcanic crater (e.g. LUSI mud volcano, East Java, Davies et al. 2007). This was followed by initiation of focussed collapse of the edifice floor and development of the asymmetric caldera fault system, possibly as a result of localized depletion of the system’s source region. Further extrusive pulses took place during this phase resulting in the deposition of the edifice’s growth section (Stage II). We speculate that upon initiation of this phase the eruptive source point moved from the pioneer cone crater to the

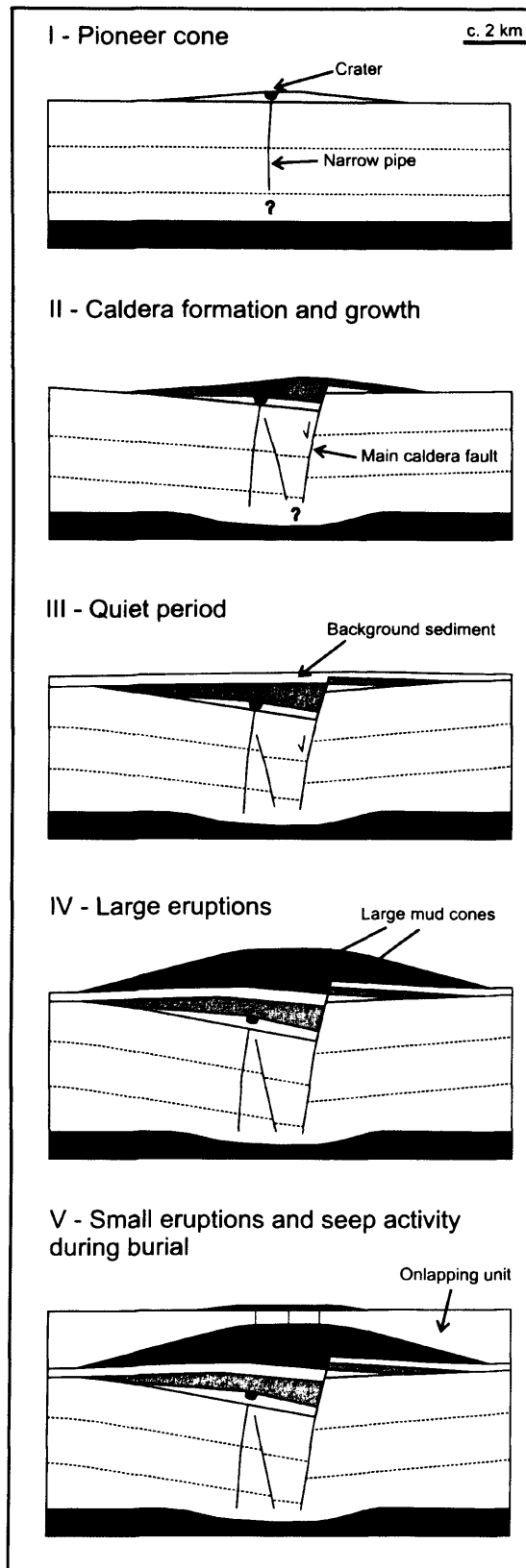


Figure 3.8 Schematic diagram showing a 5 stage model for the evolution and eruptive history of large mud volcano systems, based on the analysis of Chirag. See text for discussion.

caldera fault itself. Towards the end of the growth phase a break in eruptive activity resulted in the deposition of a layer of non-eruptive background sediment (Stage III). Later pulses of extrusion resulted in the deposition of large mud cones (Stage IV). By this stage caldera growth was minimal.

Following the phase of edifice construction, mud volcanism at Chirag appears to have continued during the deposition of the onlapping unit that overlies the stacked mud cones (Stage V). This period of extrusion did not result in the construction of mud cones as observed within the main edifice. This may be due to a lower eruptive volume, an increased background sedimentation rate, acceleration of fold growth or a reduction in the viscosity of the erupted mud. Fluids and sediment erupted during this late stage of the system's evolution may be the result of remobilization of previously erupted material within the underlying edifice as it is buried and compacted (Fig. 3.2).

3.5.2 Implications for fluid and sediment eruption

The composition of the Chirag edifice as a number of individual component mud cones suggests it was constructed by a number of discrete extrusive periods, rather than a single uninterrupted episode. With an average sediment volume of approximately 2.7 km^3 as the record of each pulse; each one is likely to have involved the release of considerable volumes of fluid (both liquids and gases) from the host sedimentary basin.

Pulsed fluid expulsion of this kind reflects periodic activity of the hydrodynamic system and supports the idea of some form of "on-off" trigger mechanism controlling the eruption pattern. Reasons for this pattern are uncertain. Possibilities range from repeated mechanical seal-failure and resealing events within the conduit system (Roberts and Nunn 1995; Sibson et al. 1988), to some form of temporal variation in the deeper hydrodynamic drive of the system and mud source output rate. Cyclical and pulsed fluid expulsion from sedimentary basins in general is a widely reported phenomenon observed in a range of tectonic settings (Bons and van Milligen 2001; Carson and Scream 1998; Hallager et al. 1990; MacDonald et al. 2000; Roberts and Nunn 1995).

This study suggests that pulsed fluid flow through large, long-lived mud volcano systems may be a volumetrically significant process of fluid and sediment expulsion from sedimentary basins. It highlights the importance of pulsed fluid-mud

expulsion patterns in controlling the internal architecture of large mud volcano edifices.

3.5.3 Comparison with igneous volcano systems

Difficulties in assessing caldera structure within the igneous realm arise because studies of most modern calderas are limited due to superficial exposure, their large dimensions, overprinting by other structures and deep erosion (Beresford and Cole 2000; Branney 1995; Lipman 1997; Smith et al. 2006). Well-imaged analogous systems from other volcanological domains are therefore of potentially high value to the study of igneous caldera structure and formation. Chirag is a pristine example of a well-imaged complex mud volcano system within which we can observe characteristics of both structural and eruptive style that are similar to many igneous volcano systems. These similarities highlight the potential of large mud volcano systems to act as important analogues for igneous volcano systems.

Firstly, the maximum displacement on the central trapdoor caldera fault is approximately 480 m which is comparable to direct measurements taken from the late Palaeozoic Glencoe and Ben Nevis calderas of Scotland, where at least 300 and 450 m, respectively, of downfaulting has been determined (Bailey and Maufe 1960). The 2 km diameter of the Chirag caldera falls within the broad range of typical igneous caldera sizes (<1 km – 40 x 75 km diameter) and has most in common with basaltic and andesitic calderas (Lipman 2000).

Secondly, characteristics of the volcano's eruptive history show a close similarity to igneous volcano systems. For example, Lipman (2000) has proposed a model of caldera-forming eruption cycles based on data from a range of igneous volcanoes. First is a phase of pre-collapse volcanism that is often sourced from a discrete central vent followed by a ring-vent phase and caldera-collapse (Cole et al. 2004; Kennedy et al. 2004). Finally the system undergoes a resurgence of magmatism that is most commonly focussed on the caldera fault zone. This model closely matches the evolutionary history of the Chirag edifice described above and depicted in Fig. 3.8.

3.6 Conclusions

3D seismic reflection data have been used in this study to describe the internal architecture of a large mud volcanic edifice leading to a reconstruction of the volcano system's eruptive history. In doing so we have recorded the evolutionary history of a large focussed fluid flow system in a tectonically active sedimentary basin. The key elements of this eruptive history have been presented in a new model of mud volcano system evolution, which may be applicable to other large mud volcano systems. Characteristics of the eruptive history highlight the importance of pulsed fluid flow through long-lived mud volcano systems as a mechanism of fluid and sediment expulsion from sedimentary basins. The duration and frequency of each pulse is important in controlling the internal architecture of large mud volcano edifices. Strong structural and evolutionary similarities can be observed between the studied mud volcano system and magmatic volcanoes. This supports the notion that large mud volcano systems may act as important analogues for igneous volcano systems.

3.7 Acknowledgements

The authors would like to thank BP for the provision of data used in this study and NERC for provision of award number NER/S/C/2004/12724 that supports the research. We are also grateful to Schlumberger GeoQuest for the provision of IESX and GeoViz software package. We thank Sverre Planke and Ben Clennell for helpful reviews and members of the 3D Lab at Cardiff University for helpful discussion. The technical conclusions presented here do not necessarily represent the opinions of BP or the AIOC Partnership.

CHAPTER FOUR

4.0 Phase-reversed seabed reflections in seismic data: examples related to mud volcanoes from the South Caspian Sea¹

4.1 Abstract

The sediment-water interface is usually marked by an increase in acoustic impedance and is therefore displayed in a seismic section as a positive polarity reflection. Here we use the term “seabed phase reversal” to describe areas of seafloor which are instead expressed as a negative polarity reflection in seismic data. We describe in detail a number of examples of seafloor phase reversals and use a simple 1D geophysical model to test the hypothesis that they are the result of the presence of gas within the seafloor sediment. Our examples are all related to seismically-imaged mud volcanoes located within the South Caspian Sea. Sections of phase-reversed seafloor at the summit area of these volcanoes have been mapped to reveal the existence of seafloor mud pools (salses) and recently erupted mud flows which show a strong similarity to smaller scale features at onshore volcanoes in Azerbaijan. Synthetic geophysical modelling indicates that under the physical conditions likely to occur when the seabed sediment is gas-bearing the seafloor will be expressed as a strong negative polarity reflection. Unlike other indicators of seafloor gas, such as pockmarks, which merely record the transient expulsion of fluids from sedimentary basins, seafloor phase reversals indicate the presence of gas in marine sediment at the time of survey acquisition. They therefore are of significance to engineering and site survey operations as well as the identification of biological communities and gas flux calculations.

¹Published as:

Evans R.J. et al. 2007. Phase-reversed seabed reflections in seismic data: examples related to mud volcanoes from the South Caspian Sea. *Geo-Marine Letters*, 27(2/3), pp. 203-212.

4.2 Introduction

The acoustic properties of the sediment-water interface are of considerable interest in underwater acoustics, geophysics, ocean engineering and naval applications (Anderson and Bryant 1990; Gorgas et al. 2003; Hamilton and Bachman 1982). The presence of gas in seabed sediment can significantly modify its acoustic and physical properties and evidence of gas is frequently observed in seismic profiles (Anderson and Bryant 1990; Gorgas et al. 2003; Hamilton and Bachman 1982; Judd and Hovland 1992; Yuan et al. 1992). Acoustic phenomena such as gas chimneys, reduced signal to noise and bright spots are accepted as generally reliable indicators of the presence of gas in a section (Fannin 1980; Gorgas et al. 2003; Hovland 2003; Judd and Hovland 1992; Schroot et al. 2005).

However, one particular feature that is often seen but so far has gone without rigorous geophysical examination is the expression of the seabed as a negative polarity reflection in seismic data (here termed “seabed phase reversals”). In general, we expect a positive polarity reflection at the seabed as the acoustic impedance of seabed sediment is usually greater than that of seawater. We have found many examples where this is not the case in our South Caspian Basin study area (Fig. 4.1a). All of these are related to mud volcanoes and are most likely to be caused by the presence of gas within the seabed sediments (Fig. 4.1b). In this study we aim to describe and explain the phenomena of seabed phase reversals using seismic data from an area of the South Caspian Sea located approximately 100 km SE of Baku, offshore Azerbaijan (Fig. 4.1a), combined with field observations and reference to published information on the geophysical properties of gas-bearing sediment.

Previous studies have noted the occurrence of seabed phase reversals and “soft-bottom” areas of negative acoustic impedance associated with mud volcanoes (Fowler et al. 2000), mud domes (Fowler et al. 2000; Roberts 1996; Sager et al. 2003) and other gas seepages (Schroot et al. 2005). However, they have not been described in detail and no attempt has been made to explain them in terms of the physical conditions that cause them. Phase reversals associated with sub-seabed gas accumulations are more widely recognized as an important indicator of shallow gas in seismic data (Anderson and Bryant 1990; Judd and Hovland 1992; Yin et al. 2003). The gas associated with acoustic phenomena is generally considered to be methane (Judd and Hovland 1982).

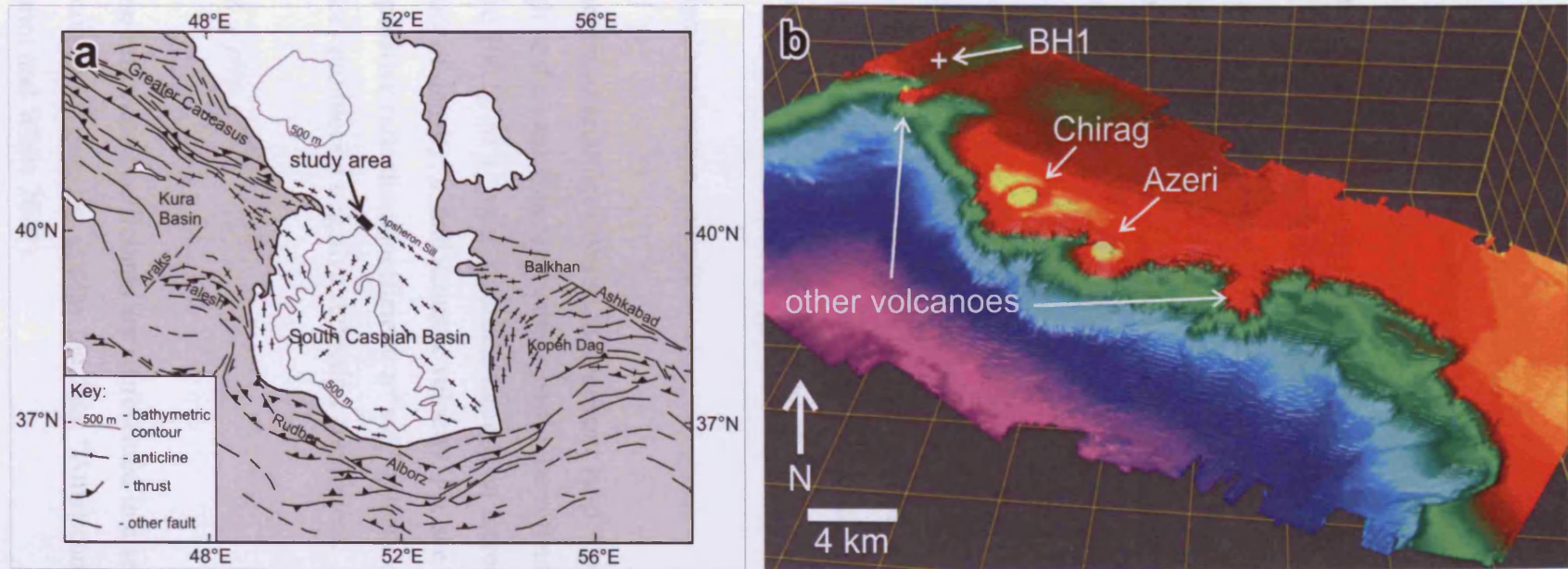


Figure 4.1 (a) Tectonic map of the South Caspian Basin and surrounding area showing position of study area within South Caspian Sea. Modified from (Jackson et al. 2002). (b) 3D seabed depth map of the study area seabed showing the position of major mud volcanoes at the shelf break.

4.2.1 Mud volcanoes and fluid expulsion

Mud volcanoes are important focussed fluid flow systems that facilitate the expulsion of liquid, gas and sediment to the Earth's surface from up to 20 kilometres depth (Dimitrov 2002; Kopf 2002). They have been documented in a range of tectonic settings and tens of thousands appear to be present globally (Davies and Stewart 2005; Evans et al. 2007a; Kopf 2002; Milkov et al. 2003; Stewart and Davies 2006). Erupted gas, which is generally >95% methane, is very commonly associated with mud volcanic eruption (Judd 2005; Kopf 2002).

Where mud volcanoes are present onshore, evidence for methane expulsion is abundant (Hovland et al. 1997; Etiope et al. 2004). This can include bubbling mud pools (termed salses, Fig. 4.2a) and large (>100 m high) gas flares that result from the ignition of methane during eruption (Planke et al. 2003). The deposits of mud volcanoes also show evidence to suggest that they are gas-bearing when erupted, in the form of small (2-4 mm diameter) ellipsoidal voids observed within terrestrial mud flows (Fig. 4.2b). These are similar in shape, size and process of origin to gas-expulsion vesicles in lava flows (Cashman et al. 2000).

4.2.2 Seismic reflection polarity

For symmetrical seismic wavelets, a dominant loop “polarity” describes whether it is the trough or the peak that represents a particular reflection type; hard or soft (Simm and White 2002). At a “hard” interface there is an increase in acoustic impedance (Z , the product of density, ρ , and acoustic velocity, V_p , see Eq. 4.1 below) and this gives rise to a positive reflection coefficient; a “soft” interface (decrease in acoustic impedance) produces a negative reflection coefficient.

$$Z = \rho V_p \quad \text{(Equation 4.1)}$$

How these reflection coefficients are represented in a seismic section depends on the polarity convention used to display the data; “American” or “European” (Brown 1999; Simm and White 2002).

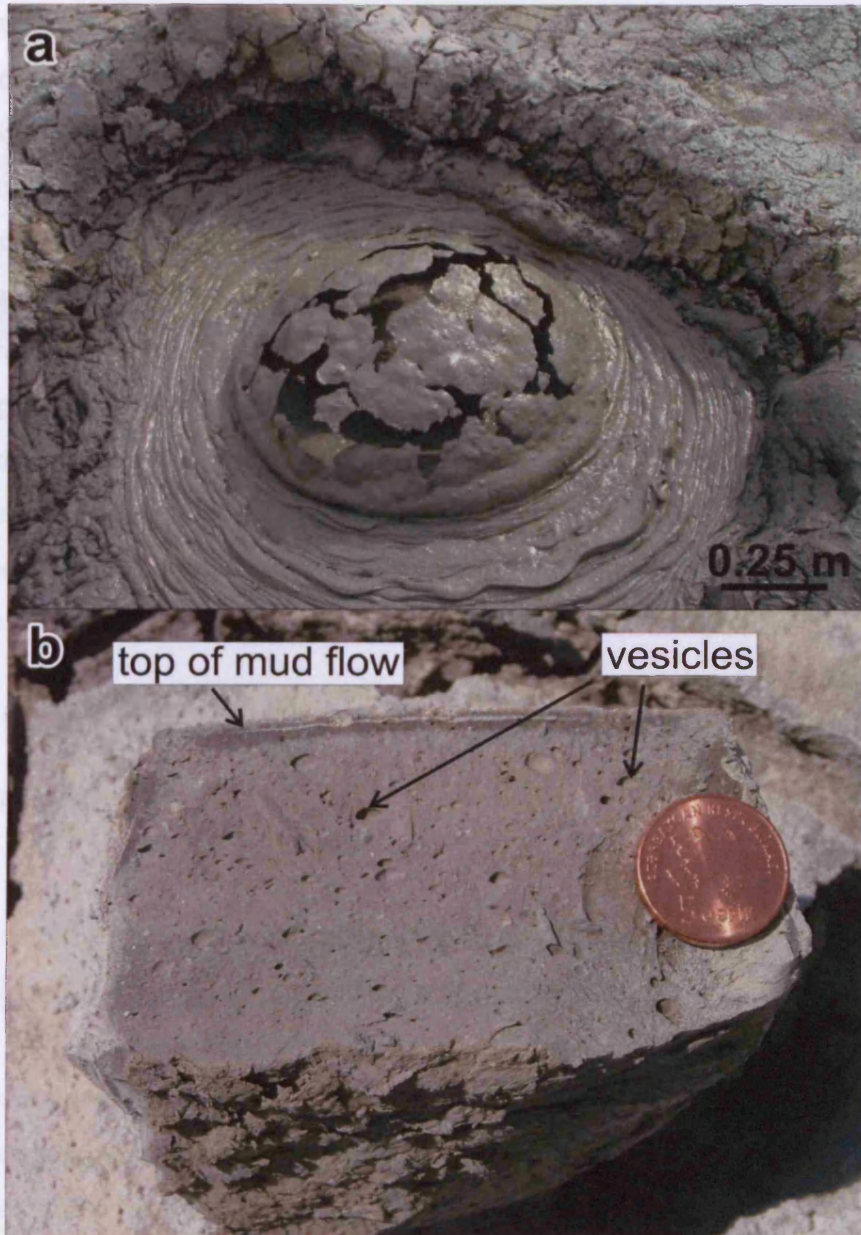


Figure 4.2 Evidence for gas expulsion during mud volcanic extrusion: (a) Photograph of a bursting gas bubble within a gryphon (small mud cone) at the summit of an Azerbaijan mud volcano. (b) Hand specimen-scale evidence for gas release from mud volcano deposits. Photograph of a vertical slice through a recent Azerbaijan volcano mud flow showing gas vesicles within the sediment. Coin for scale.

In general, we expect an increase in acoustic impedance across the sediment water interface because seabed sediment usually has a greater bulk density and hence acoustic impedance than seawater. In cases where the acoustic velocity of sediment is lower than that of seawater (not usually more than 3% lower), the density contrast between the two is still sufficient to account for an increase in acoustic impedance (Hamilton 1970; Hamilton and Bachman 1982).

However, if gas is present within the seabed sediment, its physical and acoustic properties are likely to be significantly modified (Fu et al. 1996; Hamilton 1970; Hamilton and Bachman 1982). Important modifications include a decrease in the sediment's bulk modulus (Anderson 1992), bulk density (ρ) and shear modulus (μ). These changes cause a reduction in the sediment's acoustic velocity (V_p , see Eq. 4.2 below).

$$V_p = \sqrt{\frac{\kappa + \frac{4}{3}\mu}{\rho}} \quad (\text{Equation 4.2})$$

The acoustic impedance of gas-bearing sediments will therefore be lower than of the same sediment if it were 100% saturated with seawater. If the volume of gas is sufficient to lower the sediment's acoustic impedance to less than that of the seawater then the seabed will be expressed as a negative polarity reflection in a seismic section. It is appropriate to term a lateral change in seismic reflection polarity from positive to negative a "phase reversal" as it is equivalent to a phase shift of 180° (Simm and White 2002).

4.3 Materials and methods

We begin by describing examples of mud volcano-related seabed phase reversals from the South Caspian Sea that are imaged by 3D and "high-resolution" 2D seismic reflection data. We then test the hypothesis that these phase reversals are the result of gas presence by constructing synthetic seismograms from sonic and density calibrations of the shallow sediments and the water column of the area, under normal and gassy conditions.

4.3.1 Seismic reflection data

The 3D seismic data image a number of kilometre-scale mud volcanoes, some of which are believed to be currently active as sites of fluid and sediment expulsion (Fig. 4.1b). Line spacing of the 3D data is 12.5 m and vertical resolution at a depth of 100 m is approximately 8 m. These data conform to the SEG (Society of Exploration Geophysicists) standard American polarity convention whereby an increase in acoustic impedance across an interface is represented by an amplitude peak (coloured red), a decrease in acoustic impedance is represented by an amplitude trough (coloured black, Brown 1999). The “high-resolution” 2D data also conform to the SEG American polarity convention although a positive polarity reflection is coloured blue and a negative is coloured red. The vertical resolution of these data at approximately 100 m depth is approximately 4 m although coverage is restricted to a small number of lines.

4.3.2 Synthetic seismic modelling

The parameters used to model both normal and gassy seabed conditions have been constrained by wireline data acquired within a shallow site investigation borehole located in the study area (BH1 in Fig. 4.1b) combined with details from a range of other sources. These properties and their sources are shown in the well log curves in Figure 4.3. Synthetic seismograms were generated from the geological model using the Landmark Graphic Corporation software SynTool. The wavelet used is a zero-phase 50 Hz Ricker.

For normal, non-gassy seabed conditions we have used a combination of shallow sonic log and extrapolated well checkshot survey data to constrain the seismic velocity of the seabed sediment (Fig. 4.3a). For sediment density we have modified a shallow density profile from within BH1 to reflect the likely conditions at the seabed as suggested by Hamilton and Bachman (1982, Fig. 4.3a). Our resultant values of 1459 m sec^{-1} V_p and 1.48 g cm^{-3} ρ are in good agreement with published values for the average velocity and bulk density of seabed silt in a continental shelf setting (Hamilton and Bachman 1982).

The geological model has been adapted to predict the response of the seismic data to the presence of gas within the seabed sediment by substituting the likely properties

of gas-bearing seabed sediments from a range of other studies into the sonic and density profiles measured in BH1 (Fig. 4.3b). According to published work on gas-bearing sediment acoustics, the acoustic velocity of the seabed sediment is likely to be reduced by between 15-50% from normal (Anderson and Bryant 1990; Edrington and Calloway 1984; Fu et al. 1996; Hamilton 1970; Hamilton and Bachman 1982; Yuan et al. 1992). At the centre of this suggested range a 32.5% reduction in sediment acoustic velocity from our non-gassy value is 984 m sec^{-1} . We take this value to be a fair estimate of the velocity of gas-bearing seabed sediment and use it in our calculations here. The bulk density of gas-bearing mud volcano deposits is poorly constrained due to a lack of direct measurements within the study area or elsewhere. However, a recent submersible investigation of a Nile Delta mud volcano has found that an area of seafloor that appears phase-reversed in seismic data consists of very soft and fluid clay which easily moves into suspension with only a slight disturbance and is very slow to settle (E. Deville 2006 *pers. comm.*). The sediment contains numerous gas bubbles which stream from the surface when disturbed by sampling equipment. It is therefore likely that the gas-bearing sediment in this example has a bulk density only slightly greater than that of seawater. Direct measurements of mud flows associated with mud volcanoes in the Mediterranean Ridge have yielded density values of as low as 1.2 g cm^{-3} (Kopf and Behrmann 2000). We adopt this value as our chosen density value for gas-bearing sediment.

The velocity of Caspian Sea water is constrained as 1453 msec^{-1} by direct measurements of velocity throughout the water column and is integrated into our geophysical model (Fig. 4.3). The water density at the seabed has been calculated as 1.028 g cm^{-3} using the equation of state for seawater (Fofonoff 1985). The value was calculated for a depth of 150 m, a salinity value for the Caspian bottom waters of 13 Practical Salinity Units (Millero and Chetirkin 1980), and a temperature value of 7°C as indicated by recent unpublished direct measurements.

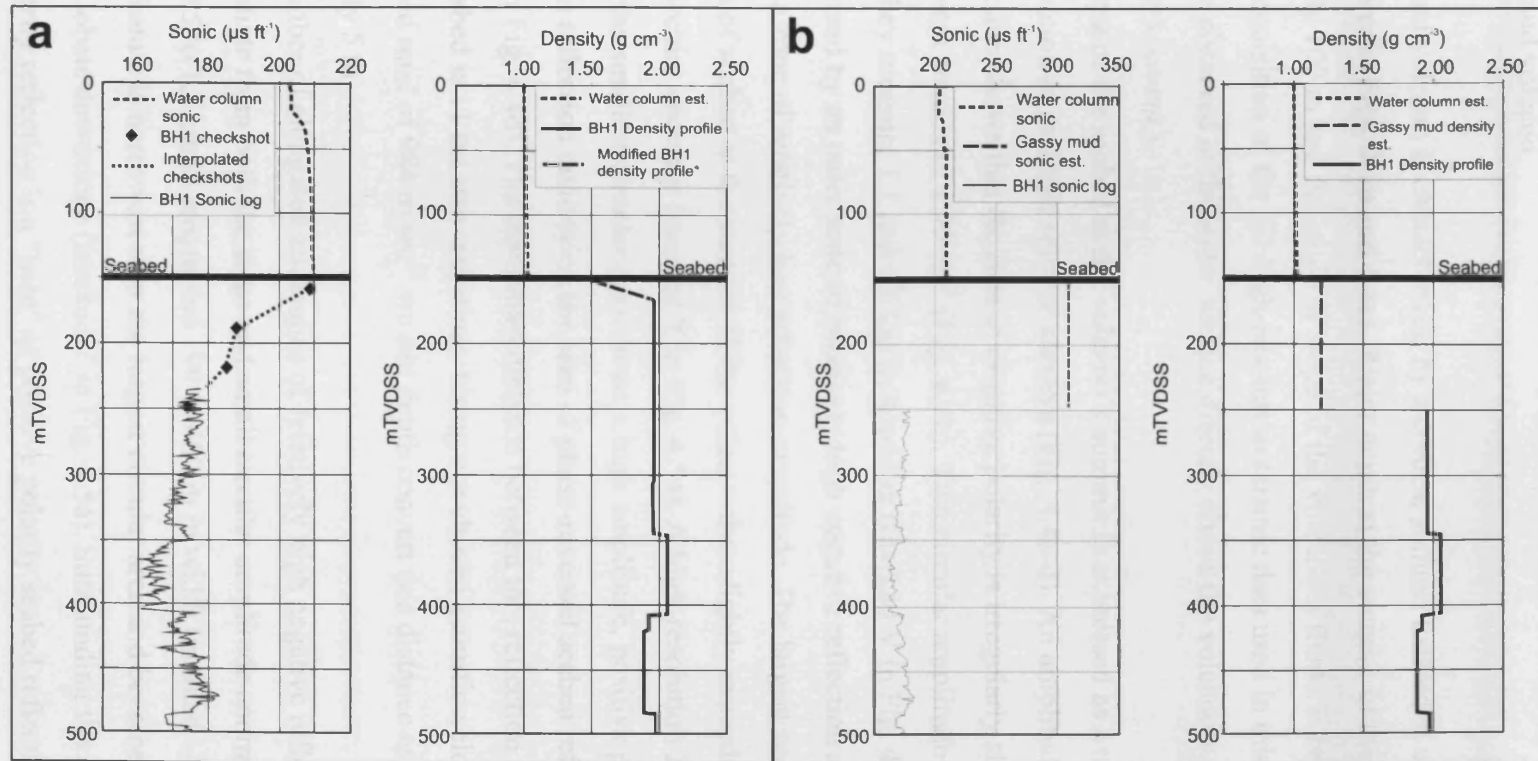


Figure 4.3 Composite depth profile curves showing geophysical model input data: (a) Composite sonic and density profiles for physical properties of normal non-gassy seabed conditions. (b) Composite sonic and density profiles for physical properties of gassy seabed conditions. Line styles indicate the data source for both figure parts. See text for further discussion. TVDSS = true vertical distance sub-sea. *Data source Hamilton and Bachman (1982).

4.4 Seismic interpretation

3.4.1 Azeri mud volcano

The Azeri mud volcano is characterized by a conical summit located at a well-defined shelf-slope break (Figs. 4.1b and 4.4a). Water depth at the summit of the volcano is approximately 100 m and the angle of slope of the volcanoes flanks is between 3 and 4°. During acquisition of the 2D high-resolution seismic data used in this study gas bubbles were observed at the water surface directly above the volcano's summit (A. Hill 2005, *pers. comm.*).

An area of the seabed at the volcano's summit is expressed as a negative polarity reflection in multiple seismic surveys (Fig. 4.4a-d). An amplitude map of the seabed reflection shows that the area of negative polarity is irregularly shaped in plan view and covers an area of 1.95 km² (Fig. 4.4b). Two circular amplitude anomalies are visible; they measure 1.1 and 0.6 km in diameter (marked V in Fig. 4.4b). Both are characterized by an outer zone of relatively high negative reflection amplitude surrounding a zone of relatively low reflection amplitude. The largest zone is located on a flat area of seabed at the summit of the volcano that slightly exceeds the surface area of the circular anomaly (marked Y in Fig. 4.5a). A high-resolution 2D seismic line through the smallest circular area shows a high amplitude, positive polarity, convex-down reflection underlying the area of phase-reversed seabed reflection (marked X in Fig. 4.4d). The maximum distance between this reflection and the overlying seabed is 11 ms two-way-time. Using our chosen acoustic velocity for gas-bearing seabed mud of 984 m sec⁻¹ we can depth convert this distance as approximately 5 m.

A number of elongated anomalies of relatively high negative reflection amplitude radiate from both the large and small circular amplitude anomalies. These range from 0.5 to 1.2 km in length and 190 to 400 m in width (marked U in Fig. 4.4b). The largest feature is narrowest near the largest circular area and becomes wider and increasingly lobate downslope (marked Z in Fig. 4.5a). Surrounding the area of negative polarity reflection is a "halo" of positive polarity seabed reflection that has a reduced amplitude (marked W in Fig. 4.4b). Beneath the area of negative polarity reflection, the seismic image quality is poor, possibly as a result of attenuation and scattering of acoustic energy due to gas. A number of clear seabed multiples can be

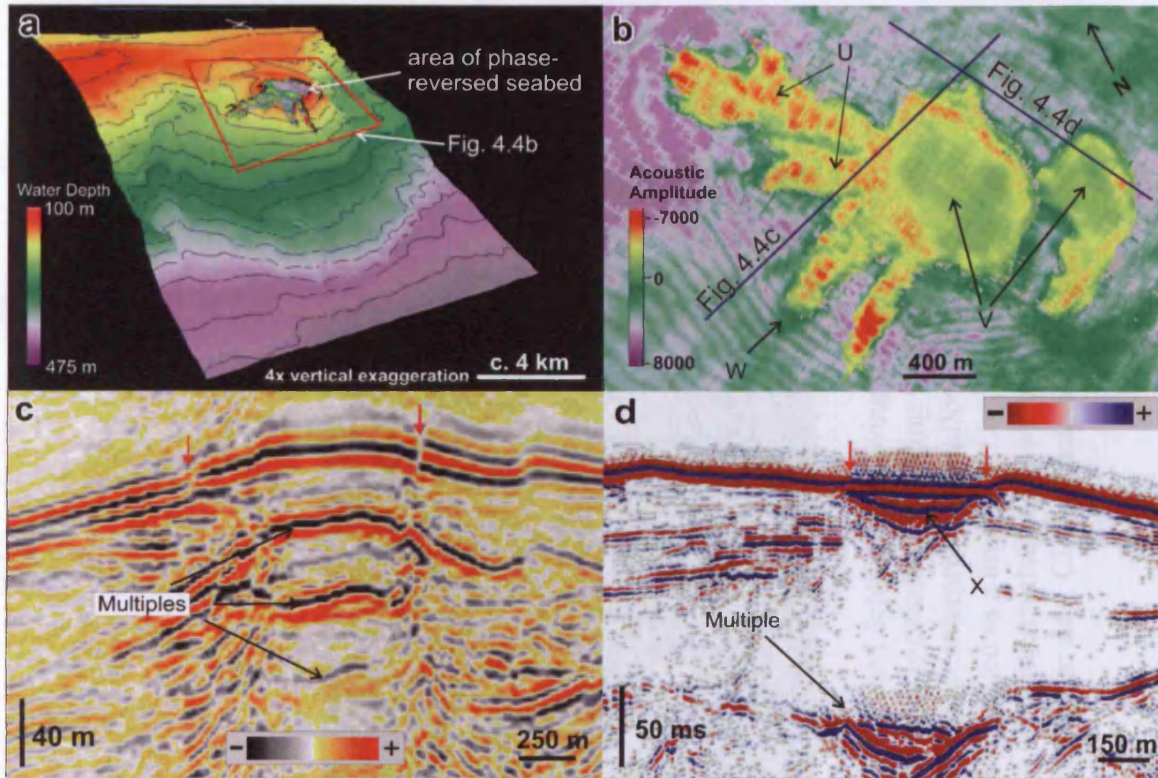


Figure 4.4 The Azeri mud volcano: (a) 3D bathymetric map of the seabed at the site of the Azeri mud volcano. Note the conical shape of the volcano's summit and the area of phase-reversed seabed reflection at the volcano summit. The phase-reversed section is coloured according to its acoustic amplitude; see Fig. 4.4b for further details. (b) Acoustic amplitude map of the phase-reversed section of seafloor at the Azeri mud volcano summit. U= Linear negative amplitude anomalies interpreted as seafloor mudflows, V= Circular amplitude anomalies of relatively low reflection amplitude interpreted as seafloor salses, W= "halo" of reduced positive reflection amplitude surrounding phase-reversed section of seafloor reflection; this is interpreted to be the result of the progressive de-gassing of gas-bearing sediment within the phase-reversed area. Map location shown on Fig. 4.4a. (c) Representative seismic section through the Azeri volcano showing the character of the phase reversal. The seabed phase reversal occurs in the area between the vertical arrows. See Fig. 4.4b for section location (d) "High-resolution" seismic profile through the Azeri volcano showing the character of the phase reversal, which occurs between the vertical arrows. X= The convex-downward positive polarity reflection interpreted as the base of a seafloor salse. See Fig. 4.4b for section location.

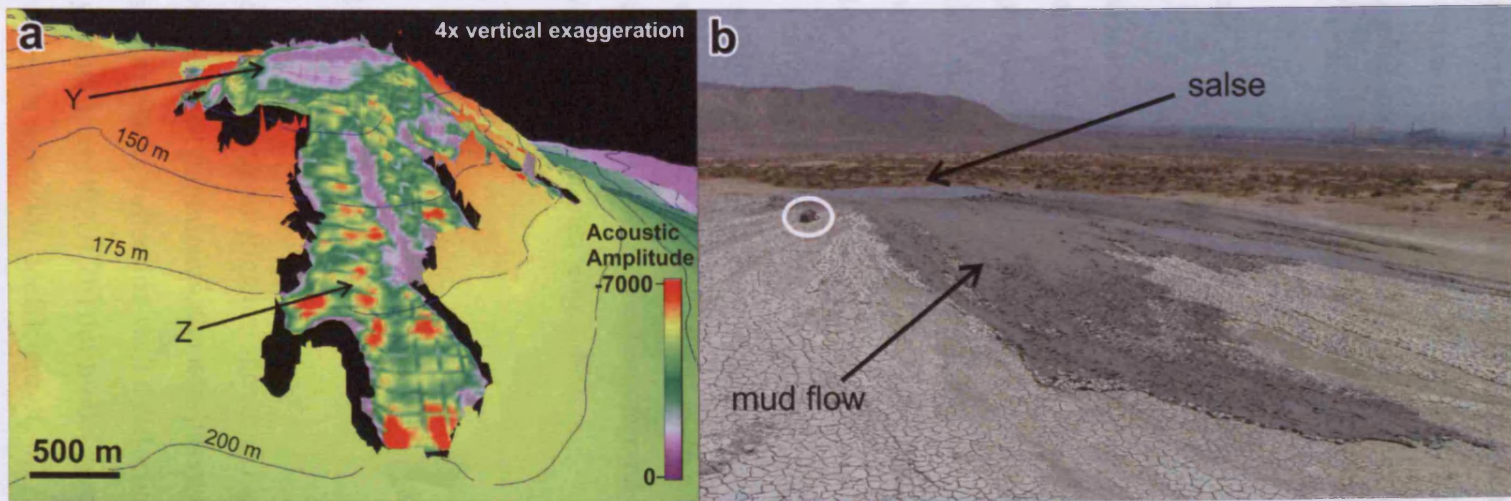


Figure 4.5 Seafloor salse and mudflows of the Azeri mud volcano: (a) 3D seabed depth map showing the relationship between the seafloor salse and mud flows. The phase-reversed area of seafloor is coloured according to acoustic amplitude. Y= Circular amplitude anomaly that corresponds to flat summit area of volcano; interpreted as seafloor salse. Z= Linear and lobate amplitude anomaly radiating from the seafloor salse; this is interpreted as a mudflow. Location of phase-reversed area is shown on Fig. 4.4a. (b) Photograph of the Garadag mud volcano, Azerbaijan showing mud flows originating from a salse similar to that observed at Azeri mud volcano in seismic data. Circled rucksack for scale.

observed in the blanked zone (Fig. 4.4c and d). These are only present in the area beneath the negative polarity seabed reflection. Their closely repeating pattern shows a strong similarity to the geophysical artefact “acoustic ringing” which has been observed beneath the area of negative polarity reflection. The seismic image quality is poor, possibly as a result of attenuation and scattering of acoustic energy due to gas. A number of clear seabed multiples can be identified in other areas where gas is present in the seabed sediment (Anderson and Bryant 1990).

4.4.2 Chirag mud volcano

The Chirag mud volcano is the largest in the study area and consists of a buried edifice complex of up to 1.4 km thickness (Evans et al. 2007a). Like Azeri, Chirag is situated at the shelf-slope break in approximately 110 m of water but is characterized by a flat rather than conical summit (Fig. 4.6a). At the centre of this summit is a sub-circular moat that is approximately 12 m deep and 450 m wide. It surrounds an area of slightly convex-up seafloor that measures up to 1.7 km in diameter and covers an area of 2.2 km². This part of seafloor is expressed as a negative polarity reflection in multiple seismic surveys (Fig. 4.6b). No obvious amplitude anomalies are present within or outside this area of negative polarity reflection. In a similar manner to Azeri, the area beneath this negative polarity seabed is characterized by poor image quality and a number of acoustic ringing multiples (Fig. 4.6b).

4.5 Results

4.5.1 Synthetic seismograms

The results of the synthetic seismic modelling are shown in Figure 4.7. It can be seen that, according to our chosen input parameters, the non-gassy sediment-water interface produces a positive polarity reflection with a reflection coefficient of 0.18 (Fig. 4.7a). Under gassy conditions (Fig. 4.7b) our model predicts that a negative polarity seabed reflection with a reflection coefficient of -0.12 would be created. This suggests that a negative polarity seabed reflection is a geophysical possibility when the seabed sediment is gassy. In addition this model shows a clear very high amplitude reflection at the base of the gas bearing section of mud (250 m depth in Fig.

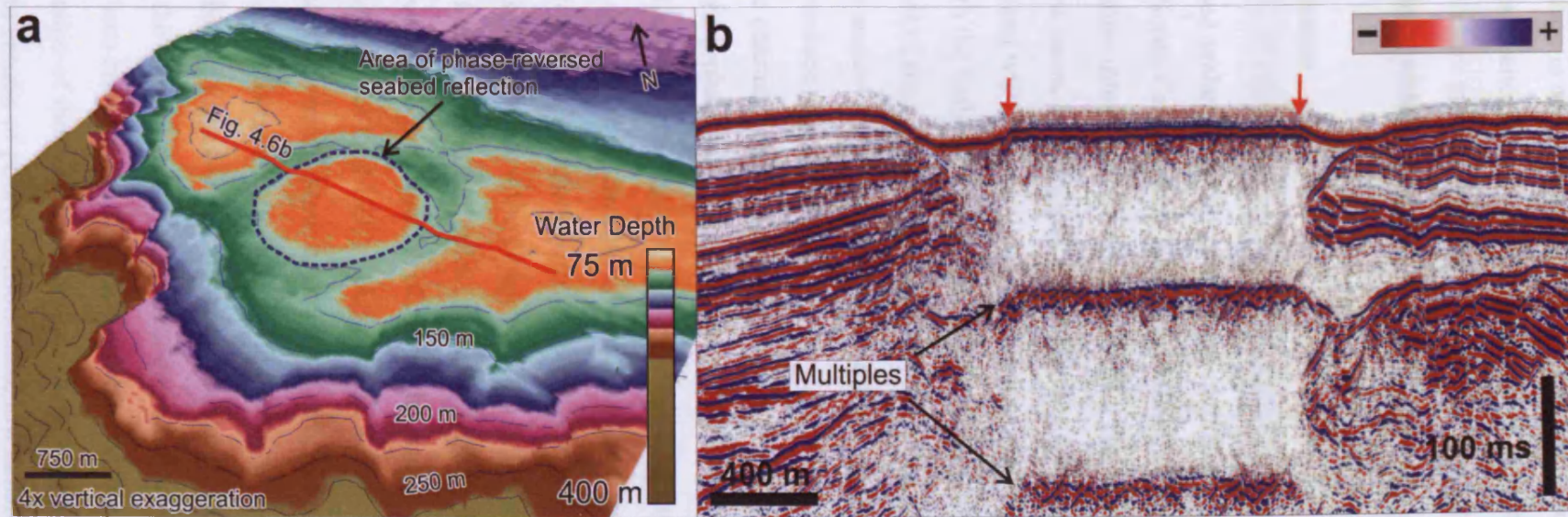


Figure 4.6 The Chirag mud volcano: (a) 3D seabed bathymetric map showing morphology of the volcano at the seabed. An area of phase-reversed seabed reflection is marked by the blue dashed line. (b) “High-resolution” seismic profile through the Chirag volcano showing the character of the phase reversal. See Figure 6a for section location. Vertical arrows indicate the position of the blue line shown in Figure 4.6a.

4.7b). A similar reflection is observed in the seismic data as the convex-down positive polarity reflection 11 ms beneath the Azeri volcano seabed (Fig. 4.4d). Both the reflection coefficient values predicted by our model are sufficient to produce a clear high amplitude reflection, which is consistent with the real data.

4.5.2 Seismic interpretation

Areas of phase-reversed seabed reflection have been identified at two large mud volcanoes within the South Caspian Sea. In both cases the possibility of faulting accounting for the feature interpreted as a phase reversal can be ruled out. This is due to the fact that, in most cases, fault-related interpretations would require the phase-reversed area to be raised with respect to the surrounding seabed (e.g. Fig. 4.4c), which does not fit with the bathymetry data. Where the phase-reversed area is located slightly below the level of the surrounding seabed the clear high amplitude and zero-phase character of the negative polarity reflection strongly suggests that it represents the sediment-water interface (e.g. Fig. 4.4d).

In all cases the character of the phase-reversed wavelet is similar and almost always appears to be zero-phase indicating that the polarity has been reversed a full 180° (Brown 1999). This suggests that the feature cannot be accounted for by a smaller degree phase shift ($<180^\circ$), the kind of which can be observed in association with other direct hydrocarbon indicators (Brown 1999). The presence of considerable blanking of the seismic record below the phase-reversed reflections together with the presence of a series of clear seabed multiples (acoustic ringing) is evidence to link the origin of the phase reversals to the presence of gas in the seabed sediment (Anderson and Bryant 1990; Judd and Hovland 1992; Schroot et al. 2005).

At Azeri the complex areal extent of the phase-reversed seabed area reveals details of the depositional processes associated with the volcano's eruption. The elongated features radiating from two circular areas are interpreted as mud flows that have originated from the summit area of the volcano. Each flow is observed to originate from one of two circular and flat phase reversed areas of seafloor. The phase-reversed expression of these areas in the seismic data indicates that the seabed within them is likely to consist of poorly consolidated, low density and low acoustic velocity, gas-bearing sediment. They are therefore most likely to consist of recently erupted and deposited mud volcanic sediment (Roberts et al. 2006). Their lack of

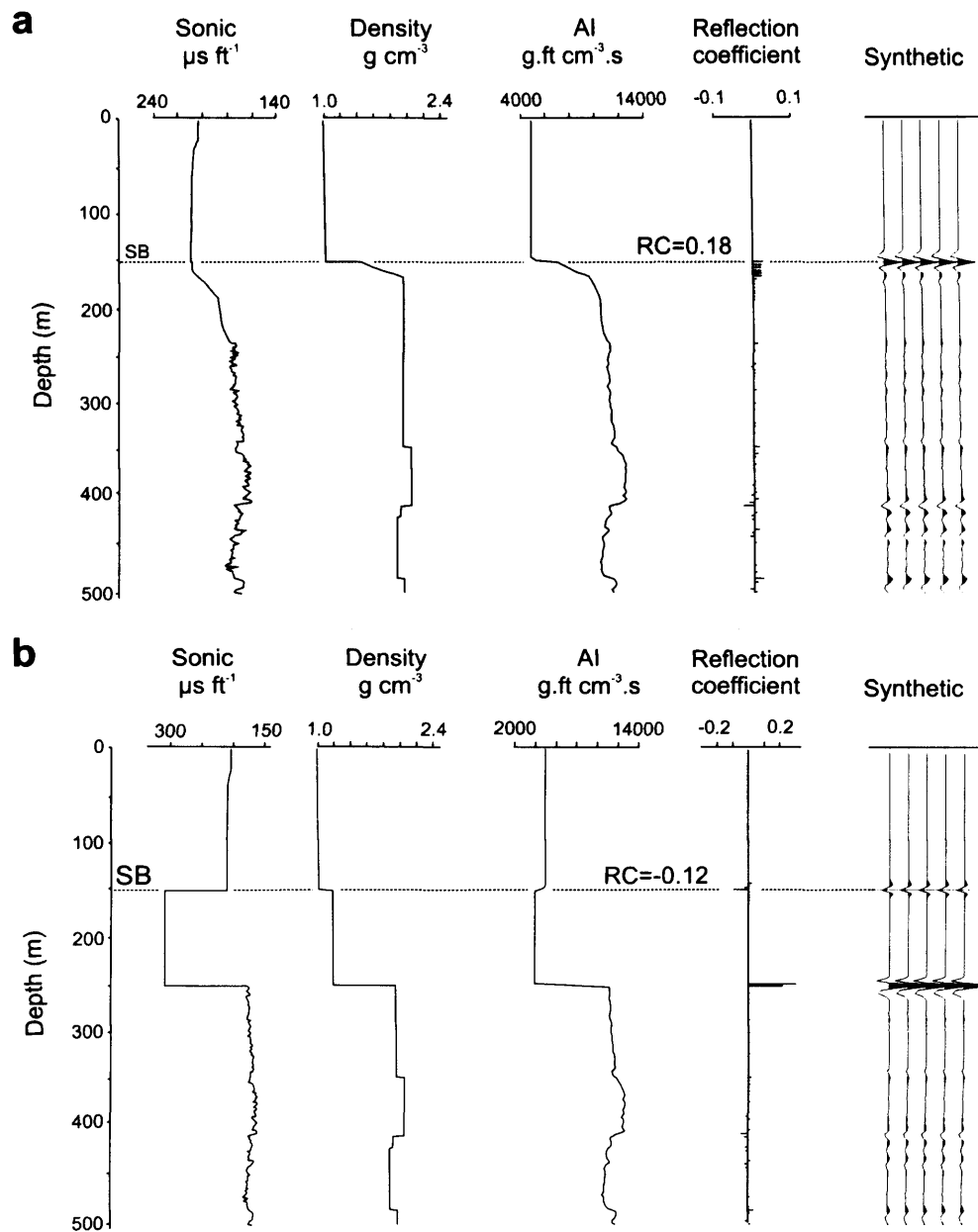


Figure 4.7 Results of synthetic seismic modelling: SynTool synthetic seismogram panel showing (a) Results of non-gassy geological model convolved with a 50 Hz zero-phase Ricker wavelet. (b) Results of gassy seabed geological model convolved with a 50 Hz zero-phase Ricker wavelet. AI = acoustic impedance, SB = seabed

bathymetric relief and sub-circular extent suggests one possibility to be that the circular zones represent submarine salses, similar to those observed on land (Fig. 4.5b). This interpretation is supported by the positive polarity convex-down geometry of the reflection that underlies the smallest Azeri circular area, which we interpret as the base of one of the seafloor salses (Fig. 4.4d). Our synthetic modelling has produced a similar reflection to this at the base of the section of gassy sediment that represents the interface between gassy and non-gassy sediment (Fig. 4.7).

The slightly convex-up bathymetric expression of the Chirag phase-reversed area indicates that is not likely to represent the surface of a seafloor salse as seen at Azeri. Instead we interpret this zone to represent a subdued area of predominantly recent mud extrusion consisting of firmer and more consolidated gassy sediment.

4.6 Discussion

The seismic interpretation and synthetic modelling presented in this study indicates that seabed phase reversals in seismic data are most likely to be the result of the presence of low density and low acoustic velocity, gassy mud volcanic sediment at the seabed. At Azeri the phase-reversed zone is likely to consist of a pair of submarine salses filled with very poorly consolidated gassy sediment that source a series of mud flows. Similar features have been identified at the centre of mud mounds in the Barbados accretionary prism and have been termed “mud lakes” (Lance et al. 1998). At Chirag the circular phase-reversed zone is likely to consist of an area of a firmer and more consolidated area of gassy sediment that has formed a slight build up on the seafloor.

The presence of a number of kilometre-scale mud flows originating from the two submarine salses at Azeri is an indication that they can be the source of considerable volumes of eruptive material. The fact that these flows are phase-reversed indicates that extruded material was gas-bearing when erupted and remained so as it is transported and deposited; an interpretation supported by the presence of gas-expulsion vesicles within terrestrial mud volcano flows (Fig. 4.2b). Many small salses in the mud volcanoes of Azerbaijan act as the source points for numerous small-scale mud flows in a manner directly analogous to that suggested by the Azeri volcano seabed image (Fig. 4.5b). Using eruptive patterns of onshore salses we can infer that mud delivered from the feeder system is not immediately deposited as flows

or other depositional features. It is likely that flows will occur only when the salse level rises to a point when it can breach its edges. Prior to this any mud and gas delivered to the surface is likely to be temporarily stored at the seabed within the salse. Indeed, the presence of a phase-reversed seabed reflection in general suggests that some of the gas delivered to the surface is retained within the sediment and not immediately released to the atmosphere. During this “lag time” between gas delivery to the surface and release to the atmosphere the gas is available for oxidation by methanotrophic bacteria (Kruger et al. 2005). The duration of the lag time may therefore be an important consideration when calculating methane flux from mud volcanoes as it can influence the net amount of gas eventually delivered to the ocean and atmosphere.

The reliable identification of areas of gassy seabed sediment is of vital importance to underwater engineering operations as they are likely to represent an area of difficult ground in terms of foundation location, drilling or acoustic survey design (Sills and Wheeler 1992). For many years acoustic phenomena such as zones of acoustic turbidity and gas chimneys have been utilised for shallow gas hazard identification. However, only a limited number of these phenomena are able to confirm the actual seepage of fluids through the seabed (e.g. hydroacoustic “plumes”, (Greinert et al. 2006; Hovland 2003; Parnell and Schwab 2003). Morphological features such as pockmarks, and indeed mud volcanoes, are often relied upon for this purpose but these alone are merely a record of fluid flow at one time and do not necessarily indicate the fluid expulsion system to be presently active. Indeed some mud volcanoes have been found to be covered with non-volcanic sediment suggesting prolonged periods of inactivity (Kopf and Behrmann 2000). If coupled with a seabed phase reversal then mud volcanoes, pockmarks and flat areas of seafloor become more significant as indicators of the very recent expulsion of gas through the seabed, and the presence of patches of gas-bearing sediment. They therefore have significance to engineering and site surveying operations as well as the identification of likely sites of chemosynthetic biological communities.

4.7 Conclusions

This study has documented examples of seabed phase reversals associated with mud volcanoes and has shown that the most likely cause of their occurrence is the presence

of gas within the seabed sediment. Mapping the lateral extent of phase-reversed zones using 3D seismic data may be an effective approach in identifying and imaging recently-erupted mud volcano deposits.

The low topographic relief of some phase-reversed zones together with their circular shape suggests an origin similar to that of salses identified in other areas, particularly on land. This indicates that the source point of mud volcano edifices can be the site of mud and fluid storage prior to flow deposition sourced from the margins of the salse. Other phase-reversed areas may consist of firmer and more consolidated zones of gassy sediment extrusion and accumulation.

In general, seabed phase reversals indicate the presence of gassy seabed conditions and are therefore important gas-indicators for surveying or engineering operations. They further indicate the temporary storage of gas within erupted seabed sediment prior to its release into the water column or atmosphere. During this lag time between eruption, gas delivery to the surface and its subsequent release the total volume of erupted methane is likely to be reduced by microbial oxidation. Therefore a consideration of the duration of the lag time may be important to calculations of methane flux to the atmosphere from mud volcanoes.

The synthetic seismic modelling carried out in this study has demonstrated that, under the physical conditions typical of gassy seabed sediment, areas of seabed can be expressed as negative polarity reflections in seismic data. This strengthens our interpretation of the seabed anomalies as gas-related phase reversals.

4.8 Acknowledgements

The authors would like to acknowledge the National Environment Research Council (NERC) for provision of award number NER/S/C/2004/12724 that supports this research. Also BP Azerbaijan for provision of seismic and well data and Schlumberger Geoquest for provision of IESX and GeoViz interpretation software. We are grateful to Alan Judd and another anonymous reviewer for their helpful reviews and comments. Andrew Hill, Eric Deville and Mads Huuse are thanked for help with data provision and technical discussion.

CHAPTER FIVE

5.0 Mud volcano subsidence craters onshore and offshore Azerbaijan¹

5.1 Abstract

Circular depressions bound by inward-dipping faults found at the upper terminations of large mud volcano systems (>500 m diameter) are termed “mud volcano subsidence craters”. From new mapping we describe a series of common structural and morphological features found at a number of craters and propose a mechanism for crater formation. A typical example consists of concentric zones including an outermost topographic rim, inward-dipping circular fault system, “moat” and raised central “pedestal” of freshly extruded mud volcanic sediment. This distinctive “moat and pedestal” morphology can be explained in terms of the quantity and rheology of extruded mud. Potential mechanisms to explain the formation of the craters are an origin as a slope movement, a forceful excavation formed during an explosive eruption or a collapse feature induced by subsurface evacuation and compaction. The association of fresh mud volcanic deposits with crater subsidence together with a 3D spatial relationship between craters, extrusives and feeder conduits leads us to conclude that the latter mechanism is the most likely. Mud volcano craters may therefore be analogous to other collapse structures such as calderas, dissolution collapse sinkholes and collapse depressions that all form as a result of removal of material from the subsurface.

¹Published as:

Evans R.J. et al. *The structure and formation of mud volcano summit calderas. Journal of The Geological Society, London. 165: 769-780.*

5.2 Introduction

The mud volcanoes of Azerbaijan are amongst the largest, most active and most extensively studied in the world (Aliyev et al. 2002; Etiope and Milkov 2004; Guliyev and Feizullayev 1995; Yusifov and Rabinowitz 2004). However, a particular difficulty is relating structures apparent in the surface expression of mud volcanoes to the processes occurring within the subsurface. Further knowledge gaps exist in our understanding of the mechanisms controlling the growth and evolution of large (>500 m diameter) mud volcano edifices from their inception through to extinction and burial.

This study focuses on seismic scale (>15 m size) structural and morphological features found at the upper termination of large mud volcano systems. Particular focus is given to broadly circular depressions (300-2500 m diameter) that are referred to here as craters (Kopf 2002). Craters from two active volcanoes exposed onshore in Azerbaijan and others within the South Caspian Sea are described in detail using field maps and remotely sensed data (Fig. 5.1). A number of structural and morphological elements are common to all the craters, which has enabled us to synthesize a generalized model of mud volcano crater structure. cursory examination of published mud volcano crater examples from other areas indicates that similar mud volcano craters could be found elsewhere. Insights from offshore seismic reflection data supplement our onshore mapping and lead to a discussion of the mechanisms of crater formation in the Azerbaijan mud volcanoes. Parallels can be drawn between the mud volcano craters described here and circular structures from other geological settings, including igneous volcanic calderas.

5.3 Geological setting, methods and datasets

With up to 30% of the world's known population of mud volcanoes located in eastern Azerbaijan and the South Caspian Sea, the region has long been acknowledged as an ideal natural laboratory for the study of mud volcanic geology (Aliyev et al. 2002; Guliyev and Feizullayev 1995; Milkov 2000; Yusifov and Rabinowitz 2004). Prolific mud volcanism in the area is thought to be the result of a combination of factors including rapid sedimentation during the last 5.5 Ma, tectonic compression, the presence of a thick overpressured shale layer at depth and hydrocarbon maturation

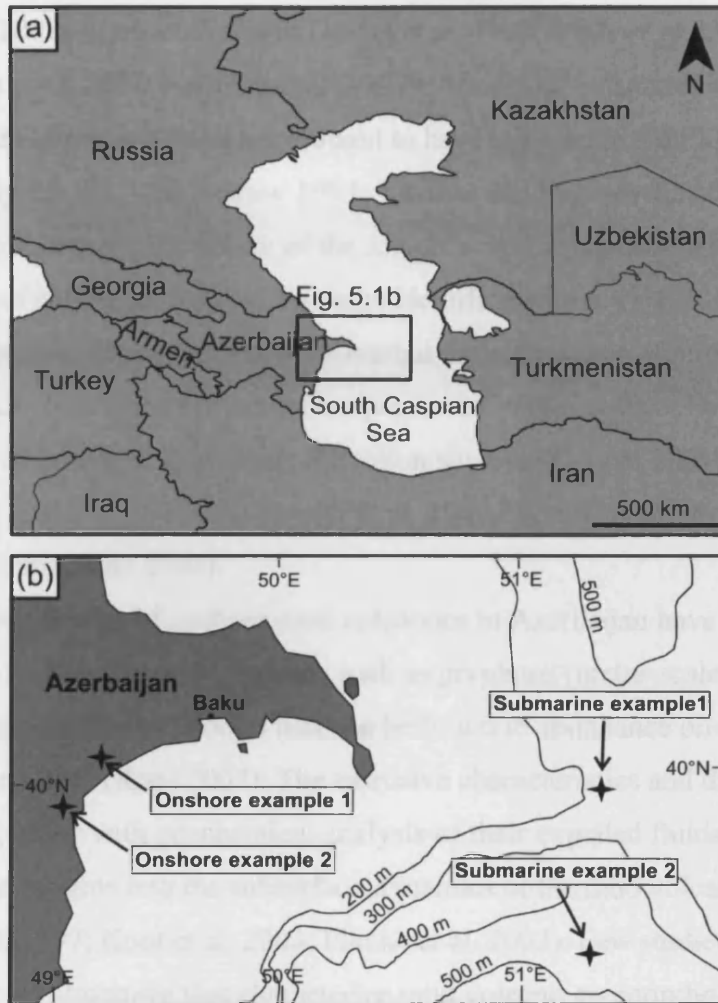


Figure 5.1 (a) Map of the Caspian Sea and surrounding countries showing the position of study area indicated as the black box. (b) Map of eastern Azerbaijan and the South Caspian Sea showing the position of the onshore and submarine crater examples described in this study. Location of map shown in (a).

(Aliyev et al. 2002; Allen et al. 2003; Devlin et al. 1999; Guliyev and Feizullayev 1995; Jackson et al. 2002; Nadirov et al. 1997). Almost all volcanoes are located in the crests of anticlines and most are thought to have initiated in the Pliocene (approximately 3.5 Ma; (Narimanov 1993; Yusifov and Rabinowitz 2004).

Offshore, the prolific nature of the region's mud volcanism is reflected in the large number of submarine volcano systems identified within the South Caspian Sea. Again, the locations of most of these are related to the presence of large folds. Kilometre-scale mud volcano systems are preserved in the crests of large anticlines and are often well imaged by seismic reflection surveys (Cooper 2001; Davies and Stewart 2005; Evans et al. 2007a; Fowler et al. 2000; Stewart and Davies 2006; Yusifov and Rabinowitz 2004).

Previous studies of onshore mud volcanoes in Azerbaijan have focussed on the morphology of minor extrusive features such as gryphons (metre-scale mud cones) and salses (metre-scale mud pools) that can be found in abundance on most active mud volcano edifices (Kopf 2002). The extrusive characteristics and distribution of these features, along with geochemical analysis of their expelled fluids have so far provided some insights into the subsurface dynamics of the mud volcano system (Hovland et al. 1997; Kopf et al. 2003; Planke et al. 2003). Few studies have focussed on the large scale structures that characterize mud volcano geomorphology at outcrop (cf. Planke et al. 2003).

Data for this study are derived from field mapping of onshore mud volcanoes combined with bathymetry and seismic reflection data from two areas within the South Caspian Sea (Fig. 5.1b). Mapping volcanoes in the field was carried out using a handheld Global Positioning System (GPS) receiver, with a positional accuracy of 5 m, together with IKONOS satellite images and Digital Elevation Model (DEM) data where available (Doyle 1984). Our first onshore example is imaged by a 15 m resolution DEM and a spatially referenced colour IKONOS satellite image. Our second is not covered by these data and has been mapped using a GPS only. Seismic data used to image one submarine example are 1995 vintage "high-resolution" 2D and conventional resolution 3D, both acquired using towed streamers. Vertical resolution ($\lambda/4$) at a depth of approximately 500 m is 4 m and 12 m respectively (Brown 1999). An increase in acoustic impedance across an interface in the 2D survey is represented by an amplitude peak and is coloured blue. Bathymetry data that image another

submarine example are derived from a 3D seismic survey and are displayed so that one pixel represents an area measuring 25 x 25 m.

5.4 Crater mapping

This section provides a description of four mud volcano craters that all show a strong degree of geomorphological similarity. Two examples of onshore mud volcano craters are located in eastern Azerbaijan and two submarine examples are located in the South Caspian Sea (Fig. 5.1b). A summary of each description is shown in Table 5.1.

5.4.1 Onshore example 1

The Qaraqus–Dagi mud volcano system (QD) is located 26 km southwest of Baku and is covered by a 15 m resolution DEM and an IKONOS satellite image (Fig. 5.1b). The large conical edifice of the volcano measures approximately 6.3 x 3.4 km in areal extent and 385 m in height (Figs 5.2a-e). The total volume of erupted material within the edifice is estimated as approximately 2.3 km³. It is bound to the east and west by prominent north-south trending topographic ridges (Figs 5.2 & 5.3). Mud flows originating from the summit area of the edifice have therefore been restricted to either a northerly or southerly transport direction (Figs 5.2a & 5.3). Large and lobate mud flows are present on the south flank of the edifice. The largest of these single flows measures approximately 3 km in length and 1.6 km in width (Fig. 5.3).

At the summit of the edifice is a circular depression measuring approximately 850 m in diameter, which we term the crater (Figs 5.2, 5.3 & 5.4). Field mapping and topographic maps coloured according to the slope angle of the land surface (slope maps) were used to identify a curved topographic ridge, here termed the rim, that marks the topographic boundary of the crater (Figs 5.2b, 5.3 & 5.4). Rim height reaches a maximum of approximately 15 m on the northern side of the crater and progressively decreases in height towards the south until it disappears. It therefore only traverses approximately 290° of arc around the crater circumference (Table 5.1; Figs 5.3 & 5.4). Consequently the crater is open to the south where the large and lobate series of mud flows originate (Figs 5.2d, 5.3 & 5.4). Like the rest of this edifice, the rim is comprised of mud volcanic sediment, a relatively soft material evidenced by the fluvial rills and canyoning on the edifice flanks. The inward-facing side of the rim





Name	Max. diameter (m)	Slope	W/L	Max. rim height (m)	Moat	Rim arc
Qaraqus-Dagi	850	N/A	1.1	15	Y	
Gora Kagniza-Dag	325	N/A	0.9	2	N	
Chirag	2500	0.4°	1.0	12	Y	
Alov	2700	0.3°	1.0	15	Y	

Table 5.1 Summary table of the principal dimensions, geomorphological and structural characteristics of each crater described in this study. Slope = angle of slope crater is located on; W/L = crater width/length ratio.

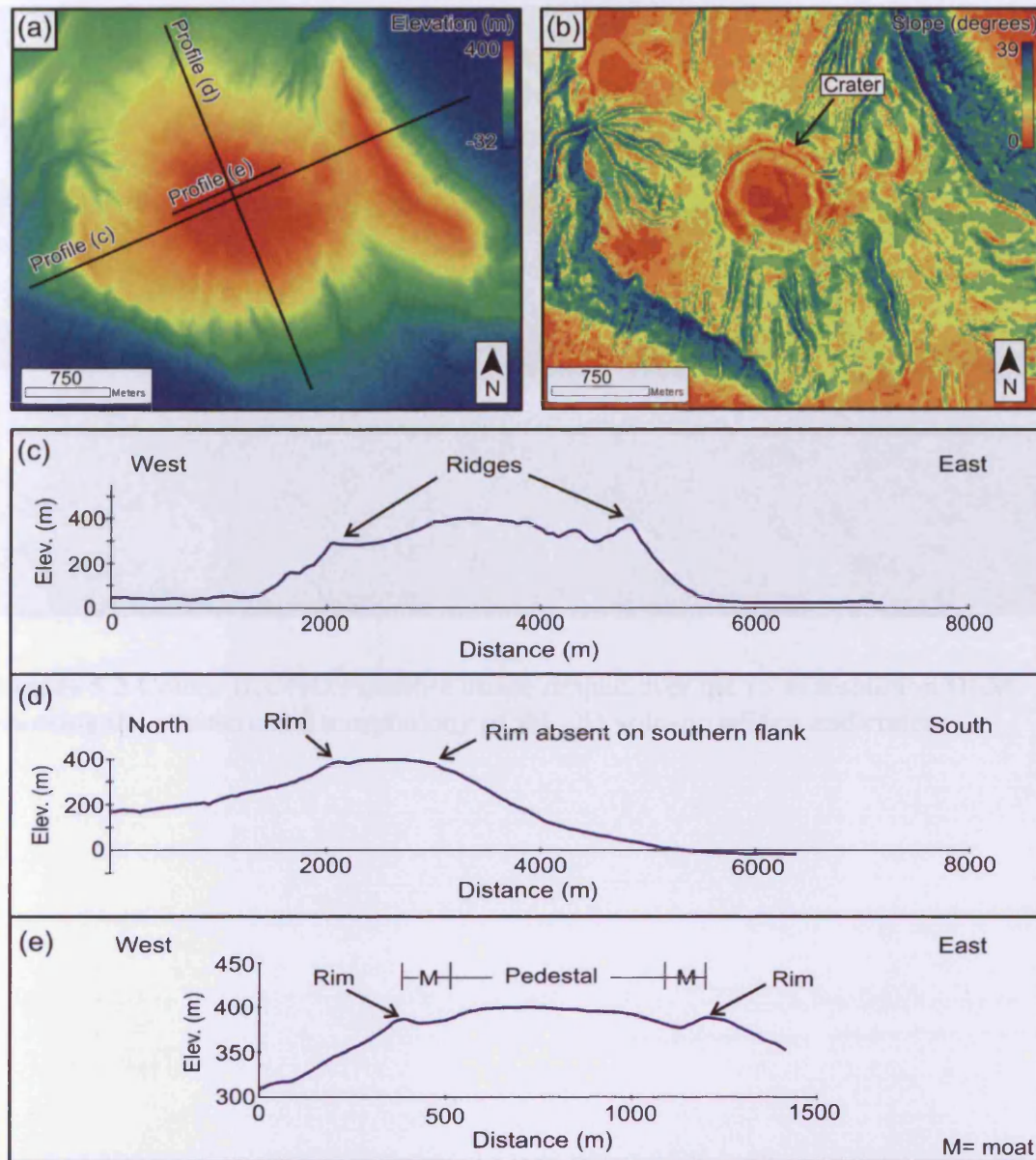


Figure 5.2 The Qaraqus–Dagi mud volcano (QD in this and subsequent Figures). (a) Topographic map of the QD volcano edifice derived from 15 m resolution Digital Elevation Model. Note the position of topographic profiles. (b) Slope map showing the position and morphology of the summit crater. (c) Transverse topographic profile showing the position of laterally confining ridges. (d) Longitudinal topographic profile showing the position of the crater rim and open southeastern crater margin. (e) Zoom-in transverse topographic profile showing characteristic “moat and pedestal” morphology of the QD crater. Note the difference in scale to profiles (c) and (d).

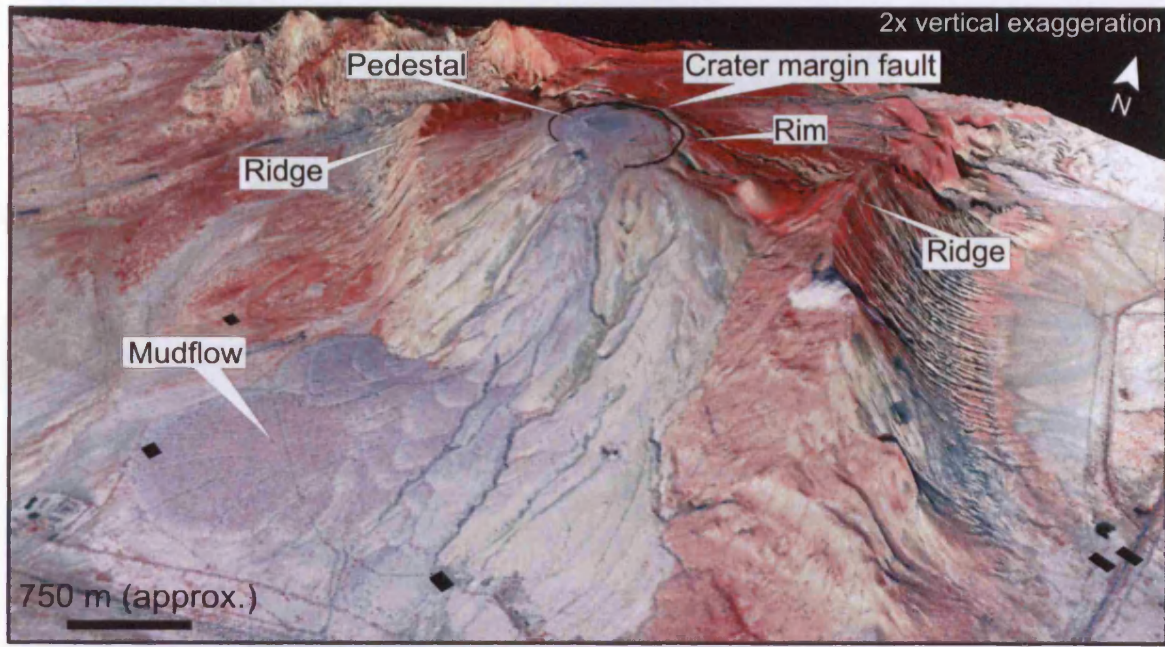


Figure 5.3 Colour IKONOS satellite image draped over the 15 m resolution DEM showing the structure and morphology of the QD volcano edifice and crater.

Figure 5.4 (a) Uninterpreted and (b) interpreted colour IKONOS satellite image of the QD mud volcano crater labelled to show the key structural and morphological elements that constitute the crater. Shaded grey areas signify mud breccia deposits.

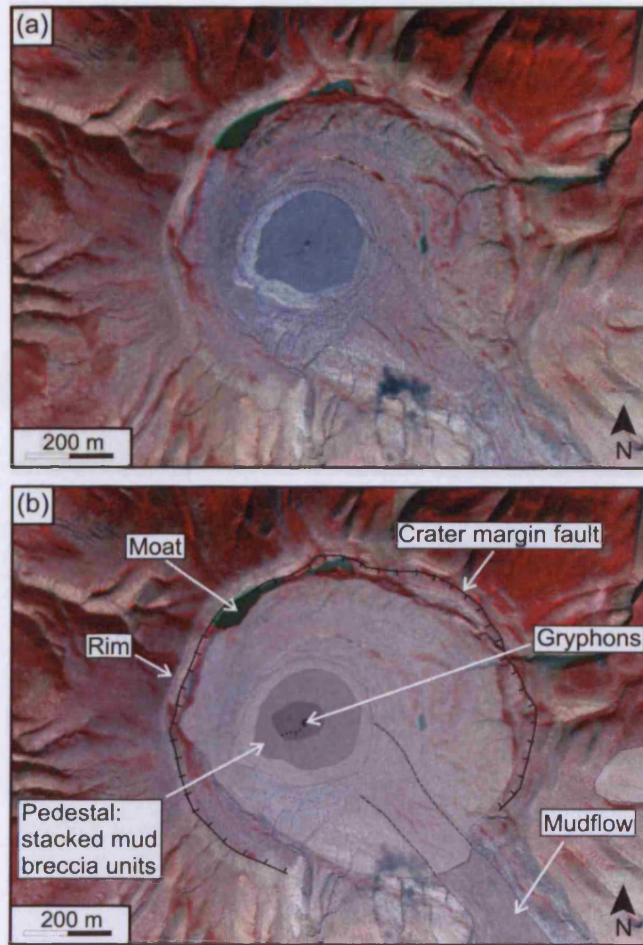


Figure 5.4 (a) Uninterpreted and (b) interpreted colour IKONOS satellite image of the QD mud volcano crater labelled to show the key structural and geomorphological elements that constitute the crater. Shaded grey areas signify mud breccia deposits.

maximum rim height is approximately 15 m. The field photograph showing the relationship of concentric stacked mud breccia units within the crater pedestal. Note the increased level of weathering and vegetation of the water-poor (dry) side of mud flows.

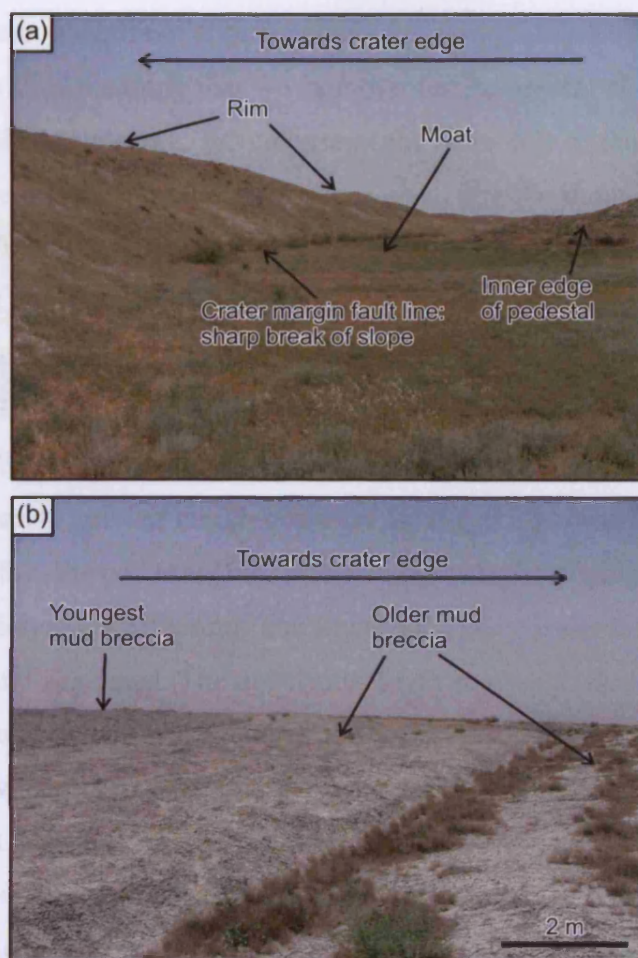


Figure 5.5 (a) Field photograph illustrating the crater rim, crater margin fault line, moat and pedestal of the QD mud volcano crater. Note the sharp break of slope at the outer edge of the moat taken to indicate the position of the crater margin fault line. Maximum rim height is approximately 15 m. (b) Field photograph showing the relationship of concentric stacked mud breccia units within the crater's pedestal. Note the increased level of weathering and vegetation of the outermost (older) units of mud breccia.

dips towards the crater centre at approximately 25° (Fig. 5.5a). The surface is vegetated and bevelled meaning that we cannot infer the present slope to represent that of any controlling structure. At the base of the inner side of the rim a sharp break of slope marks the transition to the crater floor and a circular moat-like depression that is between 20 and 60 m in width (Fig. 5.5a). Inwards of this moat is a circular “pedestal”, raised 20 m above the moat that consists of grey fined grained sediment embedded with numerous angular clasts of shale and sandstone measuring up to 10 cm (Figs 5.2e, 5.3, 5.4 & 5.5b). This sediment is the typical product of mud volcanic eruption and has been previously termed mud breccia due to its variety of clast sizes (Kopf 2002). Separate units of mud breccia are arranged into broadly concentric stacked layers within the pedestal (Fig. 5.5b). Layers can be distinguished by their degree of vegetation and weathering. The lowermost layer is the thickest, widest, most weathered and vegetated. The uppermost layer is unvegetated, its sediment very firm and its top surface highly irregular. Comparing this layer to other mud breccia deposits of a known age from elsewhere in Azerbaijan indicates that it was probably erupted in the last few decades (Planke et al. 2003). At the centre of the pedestal are a small number of active gryphons (Fig. 5.4). These are surrounded by a discontinuous dilatational fracture zone approximately 15 m in diameter that forms an incomplete circle around the gryphons.

5.4.2 Onshore example 2

The Gora Kagniza–Dag mud volcano (GKD) is one of many located near the town of Gobustan, 55 km southwest of Baku (Fig. 5.1b). The edifice of the volcano measures approximately 4 x 4 km in aerial extent, 400 m in height and contains an estimated sediment volume of approximately 1.6 km^3 (Fig. 5.6a). Unlike the QD volcano edifice this example is not covered by satellite imagery or a DEM. From a distance the flat top of the edifice is clearly visible, a characteristic common to a number of other large examples in the region (Fig. 5.6a). Upon close investigation and mapping we have found the summit area to consist of a roughly circular crater measuring approximately 325 m in diameter (Fig. 5.6b).

The outer boundary of the crater is once again marked by a topographic rim that, in this instance, is located at the top of a curved scarp that dips towards the crater centre at approximately 45° (Fig. 5.6b-d). In contrast to the QD edifice, this scarp is

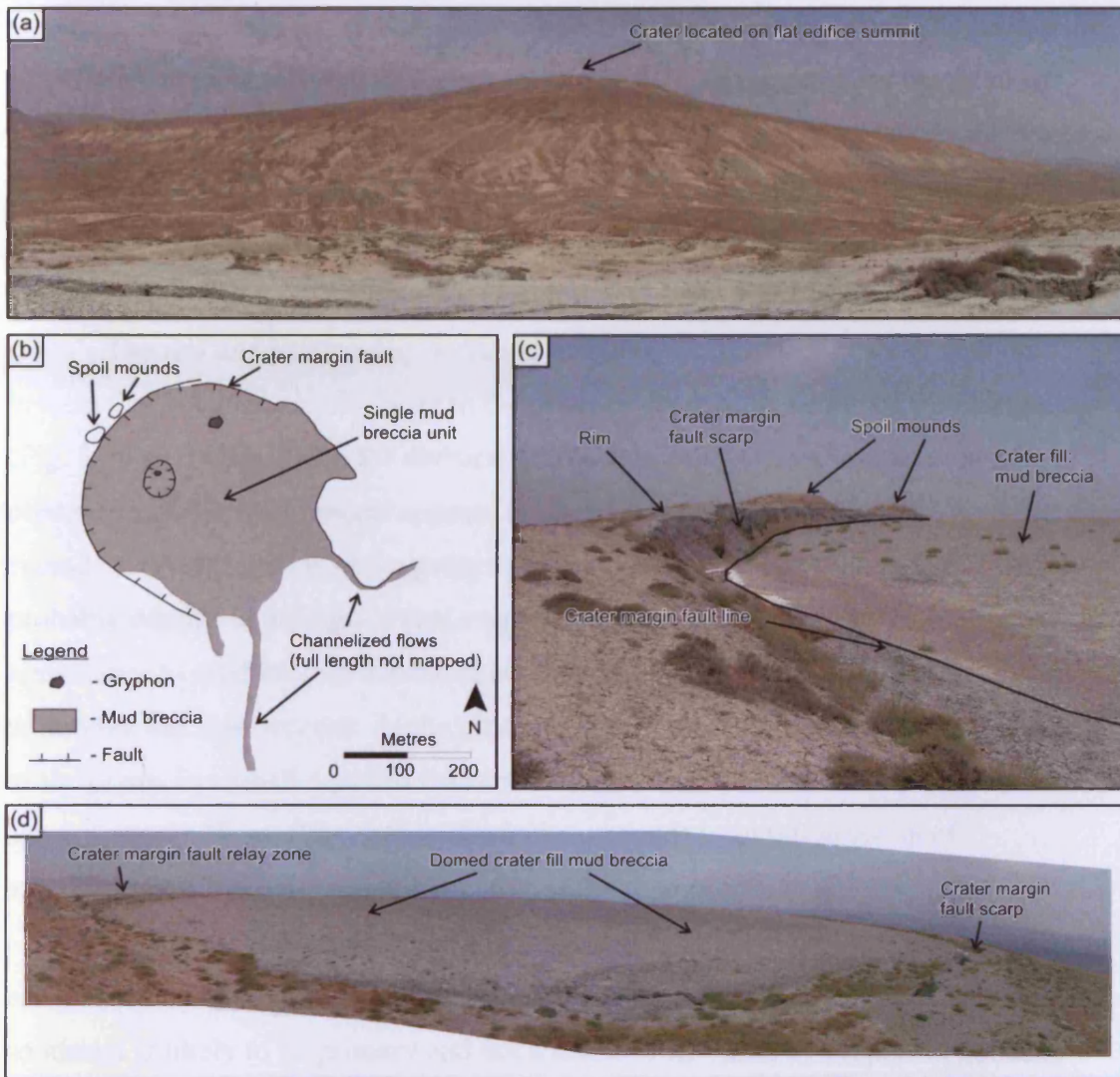


Figure 5.6 The Gora Kagniza–Dag mud volcano system (GKD). (a) Field photograph showing the large scale morphology of the volcano system’s kilometre-scale edifice. The edifice width at its base is approximately 4 km and it is approximately 400 m high. Note the distinctive flat top of the edifice. (b) Simplified geological map of the volcano crater labelled to show its main structural and geomorphological features. (c) Field photograph of the crater margin labelled to show its rim, crater margin fault scarp and fill. Note the absence of the moat. Scarp is 2 m high. (c) Field photograph showing the curved crater rim and crater margin fault scarp surrounding a single domed unit of mud volcanic breccia. Note the position of the crater margin fault relay zone. Horizontal crater width is approximately 325 m.

unvegetated and does not appear to have been significantly weathered, suggesting the slope angle is more relevant to the causal mechanism. The maximum height of the scarp is approximately 2 m. Towards the southeast the scarp progressively decreases in height around the circumference of the crater until it disappears completely (Fig. 5.6b). In places the scarp is offset by structures similar to relay ramps described from extensional fault systems (Fig. 5.6d; (Trudgill and Cartwright 1994).

The rim and scarp partly surround a slightly domed area of fresh grey mud breccia that is similar in character to the deposits seen in the centre of the QD crater (Fig. 5.6b-d). No evidence for division of this unit into separate layers could be observed and the mud breccia appears to have been deposited during one eruptive episode. The sediment is not vegetated or highly weathered indicating that it was probably deposited during a recent eruptive episode. Again it is similar in its appearance to mud breccia deposited at other volcanoes during eruptions occurring within the last few decades. At the centre of the mud breccia unit, at the highest point of the dome, is a small down to the centre circular fault that offsets the land surface by approximately 30 cm (Fig. 5.6b). The fault surrounds a central gryphon of approximately 1 m height that was active at the time of investigation.

In plan view the mud breccia unit is roughly circular and does not overstep the scarp or rim at any point indicating that the reduction in scarp height towards the southeast is likely to be primary and not a result of its burial by erupted sediments. Where the scarp is present the mud breccia extends right up to its base and no moat-like circular depression is present (Fig. 5.6b, c). Where the scarp is absent on the southeastern side of the crater the mud breccia deposit passes into a number of narrow flows that appear to have been channelled into fluvial gullies cut into the edifice flank (Fig. 5.6b).

5.4.3 Submarine example 1

The Chirag mud volcano system is located in the South Caspian Sea within the crest of the Apsheron anticline and is one of the largest known to exist (Figs 5.1b & 5.7). At the seabed there is a circular crater similar to those observed at the onshore examples previously described, albeit at a larger scale (crater diameter = 2.5 km, Fig. 5.8). This crater and the rest of the volcano system is imaged by high-resolution 2D seismic data that were acquired and processed to image the shallow section in detail

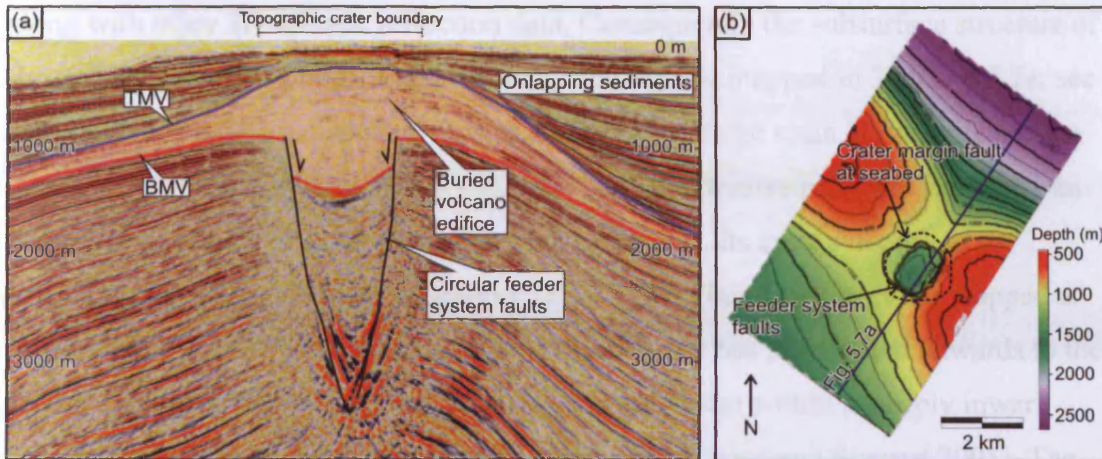


Figure 5.7 (a) 3D seismic reflection profile showing the subsurface seismic architecture of the mud volcano system, including onlapping sediments, the buried volcano edifice and ring-like downward tapering feeder system faults. TMV= top volcano edifice reflection, BMV= base mud volcano reflection. Section location shown in (b) a 3D seismic depth map of the BMV seismic reflection showing the position of the circular feeder system faults and the location of the crater margin fault at the seabed (dashed line).

along with other 3D seismic reflection data. Consequently the subsurface structure of the system's extrusive edifice and feeder system can be mapped in 3D (Fig. 5.7a; see also Davies and Stewart 2005; Evans et al. 2007a). A large scale 3D seismic section through the volcano system shows that its principal extrusive edifice is buried by an overlapping sequence of largely non-eruptive sediments, its crest a depth of approximately 200 m below the seafloor (Fig. 5.7a). Therefore the crater mapped at this example is analogous to the onshore examples but has propagated upwards to the seafloor. Underlying the buried edifice is a feeder system within a steeply inward dipping circular extensional fault system (Fig. 5.7a; Davies and Stewart 2005). The upper tips of these faults correspond closely to the outer limits of the seabed crater (Fig. 5.7b).

The topographic boundary of the seabed crater is marked by a curved rim which, like both onshore examples is partly continuous (Table 5.1; Fig. 5.8b). In places it appears to be scalloped and degraded leading to gaps or recessed sections of the crater edge (Fig. 5.8b). The rim surrounds a clear moat-like depression measuring approximately 450 m in width and 12 m depth. Inwards of the moat is a circular raised pedestal that is 1.5 km in diameter. Overall the crater is circular and has a width/length ratio (W/L) of 1.0 (Table 5.1; Fig. 5.8b).

A high-resolution 2D seismic profile yields detailed information on subsurface structure and fluid properties within the Chirag crater beyond what can be observed from bathymetry data alone (Fig. 5.9). A large portion of this profile features a highly disrupted zone of acoustic blanking which is most likely due to the presence of gas within the section (Fig. 5.9a, Judd and Hovland 1992; Parnell and Schwab 2003). A number of important observations are now listed with reference to Figure 5.9 which shows the uninterpreted seismic line (Fig. 5.9a) and a line drawing highlighting these observations (Fig. 5.9b).

Beginning at the crater centre it can be seen that the circular raised pedestal is expressed as negative polarity seismic reflection, opposite to what is generally expected at the geophysical interface between seawater and sediment (Simm and White 2002). Seismic amplitude maps of the seafloor reflection show that the phase-reversed area exactly matches the shape and extent of the pedestal (Fig. 5.10a). Towards both the edges of the crater the termination and offset of shallow reflections enables the interpretation of a number of inward dipping extensional faults (marked A in Fig. 5.9b). These faults dip towards the crater centre at between 13 and 20° and

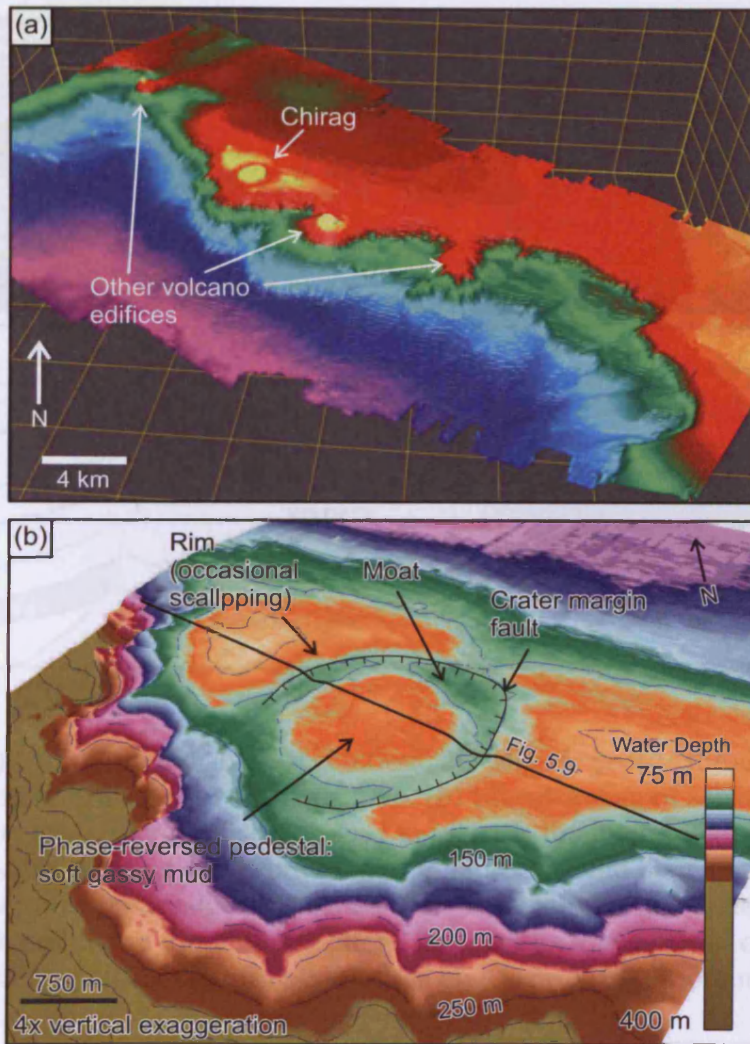


Figure 5.8 (a) 3D bathymetric map of the Apsheron anticline seabed area showing the position of Chirag and other large mud volcano systems at the shelf break. (b) 3D bathymetric map interpreted to show the main structural elements of the Chirag mud volcano crater.

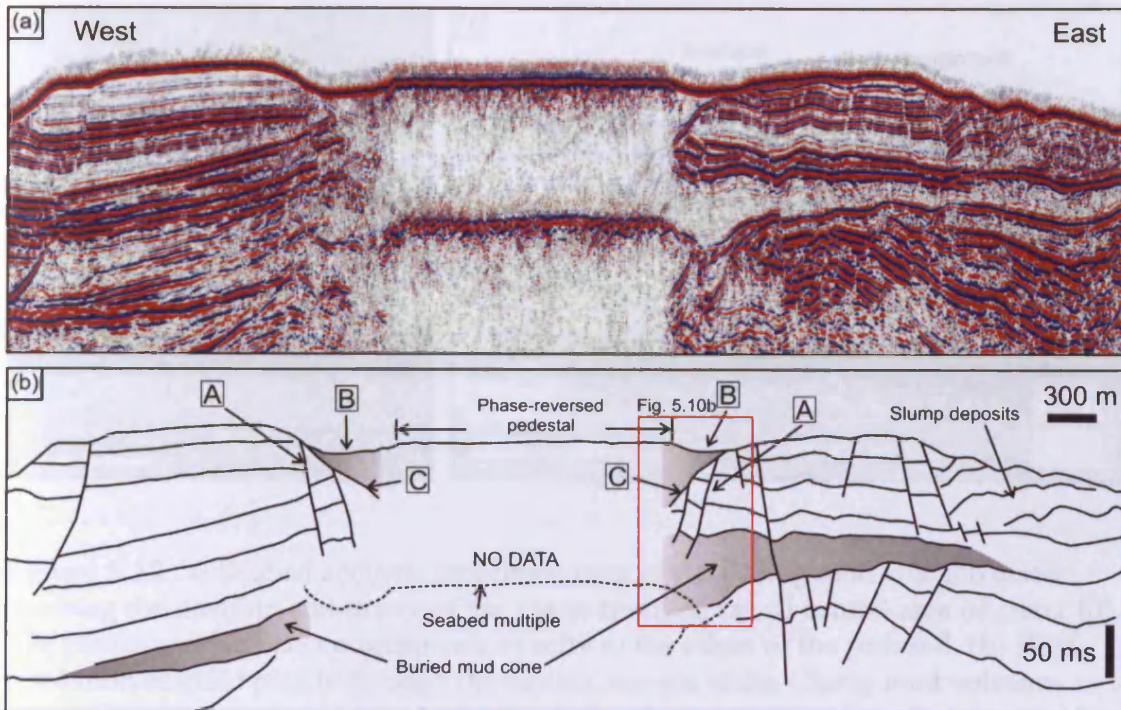


Figure 5.9 (a) Uninterpreted “high-resolution” 2D seismic profile through the Chirag crater. Location section is shown in Fig. 5.8b. (b) Line drawing of seismic section in (a) showing the key structural features used to assist in the interpretation of the crater structure. Note the position of the crater margin faults (A) and their spatial coincidence with the outer edge of the moat (B). Truncation of the crater margin fault blocks beneath an inward dipping reflection (C) suggests that a period of crater edge degradation occurred after the formation of the crater, prior to its continued filling.

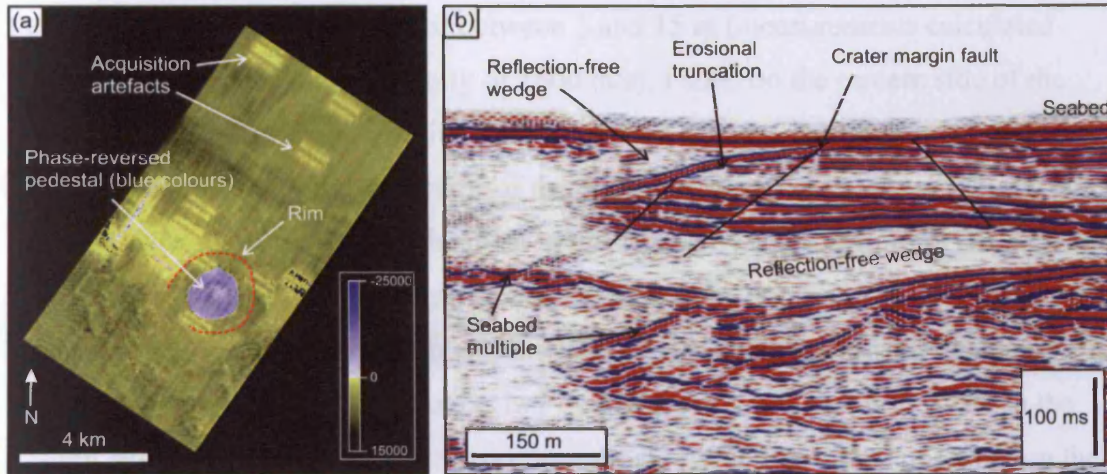


Figure 5.10 (a) Seabed acoustic amplitude map of the Chirag mud volcano crater showing the position and extent of the phase-reversed raised central area of crater fill. The phase-reversed area corresponds exactly to the edges of the pedestal. (b) High-resolution seismic profile through the eastern margin of the Chirag mud volcano crater displayed at approximately $V= 3 \times H$ the show the truncation of crater margin fault tips against the inward and inward dipping reflection overlying them. Note the position of the reflection-free wedge shaped seismic facies unit beneath the lower fault tips interpreted as a buried unit of mud volcano sediment. Location of section is shown in Fig. 5.9b

5.1.4 Submarine example 2

Located approximately 90 km south of submarine example 1 is an area of the South Indian Sea featuring a number of large (>500 m diameter) mud volcano systems (Fig. 5.10). These are imaged by the seabed reflection pick of a 3D seismic survey displayed so that one pixel represents an area measuring 25 x 25 m (Fig. 5.11). All the volcanoes are located in an area where the seafloor dips south at approximately 1:1. Most are located near a well defined shelf break that is characterized by numerous widely spaced surges that indicate its degradation by retrogressive slope movements (Fig. 5.11a, Varma 1978).

Using bathymetric slope maps it is clear that a number of the volcanoes in this area display a crater-like seabed morphology similar to that observed at all other examples (Fig. 5.11). None appear to be located directly on top of a conical edifice and therefore, like the Chirag system, they may be located in sediments that have eroded previous conical constructions. The craters range in size from 0.5-1.6 km diameter, all are surrounded by a partly continuous rim and are near perfectly circular ($A/L = 1.0$; Table 3.1). The rim surrounds an inward-facing area of seabed that dips

have extensional displacements of between 3 and 15 m (measurements calculated assuming a sediment sound velocity of 1600 m/s). Faults on the eastern side of the crater are mildly listric and hangingwall reflections appear to be slightly rotated. On both sides of the crater the upper tips of the outermost faults are seen to spatially coincide with the outer edge of the moat at the seabed (marked B in Fig. 5.9b). On the eastern side of the crater hangingwall reflections and the upper tips of the extensional faults are truncated against a high amplitude reflection that dips toward the crater centre at approximately 4° (marked C in Fig. 5.9b). Although this is clearest on the eastern side of the crater a similar, lower amplitude reflection can be observed on the western side of the crater dipping towards the crater centre at a similar magnitude. When viewed at a smaller vertical exaggeration, the area between this reflection and the seabed on the eastern side of the crater can be examined in more detail (Fig. 5.10b). It is seen as a wedge shaped reflection-free seismic facies unit that thins away from the crater centre. It exhibits what appears to be an onlapping relationship to underlying truncated hangingwall reflections and fault tips (marked “erosional truncation” in Fig. 5.10b).

5.4.4 Submarine example 2

Located approximately 90 km south of submarine example 1 is an area of the South Caspian Sea featuring a number of large (>500 m diameter) mud volcano systems (Fig. 5.1b). These are imaged by the seabed reflection pick of a 3D seismic survey displayed so that one pixel represents an area measuring 25 x 25 m (Fig. 5.11). All the volcanoes are located in an area where the seafloor dips south at approximately 0.3° . Most are located near a well defined shelf break that is characterized by numerous mildly arcuate scarps that indicate its degradation by retrogressive slope movements (Fig. 5.11a, Varnes 1978).

Using bathymetric slope maps it is clear that a number of the volcanoes in this area display a crater-like seabed morphology similar to that observed at all other examples (Fig. 5.11). None appear to be located directly on top of a conical edifice and therefore, like the Chirag crater, they may be located in sediments that have buried previous eruptive constructions. The craters range in size from 0.5-1.6 km diameter; all are surrounded by a partly continuous rim and are near perfectly circular (W/L = 1.0; Table 5.1). The rim surrounds an inward-facing area of seabed that dips

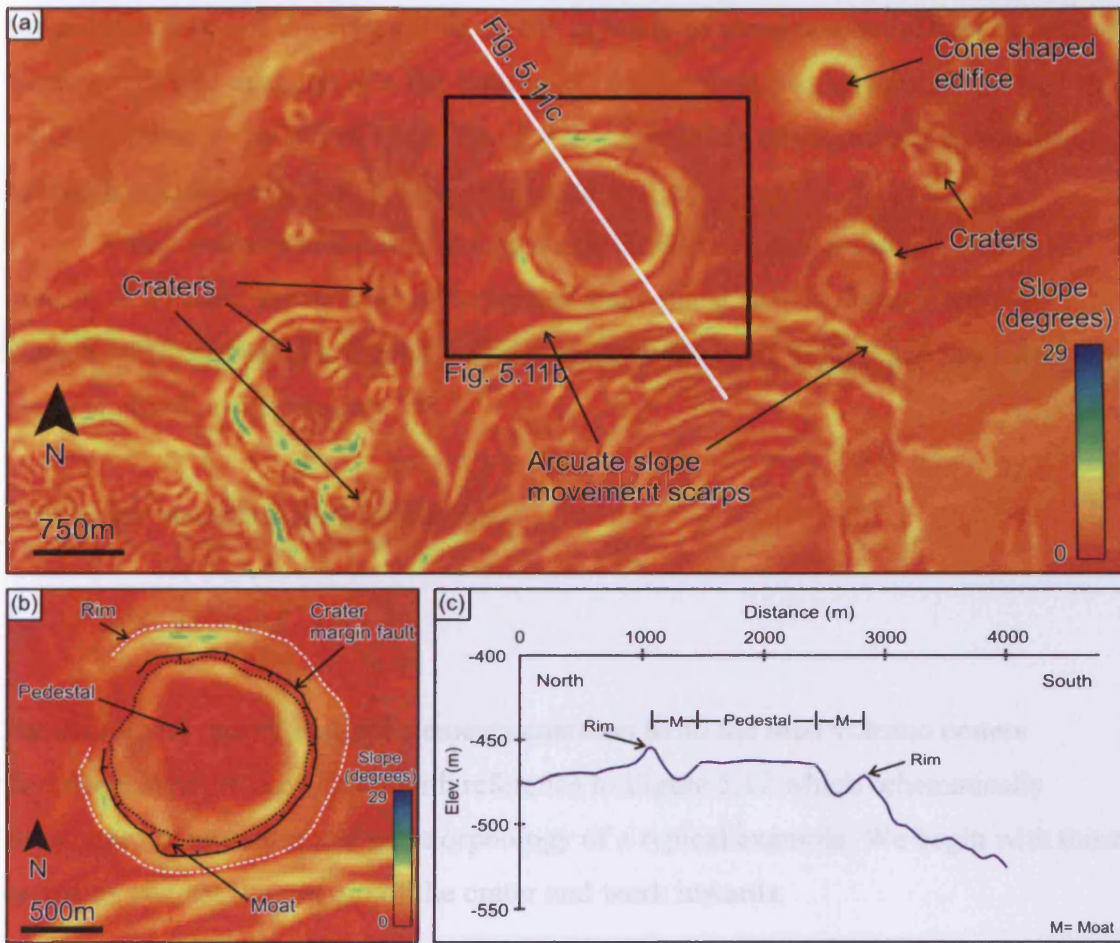


Figure 5.11 (a) Bathymetric map of a selected area of seafloor from submarine example 2 area seabed coloured according to the angle of seabed slope. Note the position of six circular mud volcano craters and the cone shaped mud volcano edifice to the north. (b) Zoom in slope bathymetric map labelled to show the structural and geomorphological elements of one of the area's craters. Slope direction is to the south. Map location is shown in (a). (c) Bathymetric profile through the largest mud volcano crater showing the characteristic "moat and pedestal" morphology of the largest crater in the area. Profile location is shown in (a).

... Using the data, specific features of craters, which is difficult to be predicted by relatively small-scale mass wasting processes occurring after its formation. When the rim is absent the crater is open which, in some cases, allows eroded material to leave the craters and flow down the flanks of the edifice (e.g. Figs 5.3 & 5.4).

Crater margin fault

The inner flank of the rim is marked either by an inward dipping scarp (Fig. 5.11b) or a slope with a pronounced break at its base (Figs 5.11a & 5.11c). These geomorphological characteristics together with the presence of inward dipping extensional faults at this point in the Chirag seismic profile (Fig. 5.9) lead us to

toward the centre of the crater at up to 14°. A break of slope marks the base of this sloping area and the edge of a flat bottomed circular moat that is approximately 10 to 15 m deep and up to 225 m wide (Fig. 5.11b, c). Inwards of the moat is a pedestal of low bathymetric relief that is broadly circular in plan view (Fig. 5.11a-c).

Other volcano systems in the area exhibit different seabed morphology and, instead of a crater, are defined by a circular and conical shaped dome. The cone shaped edifice labelled in Figure 5.11a is approximately 35 m high and has a flank slope angle of approximately 10°.

5.5 Crater structure and formation

5.5.1 Crater structure

Structural and morphological elements common to all the mud volcano craters described here are now listed with reference to Figure 5.12 which schematically illustrates the structure and geomorphology of a typical example. We begin with those elements nearest the margin of the crater and work inwards.

Rim

Defining the topographic boundary of the crater is the rim which is broadly circular in plan view. As the rim effectively represents the footwall high of the crater margin fault (see below), its height is controlled by the amount of fault displacement.

Typically this is between 12 and 15 m but it may be as low as 2 m in some craters (Table 5.1). The rim may not be present around 100% of the crater's circumference. At Chirag the rim appears scalloped in places, which is indicative of its degradation by relatively small scale mass wasting processes occurring after its formation. Where the rim is absent the crater is open which, in some cases, allows erupted material to leave the crater and flow down the flanks of the edifice (e.g. Figs 5.3 & 5.4).

Crater margin fault

The inner flank of the rim is marked either by an inward dipping scarp (Fig. 5.6b-d) or a slope with a pronounced break at its base (Figs 5.5a & 5.11b). These geomorphological characteristics together with the observation of inward dipping extensional faults at this point in the Chirag seismic profile (Fig. 5.9) lead us to

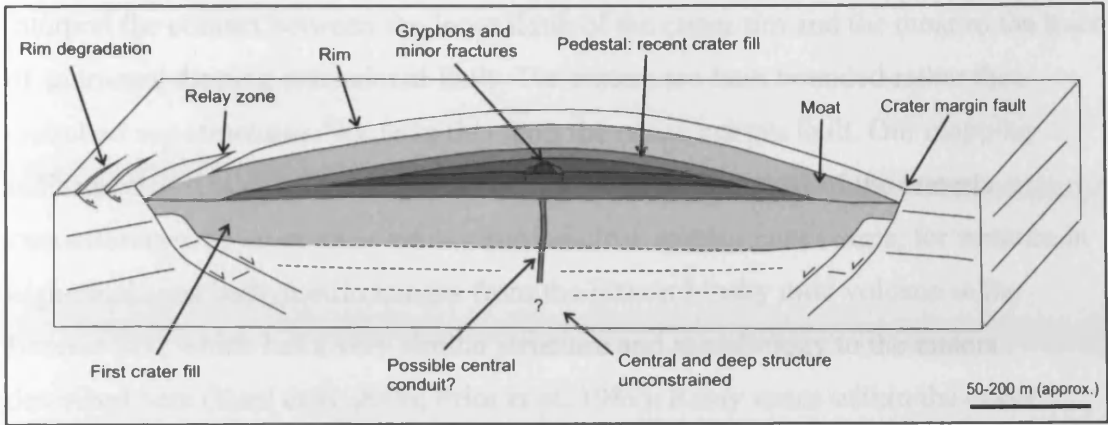


Figure 5.12 Schematic block diagram illustrating the principal structural and morphological elements of a typical circular mud volcano crater identified in this study. Dashed lines indicate areas of tentative interpretation. See text for discussion.

interpret the contact between the inner flank of the crater rim and the moat as the trace of an inward dipping extensional fault. The craters are fault bounded rather than unfaulted sag structures. We term this fault the crater margin fault. Our mapping indicates that it is circular and probably continues around most of the crater's circumference. In other areas we see similar clear arcuate fault scarps, for instance in high-resolution bathymetric images from the Håkon Mosby mud volcano in the Barents Sea, which has a very similar structure and morphology to the craters described here (Kaul et al. 2006; Prior et al. 1989). Relay zones within the crater margin fault scarp at the GKD crater indicate that it is likely to consist of a number of discrete arcuate segments rather than a single continuous fault plane. In all instances where the dip of the crater margin fault can be measured with any degree of confidence it is in the range of 13-45°.

In the Chirag seismic profile we have observed truncation of the upper crater margin fault tips and hangingwall reflections against the base of a wedge shaped reflection-free seismic facies unit that oversteps and onlaps the fault blocks (unit base marked C in Fig. 5.9b). Seismic facies characteristics of the wedge shaped unit together with its cross-sectional geometry indicate that it is likely to consist of relatively massive and structureless sediments that originated from the volcano centre. We interpret it as a unit of mud volcanic sediment that was extruded onto eroded crater margin fault blocks. At Chirag the seismic stratigraphic relationship of this unit to the underlying fault tips and the truncation of the hangingwall reflections indicate that the extrusion occurred after the faulting and a period of hangingwall degradation.

Moat and Pedestal

In several examples a circular depression, termed the moat, occurs between the inner margin of the rim and the outer margin of a raised circular area, termed the pedestal. In profile these features produce a clear "moat and pedestal" morphology which we believe to be characteristic of most of the craters described here (e.g. Fig. 5.11c).

Our mapping reveals that the raised topographic expression of the pedestal is a result of the build up of relatively fresh mud breccia deposits that comprise the most recent crater fill. Onshore this is evidenced by the presence of circular areas of relatively fresh mud breccia that spatially correspond to areal extent of the pedestal. Offshore the phase-reversed expression of the Chirag crater pedestal indicates it to

consist of low density and seismic velocity gas-rich mud volcanic sediment (Evans et al. 2007b; Roberts et al. 2006).

Within the QD crater it is the extrusion of high viscosity mud breccia that has led to the raised topography and pronounced edges of the pedestal and the formation of the moat. Stacking of successively smaller and younger concentric subcircular layers of high viscosity mud breccia can be identified – the stacking pattern is well represented by the models developed by (Murton and Biggs 2003). Dark grey colouring and absence of any vegetation within the uppermost mud breccia layer indicates that it is likely to have been erupted and deposited recently (approximately <30 years). Comparing the approximate volume and sedimentary character of this layer to those seen at other more frequently monitored volcanoes in which eruptions have been observed indicates that the eruption responsible for its deposition was likely to have been explosive and was probably noticeable from areas far outside the crater (e.g. Lokbatan; Planke et al. 2003).

The oldest and largest mud breccia layer at the QD volcano does not extend up to the inner flank of the rim and the moat and pedestal morphology is preserved (Figs 5.2e & 5.5a). At GKD a single recent extrusion has filled the crater to the base of its rim meaning there is no moat and pedestal morphology (Fig. 5.6b-d).

Gryphons

Onshore craters usually have a small zone of active fluid extrusions – gryphons, salses and mofettes located in the centre of the crater, occasionally surrounded by a concentric tensile fracture. These features may also be present offshore but are below the resolution limits of currently available seismic data. Their existence suggests the presence of some form of central conduit system. It is not clear whether such a conduit was responsible for feeding the principal pedestal building eruptions.

5.5.2 Crater formation

The structural and geomorphological similarity of the craters described in this study suggests that they share a causal mechanism. Identification of this mechanism must take account of all the observations made in the field and in remotely sensed offshore data including; the vertical offset of the land surface or seabed and the formation of the crater margin fault; the very shallow dip (13-45°) of the crater margin fault; the

circular shape of the craters (W/L ratios typically c.1.0) and the common occurrence of recently erupted mud breccia that forms the pedestal. We consider the following options as potential crater forming mechanisms: 1) Slope movement unrelated to mud volcanic processes; 2) Excavation during an explosive eruption; 3) Failure induced by subsurface evacuation and compaction occurring in association with the extrusion of sediment and fluid.

Slope movement mechanism: Some evidence to support this possibility is the incomplete rim and crater margin fault line observed at the onshore craters; a characteristic that could be used to interpret the crater margin fault as some form of scarp at the head of a rotational slope movement (Martinsen 1994; Varnes 1978). This origin for the craters is considered unlikely for a number of reasons. Firstly, it is not consistent with the near perfectly circular shape of most of the craters (W/L ratios c.1.0; Table 5.1). This contrasts the more linear pattern of headscarp fault lines from typical slope movement structures and the elongate and trench-like collapse scarps formed by sector collapse of large igneous volcanic cones (Acocella 2005; Martinsen 1994; Ponomareva et al. 2006; Tibaldi 2001; Varnes 1978). At both submarine examples in this study there is a clear morphological contrast between the circular craters and the more linear slope movement headscarps at the nearby shelf break (Figs 5.8 & 5.11a). Furthermore, slope maps from submarine example 2 clearly show the closure of the largest circular crater against the direction of slope which further precludes a simple slope movement or sector collapse origin (Fig. 5.11a, b). Finally, no gravity-induced slope movement processes that are known to us can explain the presence or shape of the pedestal of fresh mud breccia at the centre of the craters.

Explosive excavation mechanism: An origin as a filled explosive crater provides a means of explaining the erosional truncation observed in the hangingwalls of the crater margin faults (Figs 5.9 & 5.10b). In this scenario crater formation would begin with an explosive eruption blasting away near surface sediment forming an excavated void, similar in morphology to a large pockmark (Hovland and Judd 1988). Collapse of adjacent sediment into this void produces the surrounding faults in a manner similar to the formation of complex impact craters (Melosh and Ivanov 1999). Filling of the crater by ejected and other sediments in the period after the explosive eruption then produces the onlapping relationship of mud breccia deposits onto the truncated crater margin fault tips and eroded faults blocks. However, it is not clear how larger explosions would produce negative topographic features (crater) while

smaller events produce positive topography (pedestal). There are no historical records of explosions in line with this mechanism – there are many records, which testify to non-explosive eruptions. Furthermore, the size of the largest known explosive mud volcano craters challenges the explosive mechanism since they are far smaller than the diameter of our examples (Evans et al. 2007a; Planke et al. 2003; Stewart and Davies 2006).

Subsurface evacuation and compaction mechanism (Fig. 5.13): In this scenario the formation of the crater is genetically associated with the expulsion of fluids and sediments from the subsurface, either during discrete eruptions or ongoing fluid escape representing dewatering or degassing at depth. Vertical displacement and faulting of the land surface or seabed takes place due to volume loss within a subjacent source domain that evacuates of fluid and sediment and therefore compacts at a greater rate than surrounding areas. As the surface collapses the evacuated sediment is extruded and fills the depression (Fig. 5.13a). At a point in time before the depression is completely filled the exposed hangingwalls of the crater margin faults degrade by small (sub-seismic) episodes of mass wasting resulting in the truncation of the crater margin fault scarps and hangingwall reflections (Fig. 5.13a). Scalping of the crater rim at Chirag indicates that this process is continuing up until the present day (Fig. 5.8b). As filling of the depression continues the onlap of mud volcanic sediments onto the degraded fault scarps creates an unconformity between the base of the further crater fill and the pre-crater collapsed sediments (Fig. 5.13b). Later stages of crater formation involve the eruption of more mud volcanic sediment into the crater centre which forms the pedestal of mud breccia (Fig. 5.13c). The mechanical properties and volume of the erupted sediment at this time will determine the morphology and extent of the pedestal and control the formation of the moat. Eruptions producing small volumes of high viscosity mud breccia best favour preservation of the moat. High volume low viscosity eruptions are more likely to reach or overstep the crater rim.

We consider this mechanism of formation to best satisfy the constraints imposed by the geomorphology and structure of each crater. It is supported principally by the vertical offset of the surface that is in direct spatial coincidence with the crater fill pedestal. The spatial coincidence of the Chirag crater edges to the volcano's circular feeder system also argues for an origin mechanism related to eruptive processes and fluid extrusion from the subsurface (Fig. 5.7b). From the data

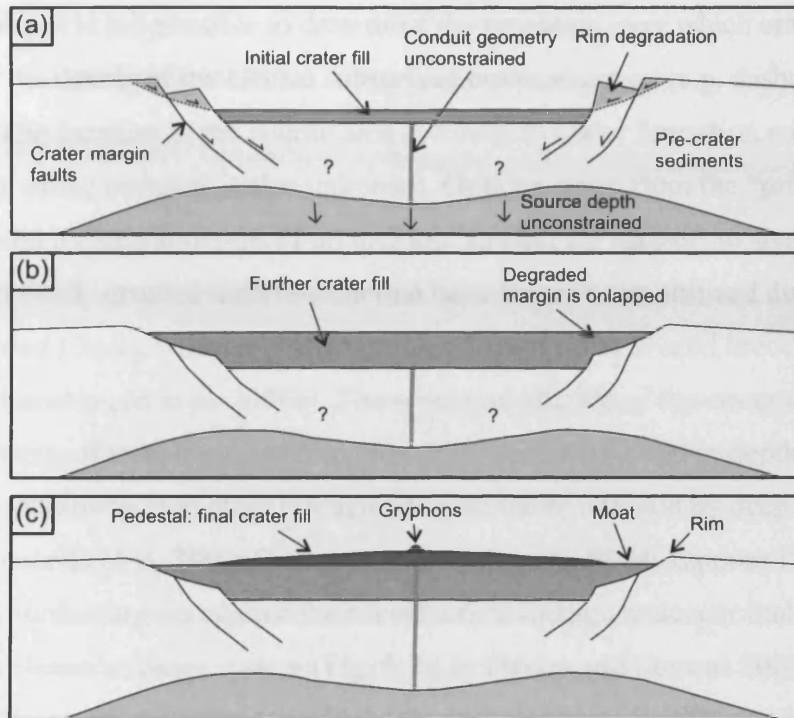


Figure 5.13 Schematic depiction of the formation of mud volcano craters as collapse features induced by subsurface volume changes occurring during and eruption. (a) Evacuation and deflation of subsurface source region during eruption inducing crater formation. Degradation of the crater rim by small slope movements creates the erosional truncation observed at the crater margin. (b) Further crater fill leads to onlapping of the degraded crater margins. (c) Final crater fill is deposited as the pedestal and central gryphons. In this example mud breccia does not reach the rim and the moat is preserved. This may not be the case for all mud volcano craters.

presented here it is not possible to determine the timescale over which craters form in this way or the details of the central subsurface crater structure (e.g. dashed lines in Fig. 5.12). The location of the source area involved in crater formation and the construction of the pedestal is also unknown. Options range from the “primary” mud source domain located at depths of up to 5 km beneath the surface, to shallow buried units of previously erupted mud breccia that have become remobilized during burial (e.g. the buried Chirag volcano edifice or other buried units of mud breccia; Ø et al. 2003; Van Rensbergen et al. 2005a). The structural attitude of the crater margin faults argues in favour of a shallow source region (approximately <400 m depth) as they dip much more shallowly than other circular collapse faults initiated by deep volume changes (Acocella et al. 2000; Branney 1995; Cole et al. 2004; Lipman 1997). The shallow dip further argues against their mechanical linkage to deeper faults that exist within the volcano’s feeder system (Fig. 5.7a, b; Davies and Stewart 2005, Evans et al. 2007a). However, the extent to which this fault dip angle is influenced by the mechanical properties of the near surface sediment is unconstrained meaning that we cannot completely rule out a deep location for the source region involved in crater formation. Further work is required to better constrain this aspect of crater formation.

5.6 Discussion

5.6.1 Other mud volcano craters

Structural and geomorphological similarities have been observed between two well exposed and relatively fresh onshore craters and well imaged submarine mud volcano craters in this study. This fact, together with the similarity of a number of other craters in Azerbaijan and elsewhere, suggests that the characteristic crater morphology is not restricted only to the examples described here.

Similar craters can be found at other volcanoes in eastern Azerbaijan whose general structure is similar to that described in our model. Indeed, many of the region’s volcanic edifices are of a broadly circular shape in plan view and have flat or bulging summit areas flanked by a rim (Judd and Hovland 2007). One example is the Dashgil mud volcano edifice where Hovland et al. (1997) have identified an uneven summit rim surrounding an otherwise flat summit plateau. The rim outlines what is described as a summit “caldera”, bound partly by a 3 m high escarpment that encloses

a number of minor eruptive features including gryphons and salses (Planke et al. 2003; Skinner and Tanaka 2007).

Outside of the Caspian region mud volcanoes of comparable size to our examples have summit craters with a similar morphology to those described here. Offshore Trinidad for example, exist a number of circular craters at the summits of conical mud volcano edifices. (Deville et al. 2006) have termed these “calderas” and suggest that during their development they become progressively filled by extruded sediments. In other examples bathymetric surveys have identified craters with a clear “moat and pedestal” morphology. Examples include the Al Idrissi and Mercator mud volcanoes in the Gulf of Cadiz (Van Rensbergen et al. 2005b). These are partially filled by a series of recently extruded deposits comprising a central mud dome that is comparable in size and shape to the pedestal. Somoza et al. (2003) have also identified a number of mud volcano edifices from this area that are rimmed by circular collapse structures, similar in morphology to the moats described here, that are thought to be the result of degassing during mud extrusion. A further example of a clear “moat and pedestal” crater is an unnamed 220 m wide seafloor fluid expulsion feature from the Gulf of Mexico that shows a clear rim, moat and slightly domed central pedestal (George 2006).

However, the summit collapse features and general morphology of some other mud volcano edifices are not similar to the craters we have described. For example, a small number of mud volcano edifices in Azerbaijan feature elliptical and open ended craters with localized evidence for axis-parallel strike-slip displacement (Planke et al. 2003). Further work is required to constrain the origin of these structures and compare them to the circular craters described here.

It also must be highlighted that not all mud volcano systems feature craters or any other form of collapse structure at their upper terminations. Examples include the cone shaped edifice shown in Figure 5.11a and others within the South Caspian Sea. The absence of craters in these instances may be due to differences in the subsurface geometry compared to the examples studied here. It is also noted that in our favoured structural model, if pedestal growth exceeds the crater volume the crater morphology will be buried and replaced by a dome structure.

5.6.2 Circular collapse structures

A wide range of fluid dynamic, tectonic or igneous processes can result in the formation of circular geological structures (Stewart 1999b). This study provides a detailed description of a new circular geological structure that has not been previously described, the mud volcano crater. The key characteristics of mud volcano craters which may be used to distinguish them from other circular structures are: 1) The location at the summit of a conical mud volcano edifice or an area of seafloor directly above the root zone and feeder system of an otherwise known mud volcano system; 2) A partly continuous topographic rim 2 to 15 m in height that bounds a circular depression 300 to 2500 m in diameter with W/L ratios of approximately 1.0; 3) The presence within this depression of an inward dipping circular extensional fault system and evidence for fault controlled vertical displacement of the surface; 4) The presence of mud volcanic deposits, typically circular in planform, occupying the centre of the crater; 5) A characteristic “moat and pedestal” morphology within the crater’s interior; 6) Metre-scale gryphons or other minor extrusive features at the centre of the crater pedestal.

Although the craters described here are genetically associated with mud volcanic eruptions, they contrast other sedimentary or igneous craters that form as a result of excavation during explosive eruptions (Pike 1974). To distinguish these two styles of crater formation we would suggest that the prefix “explosive” be applied to craters formed by excavation during violent eruptions and “subsidence” to those described in this study. Considering the size of present day mud volcano craters formed during recent explosive eruptions (e.g. Lokbatan, Planke et al. 2003), we would expect explosive mud volcano craters to generally be at least an order of magnitude smaller than typical subsidence craters. Other explosive craters such as giant pockmarks formed by violent eruptions of gas however, can be comparable in size to the subsidence craters described here (Cole et al. 2000).

In a purely morphological sense mud volcano subsidence craters are similar to many circular geological structures including kettle holes, pingoes, and diatremes. They share most similarity with fault-bound circular structures such as impact craters, calderas, pit craters, collapse depressions and dissolution collapse sinkholes (Acocella 2006; Bertoni and Cartwright 2005; Judd and Hovland 2007; Murton and Biggs 2003; Pike 1974; Prior and Coleman 1982; Roche et al. 2001). With the exception of impact

craters all these circular structures form as a result of point-centred volume change in areas subjacent to the structure (Stewart 1999b). Calderas are well known igneous volcanic structures that form when the roof of a magma chamber collapses during its evacuation (Lipman 1997). Like mud volcano subsidence craters a proportion of the material from the evacuating source region is often deposited within the depression formed at the surface. Pike (1974) has described such features as “craters of net accumulation” which contrast “craters of excavation” formed by excavation during impacts or blasting. A similar process occurs in the formation collapse depressions. These subcircular sedimentary failures show a large degree of morphological similarity to the subsidence craters described here. They form as a result of the evacuation of fluids from the shallow subsurface and are found in areas of rapid sedimentation such as the Mississippi Delta (Judd and Hovland 2007; Prior and Coleman 1982).

We consider the mud volcano subsidence craters described in this study to be potentially useful analogues for other circular collapse structures, particularly fault-bound structures such as magmatic calderas, pit craters, dissolution collapse sinkholes and collapse depressions that form due to subsurface volume change. The dynamic nature of active mud volcanism in Azerbaijan and other mud volcano provinces means that structures associated with their activity are evolving over timescales as short as months or even days. Mud volcano subsidence craters may therefore present an opportunity to study the formation of large scale subsidence features in what is effectively “real time”.

5.7 Conclusions

Circular depressions bound by inward-facing faults at the upper terminations of large (>500 m diameter) mud volcano systems are termed “mud volcano subsidence craters”. They range in size from 325 m to 2.5 km in diameter. Common structural and geomorphological elements are observed at a range of onshore craters from Azerbaijan together with geophysically imaged craters on the seabed of the South Caspian Sea.

Based on our mapping we have shown a typical mud volcano subsidence crater to feature a subcircular rim that defines its topographic boundary, a crater margin fault system, a moat and a series of mud breccia deposits that constitute the

central pedestal. cursory examination of mud volcanoes from other areas indicates that similar craters may be found outside of the study area.

The geomorphological similarity of all the crater examples suggests that a common mechanism is responsible for their formation. Our preferred origin mechanism for the craters is as collapse features induced by subsurface sediment and fluid evacuation occurring during eruptions.

This study is the first to identify similar geomorphological features at mud volcanoes within and outside a particular mud volcano province and is therefore a step towards building a generic understanding of the processes involved in the evolution of large mud volcano systems. It highlights the potential of surface structures for constraining the subsurface architecture and dynamic evolution of large mud volcano systems. We propose that mud volcano subsidence craters may be potentially useful analogues for other large scale circular geological structures, including magmatic calderas.

5.8 Acknowledgements

We are grateful to the National Environment Research Council (NERC) for provision of award number NER/S/C/2004/12724 that supports this research. Also acknowledged are Schlumberger Geoquest for provision of IESX and GeoViz seismic interpretation software and BP Azerbaijan for provision of seismic and other data. T. Evans and S. Bull are thanked for assistance during fieldwork and M. Joly for help with data provision. J. Cartwright, S. Higgins and other members of the 3DLab in Cardiff University are thanked for helpful discussion.

CHAPTER SIX

6.0 Summary and Discussion

6.1 Introduction

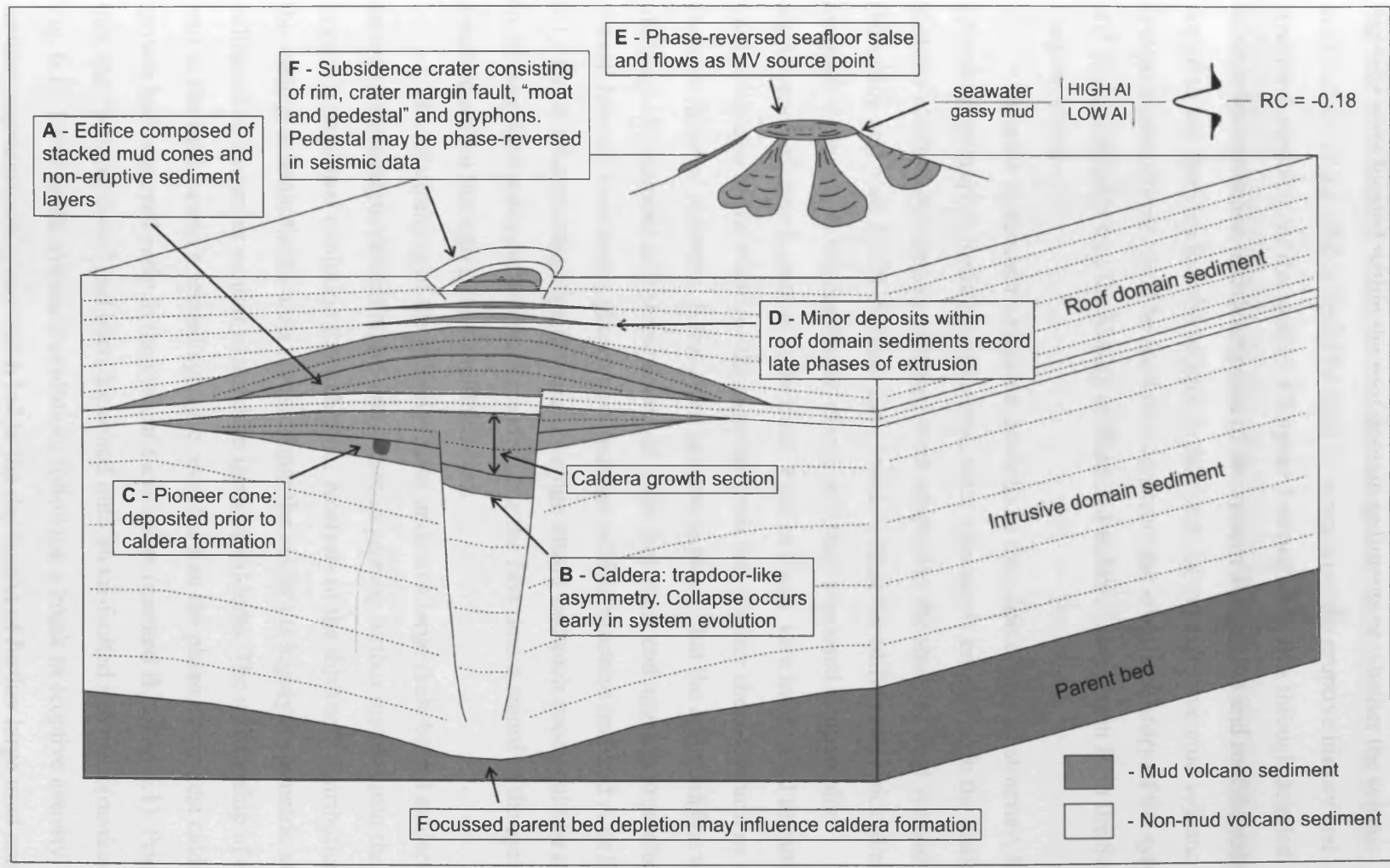
This project has used industrially acquired 2D and 3D seismic data, field maps and well data to perform a detailed analysis of the structure, evolution and geophysical expression of the extrusive and roof domains of mud volcano systems from Azerbaijan and the South Caspian Sea. The use of multiple data types has led to a thorough coverage of the various structural and sedimentary constructions and features found within these structural domains. This chapter now aims to summarize the key scientific results of each core research chapter and draw them together into a generalized structural model of large volcano systems from the South Caspian Basin. It then aims to assess the significance of the project results for various aspects of mud volcanic geology and related topics. The chapter is concluded with a brief discussion of the implications for economic and engineering geology and a number of suggestions for future work.

6.2 Summary of results: a generalized structural model

The following sub-Sections summarize the main scientific results of each core research chapter. They are illustrated with reference to Figure 6.1 which schematically depicts the structural configuration of the extrusive and roof domains of a typical South Caspian Basin mud volcano system.

6.2.1 Edifice internal structure and eruptive history (chapter 3)

Chapter 3 focussed on the largest known mud volcano system in the world that is imaged by seismic reflection data- the Chirag mud volcano system. Prior to the onset of this project a previous study had introduced this mud volcano system and its gross seismic architecture. This had revealed that the system consisted of a large buried edifice covered by onlapping roof domain sediments (Davies and Stewart 2005).



6 - 2

Figure 6.1 A generalized structural model for a typical South Caspian Sea mud volcano system drawn and annotated to highlight the most significant findings of this project. See text for further discussion and explanation of letter annotations.

These feature had however, not been mapped or described in detail. Consequently little was known about the internal structure of the edifice, whether any mud volcanic deposits were located within the roof domain sediments or whether the seismic architecture of the edifice could be used to reconstruct the eruptive history and structural evolution of the system. **Chapter 3** aimed to do this through detailed seismic interpretation and description of the system's extrusive and roof domains. It aimed to test the idea that the seismic architecture of the extrusive mud volcano system constructions could be used to reconstruct the eruptive history of the system and to gain insights into the history of fluid and sediment expulsion from the South Caspian Basin

In order to conduct a rigorous analysis of the edifice internal structure, basic seismic stratigraphic methods and terms, more commonly employed in the analysis of shallow marine sedimentary systems, were adapted to the study of mud volcanism (Mitchum and Vail 1977). Seismic facies units within the edifice were picked and mapped according to the continuity, clarity and their supposed stratigraphic significance of their bounding reflections. Four of these were interpreted as buried mud cones due to their wedge-like external form and another sheet-like unit as a non-eruptive layer of sediment. It therefore became apparent that the entire edifice was made up of a number of discrete sediment units that stack and aggrade to produce the overall biconic (two cones placed base to base) edifice structure (marked A in Fig. 6.1). Good seismic image quality and coverage meant that each cone could be mapped in 3D and their main dimensions recorded. For the first time a record of the system's eruptive output through time was established.

The relationship of the seismic facies units to a large fault-bound caldera at the centre of the system proved highly important in gaining further insights into the system's structural evolution through time. Analysis of the thickness distribution of the various seismic facies units revealed that the caldera is highly asymmetric and collapsed in a manner similar to trapdoor igneous calderas. The relationship of each unit to the caldera and a related synform revealed that the phase of greatest caldera growth had occurred early in the system's evolution (marked B in Fig. 6.1). Prior to this, the "pioneer cone" had been deposited onto an un-faulted substrate (marked C in Fig. 6.1). Later in the system's evolution, following a break in eruptive activity, further eruptions took place which led to the deposition of further large mud cones. These were not affected by further periods of caldera collapse and are of a relatively

uniform thickness all around the edifice. A relative structural chronology was therefore established for the main edifice and its history of growth and collapse was documented.

Within the roof domain sediments evidence for further mud volcanic activity was identified that post-dated the main phase of edifice construction. Amplitude maps of seismic horizons within the roof domain showed the presence of linear and radial amplitude anomalies which were interpreted as further, thinner, mud volcanic deposits (marked D in Fig. 6.1). Minor extrusion had therefore taken place after the main phase of edifice construction during the burial of the principal edifice.

Chapter 3 clearly demonstrated the power of 3D seismic data as a tool for the investigation of mud volcano systems. It showed that the extrusive constructions within the system can be large enough to be well-imaged and interpreted in a classic seismic stratigraphic context. It very much supports the notion that seismic analysis of large mud volcano systems can be used to reconstruct the system's eruptive history and gain insights in to the history of basinal fluid and sediment expulsion.

6.2.2 Seabed phase reversal analysis (Chapter 4)

For the first time **chapter 4** documented in detail the phenomenon of seabed phase reversals in seismic reflection data. A phase reversal can be defined as a lateral change in seismic reflection polarity resulting from a change in the nature of the geophysical interface. Generally the seabed is marked by a positive polarity seismic reflection since seabed sediment generally has a higher acoustic impedance than seawater. A seabed phase reversal therefore occurs when the seabed reflection changes laterally to a negative polarity reflection which contrasts the surrounding positive polarity reflection. Prior to this project seabed phase reversals had been casually noted in other studies but no attempt had been made to describe them in detail, account for their occurrence or highlight their significance to mud volcanism. These were the principal aims of **chapter 4**, which included first a description of two areas of phase-reversed seabed at the upper terminations of large mud volcano systems and then used a geophysical model to constrain their most likely cause.

Seismic descriptions of phase-reversed areas of seabed were made at the Chirag and Azeri mud volcanoes. In both cases the area of negative polarity seafloor reflection was found to be clear and continuous over a large area. At Chirag the phase

reversal corresponded to the crater pedestal which is investigated further in **chapter 5**. At Azeri the phase-reversed area was found to cover an irregularly shaped area interpreted to represent two seabed salses and a number of kilometre-scale lobate mud flows. These were probably sourced from the salses once the fill breached the salse edges (marked E in Fig 6.1). A synformal reflection interpreted to represent the base of one salse was identified that indicated a salse depth of approximately 5 m near its edge. This mapping provided a clear picture of the architecture of the volcano's source point and the pattern of recent mud extrusions. Other studies have achieved this to some extent but none have documented such detailed evidence for the presence of salses and associated mud flows. None have identified extrusive depositional features as phase-reversed amplitude anomalies.

The second part of **chapter 4** aimed at better constraining the likely origin of seabed phase reversals. Since subsurface phase reversals are known to be the result of gas in the section and mud volcanoes are known as sites of voluminous gas expulsion, an obvious hypothesis to test was that seabed phase reversals are the result of gas within the seafloor sediment. This test took the form of a simple geological and geophysical model derived from data from a nearby borehole. Sonic, density and checkshot data were used together with published measurements for seabed sediment density and seismic velocity to establish the likely acoustic impedance change across the study area seafloor. Other published information was then used to reduce these values by an amount likely to occur when gas was present in the sediment. The results suggested that the under normal conditions the seabed reflection would be positive polarity and under gassy conditions it would negative polarity. The hypothesis that seafloor phase reversals are the result of gas in the sediment was verified.

Chapter 4 introduced and explained an acoustic phenomenon that is potentially very useful to the study of mud volcanism. It showed that phase-reversed areas of seafloor can be mapped using seismic data to reveal important details of the source point architecture, sediment distribution and fluid content. All of these are yet again important in enhancing the understanding of the way that mud volcano systems evolve and they way sediments and fluids are expelled from sedimentary basins.

6.2.3 Crater mapping and analysis (chapter 5)

Chapter 5 reported a multidisciplinary study into the structure and origin of an interesting and widely observed mud volcano source point structure- the mud volcano crater. The investigation utilised field mapping, seismic, satellite and digital elevation data to provide a thorough coverage of submarine and onshore craters from Azerbaijan and the South Caspian Sea. This enabled both the gross crater architecture and outcrop-scale structure to be analysed and visualized leading to the construction of a generic model for crater structure and an informed discussion of potential crater origin mechanisms. Prior to this study mud volcano source point structure had been investigated by others but no studies had identified mud volcano craters of the kind described in **chapter 5**. It had not been identified that similar collapse structures could be found at a range of examples and no terminology or origin mechanism had been proposed to assist with better describing or understanding this kind of mud volcano source point.

Through the description of a range of examples and the ground-truthing of remotely imaged craters with onshore observations, a generic model for crater structure was compiled. Starting at the edge of the crater this consisted of a topographic rim, circular crater margin fault, moat, pedestal and central gryphons (marked F in Fig. 6.1). A number of examples were described that displayed this morphology and it was noted that the striking “moat and pedestal” topographic pattern appears characteristic to a number of craters. Some craters were found to be located at the crests of conical edifices, others in roof domain sediments that overly buried edifices and feeder conduit systems (marked F in Fig. 6.1).

How the craters formed was a question addressed by the study and various potential origin mechanisms were discussed. Crater origin as a collapse feature resulting from subsurface sediment and fluid evacuation emerged as the favoured choice due to the close association of the craters to recently extruded mud volcanic sediment. Mud volcano craters can therefore be viewed in a similar context to other circular collapses that result from subsurface evacuation such as igneous calderas, pit craters, dissolution collapse sinkholes and collapse depressions. The prefix “subsidence” can therefore be added to better distinguish this type of crater from other explosive types. Firmly concluding on the depth and nature of the evacuated region was not possible in this investigation due to seismic imaging problems. A relatively

shallow source unit (<400 m depth) is preferred to one deeper within the system due to the shallow dip of the crater margin faults. Linkage between these faults and deeper ones within the system's caldera is not thought likely but cannot be totally dismissed. Extrusive sediment layers within the roof domain are likely candidates for a crater fill source body but further work is required to confirm this.

Chapter 5 documented for the first time the detailed structure of an important type of mud volcano source point. It showed that surface structures at the upper terminations of large mud volcano systems have the potential for recording evidence of processes occurring in the subsurface. It provided a structural model and new terminology that would be of use to others describing mud volcano craters in the future. It is anticipated that a potentially large number of other mud volcano edifices worldwide may exhibit a similar morphology to the craters described here.

6.3 Discussion

This project aimed to document the structure, evolution and geophysical expression of the extrusive constructions of large mud volcano systems and assess their potential for acting as records of the processes and mechanisms that control the system's evolution and the history of sediment and fluid expulsion from sedimentary basins. From this broad remit three principal themes are here discussed in more detail. These presented in sub Sections 6.3.1-6.3.3.

6.3.1 Extrusive domain evolution and the record of basinal fluid expulsion

In combination, the core research Chapters document evidence for fluid and sediment expulsion from the South Caspian Basin in the form of multi-scale structural and sedimentary features of mud volcano edifices and other deposits. Various characteristics of the eruptive constructions investigated here can be interpreted to gain some insight into the way mud volcano systems evolve and how fluids and sediments are expelled from sedimentary basins. Three areas that are discussed further are: 1) the stacking arrangement of mud volcanic sediment units as evidence for pulsed fluid and sediment extrusion; 2) collapse of mud volcanic edifices, its causes and consequences and; 3) the various types of extrusive deposit and its significance for subsurface structure.

Pulsed eruptive activity and eruptive unit stacking

There are various lines of evidence identified in this project that point to aggradation of mud volcano sediment “units” into a stacked arrangement and the construction of the extrusive and roof domains as a series of discrete sediment bodies of various sizes. At the largest scale is the stacking of kilometre-scale mud cones within the Chirag volcano edifice. At a smaller scale are the stacked “pancake-like” circular units within the pedestal at the Qaraqus-Dagi edifice onshore. These observations support the findings of other studies that suggest that significant sediment expulsion from mud volcano systems is pulsed and not temporally continuous over long periods (Carson and Sreaton 1998; Kopf 1998; MacDonald et al. 2000). Pulsed fluid expulsion from sedimentary basins in general is a commonly observed phenomena (Bitzer and Ayora 2000; Bons and van Milligen 2001; Cartwright et al. 2007; Hunt 1990; Mazzini et al. 2003).

The reasons for the occurrence of pulsed fluid expulsion from sedimentary basins and mud volcano systems are not well understood. Pulsing can be considered as either the result of repeated seal failure and re-sealing events within any fluid expulsion conduit systems or variations in the fluid generation and output rates within the basin. In the context of the mud volcano system, the pulsed eruptive pattern that has been observed here could either be explained by processes occurring within the conduit or within the source domain. Both these areas of the system are susceptible to rapid changes in their physical state as a result of earthquakes and it has recently been suggested that earthquakes may play an important role in triggering eruptions (Mellors et al. 2007). Liquefaction within the parent bed may occur during an earthquake as can spontaneous hydrocarbon maturation, gas bubble excitation and groundwater level changes (Mellors et al. 2007). The conduit system may be affected if the earthquake causes it to dilate. Considering these factors along with recent earthquake-eruption statistical correlations it would appear that the episodic nature of earthquake activity may go some way to explaining the pulsed activity of mud volcanoes (Mellors et al. 2007).

For processes within the conduit to influence the eruptive pattern it needs to have some form of self-sealing property. One possible self-sealing mechanism is its blockage by impermeable material; a second is the mechanical closure of the conduit during pressure drop at the end of an eruption. In support of the former are ideas

centring on the “fault-valve” model of Sibson et al. (1988). This model envisages a cyclical increase in fluid pressure until hydrofracturing is induced and excess fluid pressure is rapidly drained from the system via the fracture. Hydrothermal self-sealing and mineral precipitation within the fracture then re-seal it leading to a renewed build-up of pressure and another cycle of expulsion. An obvious candidate for a similar conduit seal in mud volcano systems is the residual mud breccia within the conduit at the time the eruption stops. If this sediment is sufficiently impermeable and pressure within the underlying source region is too low to fracture it and carry it upwards then it will plug and seal the conduit. It can only be removed when pressure builds up to levels high enough to fracture it and remove it from the conduit. Kopf (2002) calls the breaching of a plugged conduit “explosive decompression” and cites it as a commonly occurring mechanism that facilitates short-lived explosive eruptions. A second possible self-sealing property of the conduit, independent of its fill, is its mechanical closure when pressure drops (Carson and Screamon 1998). Considering both these mechanisms it is not difficult to imagine how a mud volcano conduit can become sealed when pressure drops following an eruption. In reality it is likely to be a combination of conduit plugging and conduit closure that contributes to pulsed extrusive behaviour at an eruption timescale.

However, when longer duration periods of increased eruptive activity are considered, such as those that account for the four mud cones of the Chirag volcano edifice, it becomes more difficult to imagine how relatively small-scale physical processes within the conduit, or indeed earthquakes, could control such large variations in mud volcanic activity through time. A lower order control of pulsed extrusion seems necessary. In the context of all fluid expulsion from sedimentary basins this is likely to be due to far-field forces such as variations in tectonic activity, sedimentation rate or internal fluid generation. In the context of the South Caspian Basin and its mud volcanism these three factors are all potentially important in influencing the pulsed activity of mud volcanoes and all three are known to have undergone variations in intensity through the last 5 Ma (Allen et al. 2004; Lerche and Bagirov 1999; Lerche et al. 1997). Indeed, Yusifov and Rabinowitz (2004) suggest that sedimentation variations and gas generation pulses may be important factors controlling the regionally observed pulsed eruptive behaviour of South Caspian mud volcano systems. They have correlated regional pulses of rapid sedimentation and gas generation to “cycles” of increased mud volcanic activity. cursory analysis indicates

that these cycles may loosely correlate to the four Chirag mud cones although there is no reliable biostratigraphic information to confirm this idea.

Different sized units of erupted mud volcanic sediment observed in this project might suggest that the extrusive pulses responsible for their occurrence were either of different durations or were characterized by different rates of eruption. However, it is considered highly likely that the larger eruptive units, such as the Chirag mud cones are the product of numerous small eruptions and not one large one. Constraint on what volume of sediment is likely to be extruded during one eruption exists in the form of large tongues of mud breccia observed at the Lokbatan mud volcano that were deposited during a 2001 eruption (Planke et al 2003, Aliyev et al. 2002). The volume of approximately 0.0003 km^3 is many times less than the volume of any of the Chirag mud cones (average volume = 2.65 km^3) suggesting that one or even a small number of individual eruptions could not have been enough to construct the entire cone. At between 0.000004 and 0.002 km^3 in volume the pancake-like circular eruptive units in the Qaraqus-Dagi (QD) crater pedestal are more likely to have been deposited during one eruption. Repeated eruptions of this nature deposit further units which gradually aggrade to form edifice cones. Some large eruptions breach the summit crater rim and form large flows on the volcanoes flank. These have been observed in the field at the QD edifice and offshore at the Azeri mud volcano edifice as phase-reversed seabed amplitude anomalies. All this evidence suggests that the construction of large mud volcano edifices takes place by the gradual aggradation of relatively small pancake-like eruptive units and kilometre-scale mud flows. Periodic breaks in the eruptive frequency due to far field forces may result in the temporary dormancy of the system and the compaction and possible cementation of the extruded mud. As evidenced by the presence of non-eruptive sediment within the Chirag edifice these breaks may be of long enough duration for sediments to accumulate. Renewed extrusion in a second major phase of activity results in more small eruptions building to form a second stacked cone and so on.

An interesting observation made in the core research Chapters of this project is the various patterns of eruptive unit stacking and the trends in eruptive unit volume with time. Stacking patterns indicating both an increase and a decrease in eruptive volume through time have been observed (Fig. 6.2c and e). In other studies seismic images and numerical modelling suggest that eruptive volume remains fairly constant or decreases with time (Deville et al. 2006; Murton and Biggs 2003; Stewart and

Davies 2006; Yusifov and Rabinowitz 2004, Fig. 6.2a, b and d). Whilst the causes of these patterns are unclear numerical modelling suggests that variations in pressure drive are likely to play an important role. For example, Murton and Biggs (2003) state that the progressive increase in volcano edifice height during its construction decreases the driving pressure of the system since it increases the load on the base of the conduit mud column. Therefore in idealized circumstances a mud volcano edifice will develop an “upward-tapering” profile with each successive flow unit thinner and of smaller radius than the previous one (Fig. 6.2a). This model is well represented by some seismic images and the stacked eruptive units within the QD crater pedestal which may indicate a waning pressure drive during the pedestal construction and crater filling (6.2c). However, it very much contrasts the eruptive pattern observed within the principal Chirag volcano edifice where there is a progressive increase in mud cone volume culminating in a mud cone approximately 1.5 times larger than the first. Following the simple approach of Murton and Biggs (2003) this pattern indicates an increase in pressure drive with time (Fig. 6.2e). This could be explained by the action of far field forces, such as tectonic collision or sedimentation, or it could be due to a decrease in edifice height with time reducing the load on the base of the mud column. A further possible explanation is the progressive widening of the conduit during evolution of the system due to wall rock erosion. Whilst this mechanism and far field forces cannot be ruled out as contributing to the Chirag eruptive pattern, the findings of **Chapter 2** indicate the potential of edifice collapse and a decrease of mud column height for playing an important role. The edifice’s position within a fold saddle, the presence of a central collapse caldera and the internal seismic architecture all suggest that the edifice has undergone collapse during its construction. It appears that the onset of collapse coincides with the beginning of the progressive increase in mud cone volume (marked * in Fig. 6.2e). If this mechanism were true it would indicate that processes occurring as a result of mud volcanic eruption (e.g. edifice collapse) have the potential to influence and modify the continued development of the system. A comparison could be drawn between this and other self-organized fluid expulsion systems (Bons and van Milligen 2001).

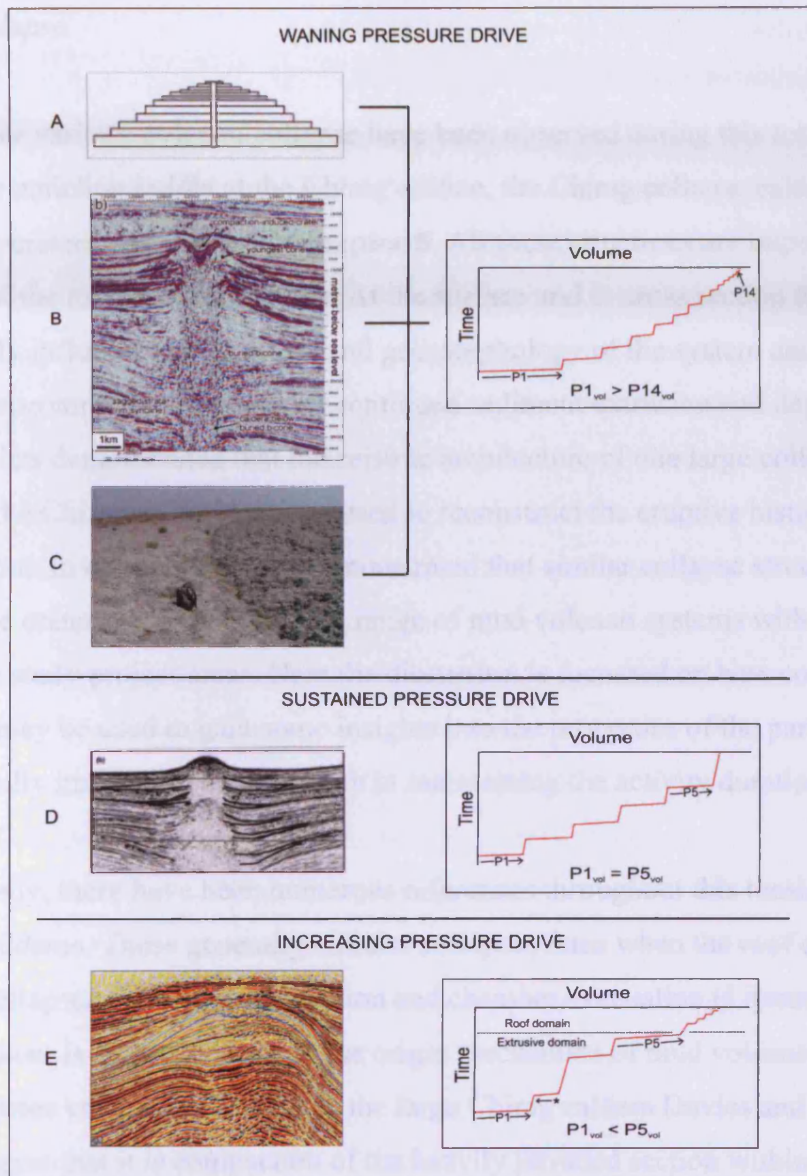


Figure 6.2 Varied styles of mud volcano sediment unit stacking within edifices as evidence for waning, sustained and increasing pressure drive with time. (a) Idealized mud volcano edifice structure based on the modelling of Murton and Biggs (2003) which is thought to represent a decreasing pressure drive with time. (b) 3D seismic image of a South Caspian Sea mud volcano edifice showing a progressive decrease in the volume of eruptive units with time (from Stewart and Davies 2006). (c) Field photograph of the Qaraqus-Dagi mud volcano crater pedestal showing the progressive decrease in eruptive unit diameter and volume with time. Each of these examples depicts a situation whereby the earliest eruptive pulses are the largest and the most recent are the smallest. (d) 2D seismic image through a South Caspian Sea mud volcano edifice showing a series of stacked mud cone each with a similar volume indicating a sustained pressure drive with time (from Yusifov and Rabinowitz 2004). (e) 3D seismic image through the Chirag mud volcano edifice showing a series of stacked eruptive units that progressively increase in volume through time. This pattern may be evidence for progressively increasing pressure drive with time.

Edifice collapse

Evidence for various styles of collapse have been observed during this research in the form of the anticline saddle at the Chirag edifice, the Chirag collapse caldera and the subsidence craters investigated in **chapter 5**. All these structures are important elements of the mud volcano system. At the surface and in cross section they significantly influence the structure and geomorphology of the system and provide important accommodation space for continued sediment extrusion and deposition. **chapter 3** has demonstrated that the seismic architecture of one large collapse structure (the Chirag caldera) can be used to reconstruct the eruptive history of the entire system. In **chapter 5** it was demonstrated that similar collapse structures (subsidence craters) can be found at a range of mud volcano systems within and outside the study project areas. Here the discussion is focussed on how collapse structures may be used to gain some insights into the properties of the parent bed and the potentially important role they play in maintaining the activity duration of the system.

Firstly, there have been numerous references throughout this thesis to igneous volcanic calderas. These generally circular collapses form when the roof of a magma chamber collapses following an eruption and chamber evacuation (Lipman 1997). A similar process is suspected here as the origin mechanism of mud volcano calderas and subsidence craters. In the case of the large Chirag caldera Davies and Stewart (2005) suggest that it is compaction of the heavily intruded section within the circular caldera faults that accounts for its occurrence. However, the fact that the caldera floor (BMV reflection) is largely coherent suggests that this might not best explain the features occurrence. Instead it is considered likely that some form of focussed evacuation of fluids and sediment from within the source region, possibly with some localized differential compaction, accounts for the formation of the collapse (Fig. 6.1). At Chirag it is not possible to determine the exact position or nature of the evacuated region. Models for igneous caldera formation suggest that it would be located near the lower tips of the caldera faults (Lipman 1997). The circular nature of the collapse suggests that the subsurface evacuation is located beneath the centre of the caldera. Its deep but laterally restricted areal extent suggests too that the evacuation zone is restricted to a relatively small area of the parent bed beneath the caldera. This may suggest that the parent bed is not highly mobilized across a large area and instead of

flowing *en masse* towards the zone of depletion when evacuation begins a relatively small zone is efficiently evacuated and collapses. A focussed collapse structure is formed in favour of a broad sag. However, at Chirag it is possible that a degree of additional ductile flow within the parent bed has occurred evidenced by the saddle within the Apsheron anticline at the location of the edifice. A combination of both processes may therefore have influenced the structure and evolution of this example.

Collapse structures within the extrusive and roof domains of mud volcano systems may play an important role in prolonging the eruptive activity of the system. This argument centres around the idea of Murton and Biggs (2003) who assume the driving force of a mud volcano system to be overpressure largely derived from the weight and density of the overburden on the parent bed. The conduit of the system is effectively a tube similar to a manometer used to measure excess pore pressure in aquifers (Brown 1994). Fluid and mud within the conduit will therefore rise to a level proportional to the level of overpressure. In the early stages of system evolution the height of the conduit ($h_{conduit}$ in Fig. 6.3a) is not sufficient to balance the pressure in the parent bed and the edifice is able to progressively increase in height through successive eruptions. At a certain point $h_{conduit}$ will reach a level where the weight of mud and fluid in it balances the pressure within the parent bed. At this point no more eruptions can occur and the edifice has reached its maximum height (Fig 6.3b). Further eruptions can only take place if the balance of pressure is once again shifted in favour of the pressure in the parent bed. This can only be achieved if the pressure within the parent bed increases by other means (i.e. hydrocarbon maturation or far field forces), an eruption occurs on the flank of the edifice or collapse of the edifice summit occurs. The latter has the effect of reducing the height of the mud column and therefore reducing the pressure at its base. This may have the effect of stimulating renewed eruptive activity until edifice height once again reaches its theoretical maximum (Fig. 6.3c). Collapse structures such as subsidence craters and calderas are therefore potentially important structures that can reduce the height of a mud column and possibly stimulate further eruptions. Again there is the suggestion that mud volcano system evolution may involve a degree of self organization and may be controlled by the formation of positive feedback loops. An eruption leads to subsurface evacuation and collapse- this reduces the mud column height and stimulates further eruptions, which in turn leads to more evacuation and so on. It is

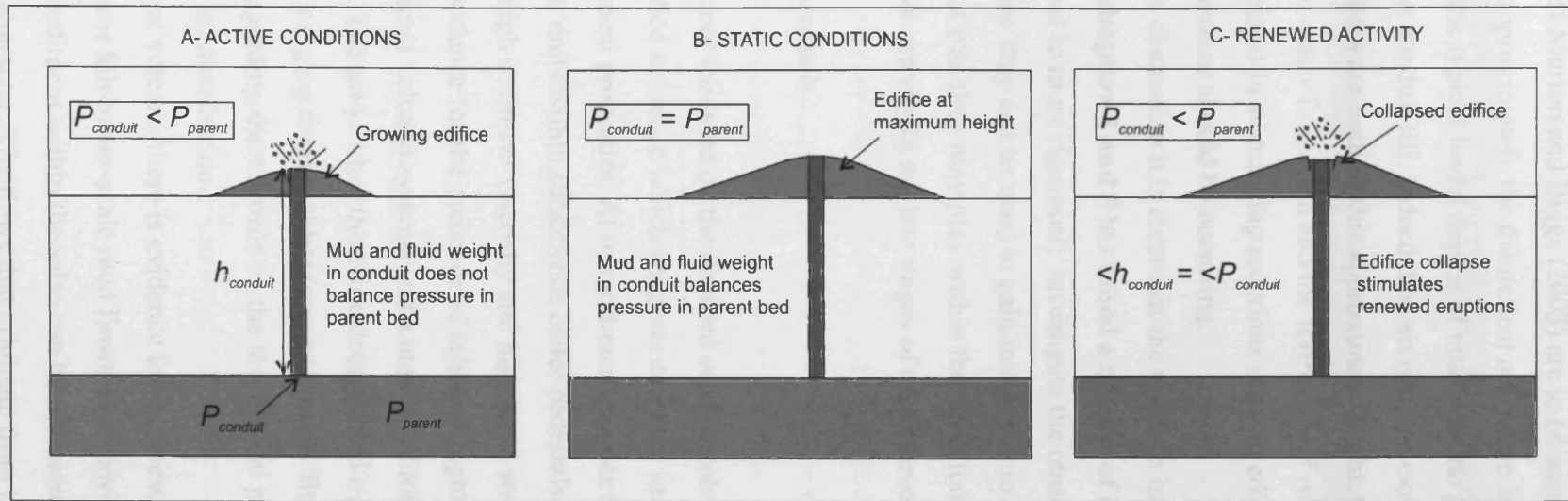


Figure 6.3 The significance of mud volcano edifice collapse: (a) Schematic depiction of a simple mud volcano system during its constructive phase. Pressure at the base of the conduit due to the weight of mud in it is not high enough to balance the pressure drive from the parent bed and the mud column and edifice grow in height. The maximum column height is reached when pressure at the base of the conduit balances the pressure drive from the parent bed as in (b). Collapse of the edifice as depicted in (c) has the effect of reducing the mud column height and reducing the pressure at its base. This may act as a stimulus for renewed eruption and the continuation of the system's activity after it has reached its theoretical maximum height.

interesting to note that few mud volcano edifices in the world are greater than 400 m in height. If the ideas of Murton and Biggs (2003) are to be accepted it could be concluded that this is approximately the theoretical maximum height of a mud volcano edifice given the typical burial depths of mud volcano parent beds and typical density of mud volcano conduit fill. Indeed the two onshore examples that both have summit subsidence craters are both of this approximate height. Collapse, through caldera and subsidence crater formation and the formation of related feedback loops, may therefore be important in stimulating eruptions once an edifice has reached a height at which no eruptions should be occurring.

From the above discussion it is clear that the research into mud volcano collapse structures in **chapters 3 and 5** has raised a number of important questions. Further work is required to more rigorously investigate the reasons for collapse structure formation, how they can be used to gain insights in to mechanical state of the parent bed and what role they may play within feedback loops that influence the continuation of eruptive activity in the late stages of edifice evolution.

Diversity of eruptive products

Whilst this project has not focussed on the detailed sedimentology of mud volcanic sediment, it has identified evidence which suggests extruded sediment can have a broad range of mechanical properties. At one extreme **chapter 5** identified rubbly mud volcanic sediment units within subsidence crater pedestals that each have abrupt edges suggestive of a high sediment viscosity and high yield strength. At the other **Chapter 4** recorded evidence for the presence of salses of highly fluid mud at the upper terminations of mud volcano systems and a number of lobate gassy flows originating from them. The project has therefore documented evidence for a spectrum of sediment properties ranging from highly viscous to highly fluid. This raises interesting questions regarding the controls on the mechanical properties of mud volcanic sediment and its distribution.

At the Azeri mud volcano there is evidence for the presence of circular seafloor salses that source kilometre-scale mud flows. By drawing analogy with onshore examples the sediment within the salse can be estimated to have a low viscosity and “soupy” character. The flows that originate from it however are lobate and bear a close resemblance to onshore flows noted in **chapter 5** that are formed by

plastic, high viscosity mud. Indeed, despite their gassy nature the Azeri seabed flows must have enough yield strength to build and support the conical edifice promontory upon which they form (Murton and Biggs 2003). These points raise the question of whether the system is somehow organized so that very low viscosity sediment remains in the salse and the higher viscosity sediment is arranged into flows. One possibility is that rapid degassing of salse overspill leads to a strengthening of the sediment and the formation of lobate flows sourced flow very fluid salse fill. This might explain why the flow retains gas bubbles for long enough to be imaged by the seismic survey. If the flow was very fluid, gas bubbles could easily escape to the water column. Onshore, for instance, gas bubbles are trapped within stiff mud due to the higher viscosity of the sediment.

A further interesting point comes from looking at the evidence for differing sediment properties at different volcanoes. Of particular interest is the difference in architecture of the Chirag subsidence crater and Azeri conical mound with circular salses. At Chirag the phase-reversed expression of the crater pedestal suggests it to be gassy, yet its raised expression suggests that it also has a degree of yield strength and viscosity more akin to the rubbly pedestal sediment in the onshore craters. At Azeri it appears that much more fluid sediment characterizes the salse fill. Why there is this contrast in eruptive styles and sediment properties is observed at two volcanoes only a short distance apart is unclear. Why should one volcano erupt very fluid sediment capable of forming a salse when another nearby erupts stiffer sediment capable of forming a pedestal? Similar differences have been observed offshore Trinidad where some mud volcanoes form fluid “mud pies” where others nearby form conical mounds (Lance et al. 1998). In this case the difference is attributed to firstly, shearing in the mud pie conduit leading to the extrusion of more fluid mud and secondly, the dissociation of gas hydrate in the vicinity of the mud pies adding more fluid to the system. In the case of Chirag and Azeri gas hydrate dissociation can be ruled out due to insufficient water depth but the possibility remains that processes within the conduit or the addition of extra fluid at Azeri might influence the properties of the erupted sediment. It may be that Azeri taps a more fluid rich area of the parent bed or a greater degree of shearing has occurred within its conduit. Once again further work is required to ground truth the inferences made here regarding sediment mechanical properties and follow up the questions posed regarding the reason for the differing mechanical properties of mud volcano sediment.

6.3.2 Geophysical expression of the extrusive and roof domains

Much of the research presented in this thesis is derived from the geophysical analysis of mud volcano systems. Indeed, the geophysical expression of the extrusive and roof domains of the system is an important theme of the project. Principally it has been seismic reflection data that has been used to describe the seabed and surface structure of the studied examples but the project has also incorporated interpretation of Digital Elevation Models (DEMs) and IKONOS satellite images to supplement the seismic and field observations. Historically, seismic reflection data that image mud volcano systems have been of very poor quality owing often to the presence of gas in the section or the small size of edifices and other system components. The use of high quality geophysical data in this project has led to a thorough and detailed geophysical analysis of the various extrusive components of the mud volcano system at the surface and in the subsurface at a range of scales.

At the largest scale seismic reflection mapping in **chapter 3** identified a large complex mud volcano edifice buried beneath roof domain sediments. This feature is up to 1.4 km thick in its central section and as such a vast amount of internal detail can be observed. At a smaller scale, within this edifice, were found a number of wedge-shaped seismic facies units each interpreted as a buried mud volcano cone. Each unit is separated from others above and below it by a discrete seismic reflection, a fact that testifies to a geophysical contrast between each sediment unit. What is responsible for this geophysical contrast has not been established here but changes in sediment consolidation, cementation, fluid and clast content are all possible causes. In **chapter 3** each mapped reflection was chosen on the basis of its continuity, clarity and seismic stratigraphic context. Interestingly, each one is negative polarity which might suggest a progressive reduction in sediment acoustic impedance with depth into the edifice. Such a pattern could be produced if the early eruptive deposits are more fluid rich than those overlying it. Without calibration to a sonic and density log however it is not possible to tell whether the reflections selected for mapping truly represent the geophysical interface between the various sediment units. In any case, the fact that each unit is imaged as a wedge suggests that the geophysical contrast follows sedimentary layering and is the result of depositional stacking and not fluid- or diagenetic-related property changes.

Mapping the shape and size of the seismic facies units within the Chirag edifice enables the constraint of their origin as wedge-shaped mud cones or sheet-like non-eruptive sediment units. This is an approach taken by other studies and is likely to be of use elsewhere (Deville et al. 2003; Yusifov and Rabinowitz 2004). Measuring the volume of the various mud cones is a useful way of determining the eruptive sediment volume pattern through time (see sub-Section 6.3.1). Analysis of this nature is a much more accurate way of measuring extruded sediment volume than surface observations since the total thickness of the deposits can be measured with a greater degree of accuracy. However, a major caveat in the calculation of erupted sediment volume is imposed by the vertical resolution limit of the seismic data. Mud cone volume can be measured but what cannot easily be determined is the proportion of non-eruptive “background” sediment within each cone that contributes to the total volume. Coring in other areas has suggested that whilst uninterrupted mud breccia beds of a thickness comparable to the thickest mud cone (approximately 195 m) can be encountered, often thin sediment layers are found interbedded with mud volcanic sediment (Jurado-Rodriguez and Martinez-Ruiz 1998; Kopf 1998; Robertson 1996). Discontinuous reflections within most of the four mud cone units suggest the presence of some internal discontinuities which may relate to the presence of thin non-eruptive units. This means that that the volume measurements of each mud cone in **chapter 3** represent a maximum estimate of the eruptive volume.

Analysis of roof domain reflections in **chapter 3** using amplitude and interval amplitude maps enabled further eruptive deposits overlying the principal edifice to be identified. This allowed for the interpretation that the activity of a mud volcano system does not finish once the phase of principal edifice construction is complete. Instead, relatively minor volumes of sediment may continue to be deposited as the edifice is buried. Whether these sediments are sourced from great depth in the source domain or whether they are the product of disequilibrium compaction within the principal edifice has not been determined. Unlike the mud cones within the principal edifice, the deposits in the roof domain are not seismically resolvable. That is they are too thin to be imaged by a separable “top” and “base” reflection. Nonetheless their presence has resulted in a clear amplitude signature at various levels within the Chirag roof domain. All anomalies are those of reduced positive amplitude. That is the strength of a positive acoustic impedance change has been reduced by the presence of

the volcanic deposit. Properties such as a high fluid content or lower grain density within the mud could produce this signature.

In terms of geophysical investigation perhaps the most significant result of this project has been the introduction and explanation of seabed phase reversals and their association with mud volcanism. Mud volcanoes are prime candidates for any gas-related geophysical phenomena since they are the sites for voluminous gas expulsion (Judd 2005). Other phenomena such as acoustic turbidity, gas chimneys and subsurface phase reversals have all been previously acknowledged as reliable indicators of gas within a section; some in association with mud volcanoes (Judd and Hovland 1992; Schroot et al. 2005; Yin et al. 2003). Seabed phase reversals have not been described before in detail. In **chapter 4** two mud volcano-related phase reversals were described and the hypothesis that they are caused by gas in the seabed sediment was tested using data from a borehole. The presence of a phase reversal in both cases suggests that the seafloor sediment is gassy but has a viscosity high enough to retain the gas for a period of time after deposition. The fact that flows at Azeri are imaged as phase-reversed indicates that the gas within them was deposited with the flow and was not otherwise injected into seabed sediment following flow deposition.

It was concluded in **chapter 4** that gas in the seabed sediment is the most likely cause of seafloor phase reversals. What was not considered was how much gas is required to create a seafloor phase reversal. It was also not considered whether seafloor sediment could be gassy and not imaged as a seafloor phase reversal. These are questions which will certainly benefit from further work. It is considered likely that to some extent the amount of gas as a percentage of the total pore fluid volume is not a significant factor in the creation of a seabed phase reversal. Theoretical calculations and experiments both suggest that significant acoustic effects are produced when gas is present even in very small amounts (Fannin 1980; Gregory 1976). Keeping bulk density at the preferred value for gassy sediments used in **chapter 4** (1.2 kg m^{-3}) a sediment seismic velocity (V_p) of 1200 m/s is required to produce a negative polarity reflection of a very low strength ($RC=-0.02$). This is equal to an 18% reduction in initial sediment V_p as chosen in **Chapter 4**. Andreassen et al. (2007), using the equations of Gregory (1976), show that a reduction in V_p of a greater magnitude than this is possible when the sediment is only 1% saturated with gas. For example, sediment with a porosity of 40% and an initial V_p of 1900 m/s is predicted to undergo a 25% reduction in V_p with only a 1% gas saturation. Beyond

approximately 4% gas saturation there is no further reduction in sediment V_p . These calculations firstly suggest that only very small amounts of gas (<1%) are required to lower sediment V_p enough to produce a phase reversal. Secondly, patches of seabed with only very small amounts of gas in the pore spaces are likely to be imaged as phase reversals. It is also apparent that phase reversals may not be useful at determining the volume of gas present in sediment since beyond 4% saturation there is no further geophysical property change.

Future work on phase reversals should investigate in more detail the gas saturation levels in phase-reversed sediments and more examples should be identified and described. **Chapter 4** does not investigate other physical consequences of gas such as attenuation and takes no account of the frequency of the seismic pulse. Both are factors that may influence the geophysical signature (Anderson and Hampton 1980). Seismic inversion of phase-reversed seabed reflections was not possible in this study since the seismic amplitude was “clipped” to reduce its volume. This analysis using seismic data with the true amplitude preserved together with focussed seabed measurement and monitoring would be a useful way of furthering the understanding of these important geophysical features.

6.4 Implications for economic and engineering geology

Since mud volcano systems are often found in close spatial association with hydrocarbon accumulations, an understanding of their internal structure and development becomes important for economic reasons. In addition, they represent a considerable hazard to drilling and engineering operations and have potential for recording important information on the history of fluid expulsion and structure development. The results of this project that may have implications for these important topics are discussed in two sub-Sections below.

6.4.1 Subsurface hazard identification

Mud volcano systems of the scale investigated in this project are significant hazards to economic drilling and engineering operations. Most notably perhaps, **chapter 4** introduced seabed phase reversals as useful indicators of gassy areas of seabed which are important to drilling or other engineering operations. However, what have not

been previously dealt with in the project are the implications that its results have for subsurface hazard identification.

Typically the anticlinal location of mud volcano systems means that hydrocarbon accumulations are located near their feeder conduits. Low rock or sediment strength, intense fracturing and large pressure variations are potential problems that may be encountered within and around this area of the system. Typically hydrocarbon wells are designed to avoid these areas and so avoid these unpredictable and potentially hazardous conditions. Seismic mapping can effectively delimit these problem areas as demonstrated in recent studies (Stewart and Davies 2006). However, in the shallower section large diameter volcano edifices act as “canopies” to the system and need to be bypassed by wells if deeper accumulations are to be accessed. The edifice represents a potentially significant hazard in which sedimentary units of high fluid content and low strength may be present. Located above numerous hydrocarbon accumulations and at over 11 km diameter the Chirag volcano edifice is a hazard that cannot be easily avoided. There is a necessity for wells to penetrate edifices of this size if deeper hydrocarbon accumulations are to be accessed. For similar reasons roof domain sediments also present a considerable risk to drilling operations since potentially weak and fluid-rich mud volcano sediments may be contained within them.

By providing a detailed account of the internal structure of the extrusive and roof domains of large South Caspian mud volcano systems, this project has gone some way towards better characterizing the hazard posed by these elements of the system. The interpretation of edifice internal units as either mud cones or non-eruptive units using their seismic architecture is a way of better predicting the sedimentary nature of a section prior to drilling. The use of amplitude maps of roof domain reflections also has proved to be a useful way of identifying potentially hazardous mud volcanic deposits that are thinner than the vertical resolution limit of the seismic data.

6.4.2 Fluid dynamic and structural history

Previous studies have identified mud volcano systems as important structures that may be used to gain insights into the deep structure and sedimentary composition of a basin as well as the prevailing hydrodynamic regime (Kopf 2002). This project has

provided further support to this notion by showing that detailed seismic interpretation of the extrusive and roof domains may be used to reconstruct the eruptive history of a large fluid expulsion conduit system and thereby gain insights into the basinal fluid dynamic regime.

At Chirag for example, the interpretation of the edifice as a series of stacked eruptive units in **chapter 3** suggests a history of pulsed fluid expulsion. In this project data has not been available that allow for the calibration of this history to the local chronostratigraphy. This could be undertaken however, if a specific dataset were acquired for the purpose. Such information would be highly valuable to petroleum geologists attempting to constrain in time periods of greatest hydrodynamic activity, seal compromise and fluid leakage to the surface. In addition **chapter 3** highlighted the importance of the large central collapse caldera to the structural evolution of the system and showed that analysis of the edifice units could lead to a reconstruction of the relative timing of caldera growth. At Chirag the steeply dipping caldera fault has a height of approximately 5 km and as such passes through important reservoir intervals beneath the edifice. As such the fault may play an important role in sealing hydrocarbon traps and preventing fluid leakage to the surface. Any information on when this fault was initiated and when it was actively propagating would be important to petroleum geologists since the periods of greatest activity may coincide with the periods of greatest fluid leakage (Carson and Scream 1998). This project has been unable to establish the absolute timing of the caldera fault activity but the genetic relationship of the caldera and the overlying edifice sediment units again suggests that dating of the edifice units may help to do this.

6.5 Project limitations and suggestions of further work

The range of data types and varying scales of investigation in this project have led to a thorough investigation of the extrusive and roof domains of South Caspian Sea mud volcano systems. However, whilst the project represents a considerable advancement of the knowledge and understanding of these aspects of mud volcanism, certain limitations have been imposed by limited data availability, data quality gaps and the relatively small number of examples available for study. The remainder of this Section now provides a discussion of the project limitations together with a number of suggestions as to how further work may be of use in overcoming them.

This project has centred on the use of 3D seismic data to better constrain the structures and origin mechanisms of large mud volcano systems. The results are testament to the power of this data type for the investigation of mud volcanoes. It is only recently that good quality 3D seismic data that cover mud volcano systems have become available. Mapping structures and sediment units in 3D and the accurate measurement of volumes and other dimensions is only now becoming possible. However, despite the large volume and high quality of seismic data available to this project only a relatively small number of mud volcano systems are imaged in enough detail to allow for meaningful seismic interpretation to take place. Whilst analysis of these examples has proved successful, the inclusion of more 3D seismic data and more well-imaged examples would allow for a more informed comparison of systems from different areas and aid with the difficult task of better classifying mud volcano systems. The study of mud volcanism using seismic data is in its infancy. It is at a stage where little is known about their basic architecture and evolution. Basic information on these aspects is still of high value to their understanding.

Chapter 5 of this project demonstrated that the integration of data types such as seismic, satellite and elevation data along with field observations has proved useful in this project. In particular, in **chapter 5**, it was shown that features observed onshore are similar to those observed offshore. No other studies have used field data to ground-truth remote data in this way. Indeed, the onshore mud volcanoes of Azerbaijan are greatly underrepresented in the literature and their potential analogue value for submarine examples has not been fully realised. In particular there is a lack of geophysical and borehole data from the Azerbaijan mud volcanoes (cf. Kadirov and Mukhtarov 2004; Mukhtarov et al. 2003), two data types that have great potential to better constrain the internal architecture of the volcano edifice and shallow structure.

The most significant limitation imposed on this project has been the lack of well data to establish the sedimentary character and absolute age of mud volcano sediment units observed in the subsurface. The reconstructed eruptive history and output volume record of the Chirag mud volcano system in **chapter 3** is therefore only referenced to relative time. Exactly how long it took for the edifice or any of its internal units to be constructed remains unknown. As discussed above in sub-Section 6.3.1 the establishment of an absolute age for the edifice and a constraint of the time it took for each internal sediment unit to be deposited may help further the understanding of the ways sediments and fluids are expelled from the subsurface.

Indeed a major gap in the knowledge of mud volcanic geology is the timescale over which they are formed. Some studies have attempted to address this question using temperature data (Kaul et al. 2006). Others studies have attempted to calibrate the history of mud volcanic eruption to time using seismic data and sedimentation rates (Summer and Westbrook 2001; Yusifov and Rabinowitz 2004). These however are based on 2D seismic data thus limiting the potential to constrain the actual sediment volume output through time.

In other aspects of this project a lack of well data or gaps in well data that were available have lead to other limitations. In **chapter 4** for example, a lack of seabed data for the physical properties of normal or gassy seabed conditions meant that existing data had to be extrapolated and constrained by other published work. The seismic velocity and density of non-gassy seabed sediment was extrapolated using data from a site survey borehole. It is believed that this represents a fair estimate of the seabed sediment properties but clearly there is some potential for error since the measurement are not from the actual study area seabed. For gassy seabed sediments also the properties had to be estimated using published data. Further studies should be focussed on obtaining more data regarding the properties of these sediments. Apparatus such as the acoustic lance is a device capable of doing this and has successfully constrained the seismic velocity of non-mud volcanic gassy sediment from other areas (Fu et al. 1995). Deployment of this device in mud volcano provinces would better constrain the properties of gassy mud volcanic sediment and lead to more detailed geophysical modelling and a better understanding of seabed phase reversals.

Outside of the scope of this project there are many aspects of mud volcanic geology that are poorly understood and would benefit from further investigation. As highlighted in Sections 2.3.1 and 2.3.2 many aspects of the understanding of the intrusive and source domains are poorly understood. With regard to the former, most notable is a lack of constraint on the architecture and diameter of the feeder conduit(s), a lack of constraint on the physical properties of sediment in the conduit between and particularly during eruptions and a poor understanding of the ways that gas actually influences the, often-quoted, buoyancy of the ascending sediment. More rigorous analysis of field exposures of mud intrusions may assist with some aspects of this understanding as would more numerical modelling of the kind already undertaken for other sedimentary intrusive systems (Gallo and Woods 2004). Significant

advancements are also likely to take place in this field as better quality seismic data becomes available. In particular there are ongoing projects focussed on producing high quality converted wave seismic data in the South Caspian Sea (Bouska and Johnston 2005). These new data are likely to lead to improved imaging of the intrusive elements of mud volcano systems since they are not subject to the gas-related imaging problems that hamper normal P-wave data acquisition. In the case of the source domain there is a large gap in the knowledge of its physical properties and the structures which control the location of large mud volcano systems. This is partly due to a lack of any boreholes that penetrate the source domain. It is also a result of the fact that most commercially acquired seismic surveys become very poorly quality at the typical depth of mud volcano parent beds

CHAPTER SEVEN

7.0 Conclusions

The investigations present in this thesis provide a wealth of information on the structure, evolution and geophysical expression of the extrusive and roof domains of mud volcano systems from the South Caspian Basin. Observations and resultant conclusions have led to insights into the eruptive history of large mud volcano systems, their history and style of eruption-related collapse, their geophysical expression both in the subsurface and at the surface and the structure and origin of different mud volcanic source points. Whilst the study is focussed on one geographic area it is anticipated that the results are relevant to mud volcano systems worldwide. The following sections list a number of statements that summarize the conclusions of this project.

7.1 General Conclusions

- Interpretation and analysis of seismic reflection data is a powerful way of investigating the structure of large mud volcano systems in the subsurface.
- Integration of these data with other data types including field maps, bathymetric maps, terrain elevation data and satellite imagery provides a comprehensive database from which to describe and investigate the extrusive constructions and features found within mud volcano systems.
- Analysis of these data types can be used to gain insights into the way large mud volcano systems evolved and reconstruct their history of activity and basinal sediment and fluid expulsion.

7.2 Mud volcano system structure and evolution

- Structural and sedimentary features found within the extrusive and roof domains of large mud volcano systems are large enough and imaged by high enough quality seismic data to allow for their 3D interpretation, mapping and analysis.

- By adapting conventional seismic stratigraphic mapping methodology to the study of mud volcanism the internal structure of large edifices can be interpreted and various seismic facies unit can be identified. Wedge-shaped and sheet-like seismic facies units can be observed. These variations in external form can be used to interpret their origin as either stacked mud cones or sheet-like non-eruptive sediments.
- Detailed 3D mapping of each stacked mud cone allows for accurate erupted sediment volumes can be measured. A volume-output history of the system can be established and breaks in the eruptive activity can be identified.
- The 3D geometry of edifice seismic facies units and their relationship to eruption-related collapse features can be analysed. These details can be used to reconstruct a history of edifice collapse.
- Combining details of both the Chirag mud volcano system's volume output and collapse history has led to the reconstruction of the system's eruptive history. This begins by the deposition of the "pioneer cone" prior to edifice collapse and caldera. A subsequent phase of caldera growth is then recorded in the thickness variation of overlying units. Following a break in eruptive activity and the deposition of a non-eruptive sediment layer further large mud cones were deposited. No caldera growth was occurring at this time.
- Seismic attribute analysis of reflections within the roof domain of a buried mud volcano system can be used to identify additional mud volcanic deposits that were erupted during the burial of the edifice by non-eruptive sediments.
- The proposed model for large mud volcano system evolution highlights the importance of pulsed sediment and fluid expulsion in controlling the internal architecture of the system. The eruptive pattern and general architecture of the system shows a strong similarity to models for igneous volcanic systems for which mud volcano systems may be analogous.

7.3 Geophysical expression of mud volcano systems and their deposits

- The use of high quality geophysical data in this project has led to a thorough and detailed geophysical analysis of the various extrusive components of the mud volcano system at the surface and in the subsurface at a range of scales.

- Seismic reflection patterns along with other geophysical anomalies and attributes can be investigated to identify mud volcanic deposits and is likely to be of use in predicting their physical properties and fluid content.
- In the subsurface mud volcano edifices are large enough for a number of a number of component units to be identified and mapped. The fact that each unit is identified as a discrete seismic reflection indicates that mud volcanic deposits can exhibit a suitably large geophysical contrast with other sediments, mud volcanic or otherwise.
- Mud volcanic deposits that are below seismic resolution may be imaged as anomalies of reduced positive amplitude and mapped in 3D to reveal the detailed pattern of mud volcanic deposition.
- At the seabed, areas at the upper terminations of large mud volcano systems may be imaged as negative polarity seismic reflections which contrast surrounding areas of positive polarity.
- These areas have been termed “seabed phase reversals”. They have been mapped in detail at two examples to reveal the pattern of recent mud extrusions. In one case this reveals a circular slightly domed area of mud volcanic deposits. At another it reveals a spectacular pattern of lobate mud flows sourced from two seabed salses (mud pools).
- Geophysical modelling utilising shallow well data and published information has demonstrated that the most likely cause of seabed phase reversals is the presence of gas within the seabed sediment.
- Seabed phase reversals are important indicators of gassy seabed conditions that indicate that a mud volcano is active at the time of survey acquisition and that sediment retains gas for some time after deposition.
- It is likely that only small amounts of gas (<1% pore fluid fraction) are required for seabed sediment to be phase-reversed in seismic data. The small change in sediment geophysical properties beyond approximately 4% gas saturation means however that they are not likely to be useful in determining how much gas is present within the sediment.

7.4 Structure and origin of mud volcanic source points

- Two types of mud volcano source point structures have been identified at the upper terminations of mud volcano systems both onshore and offshore. They are subsidence craters and seabed salses. Both have been investigated in detail using seismic, field and other remote data.
- Subsidence craters have been identified at onshore and offshore mud volcano systems as circular fault-bound depressions measuring 250 m to over 2 km in diameter.
- Onshore crater structure can be investigated through field mapping, elevation data and satellite image analysis. Offshore, 3D and hi-resolution 2D seismic data have been used to describe their architecture and constrain their subsurface structure.
- Similarities observed at a range of crater examples have lead to the construction of a generalized structural model for mud volcano craters. This features a concentric zonation of structures and deposits beginning at the edge with the rim, crater margin fault, moat, pedestal of mud volcanic sediment and central gryphons.
- Within the crater pedestal a series of recent mud breccia deposits may be stacked as a sequence of successively smaller volume and diameter eruptive units. This pattern is likely to be the result of a waning pressure drive during mud volcano evolution.
- A characteristic aspect of crater structure is created by the depressed moat and raised expression of the pedestal. This has been termed a “moat and pedestal” cross sectional morphology and is the result of incomplete filling of the crater by raised mud pools or circular layers of erupted mud breccia.
- The structural model bears a close resemblance to many other mud volcano craters and fluid expulsion features and as such is likely to be of use in describing the geomorphology and structuration of a large number of mud volcano source points worldwide.
- The preferred origin mechanism for mud volcano craters is as collapse features resulting from the subsurface evacuation of fluids and sediments during eruptions. As such they are similar to other circular structures that form in this way including calderas, collapse depressions and dissolution collapse

sinkholes. The prefix “subsidence” could be applied to distinguish this crater type from others that form by explosive excavation.

- On the seabed, mapping a phase-reversed section of seafloor has revealed the presence of the second type of mud volcano source point- the seabed salse. Salses are at least 5 m deep and can source kilometre-scale lobate mud flows found on the flanks of the edifice- a pattern which is observed at numerous onshore salses. Like these onshore examples mud flows are likely to form when salse fill reaches a point at which it breaches the salse edges.

7.5 Implications for economic and engineering geology

- Large mud volcano systems represent significant hazards for seafloor engineering and hydrocarbon drilling operations.
- The observations and subsequent results of this project have provided a useful characterization of extrusive constructions and features of the mud volcano system which may be of use in the identification and potential mitigation of mud volcano-related hazards.
- At the surface seabed phase reversals are an important indicator of gassy sediment. Such areas present a significant hazard to operations since they are sites of fluid expulsion and likely weak sediments. Seabed phase reversals therefore are useful anomalies which should be considered alongside other acoustic indicators of gassy sediment such as acoustic turbidity zones, gas chimneys and subsurface phase reversals. The mapping and analysis of mud volcano craters provides a characterization of another potential hazard commonly found in hydrocarbon provinces.
- In the subsurface the description of edifice and roof domain internal architecture has provided a detailed account of mud volcano structure which is of use in well planning and prediction of the section.
- Reconstructing the eruptive history of mud volcano systems, as described in this project is, a useful way of gaining insight into to history of basinal hydrodynamic activity and fluid expulsion. This is of use to petroleum geologists attempting to establish the history of basinal fluid generation and trap integrity.

- The reconstruction of volcano edifice collapse history is a potentially useful way of relatively dating the activity of large faults that pass through reservoir intervals and may have a role in sealing hydrocarbon accumulations.

7.6 Suggestions for further work

- Greater numbers of 3D seismic based studies of large mud volcano systems would lead to a greater number of examples from which to compare the results of this and other projects.
- The onshore mud volcanoes of Azerbaijan are understudied in terms of their structure and geomorphology and dynamic structural evolution. They are a useful resource that can be used to compare and ground-truth structures observed offshore. More studies should utilise them in their efforts to better understand mud volcanism.
- Integration of data types such as seismic, field maps, elevation data and satellite imagery is demonstrated here as a powerful tool in mud volcano investigation. Continuing this approach in future studies is likely to be useful.
- A limitation of this project has been a lack of well data or surface sampling measurements. Better integration of well and seismic data could lead to significant insights into the absolute age of mud volcanoes and better constraints on their time-averaged eruptive rates. Use of specialist sampling tools will help better constrain the true physical properties of gassy seabed sediments and enhance the understanding of seabed phase reversals.
- Elements of the mud volcano system not investigated directly in this project include the intrusive and source domains. Both are poorly understood elements of the system that would benefit from more focussed seismic- and field-based investigations.

8.0 References

A

- Abrams, M. A. and Narimanov, A. A. 1997. Geochemical evaluation of hydrocarbons and their potential sources in the western South Caspian depression, Republic of Azerbaijan. *Marine and Petroleum Geology* 14, pp. 451-468.
- Acocella, V. 2005. Modes of sector collapse of volcanic cones: insights from analogue experiments. *Journal of Geophysical Research* 110, p. B02205.
- Acocella, V. 2006. Caldera types: how end-members relate to evolutionary stages of collapse. *Geophysical Research Letters* 33, p. L18314.
- Acocella, V., Cifelli, F. and Funiciello, R. 2000. Analogue models of collapse calderas and resurgent domes. *Journal of Volcanology and Geothermal Research* 104(1-4), pp. 81-96.
- Aliyev, A., Guliyev, I. S. and Belov, I. S. 2002. *Catalogue of recorded eruptions of mud volcanoes of Azerbaijan (for period of years 1810 to 2001)*. Baku, Azerbaijan (In Russian): Nafta Press, p. 87.
- Aliyev, A. K. 1960. *Geology and hydrocarbons of the kura-Araks region*. Baku: Azerbaijan State Publisher of Hydrocarbon Literature, p. 361.
- Allen, M. B., Jackson, J. and Walker, R. 2004. Late Cenozoic reorganization of the Arabia-Eurasia collision and the comparison of short-term and long-term deformation rates. *Tectonics* 23, pp. 1-16.
- Allen, M. B., Jones, S., Ismail-zadeh, A., Simmons, M. and Anderson, L. 2002. Onset of subduction as the cause of rapid Pliocene-Quaternary subsidence in the South Caspian basin. *Geology* 30, pp. 775-778.
- Allen, M. B., Morton, A. C., Fanning, C. M., Ismail-zadeh, A. and Kroonenburg, S. B. 2006. Zircon age constrains on sediment provenance in the Caspian region. *Journal of the Geological Society, London* 163, pp. 647-655.
- Allen, M. B., Vincent, S. J., Alsop, G. I., Ismail-zadeh, A. and Flecker, R. 2003. Late Cenozoic deformation in the South Caspian region: effects of a rigid basement block within a collision zone. *Tectonophysics* 366, pp. 233-239.
- Anderson, A. L. 1992. Remote acoustic characterization of the seafloor including gassy and hydrated sediment regions. *Proceedings of the Second International Offshore and Polar Engineering Conference*. San Francisco, pp. 674-683.
- Anderson, A. L. and Bryant, W. R. 1990. Gassy sediment occurrence and properties: Northern Gulf of Mexico. *Geo-Marine Letters* 10, pp. 209-220.
- Anderson, A. L. and Hampton, L. D. 1980. Acoustics of gas-bearing sediments I. Background. *Journal of the Acoustic Society of America* 67, pp. 1865-1889.

Andreassen, K., Glad Nilssen, E. and Odegaard, C. M. 2007. Analysis of shallow gas and fluid migration within the Plio-Pleistocene sedimentary succession of the SW Barents Sea continental margin using 3D seismic data. *Geo-Marine Letters* 27, pp. 155-173.

Anketell, J. M., Celga, J. and Dzulynski, S. 1970. On the deformational structures in systems with reversed density gradients. *Annales de la Societe Geologique de Pologne* XL, pp. 3-29.

Apol'skiy, O. P. 1974. Origin of the Black Sea and South Caspian Sea troughs. *Geotectonics* 5, pp. 310-311.

Aslan, A., Warne, A. G., White, W. A., Gueva, E. H., Smyth, R. C., Raney, J. A. and Gibeaut, J. C. 2001. Mud volcanoes of the Orinoco Delta, Eastern Venezuela. *Geomorphology* 41, pp. 323-336.

B

Bailey, E. B. and Maufe, H. B. 1960. The geology of Ben Nevis and Glen Coe and the surrounding country. *Geological Survey of Britain Memoirs* 53, p. 307.

Barber, A. J., Tjokrosapoetro, S. and Charlton, T. R. 1986. Mud Volcanoes, Shale Diapirs, Wrench Faults and Melanges in Accretionary Complexes, Eastern Indonesia. *American Association of Petroleum Geologists Bulletin* 70, pp. 1729-1741.

Berberian, M. 1983. The southern Caspian: a compressional depression floored by trapped, modified oceanic crust. *Canadian Journal of Earth Science* 20, pp. 163-183.

Beresford, S. W. and Cole, J. W. 2000. Kaingaroa Ingnimbrite, Taupo Volcanic Zone: New Zealand: evidence for asymmetric caldera subsidence of the Reporoa Caldera. *New Zealand Journal of Geology and Geophysics* 43, pp. 471-481.

Bertoni, C. and Cartwright, J. A. 2005. 3D seismic analysis of circular evaporite dissolution structures, Eastern Mediterranean. *Journal of the Geological Society, London* 162, pp. 909-926.

Bitzer, K. and Ayora, C. 2000. Modeling episodic dewatering and evolution of fluid pressure/total load ratio (λ) in a sedimentary basin. *Journal of Geochemical Exploration* 69-70, pp. 569-573.

Bjorlykke, K. 1993. Fluid flow in sedimentary basins. *Sedimentary Geology* 86(1-2), pp. 137-158.

Boehm, A. and Moore, J. C. 2002. Fluidized sandstone intrusions as an indicator of palaeostress orientation, Santa Cruz, California. *Geofluids* 2, pp. 147-161.

Bons, P. D. and van Milligen, B. P. 2001. New experiment to model self-organized critical transport and accumulation of melt and hydrocarbons from their source rocks. *Geology* 29, pp. 919-922.

- Bouska, J. and Johnston, R. 2005. The first 3D/4C ocean bottom seismic surveys in the Caspian Sea: Acquisition design and processing strategy. *The Leading Edge* 24, pp. 910-922.
- Branney, M. J. 1995. Downsag and extension at calderas: new perspectives on collapse geometries from ice-melt, mining, and volcanic subsidence. *Bulletin of Volcanology* 57, pp. 303-318.
- Bredehoeft, J. D., Djevanshir, R. Dj. and Belitz, K. R. 1988. Lateral fluid flow in a compacting sand-shale sequence: South Caspian Basin. *American Association of Petroleum Geologists Bulletin* 72, pp. 416-424.
- Bristow, C. R., Gale, I. N., Fellman, E., Cox, B. M., Wilkinson, I. P. and Riding, J. B. 2000. The lithostratigraphy, biostratigraphy and hydrogeological significance of the mud springs at Templars Firs, Wootton Bassett, Wiltshire. *Proceedings of the Geologists Association* 111, pp. 231-245.
- Brown, A. R. 1999. *AAPG Memoir; 42, SEG Investigations in Geophysics; 9: Interpretation of three-dimensional seismic data. Fifth Edition* AAPG/SEG.
- Brown, K. M. 1990. The Nature and Hydrogeologic Significance of Mud Diapirs and Diatremes for Accretionary Systems. *Journal of Geophysical Research* 95, pp. 8969-8982.
- Brown, K. M. 1994. Fluids in deforming sediments. In: Maltman, A.J. ed. *The Geological Deformation of Sediments*. London: Chapman and Hall, pp. 205-237.
- Brown, K. M. and Orange, D. L. 1993. Structural aspects of diapiric melange emplacement: the Duck Creek diapir. *Journal of Structural Geology* 15(7), pp. 831-847.
- Brunet, M. F., Korotaev, M. V., Ershov, A. V. and Nikishin, A. M. 2003. The South Caspian Basin: a review of its evolution from subsidence modelling. *Sedimentary Geology* 156, pp. 119-148.
- Burykovsky, L. A., Djevanshir, R. Dj. and Chilingar, G. V. 1995. Abnormally-high formation pressures in Azerbaijan and the South Caspian Basin (as related to smectite-illite transformations during diagenesis and catagenesis). *Journal of Petroleum Science and Engineering* 13(203-218).
- C**
- Carson, B. and Screatton, E. J. 1998. Fluid flow in accretionary prisms: evidence for focussed, time-variable discharge. *Reviews of Geophysics* 36, pp. 329-351.
- Cartwright, J. and Huuse, M. 2005. 3D seismic technology: the geological 'Hubble'. *Basin Research* 17(1), pp. 1-20.

- Cartwright, J. A. 2007. The impact of 3D seismic data on the understanding of compaction, fluid flow and diagenesis in sedimentary basins. *Journal of the Geological Society, London* 164, pp. 881-894.
- Cartwright, J. A., Huuse, M. and Aplin, A. 2007. Seal bypass systems. *American Association of Petroleum Geologists Bulletin* 91, pp. 1141-1166.
- Cashman, K. V., Sturtevant, B., Papale, P. and Navon, O. 2000. Magmatic fragmentation. In: Sigurdsson, H. ed. *Encyclopaedia of Volcanoes*. Academic Press, pp. 421-430.
- Clari, P., Cavagna, S., Martire, L and Hunziker, J. 2004. A Miocene Mud Volcano and its Plumbing System: A Chaotic Complex Revisited (Monferrato, NW Italy). *Journal of Sedimentary Research* 74, pp. 662-676.
- Clemens, J. D. 1998. Observations on the origins and ascent mechanisms of granitic magmas. *Journal of the Geological Society* 155, pp. 843-851.
- Cole, D., Stewart, S. and Cartwright, J. 2000. Giant irregular pockmark craters in the Palaeogene of the Outer Moray Firth Basin, UK North Sea. *Marine and Petroleum Geology* 17(5), pp. 563-577.
- Cole, J. W., Milner, D. M. and Spinks, K. D. 2004. Calderas and caldera structures: a review. *Earth-Science Reviews* 69, pp. 1-26.
- Collinson, J. 1994. Sedimentary deformational structures. In: Maltman, A.J. ed. *The Geological Deformation of Sediments*. London: Chapman and Hall, pp. 95-125.
- Cooper, C. ed. 2001. *Mud Volcanoes of Azerbaijan visualized using 3D seismic depth cubes: The importance of overpressured fluid and gas instead on non-existent diapirs*. Proceedings of EAGE Conference: Subsurface Sediment Mobilization. Ghent, Belgium:
- Cosgrove, J. W. 2001. Hydraulic fracturing during the formation and deformation of a basin: a factor in the dewatering of low permeability sediments. *Bulletin-American Association of Petroleum Geologists* 85, pp. 737-748.
- D**
- Dadashev, F. G., Guseynov, R. A. and Aliyev, A. 1995. *Map of mud volcanoes of the Caspian Sea (explanatory text)*. Baku: Geological Institute of Azerbaijan, p. 20.
- Davies, R. J. 2003. Kilometre-scale fluidization structures formed during early burial of a deep-water slope channel on the Niger Delta. *Geology* 31(11), pp. 949-952.
- Davies, R. J. and Stewart, S. A. 2005. Emplacement of giant mud volcanoes in the South Caspian Basin: 3D seismic reflection imaging of their root zones. *Journal of the Geological Society, London* 162, pp. 1-4.

- Davies, R. J., Swarbrick, R. E., Evans, R. J. and Huuse, M. 2007. Birth of a mud volcano: East Java, 29 May 2006. *GSA Today* 17, pp. 4-9.
- Delaney, P. T., Pollard, D. D., Ziony, J. I. and McKee, E. H. 1986. Field relations between dikes and joints: emplacement processes and palaeostress analysis. *Journal of Geophysical Research* 91, pp. 4920-4938.
- Delisle, G., von Rad, U., Andruliet, H., von Daniels, C. H., Tabrez, A. R. and Inam, R. 2001. Active mud volcanoes on- and offshore Makran, Pakistan. *International Journal of Earth Sciences* 91, pp. 93-110.
- Deville, E., Battani, A., Griboulard, R., Guerlais, S., Herbin, J. P., Houzay, J. P., Muller, C. and Prinzhofer, A. 2003. The origin and processes of mud volcanism: new insights from Trinidad. In: Van Rensbergen, P. et al. eds. *Subsurface Sediment Mobilization*. Geological Society, London, Special Publication 216, pp. 475-490.
- Deville, E., Guerlais, S-H., Callec, Y., Griboulard, R., Huyghe, P., Lallemand, S., Mascle, A., Noble, M. and Schmitz, J. 2006. Liquefied vs. stratified sediment mobilization processes: Insight from the South of the Barbados accretionary prism. *Tectonophysics* 428(1-4), pp. 33-47.
- Devlin, W., Gogswell, J., Gaskins, G., Isaksen, G., Pitcher, D., Puls, D., Stanley, K. and Wall, G. 1999. South Caspian Basin: Young, cool, and full of promise. *GSA Today* 9, pp. 1-9.
- Dewey, J. F., Hamepton, M. R., Kidd, W. S. F., Saroglu, F. and Sengor, A. M. C. 1986. Shortening of continental lithosphere: the neo-tectonics of Eastern Anatolia- a young collision zone. In: Coward, M.P. and Ries, A.C. eds. *Collision tectonics*. Geological Society, London Special Publication. Vol. 19. pp. 3-36.
- Dimitrov, L. I. 2002. Mud volcanoes- the most important pathway for degassing deeply buried sediments. *Earth-Science Reviews* 59, pp. 49-76.
- Doust, H. and Omatsola, E. 1990. Niger Delta. In: Edwards, J.D. and Santogrossi, P.A. eds. *Divergent/Passive Margin Basins*. AAPG Memoir. Vol. 48. pp. 201-238.
- Doyle, F. J. 1984. Surveying and mapping with space data. *ITC Journal* 4, pp. 314-321.
- E**
- Edrington, T. S. and Calloway, T. M. 1984. Sound speed and attenuation measurements in gassy sediments in the Gulf of Mexico. *Geophysics* 49, pp. 297-299.
- Einsele, G. 1989. In situ water contents, liquid limits, and submarine mass flows due to a high liquefaction potential of slope sediments (results from DSDP and subaerial counterparts). *Geologische Rundschau* 78, pp. 821-840.

- Etioppe, G., Caracausi, A., Favara, R., Italiano, F. and Baciù, C. L. 2002. Methane emission from the mud volcanoes of Sicily (Italy). *Geophysical Research Letters* 29(8), p. 1215.
- Etioppe, G., Feyzullayev, A., Baciù, C. L. and Milkov, A. V. 2004. Methane emission from mud volcanoes in eastern Azerbaijan. *Geology* 32(6), pp. 465-468.
- Etioppe, G. and Klusman, R. W. 2002. Geologic emissions of methane to the atmosphere. *Chemosphere* 49, pp. 777-789.
- Etioppe, G. and Milkov, A. V. 2004. A new estimate of global methane flux from onshore and shallow submarine mud volcanoes to the atmosphere. *Environmental Geology* 46, pp. 997-1002.
- Evans, R. J., Davies, R. J. and Stewart, S. A. 2007a. Internal structure and eruptive history of a kilometre-scale mud volcano system, South Caspian Sea. *Basin Research* 19(1), pp. 153-163.
- Evans, R. J., Davies, R. J. and Stewart, S. A. 2007b. Phase-reversed seabed reflections in seismic data: examples related to mud volcanoes from the South Caspian Sea. *Geo-Marine Letters* 27(2/3), pp. 203-212.
- F**
- Fannin, N. G. T. 1980. The use of regional geological surveys in the North Sea and adjacent areas in the recognition of offshore hazards. In: Arduş, D.A. ed. *Offshore Site Investigation*. Graham & Trotman Limited, pp. 5-21.
- Fofonoff, P. 1985. Physical properties of seawater: A new salinity scale and equation of state for seawater. *Journal of Geophysical Research* 90(C2), pp. 3332-3342.
- Fowler, S. R., Mildenhall, J., Zalova, S., Riley, G., Elsley, G., Desplanques, A. and Guliyev, F. 2000. Mud volcanoes and structural development on Shah Deniz. *Journal of Petroleum Science and Engineering* 28(4), pp. 189-206.
- Fu, S. S., Wilkens, R. H. and Frazer, L. N. 1995. Acoustic lance: New *in situ* seafloor velocity profiles. *Journal of the Acoustic Society of America* 99, pp. 234-242.
- Fu, S. S., Wilkens, R. H. and Frazer, L. N. 1996. In situ velocity profiles in gassy sediments: Kiel Bay. *Geo-Marine Letters* 16, pp. 249-253.
- G**
- Gallo, F. and Woods, A. W. 2004. On steady homogenous sand-water flows in a vertical conduit. *Sedimentology* 51, pp. 195-210.
- Gatliff, R. W., Hitchen, K., Ritchie, J. D. and Smythe, D. K. 1984. Internal structure of the Erlend Tertiary volcanic complex north of Shetland, revealed by seismic reflection. *Journal of the Geological Society, London* 141, pp. 555-562.

- George, R. A. 2006. Advances in AUV remote-sensing technology for imaging deepwater geohazards. *The Leading Edge* 25, pp. 1478-1483.
- Gorgas, T. J., Kim, G. Y., Park, S. C., Wilkens, R. H., Kim, D. C. Lee, G. H. and Seo, Y. K. 2003. Evidence for gassy sediments on the inner shelf of SE Korea from geoaoustic properties. *Continental Shelf Research* 23, pp. 821-834.
- Grando, G. and McClay, K. 2007. Morphotectonics domains and structural styles in the Makran accretionary prism, offshore Iran. *Sedimentary Geology* 196(1-4), pp. 157-179.
- Graue, K. 2000. Mud volcanoes in deepwater Nigeria. *Marine and Petroleum Geology* 17, pp. 959-974.
- Gregory, A. R. 1976. Fluid saturation effects on dynamic elastic properties of sedimentary rocks. *Geophysics* 41, pp. 895-921.
- Greinert, J., Artemov, Y., Egorov, V., De Batist, M. and McGinnis, D. 2006. 1300-m-high rising bubbles from mud volcanoes at 2080 m in the Black Sea: Hydroacoustic characteristics and temporal variability. *Earth and Planetary Science Letters* 244, pp. 1-15.
- Griboulard, R., Bobier, C., Faugeres, J. C., Huyghe, P., Gonthier, E., Odonne, F. and Welsh, R. 1998. Recent tectonic activity in the South Barbados prism Deep-towed side-scan sonar imagery. *Tectonophysics* 284(1-2), pp. 79-99.
- Guliyev, I. S. and Feizullayev, A. A. 1995. *All about mud volcanoes*. Baku: Institute of Geology of the Azerbaijan National Academy of Sciences, p. 52.
- Guliyev, I. S. and Panahi, B. 2004. Geodynamics of the deep sedimentary basin of the Caspian Sea region: paragenetic correlation of seismicity and mud volcanism. *Geo-Marine Letters* 24, pp. 169-176.
- H**
- Hallager, W. S., Ulrich, M. R., Kyle, J. R., Gose, W. A. and Price, P. E. 1990. Evidence for episodic basin dewatering in salt-dome cap rocks *Geology* 18, pp. 716-719.
- Hamilton, E. L. 1970. Reflection coefficients and bottom losses at normal incidence computed from Pacific sediment properties. *Geophysics* 35, pp. 995-1004.
- Hamilton, E. L. and Bachman, R. T. 1982. Sound velocity and related properties of marine sediments. *Journal of the Acoustic Society of America* 72, pp. 1891-1904.
- Hansen, J. P. V., Cartwright, J. A., Huuse, M. and Clausen, O. 2005. 3D seismic expression of fluid migration and mud remobilization on the Gjallar Ridge, offshore mid-Norway. *Basin Research* 10, pp. 1365-2117.

- Harrison, W. J. and Summa, L. L. 1991. Paleohydrology of the Gulf of Mexico Basin. *American Journal of Science* 91, pp. 109-176.
- Hedberg, H. 1974. Relation of methane generation to undercompacted shales, shale diapirs and mud volcanoes. *American Association of Petroleum Geologists Bulletin* 58, pp. 661-673.
- Hempton, M. R. 1987. Constraints on Arabian plate motion and extensional history of the Red Sea. *Tectonics* 6(687-705).
- Hinds, D. J., Aliyeva, E., Allen, M. B., Davies, C. E., Kroonenburg, S. B., Simmons, M. D. and Vincent, S. J. 2004. Sedimentation in a discharge dominated fluvial-lacustrine system: the Neogene Productive Series of the South Caspian Basin, Azerbaijan. *Marine and Petroleum Geology* 21, pp. 613-638.
- Holland, C. W., Etiope, G., Milkov, A. V., Michelozzi, E. and Favali, P. 2003. Mud volcanoes discovered offshore Sicily. *Marine Geology* 199, pp. 1-6.
- Hovland, M. 1990. Suspected gas-associated clay diapirism on the seabed off Mid Norway. *Marine and Petroleum Geology* 7(3), pp. 267-276.
- Hovland, M. 2003. Geomorphological, geophysical, and geochemical evidence of fluid flow through the seabed. *Journal of Geochemical Exploration* 78-79, pp. 287-291.
- Hovland, M., Hill, A. and Stokes, D. 1997. The structure and geomorphology of the Dashgil mud volcano, Azerbaijan. *Geomorphology* 21, pp. 1-15.
- Hovland, M. and Judd, A. G. 1988. *Seabed Pockmarks and Seepages: Impact on Geology, Biology and the Marine Environment*. London: Graham and Trotman Ltd.
- Hunt, J. M. 1990. Generation and migration of petroleum from abnormally pressured fluid compartments. *AAPG Bulletin* 74, pp. 1-12.
- Hurst, A., Cartwright, J., Huuse, M., Jonk, R., Schwab, A., Duranti, D. and Cronin, B. 2003a. Significance of large-scale sand injectites as long-term fluid conduits: evidence from seismic data. *Geofluids* 3(4), pp. 263-274.
- Hurst, A., Cartwright, J. A. and Duranti, D. 2003b. Fluidization structures produced by upward injection of sand through a sealing lithology. In: Van Rensbergen, P. et al. eds. *Subsurface sediment mobilization, Geological Society, London Special Publication*. Vol. 216. pp. 123-137.
- Huseynov, D. A. and Guliyev, I. S. 2004. Mud volcanic natural phenomena in the South Caspian Basin: geology, fluid dynamics and environmental impact. *Environmental Geology* 46, pp. 1012-1023.
- Huuse, M. and Mickelson, M. 2004. Eocene sandstone intrusions in the Tampen Spur area (Norwegian North Sea Quad 34) imaged by 3D seismic data. *Marine and Petroleum Geology* 21(2), pp. 141-155.

Huuse, M., Shoulders, S. J., Netoff, D. I. and Cartwright, J. 2005. Giant sandstone pipes record basin-scale liquefaction of buried dune sands in the Middle Jurassic of SE Utah. *Terra Nova* 17(1), pp. 80-85.

I

Ivanov, V. V. and Guliyev, I. S. 1988. A physio-chemical model of mud volcanism. *Problems in the oil and gas content of the Caucasus*. Moscow: Nauka, p. 9.

J

Jackson, J., Priestly, K., Allen, M. and Berberian, M. 2002. Active tectonics of the South Caspian Basin. *Geophysics Journal International* 148, pp. 214-245.

Jackson, M. P. A., Vendeville, B. C. and Schultz-Ela, D. D. 1994. Structural dynamics of salt systems. *Annual Review of Earth and Planetary Sciences* 22, pp. 93-117.

Jolly, R. J. and Lonergan, L. 2002. Mechanisms and controls on the formation of sand intrusions. *Journal of the Geological Society, London* 159, pp. 605-617.

Jones, M. 1994. Mechanical principles of sediment deformation. In: Maltman, A.J. ed. *The Geological Deformation of Sediments*. London: Chapman and Hall, pp. 37-71.

Judd, A. G. 2005. Gas emissions from mud volcanoes. In: Martinelli, G. and Panahi, B. eds. *Mud volcanoes Geodynamics and Seismicity*. Vol. 51. Springer, pp. 147-159.

Judd, A. G. and Hovland, M. 1992. The evidence of shallow gas in marine sediments. *Continental Shelf Research* 12, pp. 1081-1097.

Judd, A. G. and Hovland, M. 2007. *Seabed Fluid Flow*. Cambridge University Press, p. 475.

Jurado-Rodriguez, M. J. and Martinez-Ruiz, F. 1998. Some clues about the Napoli and Milano mud volcanoes from an integrated log-core approach. In: Robertson, A.H.F. et al. eds. *Proceedings of the Ocean Drilling Program, Scientific Results*. Vol. 160. pp. 607-624.

K

Kadirov, F. A. and Mukhtarov, A. S. 2004. Geophysical fields, deep structure, and dynamics of the Lokbatan mud volcano. *Izvestiya-Physics of the Solid Earth* 40(4), pp. 327-333.

Kalinko, M. 1964. Mud volcanoes, reasons for their origin and fading. *VNIGRI* 40, pp. 30-54 (In Russian).

- Karig, D. E. and Morgan, J. K. 1994. Tectonic deformation; stress paths and strain histories. In: Maltman, A.J. ed. *The Geological Deformation of Sediments*. London: Chapman & Hall. pp. 167-206
- Kaul, N., Foucher, J. P. and Heesemann, M. 2006. Estimating mud expulsion rates from temperature measurements on Håkon Mosby Mud Volcano, SW Barents Sea. *Marine Geology* 229(1-2), pp. 1-14.
- Kennedy, B., Stix, J., Vallance, J. W., Lavallee, and Longpre, M. 2004. Controls on caldera structure: Results from analogue sandbox modelling. *Geological Society of America Bulletin* 116, pp. 515-524.
- Knapp, C. C., Kanpp, J. H. and Connor, J. A. 2004. Crustal-scale structure of the South Caspian Basin revealed by deep seismic reflection profiling. *Marine and Petroleum Geology* 21, pp. 1073-1081.
- Kopf, A. 1998. Mechanisms of mud extrusion on the Mediterranean Ridge Accretionary Complex. *Geo-Marine Letters* 18, pp. 97-114.
- Kopf, A. 2002. Significance of mud volcanism. *Reviews of Geophysics* 40(2), p. 1005.
- Kopf, A. 2003. Global methane emission through mud volcanoes and its past and present impact on the Earth's climate. *International Journal of Earth Sciences* 92, pp. 806-816.
- Kopf, A. and Behrmann, J. H. 2000. Extrusion dynamics of mud volcanoes on the Mediterranean Ridge accretionary complex. In: Vendeville, B. et al. eds. *From the Arctic to the Mediterranean: Salt, Shale and Igneous Diapirs in and Around Europe*. Geological Society, London, Special Publication. 174, pp. 169-204.
- Kopf, A., Dehyle, A., Lavurshin, V. Y., Polyak, B. G., Gieskes, J. M., Buachidize, G. I., Wallmann, K. and Eisenhauer, A. 2003. Isotopic evidence (He, B, C) for deep fluid and mud mobilization from mud volcanoes in the Caucasus continental collision zone. *International Journal of Earth Sciences* 92, pp. 407-425.
- Kopf, A., Klaeschen, D. and Mascle, J. 2001. Extreme efficiency of mud volcanism in dewatering accretionary prisms. *Earth and Planetary Science Letters* 189, pp. 295-313.
- Krastel, S., Spiess, V., Ivanov, M., Weinrebe, W., Bohrmann, G., Shashkin, P. and Heidersdorf, F. 2003. Acoustic investigations of mud volcanoes in the Sorokin Trough, Black Sea. *Geo-Marine Letters* 23, pp. 230-238.
- Kruger, M., Treude, T., Wolters, H., Nauhaus, K. and Boetius, A. 2005. Microbial methane turnover in different marine habitats. *Palaeogeography, Palaeoclimatology, Palaeoecology* 227, pp. 6-17.
- Kuprin, P. N. 2002. Apsheron Threshold and Its Role in the Processes of Sedimentation and Formation of Hydrological Regimes in the Southern and Middle Caspian Basins. *Water Resources* 29, pp. 473-484.

L

Lance, S., Henry, P., Le Pichon, X., Lallemand, S., Chamley, H., Rostek, F., Faugeres, J-C., Gonthier, E. and Olu, K. 1998. Submersible study of mud volcanoes seaward of the Barbados accretionary wedge: sedimentology and rheology. *Marine Geology* 145, pp. 255-292.

Lavrushin, V. U. B. G., Polyak, R., Prasolov, R. M. and Kamenskii, I. L. 1996. Sources of material in mud volcano products (based on isotopic, hydrochemical, and geological data). *Lithology and Mineral Resources* 31, pp. 557-578.

Leeder, M. 1999. Sediment grains in fluids: settling, transport and feedback. *Sedimentology and Sedimentary Basins, From Turbulence to Tectonics*. Blackwell Science, pp. 123-140.

Lerche, I. and Bagirov, E. 1999. *Impact of natural hazards on oil and gas extraction, The South Caspian Basin*. Kluwer Academic/- Plenum Publishers, p. 353.

Lerche, I., Bagirov, E., Nadirov, F., Tagliyev, M. and Guliyev, I. S. 1997. *Evolution of the South Caspian Basin: Geologic risks and probable hazards*. Baku: Institute of Geology of Azerbaijan Academy of Sciences, p. 580.

Lipman, P. W. 1997. Subsidence of ash-flow calderas: relation to caldera size and magma-chamber geometry. *Bulletin of Volcanology and Geothermal Research* 59, pp. 198-218.

Lipman, P. W. 2000. Calderas. In: Sigurdsson, H. ed. *Encyclopaedia of Volcanoes*. San Francisco: Academic Press, pp. 642-662.

Løseth, H. et al. 2003. Gas and fluid injection triggering shallow mud mobilization in the Hordaland Group, North Sea. In: Van Rensbergen, P. et al. eds. *Subsurface Sediment Mobilization*. Geological Society, London, Special Publication, Vol. 216, pp. 139-157.

Loncke, L., Mascle, J. and Fanil Scientific Parties. 2004. Mud volcanoes, gas chimneys, pockmarks and mounds in the Nile deep-sea fan (Eastern Mediterranean): geophysical evidences. *Marine and Petroleum Geology* 21, pp. 669-689.

Løseth, H., Wensaas, L., Anrntsen, B., Hanken, N., Basire, C. and Graue, K. 2001. 1000 m long gas blow-out pipes. In: *EAGE 63rd Conference and Technical Exhibition*. Amsterdam, The Netherlands.

Lowe, D. R. 1975. Water escape structures in coarse grained sediments. *Journal of Sedimentary Petrology* 44, pp. 484-501.

M

MacDonald, I. R., Buthman, D. B., Sager, W. W., Peccini, M. B. and Guinasso, N. L. 2000. Pulsed oil discharge from a mud volcano. *Geology* 28(907-910).

- Macedonio, G., Dobran, F. and Augusto, N. 1994. Erosion processes in volcanic conduits and application to the AD 79 eruption of Vesuvius. *Earth and Planetary Science Letters* 121, pp. 137-152.
- Maltman, A. J. 1994. Introduction and overview. In: Maltman, A.J. ed. *The Geological Deformation of Sediments*. London: Chapman and Hall, pp. 1-35.
- Maltman, A. J. and Bolton, A. 2003. How sediments become mobilized. In: Van Rensbergen, P. et al. eds. *Subsurface Sediment Mobilization*. Geological Society, London, Special Publication. Vol. 216. pp. 9-20.
- Martin, J. B., Kastner, M., Henry, P., LePichon, X. and Lallement, S. 1996. Chemical and isotopic evidence for sources of fluids in a mud volcano field seaward of the Barbados accretionary wedge. *Journal of Geophysical Research-Solid Earth* 101(B9), pp. 20325-20345.
- Martinsen, O. 1994. Mass movements. In: Maltman, A.J. ed. *The Geological Deformation of Sediments*. London: Chapman and Hall, pp. 127-164.
- Matthews, M. D. 1996. Migration- a view from the top. In: Schumacher, D. and Abrams, M.A. eds. *Hydrocarbon migration and its near-surface expression. AAPG Memoir 66*. pp. 139-155.
- Mazzini, A., Jonk, R., Duranti, D., Parnell, J., Cronin, B. and Hurst, A. 2003. Fluid escape from reservoirs: implications from cold seeps, fractures and injected sands Part I. The fluid flow system. *Journal of Geochemical Exploration* 78-79, pp. 293-296.
- Mazzini, A., Svensen, H., Akhmanov, G. G., Alosi, G., Planke, S., Malthe-Sorensen, A. and Istadi, B. 2007. Triggering and dynamic evolution of the LUSI mud volcano, Indonesia. *Earth and Planetary Science Letters* 261(3-4), pp. 375-388.
- McClay, K., Dooley, T. and Zamora, G. 2003. Analogue models of delta systems above ductile substrates. In: Van Rensbergen, P. et al. eds. *Subsurface Sediment Mobilization*. Geological Society London Special Publication. Vol. 216. pp. 411-429.
- Mellors, R., Kib, D., Aliyev, A., Gasanov, A. and Yetirmishli, G. 2007. Correlations between earthquakes and large mud volcano eruptions. *Journal of Geophysical Research-Solid Earth* 112(B4).
- Melosh, H. and Ivanov, B. A. 1999. Impact crater collapse. *Annual Review of Earth and Planetary Sciences* 27, pp. 385-415.
- Milkov, A. V. 2000. Worldwide distribution of submarine mud volcanoes and associated gas hydrates. *Marine Geology* 167, pp. 29-42.
- Milkov, A. V., Sassen, R., Apanasovich, T. V. and Dadashev, F. G. 2003. Global gas flux from mud volcanoes: A significant source of fossil methane in the atmosphere and the ocean. *Geophysical Research Letters* 30(2), pp. 9-1 - 9-4.

Millero, F. J. and Chetirkin, P. V. 1980. The density of Caspian Sea waters. *Deep Sea Research Part I: Oceanographic Research Papers* 27, pp. 265-271.

Mitchum, R. M. and Vail, P. R. 1977. Seismic stratigraphy and global changes of sea-level, part 7: stratigraphic interpretation of seismic reflection patterns in depositional sequences. In: Payton, C.E. ed. *Seismic Stratigraphy- Applications to Hydrocarbon Exploration*. American Association of Petroleum Geologists Memoir 26, pp. 135-144.

Morley, C. K. 2003a. Mobile shale related deformation in large deltas developed on passive and active margins. In: Van Rensbergen, P. et al. eds. *Subsurface Sediment Mobilization*. Geological Society, London Special Publication. Vol. 216. pp. 335-357.

Morley, C. K. 2003b. Outcrop examples of mudstone intrusions from the Jerudong anticline, Brunei Darussalam and inferences for hydrocarbon reservoirs. In: Van Rensbergen, P. et al. eds. *Subsurface Sediment Mobilization*. Vol. 216. Geological Society, London, Special Publication pp. 381-384.

Morley, C. K. 2007. Development of crestal normal faults associated with deepwater fold growth. *Journal of Structural Geology* 29(7), pp. 1148-1163.

Morley, C. K. and Guerin, G. 1996. Comparison of gravity-driven deformation styles and behaviour associated with mobile shales and salt. *Tectonics* 15, pp. 1154-1170.

Morton, A., Allen, M., Simmons, M., Spathopoulos, F., Still, J., Hinds, D. J., Ismailzadeh, A. and Kroonenberg, S. B. 2003. Provenance patterns in a neotectonic basin: Pliocene and Quaternary sediment supply to the South Caspian. *Basin Research* 15, pp. 321-337.

Mukhtarov, A. S., Kadirov, F. A., Guileyev, I. S., Feyzullayev, A. and Lerche, I. 2003. Temperature evolution in the Lokbatan mud volcano crater (Azerbaijan) after the eruption of 25 October 2001. *Energy Exploration & Exploitation* 21(3), pp. 187-207.

Murton, B. J. and Biggs, J. 2003. Numerical modelling of mud volcanoes and their flows using constraints from the Gulf of Cadiz. *Marine Geology* 195, pp. 223-236.

N

Nadirov, R. S., Bagirov, E., Tagiyev, M. and Lerche, I. 1997. Flexural plate subsidence, sedimentation rates, and structural development of the super-deep South Caspian Basin. *Marine and Petroleum Geology* 14, pp. 383-400.

Narimanov, A. A. 1993. The petroleum systems of the South Caspian Basin. In: Dore, A.G. et al. eds. *Basin modelling advances and applications*. Norwegian Petroleum Forening, Special Publication 3, pp. 599-608.

Novikov, L. A. and Slobodskoy, R. M. 1985. Mechanism of formation of diatremes. *International Geology Review* 21, pp. 1131-1139.

O

Osborne, M. J. and Swarbrick, R. E. 1997. Mechanisms for generating overpressure in sedimentary basins: a re-evaluation. *American Association of Petroleum Geologists Bulletin* 81, pp. 1023-1041.

Owen, G. 1987. Deformation processes in unconsolidated sands. In: Jones, M.E. and Preston, R.M.F. eds. *Deformation of Sediments and Sedimentary rocks*. Geological Society, London Special Publication Vol. 29. pp. 11-24.

Owen, G. 2003. Load structures: gravity-driven sediment mobilization in the shallow subsurface. In: Van Rensbergen, P. et al. eds. *Subsurface Sediment Mobilization*. Geological Society, London Special Publication. Vol. 216. pp. 21-34.

P

Parnell, J. and Schwab, A. 2003. Seismic evidence for the distribution and migration of fluids in sedimentary basins. *Geofluids* 3, pp. 213-217.

Paterson, S. R. and Fowler, T. K. 1993. Re-examining pluton emplacement processes. *Journal of Structural Geology* 15(2), pp. 191-206.

Pickering, K. T., Agar, S. M. and Ogawa, Y. 1988. Genesis and deformation of mud injections containing chaotic basalt-limestone-chert associations: Examples from the southwest Japan forearc. *Geology* 16, pp. 881-885.

Pike, R. J. 1974. Craters on Earth, Moon, and Mars: multivariate classification of mode of origin. *Earth and Planetary Science Letters* 22, pp. 245-255.

Planke, S., Svensen, H., Hovland, M. and Banks, D. A. 2003. Mud and fluid migration in active mud volcanoes in Azerbaijan. *Geo-Marine Letters* 23, pp. 258-268.

Planke, S., Symonds, P. A., Alvestad, E. and Skogseid, J. 2000. Seismic volcanostratigraphy of large-volume basaltic extrusive complexes on rifted margins. *Journal of Geophysical Research* 105, pp. 19335-19351.

Ponomareva, V. V., Melekestsev, I. V. and Dirksen, O. V. 2006. Sector collapses and large landslides on Late Pleistocene-Holocene volcanoes in Kamchatka, Russia. *Journal of Volcanology and Geothermal Research* 158(1-2), pp. 117-138.

Prior, D. B. and Coleman, J. M. 1982. Active slides and flows in unconsolidated marine sediments on the slopes of the Mississippi Delta. In: Saxov, S. and Nieuwenhuis, J.K. eds. *Marine slides and other mass movements*. New York: Plenum Press, pp. 21-51.

Prior, D. B., Doyle, E. H. and Kaluza, M. J. 1989. Evidence for sediment eruption on deep sea floor, Gulf of Mexico. *Science* 243(517-519).

R

- Reed, D. L., Silver, E. A., Tagudin, J. E., Shipley, T. H. and Vrolijk, P. 1990. Relations between mud volcanoes, thrust deformation, slope sedimentation, and gas hydrate offshore north Panama. *Marine and Petroleum Geology* 7, pp. 44-54.
- Reynolds, A. D., Simmons, M. D., Bowman, M. B. J., Henton, J., Brayshaw, A. C., Ali-Zade, A. A., Guliyev, I. S., Suleymanova, S. F., Ateava, E. Z., Mamedova, D. N. and Koshkarly, R. O. 1998. Implications of Outcrop Geology for Reservoirs in the Neogene Productive Series: Apsheron Peninsula, Azerbaijan. *American Association of Petroleum Geologists Bulletin* 82, pp. 25-49.
- Roberts, H. H. 1996. Surface amplitude data: 3D-seismic for interpretation of sea floor geology (Louisiana Slope). *Transactions of the Gulf Coast Association of Geological Societies*, pp. 353-362.
- Roberts, H. H., Haradge, B. A., Shedd, W. W. and Hunt, J Jr. 2006. Seafloor reflectivity- an important seismic property for interpreting fluid/gas expulsion geology and the presence of gas hydrate. *The Leading Edge* 25, pp. 620-628.
- Roberts, S. J. and Nunn, J. A. 1995. Episodic fluid expulsion from geopressed sediments. *Marine and Petroleum Geology* 12, pp. 195-204.
- Robertson, A. H. F. 1996. Mud volcanoes on the Mediterranean Ridge: initial results of the Ocean Drilling Program, Leg 160. *Geology* 24, pp. 239-242.
- Robinson, N., Ford, A., Howie, J., Manley, D., Riviere, M., Stewart, S. A. and Thomas, R. 2005. 4D time-lapse monitoring of the Chirag field. *The Leading Edge* 24, pp. 928-932.
- Roche, O., van Wyk de Vries, B. and Druitt, T. H. 2001. Sub-surface structures and collapse mechanisms of summit pit craters. *Journal of Volcanology and Geothermal Research* 105(1-2), pp. 1-18.
- I**
- Sager, W. W., MacDonald, I. R. and Hou, R. 2003. Geophysical signatures of mud mounds at hydrocarbon seeps on the Louisiana continental slope, northern Gulf of Mexico. *Marine Geology* 198, pp. 97-132.
- Samaila, N. K., Abubakar, M. B., Dike, E. F. C. and Obaje, N. G. 2006. Description of soft-sediment deformation structures in the Cretaceous Bima Sandstone from the Yola Arm, Upper Benue Trough, Northeastern Nigeria. *Journal of African Earth Sciences* 44(1), pp. 66-74.
- Schluter, H. U., Prexl, A., Gaedicke, Ch., Roeser, H., Reichert, Ch., Meyer, H. and von Daniels, C. 2002. The Makran accretionary wedge: sediment thicknesses and ages and the origin of mud volcanoes. *Marine Geology* 185(3-4), pp. 219-232.
- Schroot, B. M., Klaver, G. T. and Schuttenhelm, R. T. E. 2005. Surface and subsurface expressions of gas seepage to the seabed- examples from the Southern North Sea. *Marine and Petroleum Geology* 22, pp. 499-515.

- Sibson, R. H., Robert, F. and Poulsen, K. H. 1988. High-angle reverse faults, fluid pressure cycling and mesothermal gold-quartz deposits. *Geology* 16, pp. 551-555.
- Sigurdsson, H. 1999. *Melting the Earth; The Evolution of Ideas about Volcanic Eruptions*. New York: Oxford University Press, p. 250.
- Sigurdsson, H. 2000. *Encyclopaedia of volcanoes*. Academic Press, New York, p. 1417.
- Simm, R. and White, R. 2002. Phase, polarity and the interpreter's wavelet. *First Break* 20, pp. 277-281.
- Skinner, J. J. A. and Tanaka, K. L. 2007. Evidence for and implications of sedimentary diapirism and mud volcanism in the southern Utopia highland-lowland boundary plain, Mars. *Icarus* 186(1), pp. 41-59.
- Smith, N., Cassidy, J., Locke, C. A., Mauk, J. L. and Christie, A. B. 2006. The role of regional-scale faults in controlling a trapdoor caldera, Coromandel Peninsula, New Zealand. *Journal of Volcanology and Geothermal Research* 149, pp. 312-338.
- Somoza, L., Diaz-del-Rio, V., Leon, R., Ivanov, M., Fernandez-Puga, M. C., Gardener, J., Hernandez-Molina, F. J., Pinheiro, L. M., Rodero, J., Labato, A., Maestro, A., Vazquez, J. T., Medialdea, T. and Fernandez-Salas, L. M. 2003. Seabed morphology and hydrocarbon seepage in the Gulf of Cadiz mud volcano area: Acoustic imagery, multi-beam and ultra-high resolution seismic data. *Marine Geology* 195, pp. 153-176.
- Stewart, S. A. 1999a. Mid-Jurassic volcanic structures in the Outer Moray Firth Basin, UK. *Journal of the Geological Society, London* 156, pp. 487-499.
- Stewart, S. A. 1999b. Seismic interpretation of circular geological structures. *Petroleum Geoscience* 5, pp. 273-285.
- Stewart, S. A. 2006. Implications of passive salt diapir kinematics for reservoir segmentation by radial and concentric faults. *Marine and Petroleum Geology* 23(8), pp. 843-853.
- Stewart, S. A. and Davies, R. J. 2006. Structure and emplacement of mud volcano systems in the South Caspian Basin. *American Association of Petroleum Geologists Bulletin* 90, pp. 771-786.
- Summer, R. H. and Westbrook, G. K. 2001. Mud diapirism in front of the Barbados accretionary wedge: the influence of fracture zones and North America-South America plate motions. *Marine and Petroleum Geology* 18, pp. 591-613.

I

- Talukder, A. R., Comas, M. C. and Soto, J. I. 2003. Pliocene to Recent mud diapirism and related mud volcanoes in the Alboran Sea (Western Mediterranean). In: Van

Rensbergen, P. et al. eds. *Subsurface Sediment Mobilization*. Geological Society, London, Special Publication. Vol. 216. pp. 443-459.

Tibaldi, A. 2001. Multiple sector collapses at Stromboli volcano, Italy: how they work. *Bulletin of Volcanology* 63, pp. 112-125.

Torrance, J. K. 1983. Towards a general model of quick clay development. *Sedimentology* 30, pp. 547-555.

Trudgill, B. and Cartwright, J. 1994. Relay-ramp forms and normal-fault linkages, Canyonlands National Park, Utah. *Geological Society of America Bulletin* 106, pp. 1143-1157.

V

Van Rensbergen, P., Depreiter, D., Pannemans, B. and Henriët, J-P. 2005a. Seafloor expression of sediment extrusion and intrusion at the El Arraiche mud volcano field, Gulf of Cadiz. *Journal of Geophysical Research* 110(F2), p. F02010.

Van Rensbergen, P., Depreiter, D., Pannemand, B., Moerkerke, G., Van Rooij, D., Marsset, B., Akhmanov, G., Blinova, V., Ivanov, M. and Rachidi, M. 2005b. The El Arraiche mud volcano field at the Moroccan Atlantic slope, Gulf of Cadiz. *Marine Geology* 219(1), pp. 1-17.

Van Rensbergen, P., Hillis, R. R., Maltman, A. J. and Morley, C. K. 2003. Subsurface sediment mobilization: introduction. In: Van Rensbergen, P. et al. eds. *Subsurface Sediment Mobilization*. Geological Society, London Special Publication. Vol. 216. pp. 1-8.

Van Rensbergen, P. and Morley, C. K. 2003. Re-evaluation of mobile shale occurrences on seismic sections of the Champion and Baram deltas, offshore Brunei. In: Van Rensbergen, P. et al. eds. *Subsurface Sediment Mobilization*. Geological Society, London Special Publication. Vol. 216. pp. 395-411.

Varnes, D. J. 1978. Slope movement types and processes. In: Schuster, R.L. and Krizek, R.J. eds. *Landslides, Analysis and Control: National Academy of Sciences [Washington] Special Report*. Vol. 176. pp. 11-33.

W

Wall, G. R. T. W. and Wiener, R. W. 1998. Structural reconstruction of the South Caspian Basin: application to the Nakhchivan prospect. *Geophysics News in Azerbaijan* 4, pp. 11-13.

Wiedicke, M., Neben, S. and Spiess, V. 2001. Mud volcanoes at the front of the Makran accretionary complex, Pakistan. *Marine Geology* 172, pp. 57-73.

Y

- Yin, P., Berne, S., Vagner, P., Loubrieu, B. and Liu, Z. 2003. Mud volcanoes at the shelf margin of the East China Sea. *Marine Geology* 194, pp. 135-149.
- You, C.-F., Gieskes, J. M., Leec, T., Yuic, T-F. and Chenc, H-W. 2004. Geochemistry of mud volcano fluids in the Taiwan accretionary prism. *Applied Geochemistry* 19, pp. 695-607.
- Yuan, F., Bennell, J. D. and Davis, A. M. 1992. Acoustic and physical characteristics of gassy sediments in the Western Irish Sea. *Continental Shelf Research* 12, pp. 1121-1134.
- Yusifov, M. and Rabinowitz, P. D. 2004. Classification of mud volcanoes in the South Caspian Basin, offshore Azerbaijan. *Marine and Petroleum Geology* 21(8), pp. 965-975.

Z

- Zonenshain, L. P. and LePinchon, X. 1986. Deep basins of the Black and Caspian Seas as remnants of Mesozoic back-arc basins. *Tectonophysics* 123, pp. 181-211.

APPENDICIES

Because three of the Chapters in this thesis are presented as papers, it has in the past been necessary to provide additional Figures and Tables to supplement the Chapters and demonstrate the full extent of the body of work summarised in the papers. To this end the following appendices provide first, a list of all seismic horizons and faults mapped during this research and second, a separate Appendix of Figures and Tables for each of the core research Chapters (3-5). A caption is included with each Figure explaining its significance but they are not referred to in other parts of the Thesis. Finally a copy of the entire thesis in digital format is included on CD 1.

Appendix I- List of seismic horizons and faults.

Appendix II- Supplementary Figures to support the conclusions of Chapter 3.

Appendix III- Supplementary Figures to support the conclusions of Chapter 4.

Appendix IV- Supplementary Figures to support the conclusions of Chapter 5.

Appendix V- CD 1: Thesis in digital format.

Appendix I: List of mapped seismic horizons and faults

Tables API 1 and API 2 below present lists of all seismic horizons and faults mapped during the course of this project. Each one is noted by the name it appears in the GeoFrame project andy_acg. The first three letters of each horizon name denotes the interpreters initials and the single letter denotes the nature of the horizon (s= seed pick, z= autopicked). The context in which the horizon is used is shown as capitalized letters. AZ1= Azeri 1 mud volcano, AZ2 = Azeri 2 mud volcano, CH = Chirag mud volcano, G1-G3= Gunashli 1, 2 and 3 mud volcanoes, RG= Regional (not volcano specific). In the survey column CH= Chirag survey, CG= cg4d02 survey.

HORIZON NAME	SURVEY	DESCRIPTION
rje_s_AZ1_BMV	CG	Tentative base of Azeri 1 edifice
rje_s_AZ1_BShear	CH	Base of Azeri 1 shear (?) structure
rje_s_AZ1_BSlump	CH	Base of Azeri 1 rotational slump
rje_s_AZ1_slump1	CH	Alternative base of Azeri 1 rotational slump
rje_s_AZ1_slump2	CH	Alternative base of Azeri 1 rotational slump
rje_s_AZ1_slumpBS	CH	Alternative base of Azeri 1 rotational slump
rje_s_AZ1_TSurk	CG	Possible offset of Surakhany reflection
rje_s_AZ2_BMV2	CH	Possible second BMV above main cone
rje_s_AZ2_SB	CH	Detailed pick of Azeri 2 seabed
rje_s_AZ2_TMV2	CH	Top of possible second mud cone
rje_s_AZ2_TMV	CH	Tentative Azeri 2 TMV
rje_s_AZ2_Flat	CH	Flat concordant reflection in Azeri 2
rje_s_CH_BMV	CG	Chirag edifice BMV reflection
rje_s_CH_lowrBMV	CG	Alternative Chirag BMV
rje_s_CH_oldBMV	CG	First attempt at BMV reflection map
rje_s_CH_shalfBS	CG	Possible shallow Chirag cone- base
rje_s_CH_shalfTP	CG	Possible shallow Chirag cone- top
rje_s_CH_TUnit1	CG	Top of seismic facies unit 1
rje_s_CH_TUnit2	CG	Top of seismic facies unit 2
rje_s_CH_TUnit3	CG	Top of seismic facies unit 3
rje_s_CH_TUnit4	CG	Top of seismic facies unit 4
rje_s_G1_sag	CH	Enigmatic sag feature near Gunashli 1

rje_s_G1_seabed	CH	Gunashli 1 seabed
rje_s_G1_subBMV1	CH	Horizon below Gunashli 1 BMV
rje_s_G1_subBMV2	CH	Second horizon below Gunashli 1 BMV
rje_s_G1_subBMV3	CH	Third horizon below Gunashli 1 BMV
rje_s_G1_Test	PZ	Test horizon to assess PZA survey data
rje_s_G2_BMV	CG	Base of Gunashli 2 edifice
rje_s_G2_oldBMV	CG	Alternative Gunashli 2 BMV
rje_s_G3_FlatSp	CG	Flatspot near the Gunashli 3 volcano
rje_s_G3_int1	CG	Enigmatic reflection within Gunashli 3 edifice
rje_s_G3_subcald	CG	Reflection beneath the Gunashli 3 edifice
rje_s_RG_growth	CH	Base of onlapping anticline growth section
rje_s_RG_midant1	CG	Middle anticline surface
rje_s_RG_seabed	CG	Survey cg4d02 seabed
rje_s_RG_SubBMV0	CH	Reflection beneath regional BMV reflection
rje_s_SU_tpAP	CG	Top Apsheron tie from Gunashli field borehole
rje_s_SU_tpSur	CG	Top Surakhany tie from Gunashli field borehole
rje_z_AZ1_negtest	CH	Alternative phase reversal interpretation
rje_z_AZ1_SB	CH	Positive polarity seabed reflection at Azeri 1
rje_z_AZ1_SBneg	CH	Negative polarity seabed reflection at Azeri 1
rje_z_AZ2_BMV	CG	Tentative Azeri 2 BMV
rje_z_AZ2_subBMV1	CH	Arbitrary reflection near to Azeri 2 conduit
rje_z_AZ2_Tsura	CH	Top Surakhany reflection near to Azeri 2
rje_z_CH_BMV	CG	Chirag edifice BMV
rje_z_CH_lowBMV	CG	Lower choice of Chirag BMV
rje_z_CH_refx	CG	Reflection X in seismic facies unit 1
rje_z_CH_Seabed	CG	Chirag volcano seabed
rje_z_CH_SeabedNeg	CG	Phase-reversed seabed reflection area
rje_z_CH_SeabedViz	CH	Detailed seabed horizon created for visualizing
rje_z_CH_subBMV	CG	Reflection beneath BMV - test pre-MV doming
rje_z_CH_TMV	CG	Top of Chirag MV edifice
rje_z_CH_TUnit1	CG	Top of Seismic facies unit 1
rje_z_CH_TUnit2	CG	Top of Seismic facies unit 2
rje_z_CH_TUnit3	CG	Top of Seismic facies unit 3
rje_z_CH_TUnit4	CG	Top of Seismic facies unit 4
rje_z_CH_U1RefX	CG	Reflection X within seismic facies unit 1

rje_z_G1_BMV	CG	Base of Gunashli 1 edifice
rje_z_G1_BMV	CH	Base of Gunashli 1 edifice in Chirag Survey
rje_z_G1_seabed	CG	Gunashli 1 seabed
rje_z_G1_TMV	CG	Top of Gunashli 1 edifice
rje_z_G3_BMV	CG	Gunashli 3 edifice BMV
rje_z_G3_Th1	CG	Thrust fold culmination beneath Gunashli 3
rje_z_G3_tie	CG	Reflection beneath Gunashli 3 BMV
rje_z_G3_TMV	CG	Top of Gunashli 3 edifice
rje_z_RG_BMaykop	CG	Tentative base of the Maykop Formation
rje_z_RG_BMV	CH	Chirag BMV mapped regionally
rje_z_RG_BProd	CH	Suspected base of the Productive Series
rje_z_RG_onlap	CH	Chirag TMV reflection mapped regionally
rje_z_RG_seabed	CG	Regional seabed map
rje_z_RG_SubBMV1	CH	Regionally mapped
rje_z_RG_SubBmV2	CH	Regionally mapped
rje_z_RG_TMaykop	CH	Tentative top Maykop reflection
rje_z_SU_1	CH	BP Soil unit 1
rje_z_SU_1a	CH	BP Soil unit 1a
rje_z_SU_4	CH	BP Soil unit 4
rje_z_SU_8	CH	BP Soil unit 8
rje_z_SU_apsh	CH	BP Soil unit Apsheron Fm
rje_z_SU_int2	CH	BP Soil unit int2
rje_z_SU_int3	CH	BP Soil unit int3
seabed	CH	Seabed mapped regionally
Seabed_multiple	CH	Seawater depth x 2 to identify multiples
Seabed_multiple	CH	Seawater depth x 3 to identify multiples

Table API 1 List of mapped seismic horizons.

FAULT NAME	SURVEY	DESCRIPTION
Azeri2_crest	CH	Crestal extensional fault system near Azeri 2
Azeri2_Tube	CH	Tube the encloses Azeri 2 conduit system
Gun	CG	Extensional fault system near Gunashli 1
Gun1_crest1	CG	Extensional fault system near Gunashli 1
Gun3_1	CG	Extensional fault near Gunashli 3
Gun3_11	CG	Extensional fault near Gunashli 3
Gun_12	CG	Extensional fault near Gunashli 3
Gun3_13	CG	Extensional fault near Gunashli 3
Gun3_13	CG	Extensional fault near Gunashli 3
Gun3_14	CG	Extensional fault near Gunashli 3
Gun3_15	CG	Extensional fault near Gunashli 3
Gun3_16	CG	Extensional fault near Gunashli 3
Gun3_17	CG	Extensional fault near Gunashli 3
Gun3_3	CG	Extensional fault near Gunashli 3
Gun3_3	CG	Extensional fault near Gunashli 3
Gun3_4	CG	Extensional fault near Gunashli 3
Gun3_5	CG	Extensional fault near Gunashli 3
Gun3_6	CG	Extensional fault near Gunashli 3
Gun3_7	CG	Extensional fault near Gunashli 3
Gun3_8	CG	Extensional fault near Gunashli 3
Gun3_9	CG	Extensional fault near Gunashli 3
Gun3_BigTube	CG	Tube to enclose Gunashli 3 conduit system
Gun3_RAD	CG	Initial interpretation of Gunashli 3 caldera fault
Gun3_TD	CG	Gunashli 3 trapdoor fault
Gun3_TD_Final	CG	Final Gunashli 3 trapdoor fault
Gun3_Thrust	CG	Large thrust beneath Gunashli 3
Gun3_Tube1	CG	Alternative tube enclosing Gunashli 3 conduit
GunBMV	CG	Fault that offsets Gunashli 3 BMV reflection
REG_crest1	CH	Extensional crestal fault system mapped regionally
REG_MainAxial	CH	Extensional crestal fault system mapped regionally
REG_Thrust	CH	Thrust system in fold core mapped regionally
rje_ax10	CG	Axial outer-arc extensional fault
rje_ax11	CG	Axial outer-arc extensional fault
rje_ax12	CG	Axial outer-arc extensional fault

rje_ax13	CG	Axial outer-arc extensional fault
rje_ax14	CG	Axial outer-arc extensional fault
rje_ax15	CG	Axial outer-arc extensional fault
rje_ax16	CG	Axial outer-arc extensional fault
rje_ax1	CG	Axial outer-arc extensional fault
rje_ax2	CG	Axial outer-arc extensional fault
rje_ax3	CG	Axial outer-arc extensional fault
rje_ax4	CG	Axial outer-arc extensional fault
rje_ax5	CG	Axial outer-arc extensional fault
rje_ax6	CG	Axial outer-arc extensional fault
rje_ax7	CG	Axial outer-arc extensional fault
rje_ax8	CG	Axial outer-arc extensional fault
rje_ax9	CG	Axial outer-arc extensional fault
rje_ax5	CG	Axial outer-arc extensional fault
rje_AZ1_ed1	CH	Test of fault interp. of phase-reversed reflection
rje_azeri	CH	Tentative Azeri 1 trapdoor fault
rje_cald_OD	CG	Test of outward caldera fault dip at Chirag
rje_Circ_lft	CG	Segment of Chirag circular fault system
rje_circ_rgt	CG	Segment of Chirag circular fault system
rje_conc_ex1	CG	Segment of Chirag circular fault system
rje_conc_in	CG	Segment of Chirag circular fault system
rje_conc_mid	CG	Segment of Chirag circular fault system
rje_conc_out	CG	Segment of Chirag circular fault system
rje_gunash	CG	Tentative Gunashli 1 trapdoor
rje_TH_Ndip	CG	Thrust to the SE of Chirag volcano system
rje_TH_Sdip	CG	Thrust to the NW of Chirag volcano system
rje_thrust2	CG	Thrust in fold core
rje_thrust	CG	Thrust in fold core

Table API 2 List of mapped faults.

Appendix II: Supplementary Figures to support the conclusions of Chapter 3

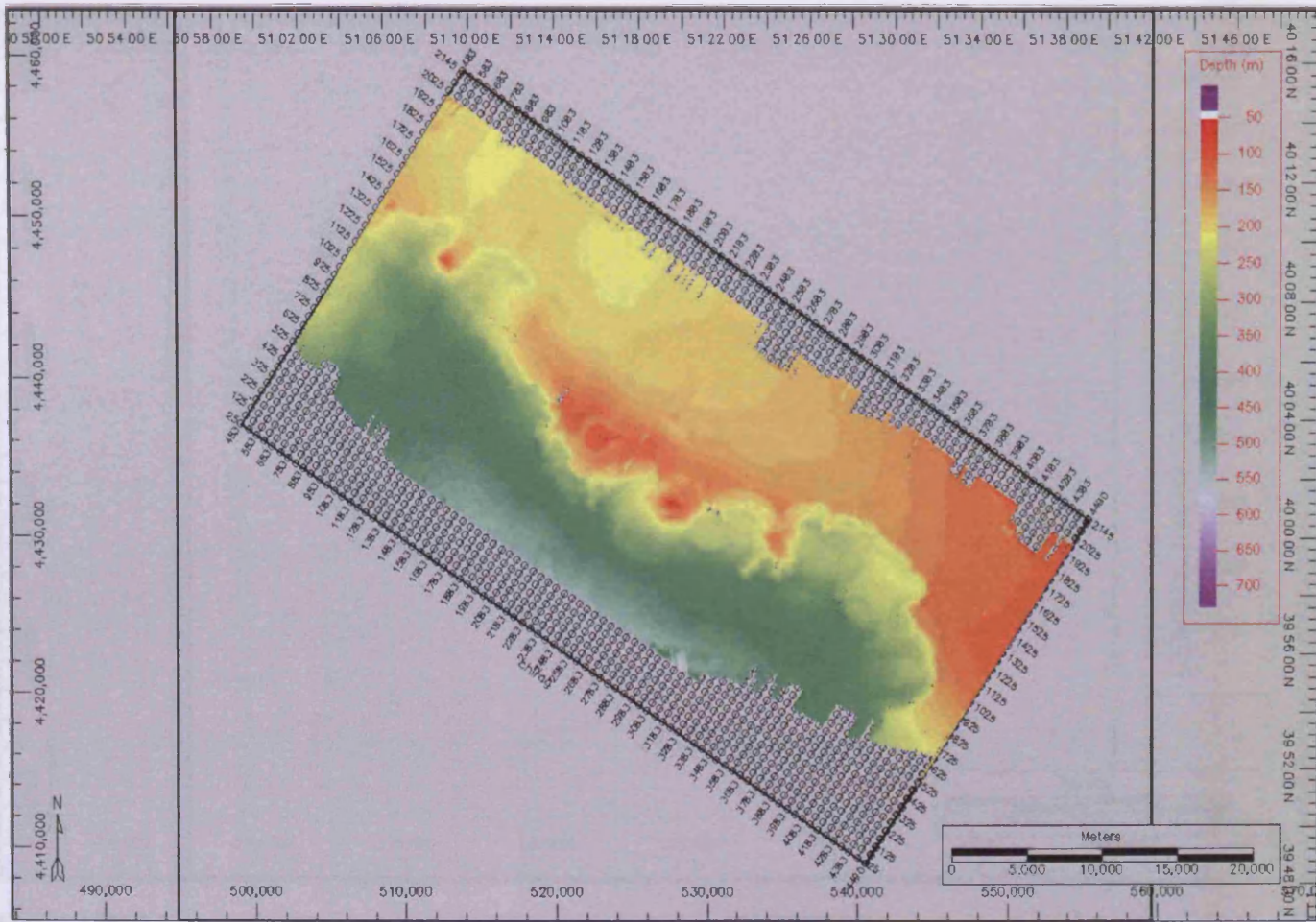


Figure APII 1 Seafloor depth map of the study area showing the position of Chirag and other major mud volcano systems as shelf-break promontories.

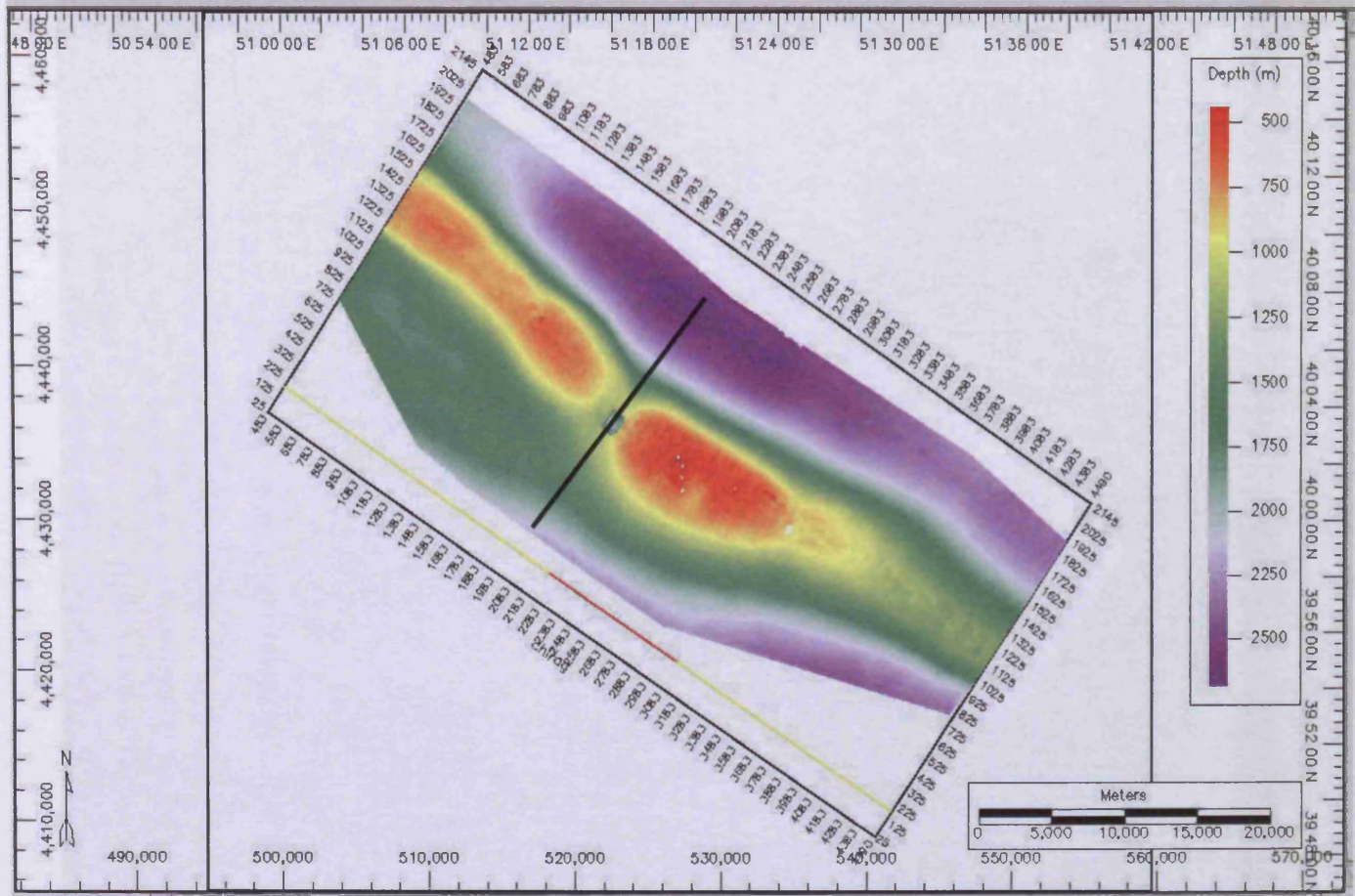


Figure API 2 Seismic depth map of the Chirag Base Mud Volcano reflection (BMV) interpreted across the study area. Chirag caldera is visible as a sharp-bounded depression. Thick black line shows section location of Figure API 5.

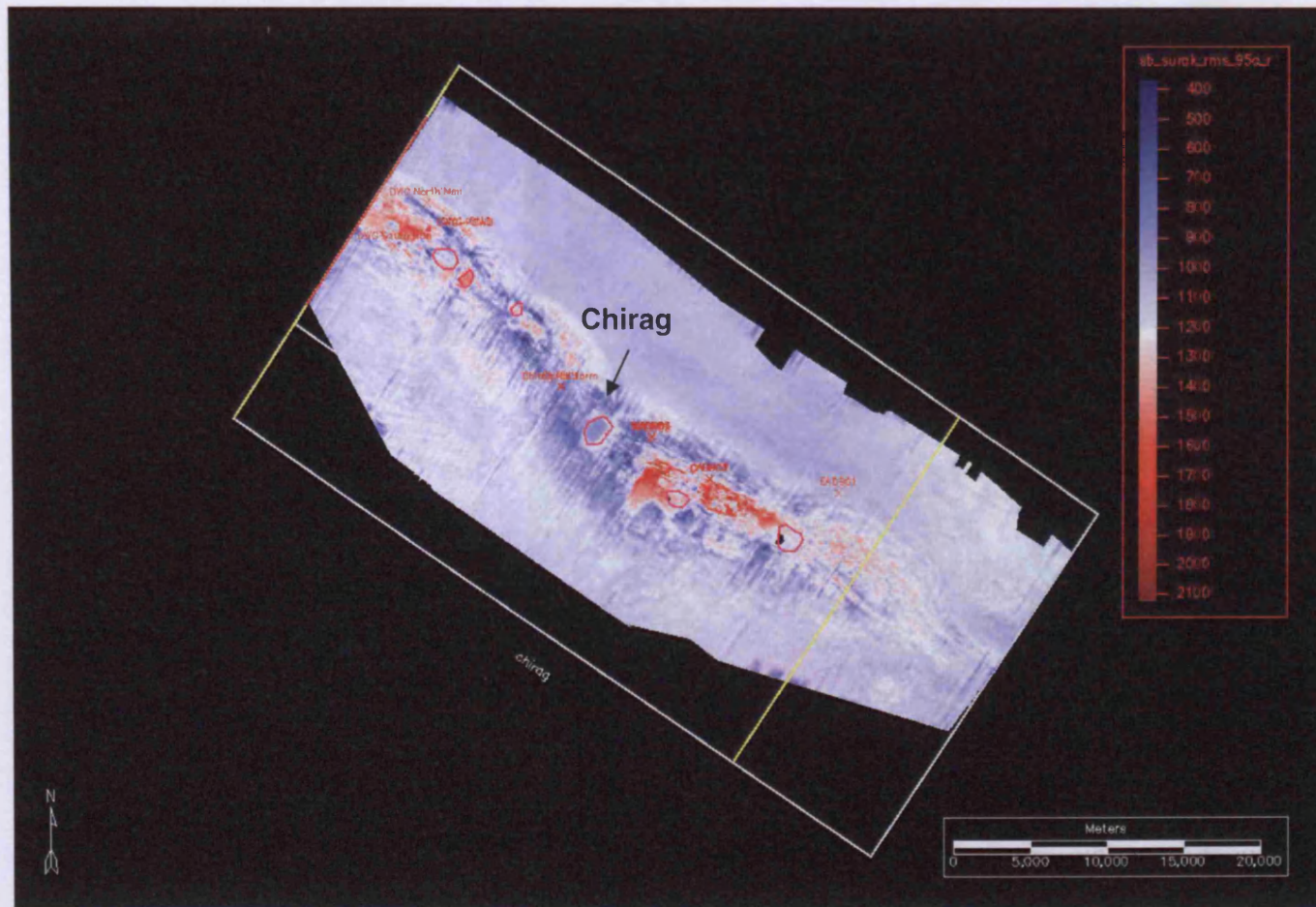


Figure APII 3 Interval Root Mean Squared (RMS) amplitude map of the interval seabed-BMV showing the large negative amplitude anomaly associated with the Chirag mud volcano system edifice. Red polygons mark locations of other mud volcano systems. Locations of industrial installations shown in red text.

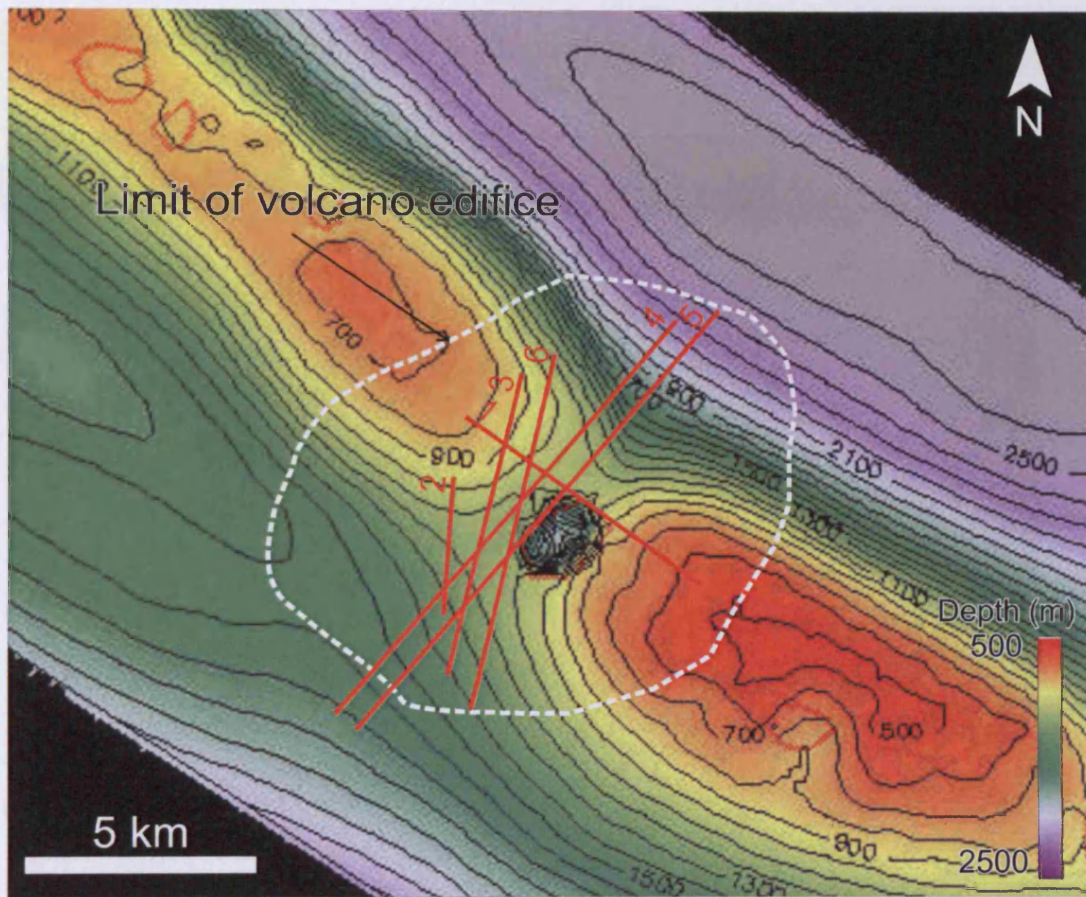


Figure APII 4 BMV reflection depth map showing location of Chirag caldera and the outer limit of the volcanic edifice. Red circles mark the locations of other mud volcano systems. White dashed line is the outer limit of the edifice. Red numbered lines 1-6 show section locations for Figures API 6, 7, 8, 11, 12 and 13 respectively. Contour interval = 200 m.

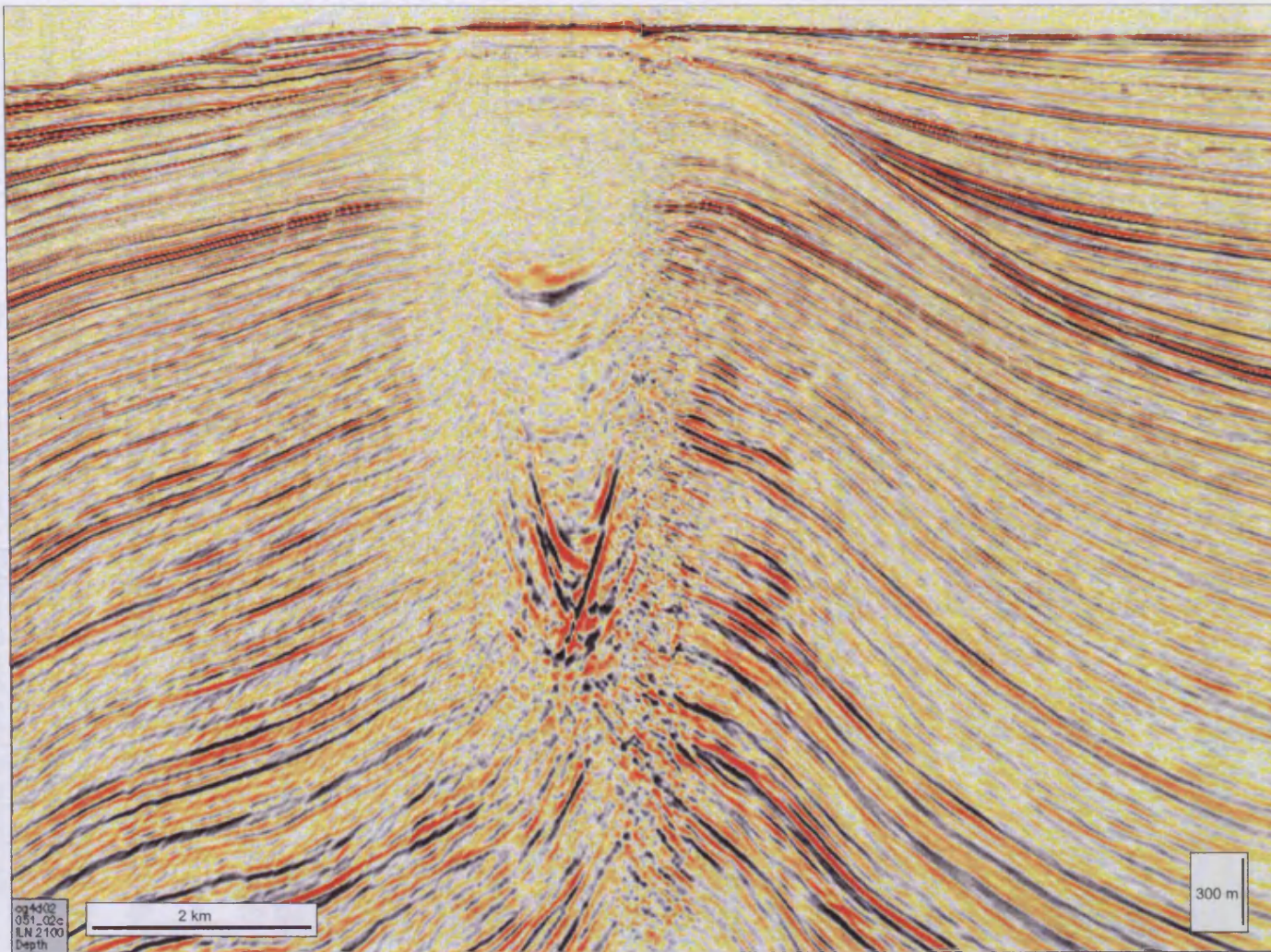


Figure APII 5 Inline 2070 showing the general seismic character of the entire Chirag mud volcano system.

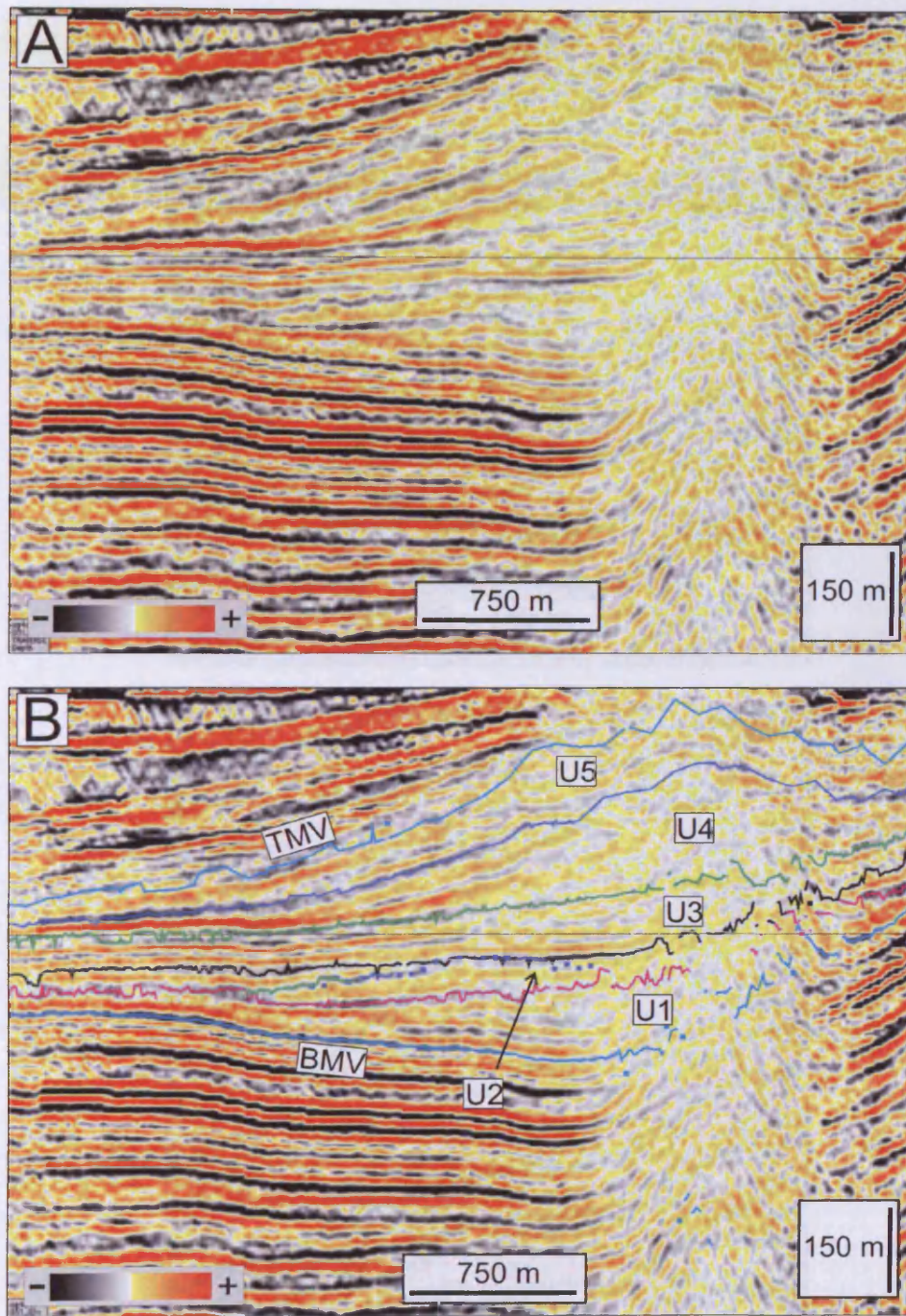


Figure APII 6 Uninterpreted (A) and interpreted (B) seismic profile through the Chirag volcano system edifice showing internal reflection detail and stacking arrangement of internal seismic facies units. Note wedge external form of units 1, 2, 4 and 5 and sheet-like external form of unit 3. Also note reflection terminations within each unit used to seismically subdivide the edifice. Section location shown in Figure API 4 (Line 1).

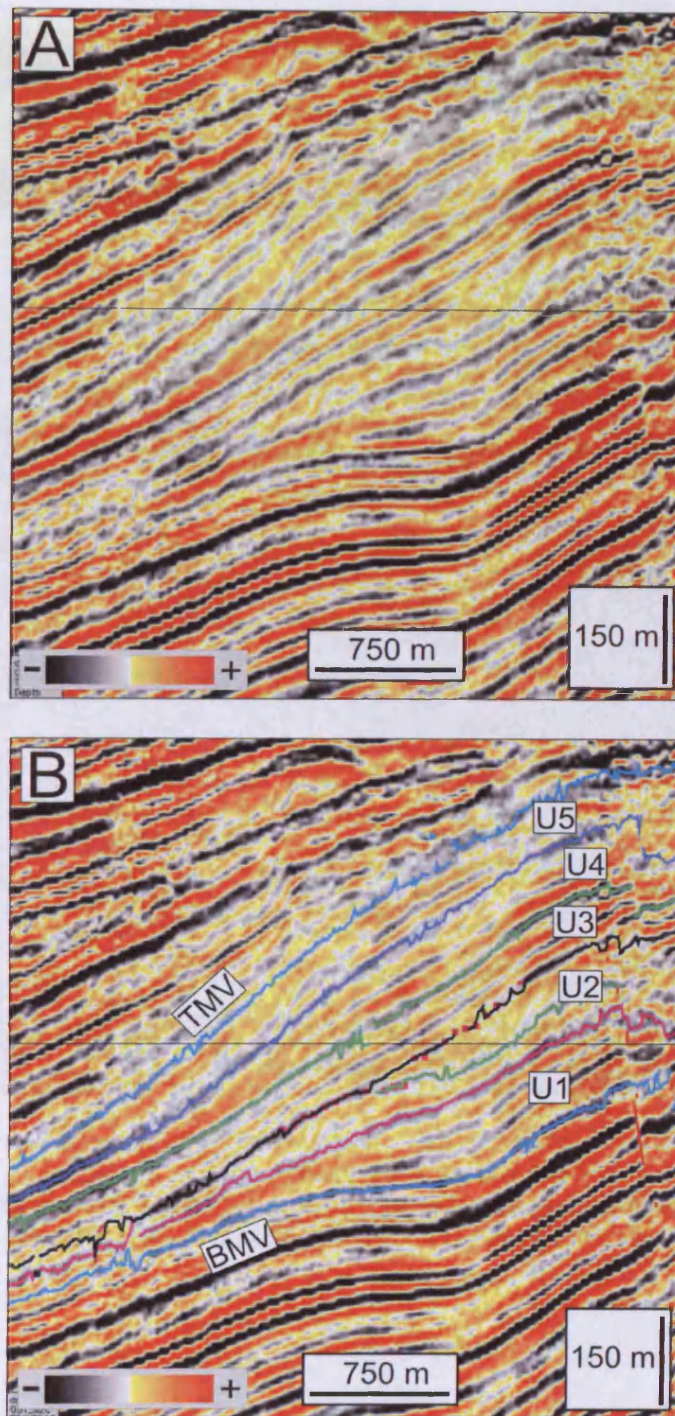


Figure APII 7 Uninterpreted (A) and interpreted (B) seismic profile through the Chirag volcano system edifice showing internal reflection detail and stacking arrangement of seismic facies units. Note wedge external form of units 1, 2, 4 and 5 and sheet-like external form of unit 3. Also note reflection terminations within each unit used to seismically subdivide the edifice. Section location shown in Figure API 4 (Line 2).

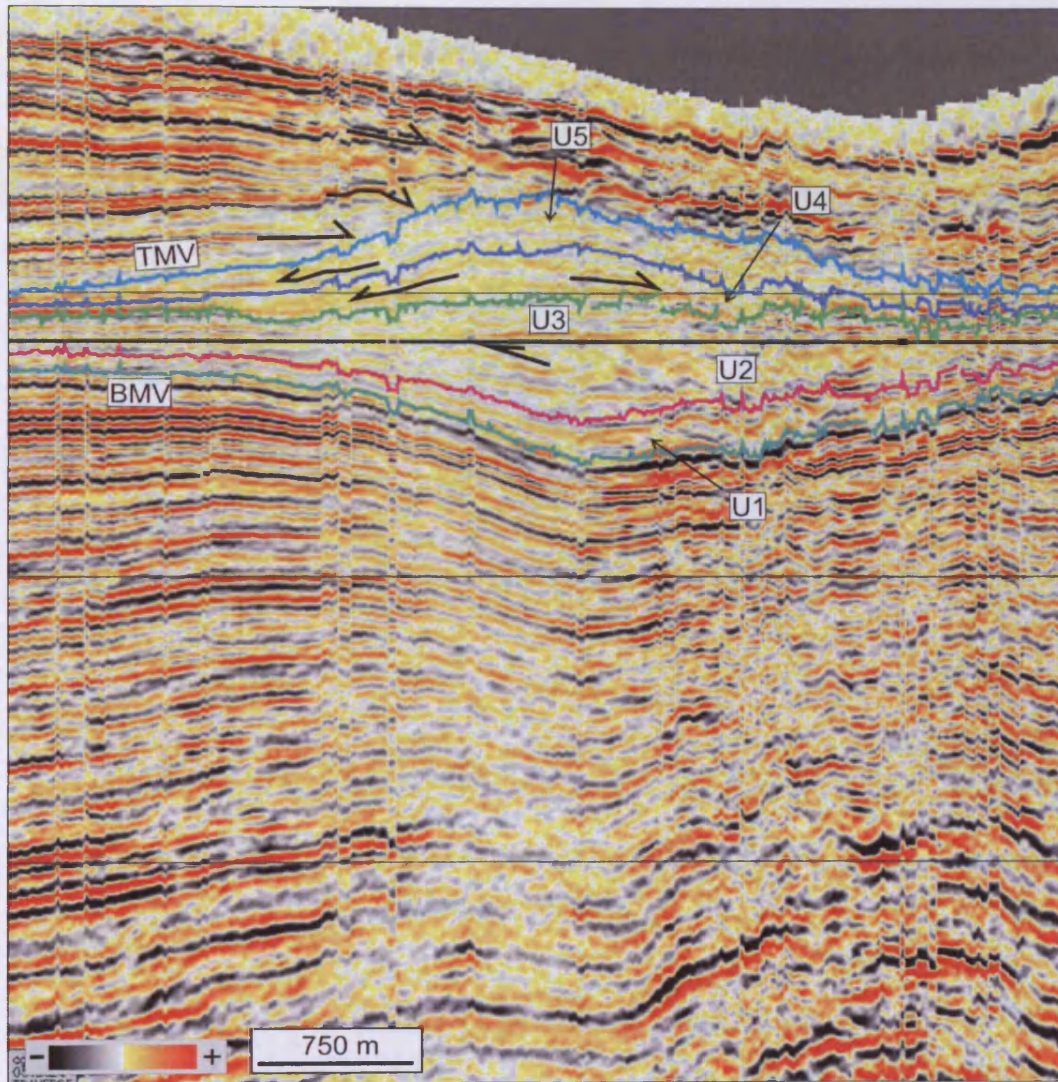


Figure APII 8 Interpreted seismic profile through the Chirag volcano system edifice flattened on the base of seismic facies unit 3 to illustrate its sheet-like external form and the clear onlap of non-eruptive sediment onto TMV. Black arrows indicate reflection terminations used to map and subdivide the edifice. Section location shown in Figure API 4 (Line 3).

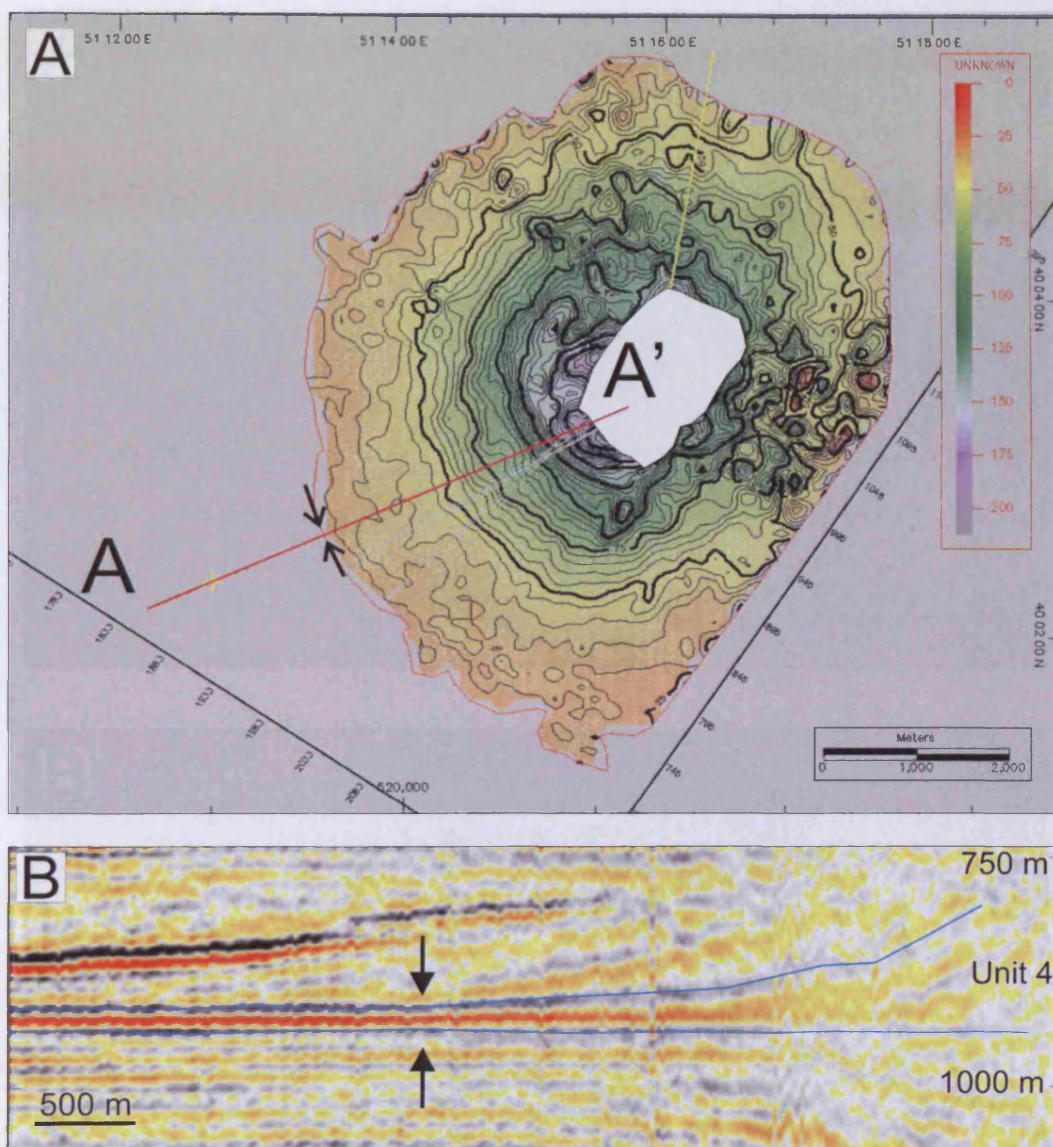


Figure APII 9 (A) Isopach map of seismic facies unit 4 illustrating the methodology used to delimit the edges of wedge-shaped seismic facies units within the edifice of the Chirag volcano system. Seismic profile A-A' is shown in (B). Black arrows in both figure parts mark the point of no further convergence of the top and base reflection of unit 4. This point was taken as the margin of all wedge shaped seismic facies units that were mapped as part of Chapter 3.

Figure APII 9 (A) Isopach map of seismic facies unit 4 illustrating the methodology used to delimit the edges of wedge-shaped seismic facies units within the edifice of the Chirag volcano system. (A) Seismic profile A-A' is shown in (B). Black arrows in both figure parts mark the point of no further convergence of the top and base reflection of unit 4. This point was taken as the margin of all wedge shaped seismic facies units that were mapped as part of Chapter 3.

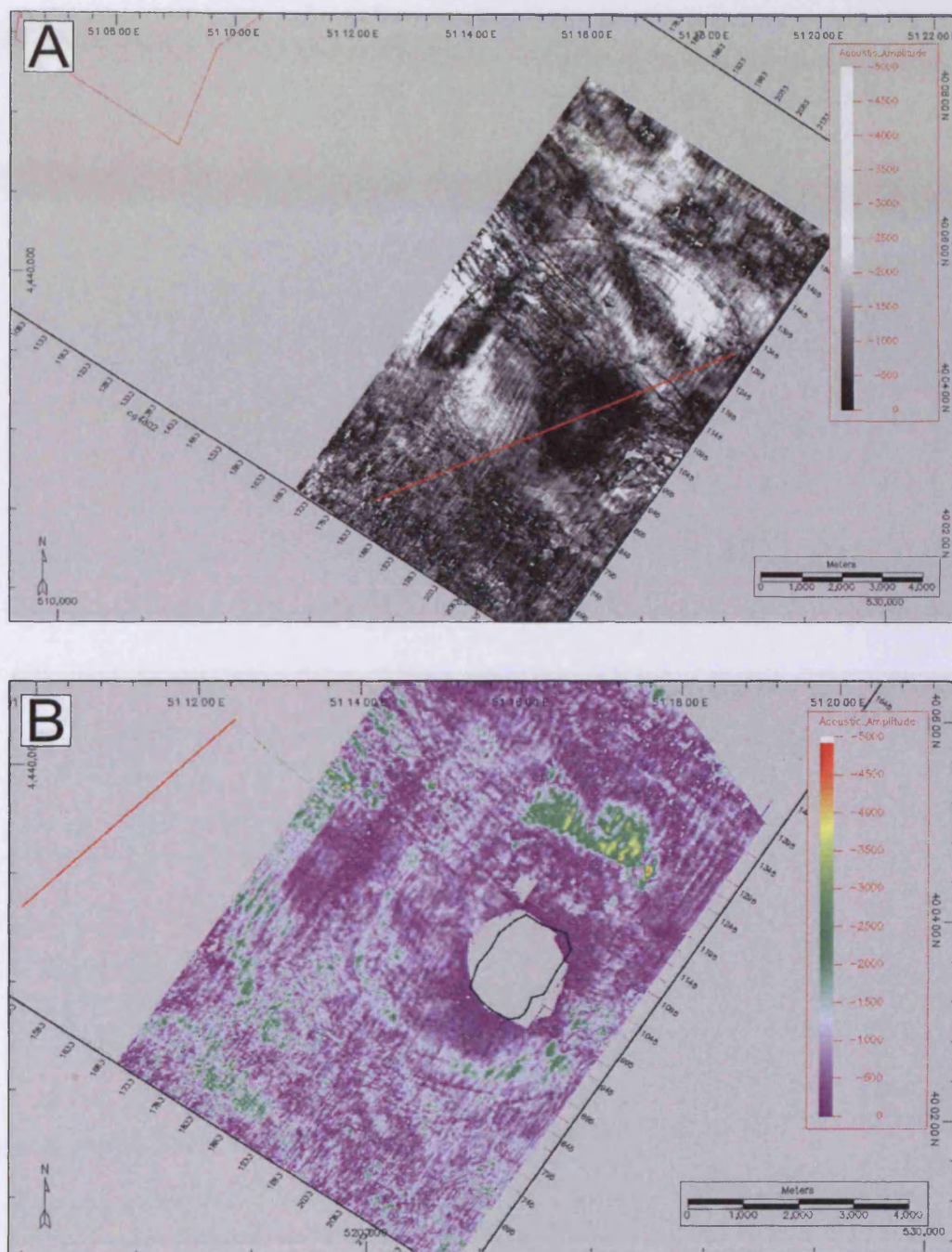


Figure APII 10 Acoustic amplitude maps for the internal reflections mapped within the Chirag volcano system edifice. (A) BMV reflection; (B) Top-unit 1 reflection; (C) Top-unit 2 reflection; (D) Top-unit 3 reflection; (E) Top-unit 4 reflection. All maps show a clear and roughly circular negative amplitude anomaly surrounding the edifice centre. They were used to investigate any potential depositional fabrics associated with each unit and assist with delimiting the margins of each one. Continued on subsequent pages.

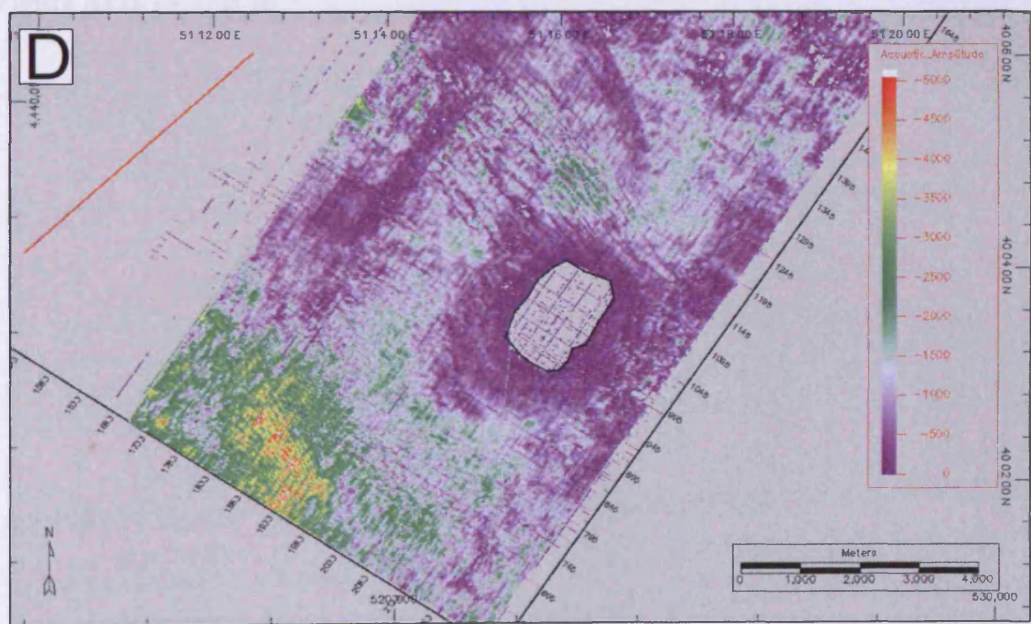
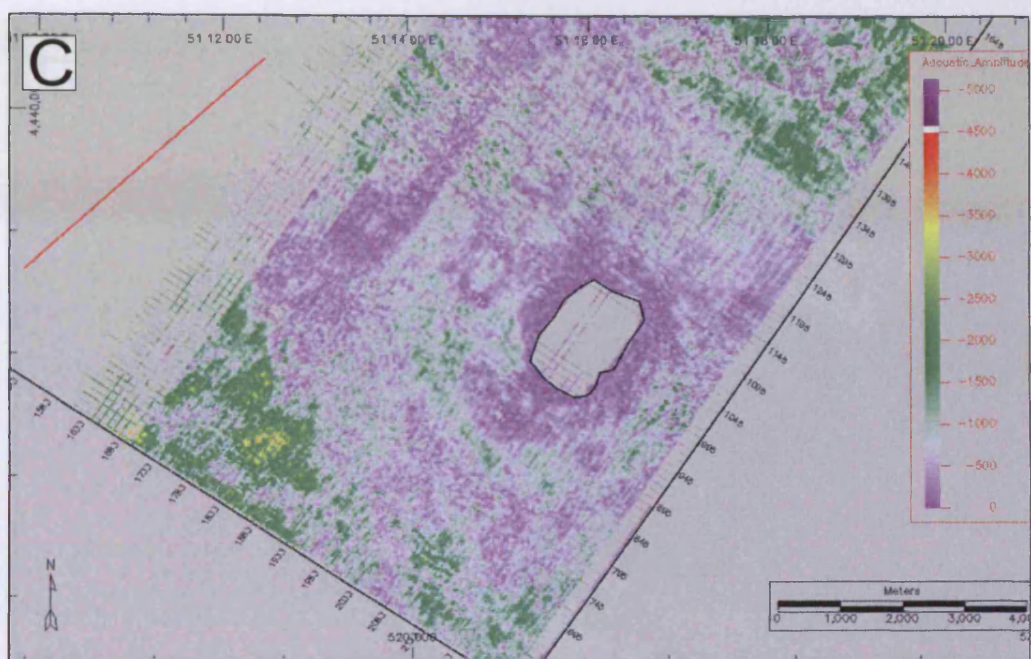


Figure APII 10 (cont'd)

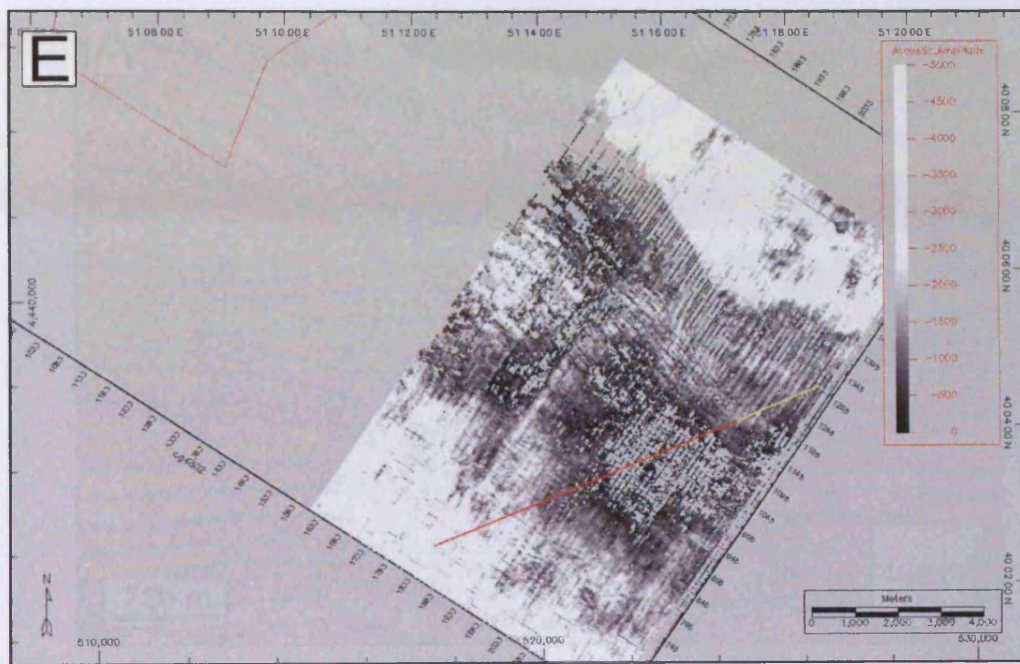


Figure APII 10 (cont'd)

Figure APII 11 shows profiles (A) and (B) interpreted (D) seismic profiles (D) in 2001 across the Chitang coal bed area showing the coal seam structure and the surrounding geological structure. Profile has been drawn on the Top view, A and B, to illustrate the structure of external part of the coal seam. A and B are the coal seam structure in the coal seam. The profile (D) shows the structure of the coal seam in the coal seam. The profile (D) shows the structure of the coal seam in the coal seam. The profile (D) shows the structure of the coal seam in the coal seam.

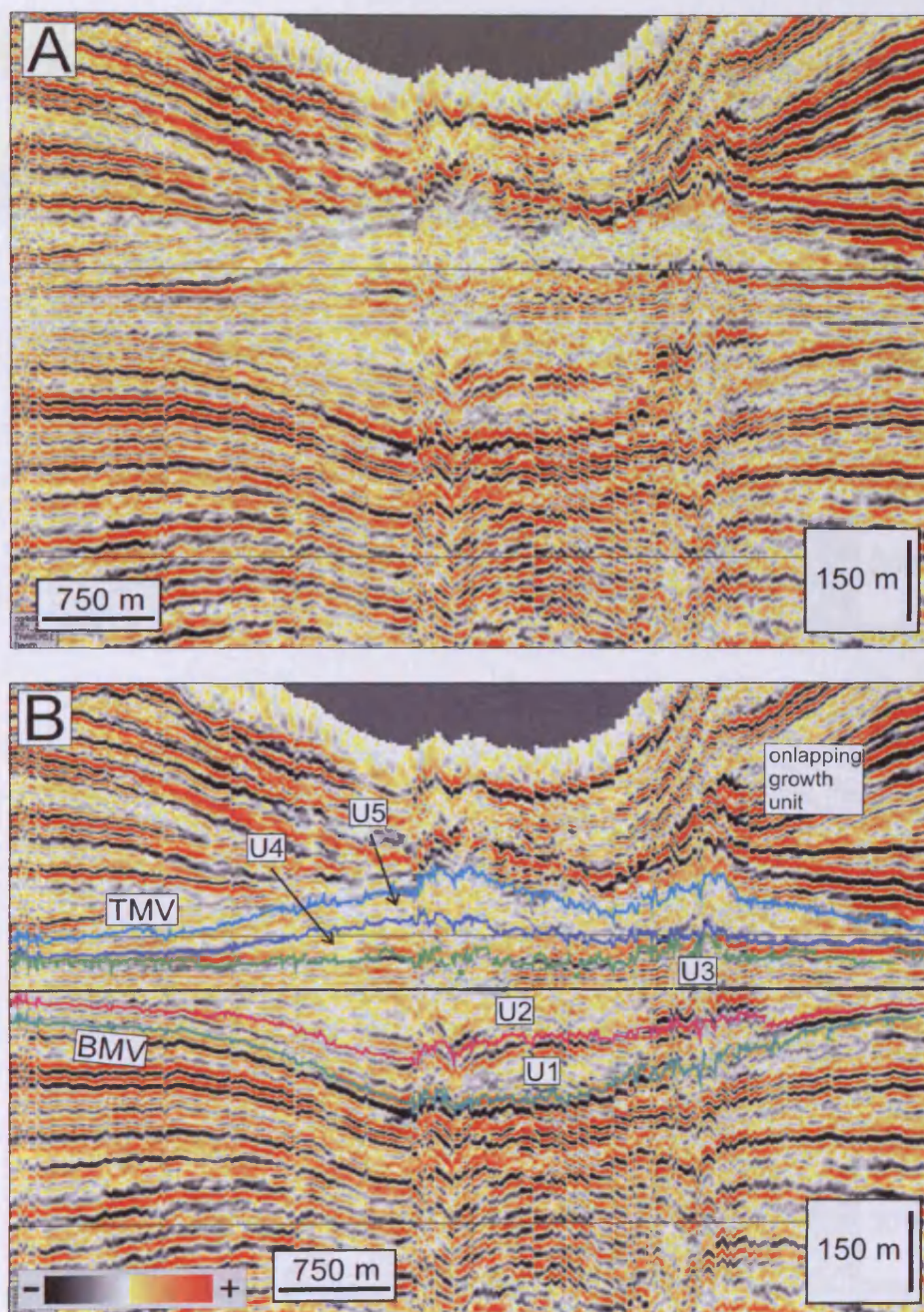


Figure APII 11 Uninterpreted (A) and interpreted (B) seismic profile (ILN 2000) through the Chirag mud volcano system edifice showing stacking arrangement of internal seismic facies units. Profile has been flattened on the Top-unit 2 reflection to illustrate the sheet-like external form of seismic facies unit 3 and the onlap of non-eruptive onto the top of the edifice (reflection TMV). Section location shown in Figure API 4 (Line 4).

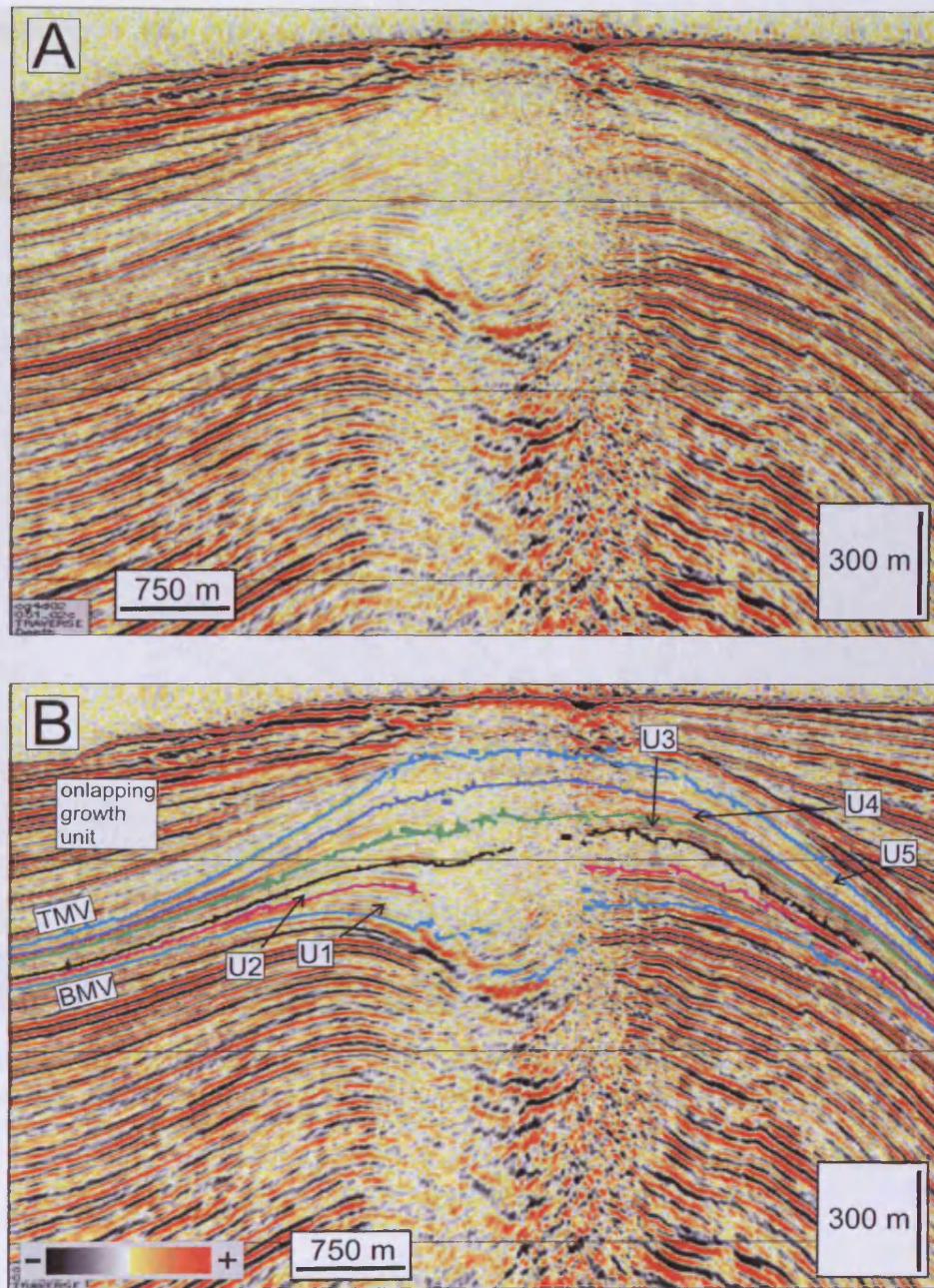


Figure APII 12 Uninterpreted (A) and interpreted (B) seismic profile through the Chirag volcano system edifice showing its internal architecture. Note the change in the BMV reflection character in the area of image deterioration on the edge of the caldera. The progressive increase in the amplitude and reduction in the frequency of the BMV reflection towards and into the caldera added confidence to the interpretation of the reflection within the blanked caldera centre. Section location shown in Figure API 4 (Line 5).

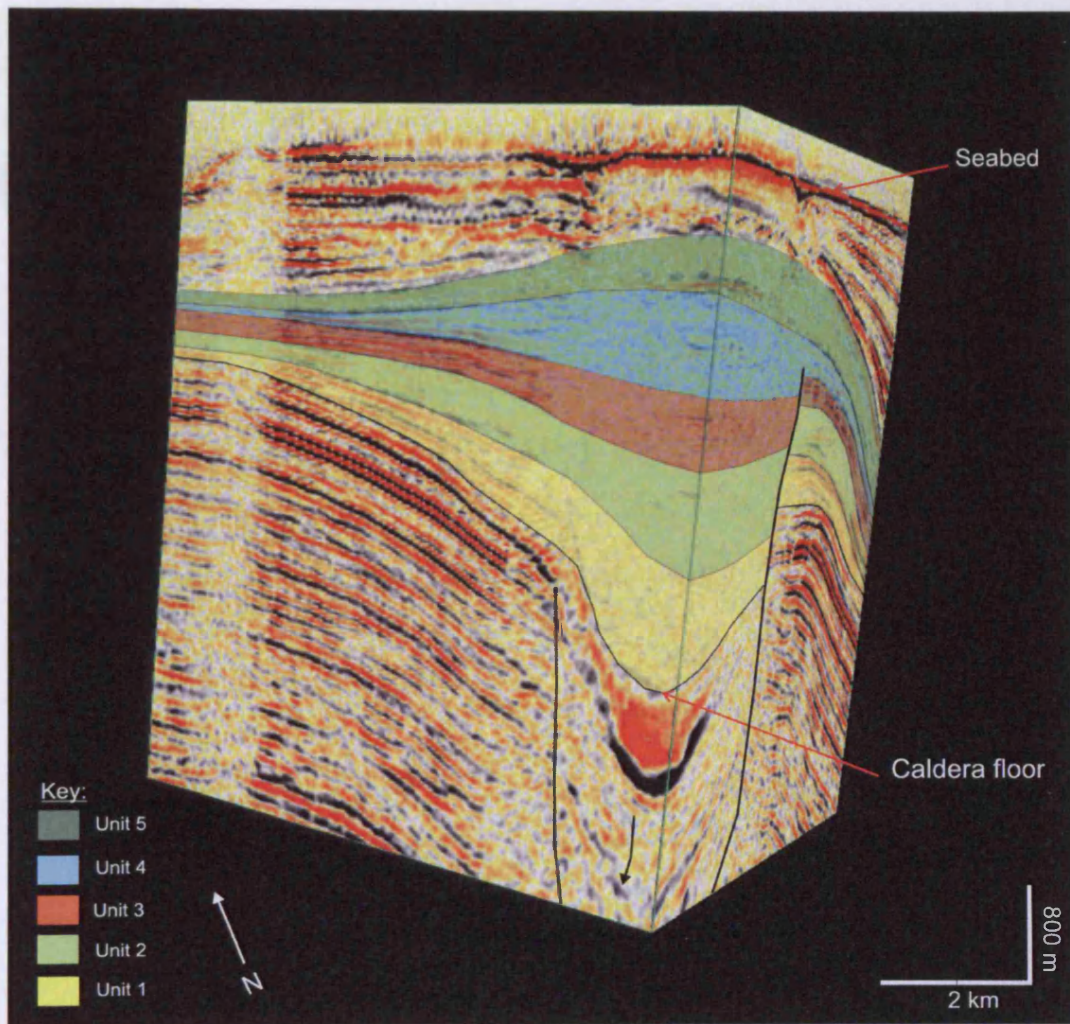


Figure APII 13 3D seismic visualisation showing the clear “trapdoor-like” asymmetry of the collapse caldera and the geometric relationship of the internal seismic facies units to it.

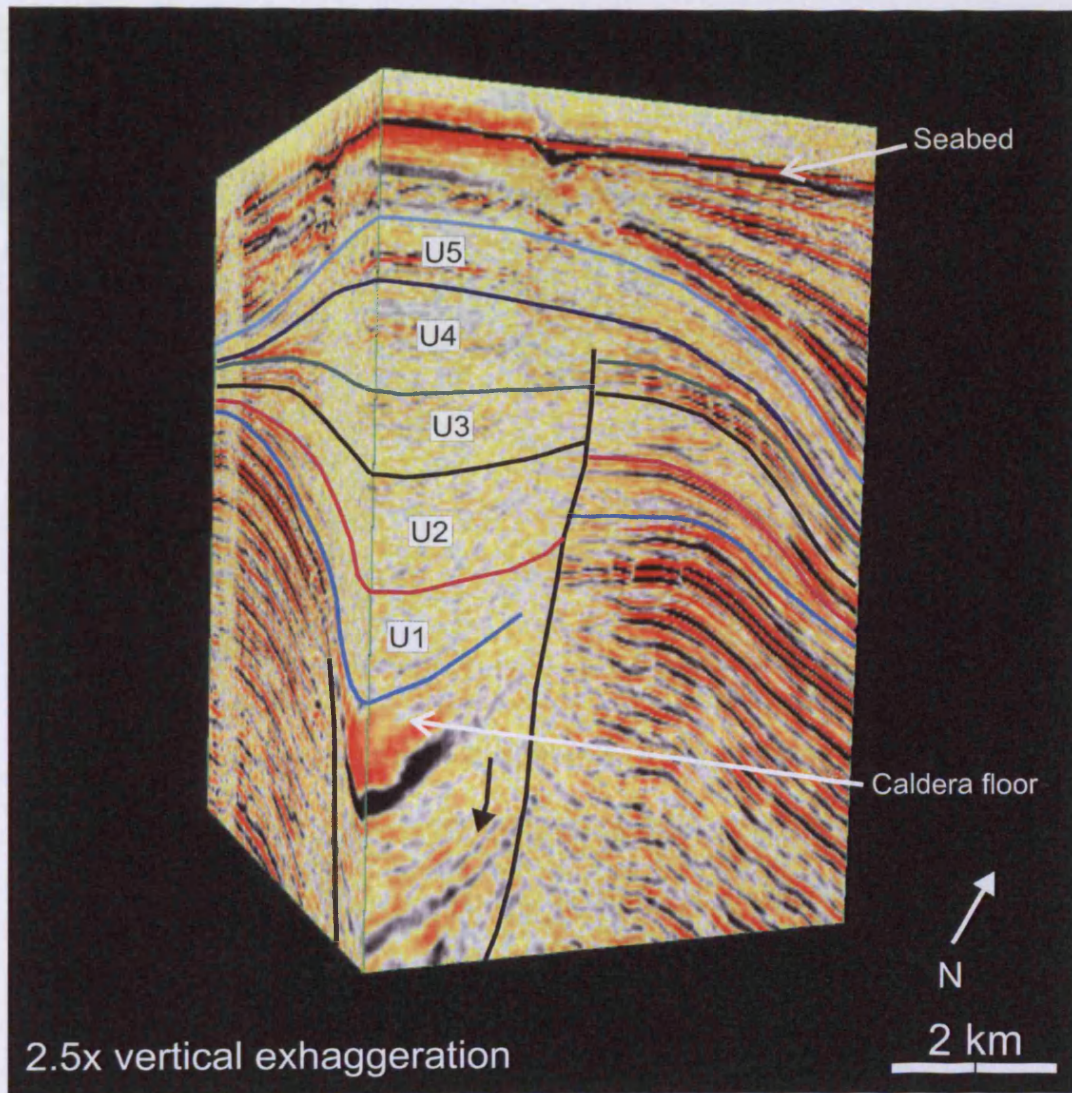


Figure APII 14 As Figure API 14 but facing NW.

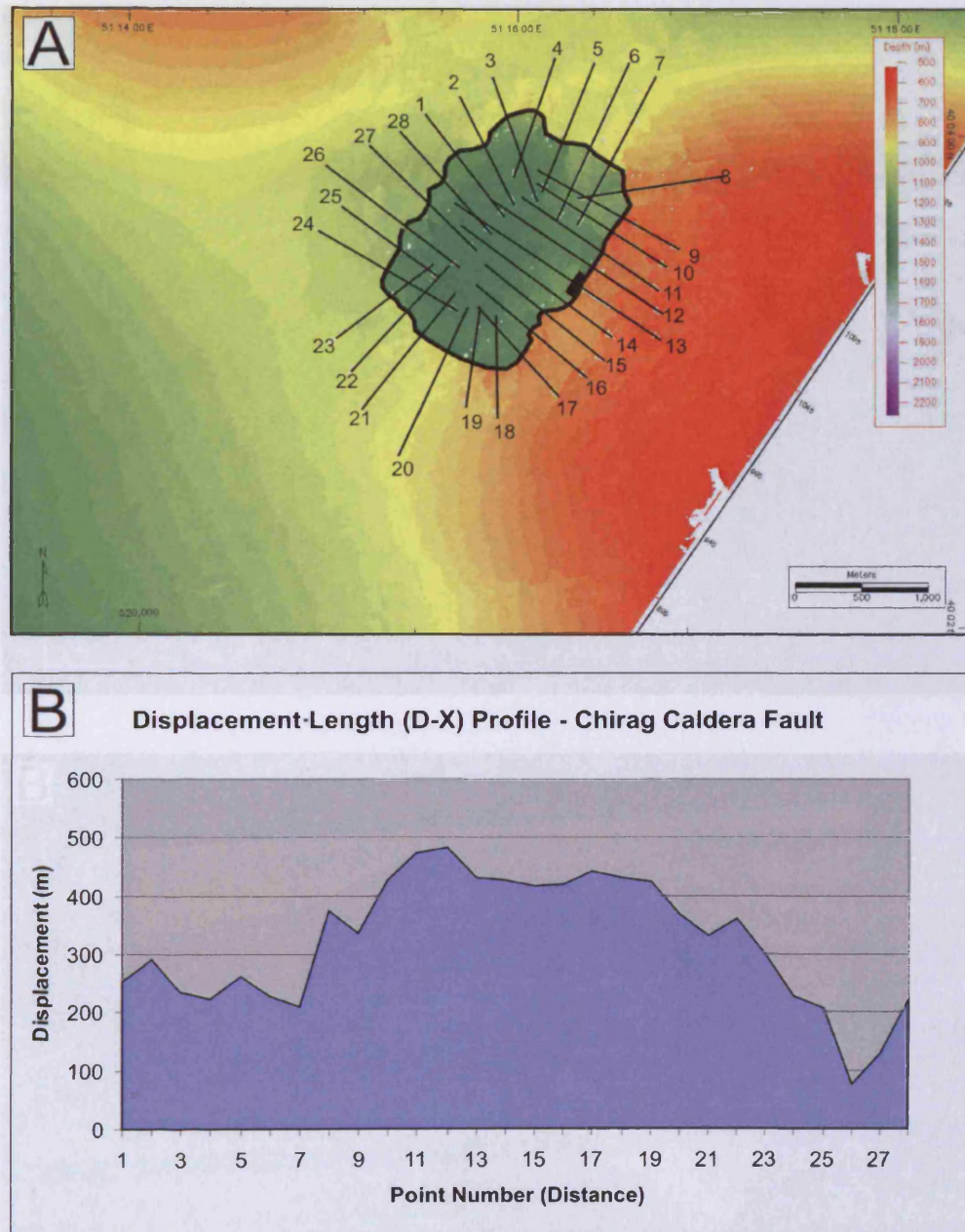
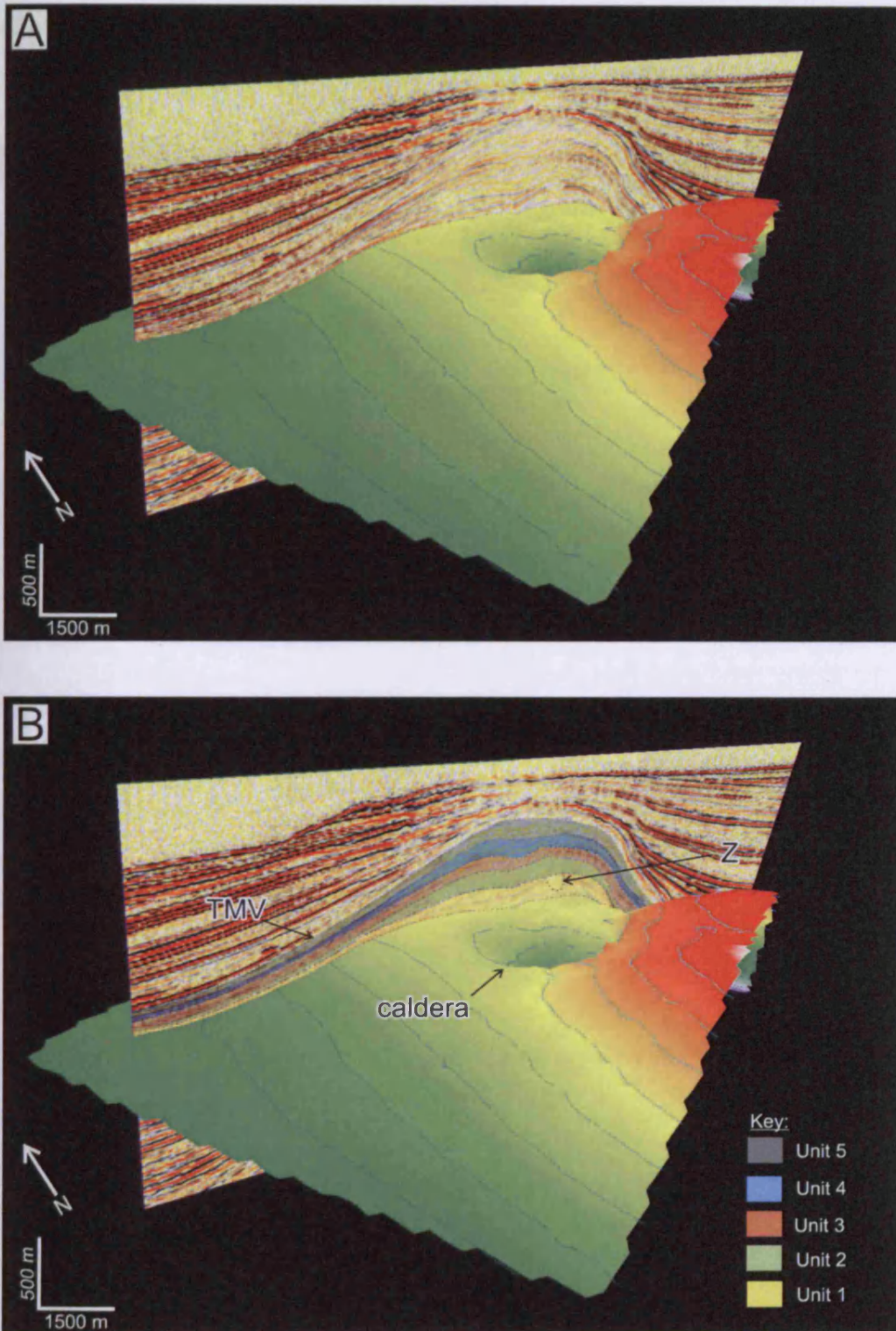


Figure AP11 15 Chirag caldera fault structural analysis: (A) Depth map of the BMV reflection showing the caldera fault as thick black line. Numbered seismic profiles (thin black lines) correspond to point numbers on the X axis of the D-X plot in (B). Dmax at point 12 = 483 m. Bell shape of profile indicates the asymmetric displacement distribution along the fault. This suggests an asymmetric “trapdoor-like” architecture of the Chirag caldera.

Figure AP11 16 (A)-(C) Selected 3D visualizations of the Chirag caldera BMV section mapped with intersecting azimuth profiles. (B) is an unprojected version of (A). Note the shape of the caldera and its position relative to the volcanic system edifice.



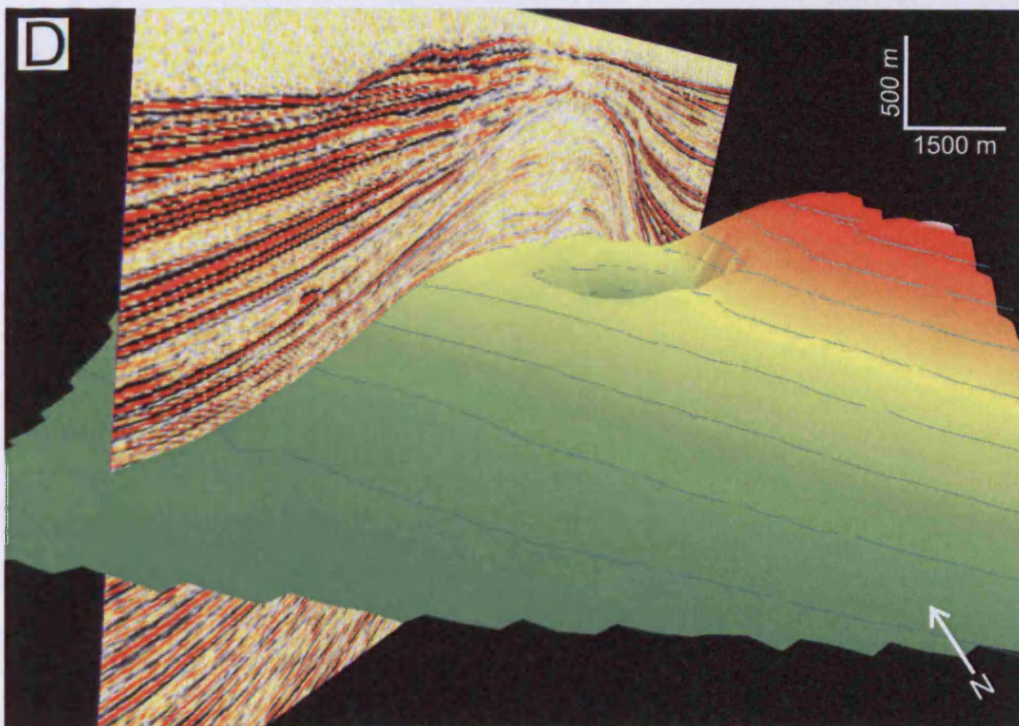
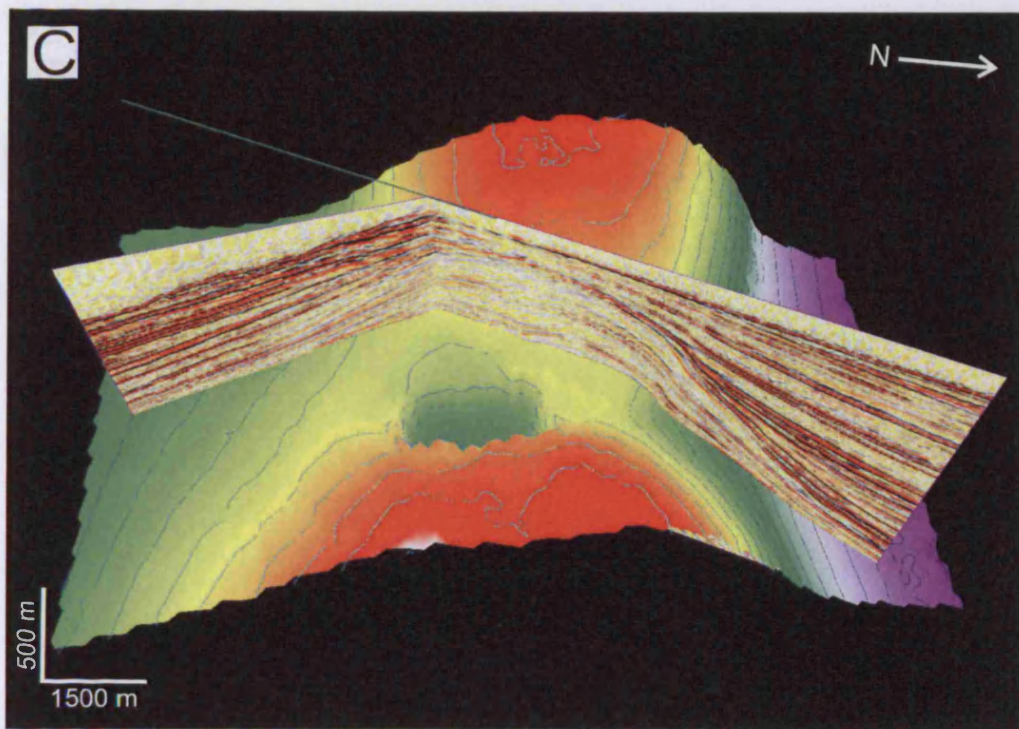


Figure APII 16 (cont'd)

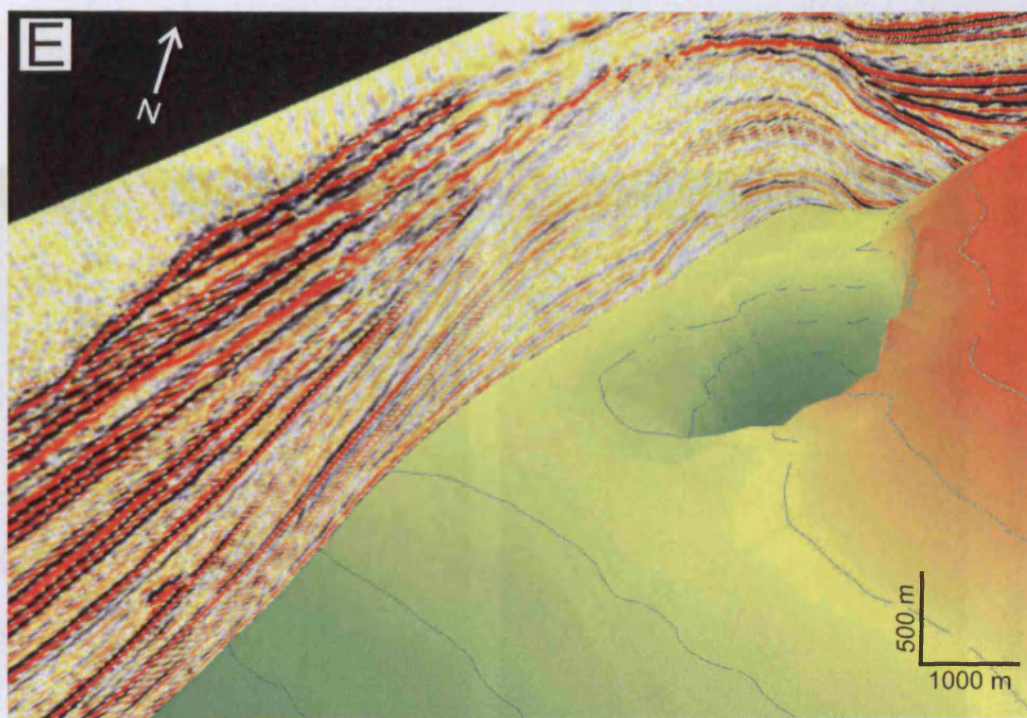


Figure AP11 16 (cont'd)



Figure AP11 16 (cont'd) shows a geological cross-section of the study area. The section is oriented North-South, as indicated by the double-headed arrow. The stratigraphic units are color-coded: yellow (top), red, black, green, and orange (bottom). The scale bar indicates a vertical distance of 500 m and a horizontal distance of 1000 m.

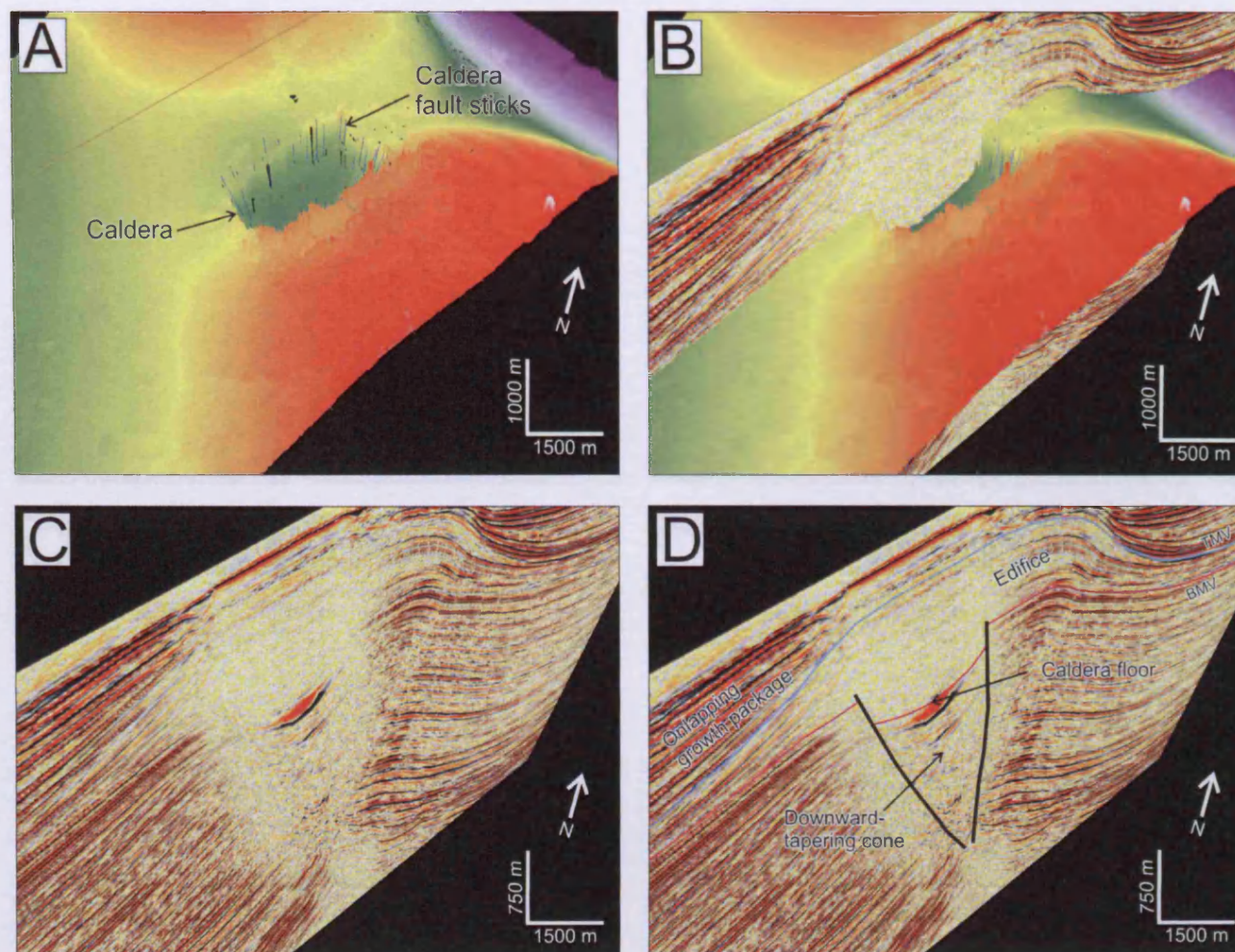


Figure APII 17 Chirag caldera visualisation: (A) 3D depth map of the BMV reflection showing position of caldera and fault sticks that were created during its mapping. (B) as (A) but with intersecting seismic Inline 2066 showing position of volcano edifice. (C) Uninterpreted 3D view of seismic Inline 2066; (D) Interpreted 3D view of seismic Inline 2066 illustrating basic structure of the edifice, caldera, bounding faults and downward-tapering cone.

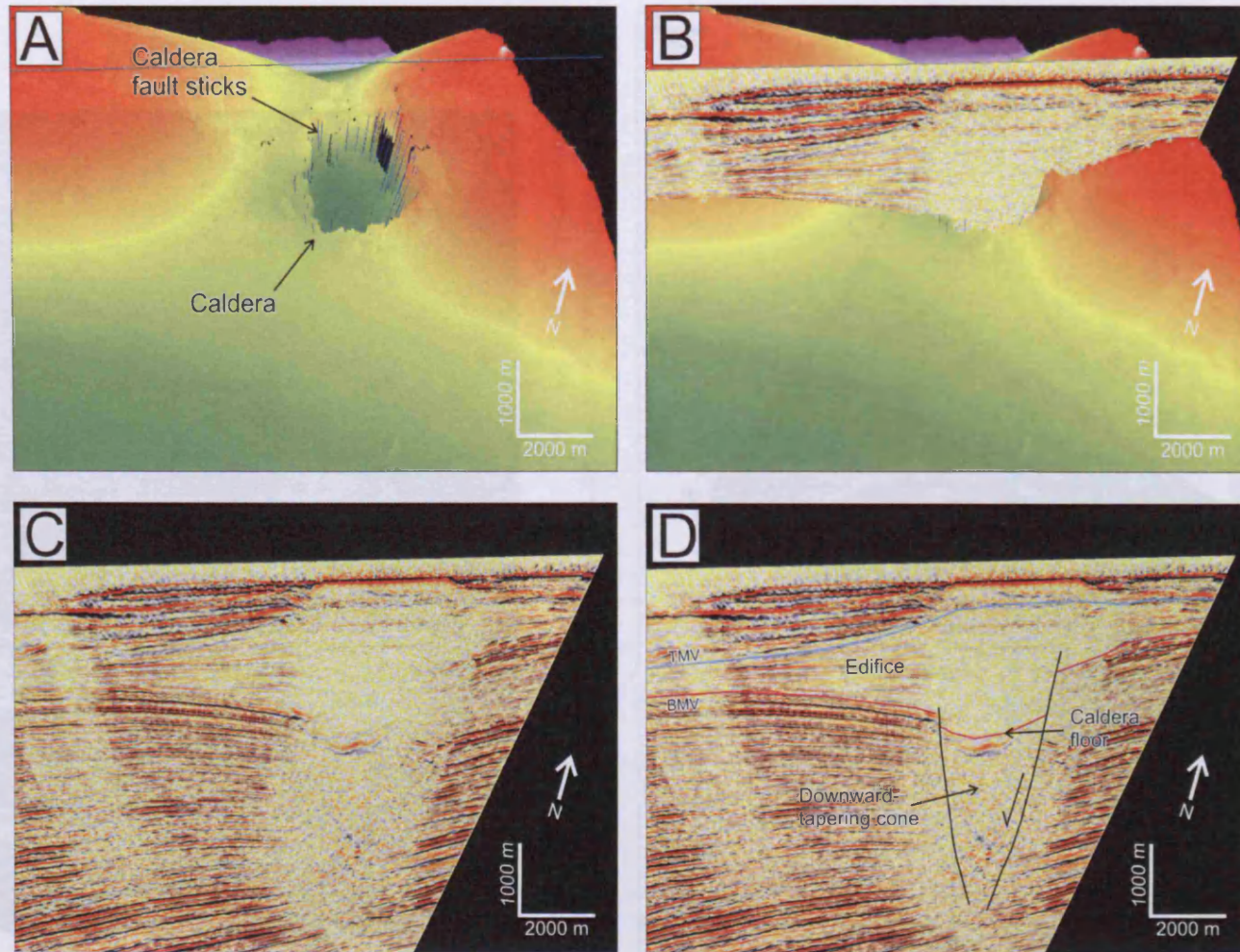


Figure APII 18 Chirag caldera visualisation: (A) 3D depth map of the BMV reflection showing position of caldera and fault sticks that were created during its mapping. (B) as (A) but with intersecting seismic Crossline 995 showing position of volcano edifice. (C) Uninterpreted 3D view of seismic crossline 995; (D) Interpreted 3D view of seismic crossline 995 illustrating basic structure of the edifice, the asymmetric architecture of the caldera, bounding faults and downward-tapering cone.

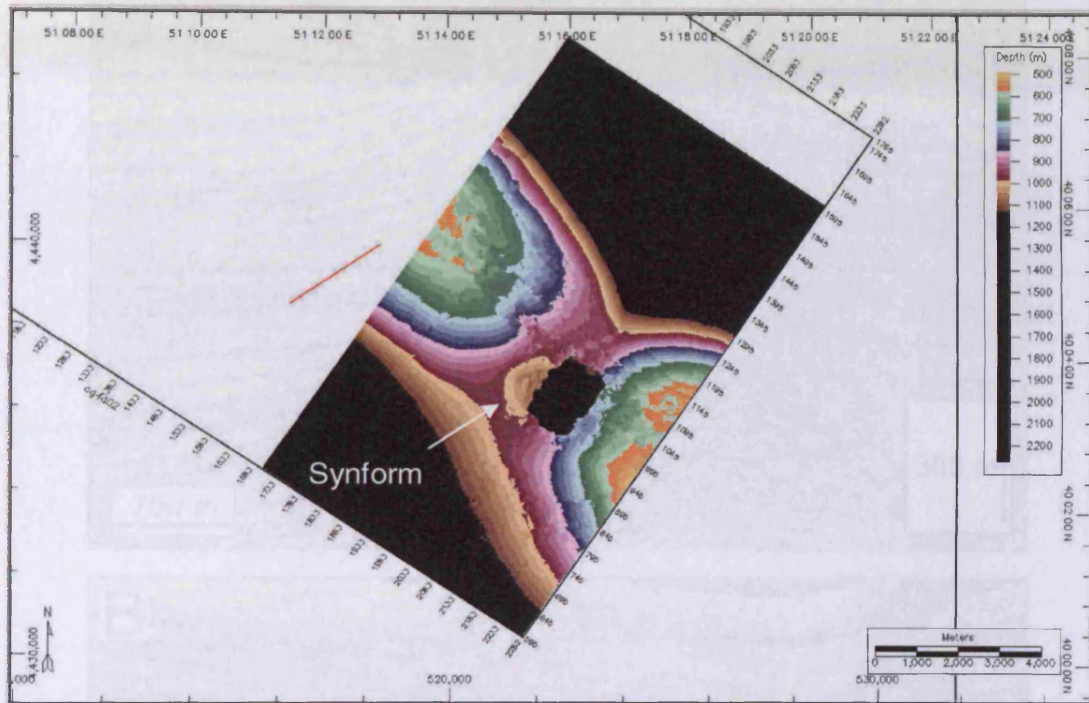


Figure APII 19 BMV reflection depth map showing Chirag volcano system caldera and adjacent hangingwall synform.

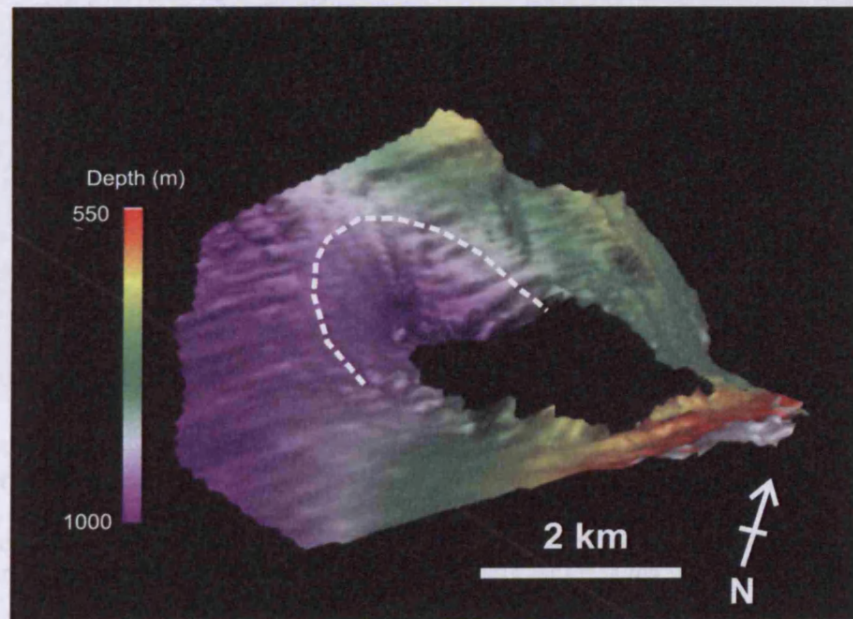


Figure APII 20 3D visualisation of the reflection "X" that is used in Chapter 3 to relatively date the onset of caldera growth. The reflection was mapped and visualised to confirm its synformal geometry and assess its geometrical similarity to the hangingwall BMV synform shown in Figure API 18. White dashed line marks approximate edge of the synform.

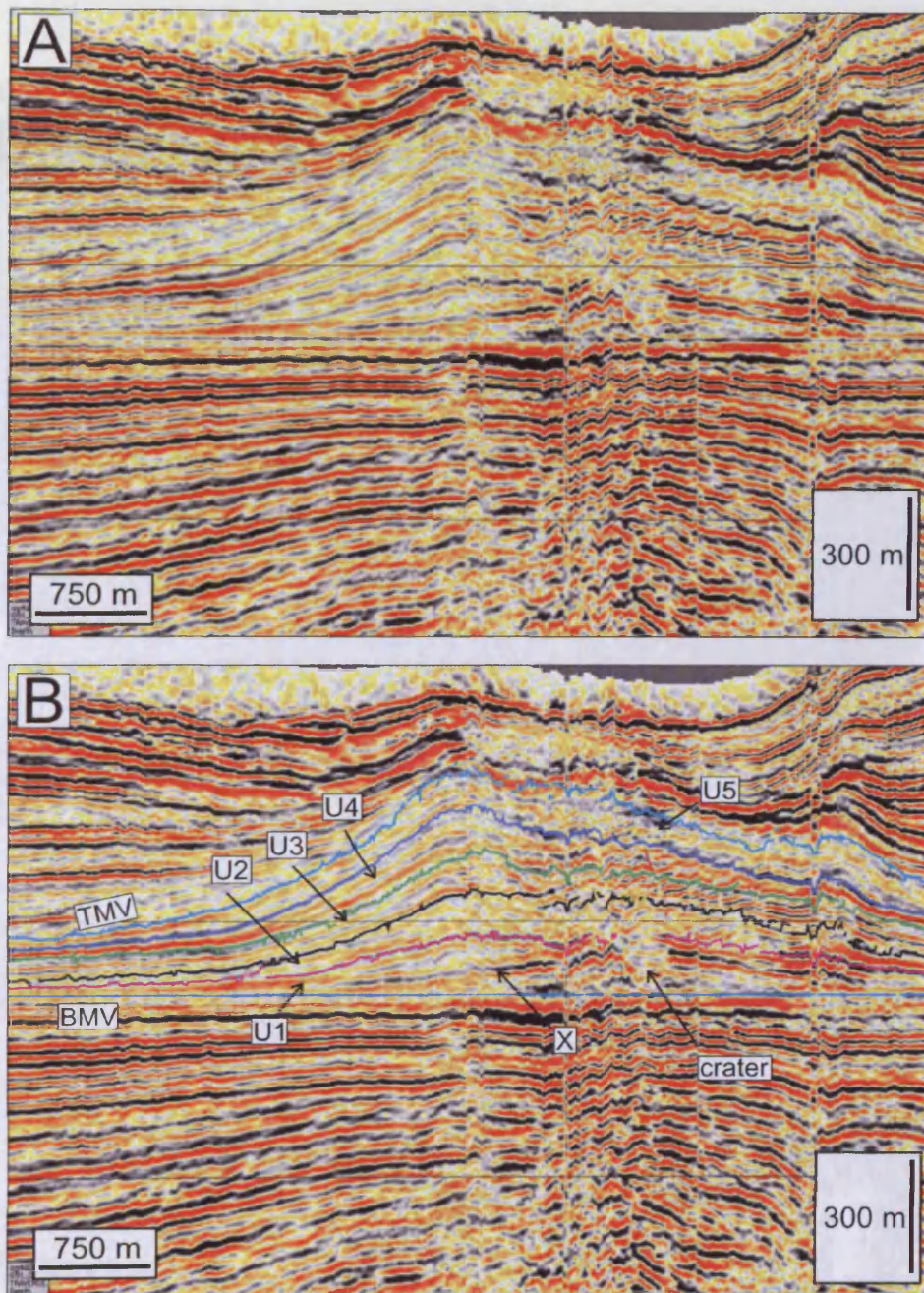


Figure APII 21 Uninterpreted and interpreted seismic profile flattened on the BMV reflection to illustrate the discordance between reflection X and the Top-unit 1 reflection (purple). The angular discordance between these reflections and the onlapping relationship of the section X-Top-unit 1 onto reflection X is used to relatively date the onset of caldera growth in Chapter 3. Section location shown in Figure API 4 (Line 6).

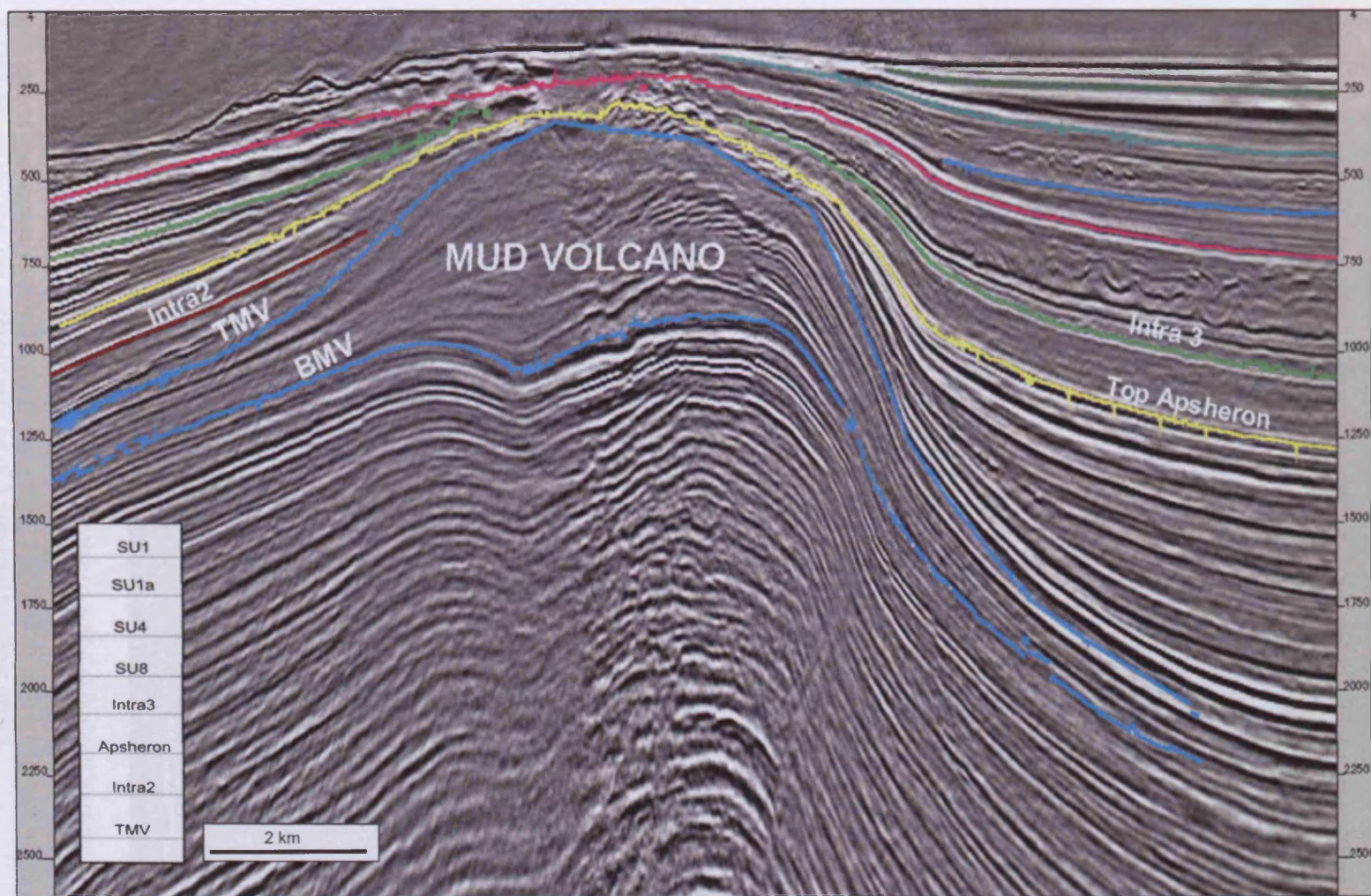


Figure APII 22 Seismic inline 2100 interpreted to show the vertical extent of the Chirag volcano system edifice (BMV-TMV) and the "Soil Unit" horizons within the onlapping growth unit overlying it. Soil units are an informal lithostratigraphic subdivision used by BP. Each unit was mapped and amplitude maps were examined to evaluate the presence of any mud volcanic deposits within the onlapping growth unit. Amplitude and interval amplitude maps within the onlapping growth unit are now shown in subsequent Figures. Depth scale in metres.

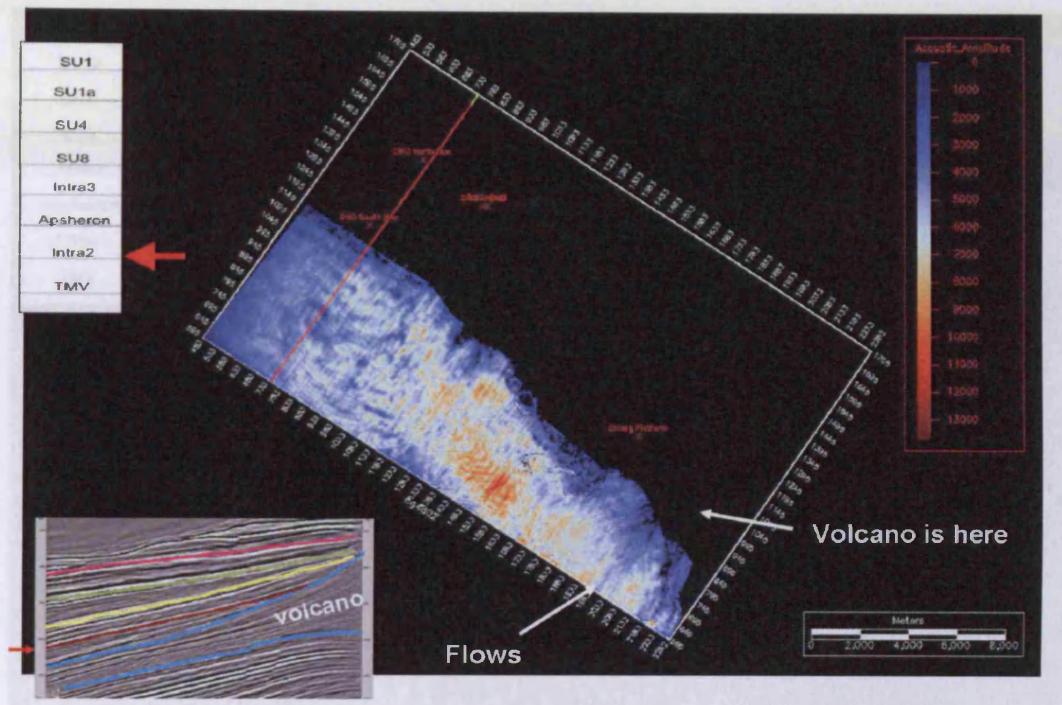


Figure APII 23 Acoustic amplitude map of the Intra2 soil unit horizon showing radial negative amplitude anomaly to the south of the Chirag mud volcano system.

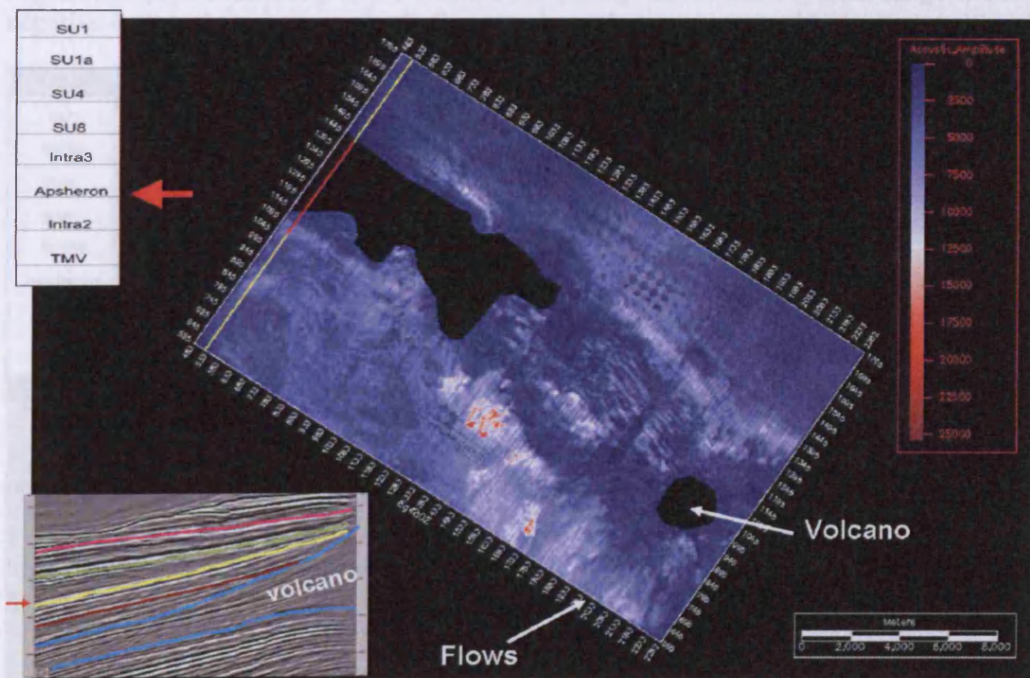


Figure APII 24 Acoustic amplitude map of the Apsheeron soil unit horizon showing radial negative amplitude anomaly to the south of the Chirag mud volcano system. Note the presence of the anomaly immediately to the west of the volcano centre, a feature which rules out the possibility that the anomaly may be of a non-mud volcanic origin.

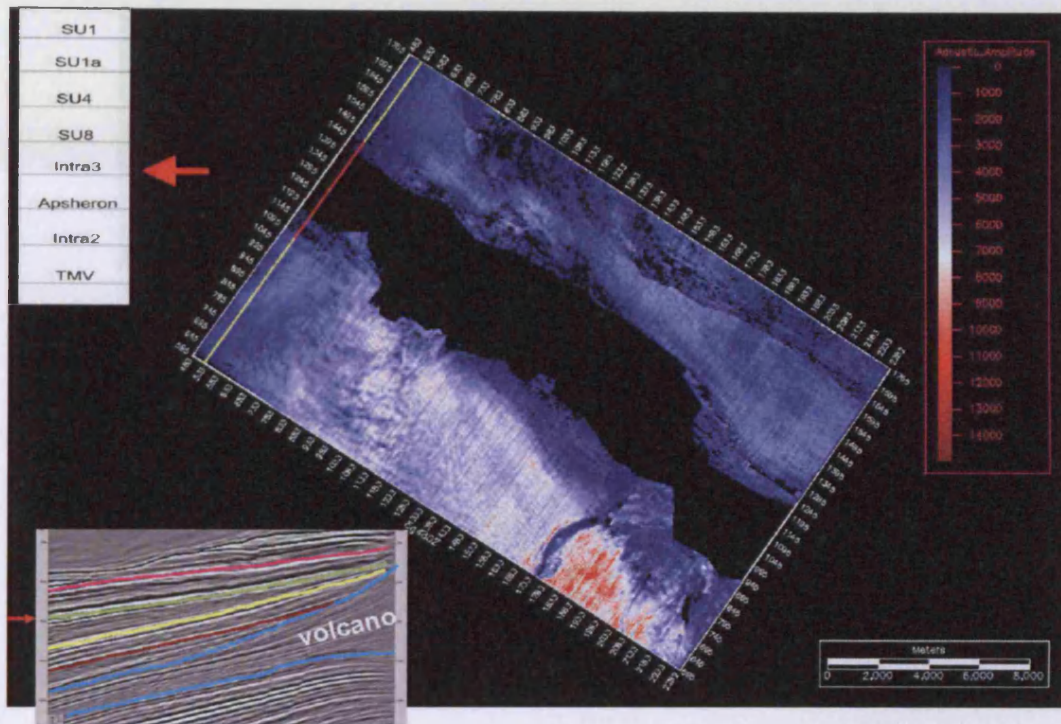


Figure API1 25 Acoustic amplitude map of the Intra3 soil unit horizon showing radial negative amplitude anomaly to the south of the Chirag mud volcano system. Large linear negative is thought to be a southerly flowing channel originating on the elevated shelfbreak.

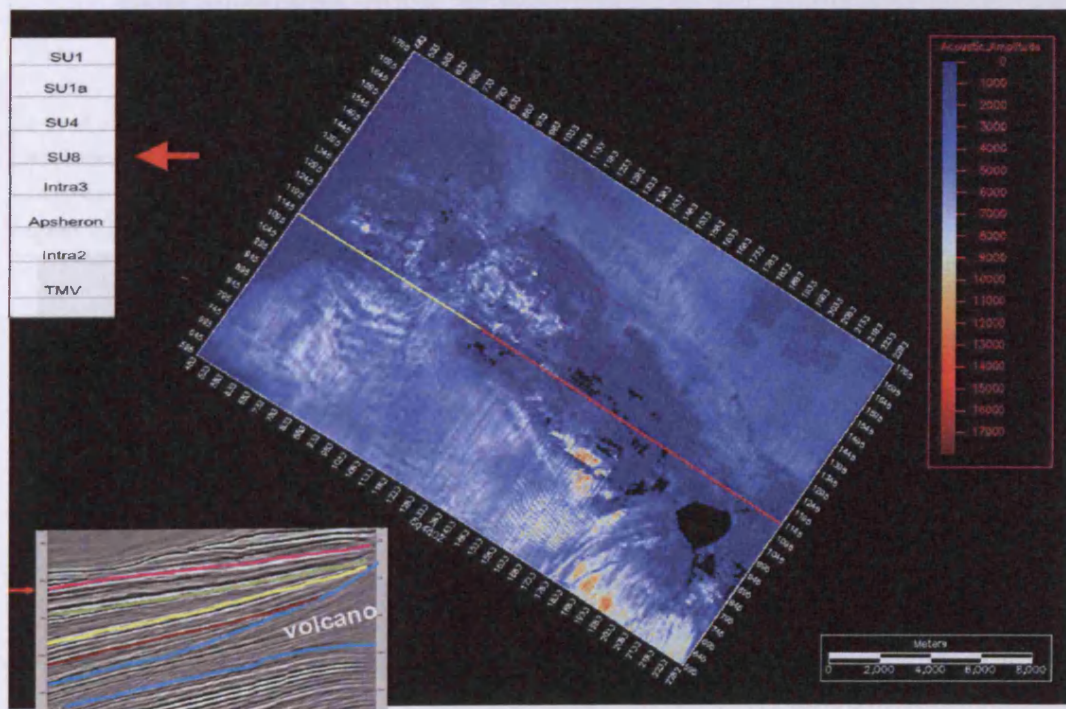


Figure API1 26 Acoustic amplitude map of the soil unit 8 horizon showing radial negative amplitude anomaly to the south of the Chirag mud volcano system.

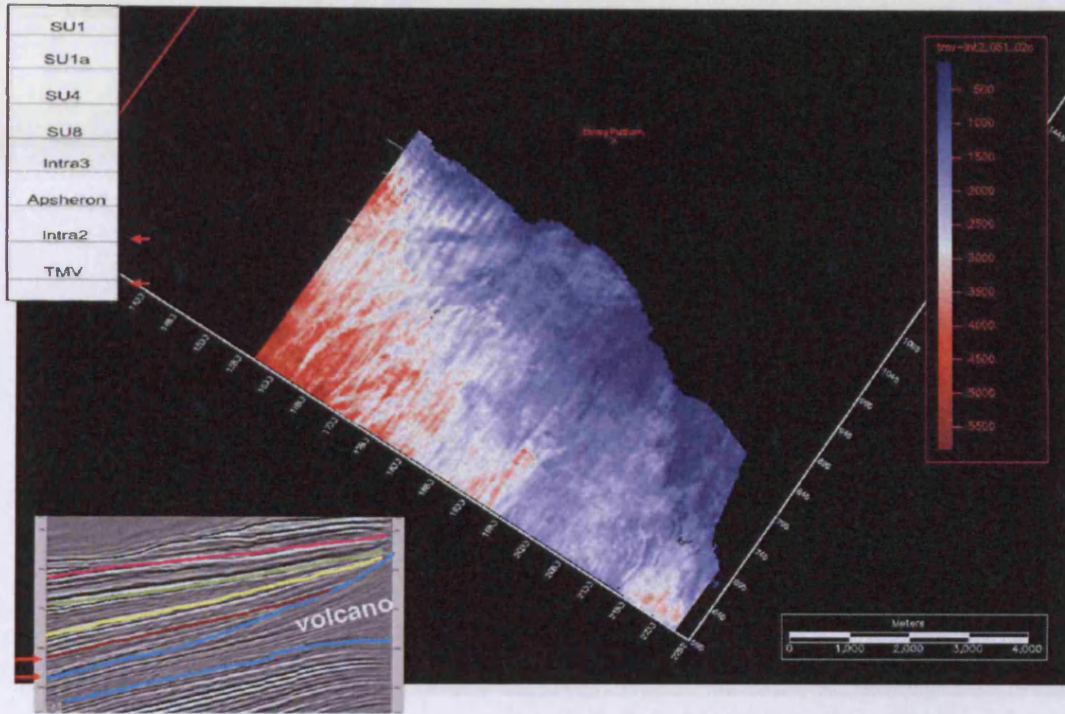


Figure API1 27 Zoom in acoustic amplitude map of the TMV-Intra2 horizon interval showing radial negative amplitude anomaly to the south of the Chirag mud volcano system.

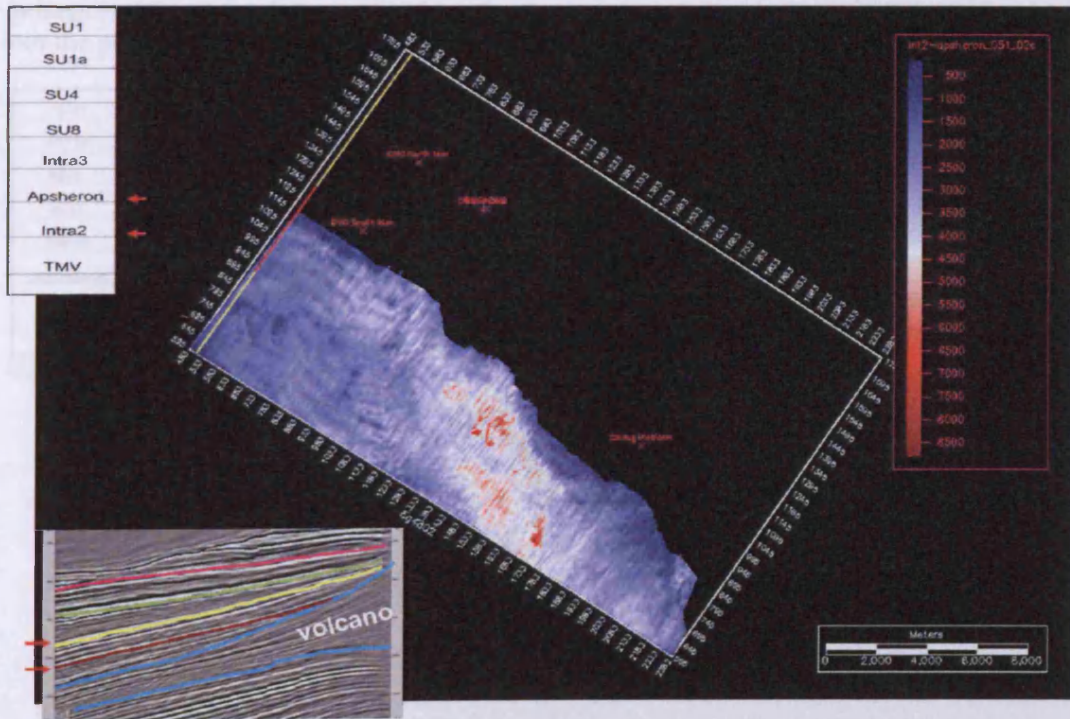


Figure API1 28 Acoustic amplitude map of the Intra2-Apsheron horizon interval showing radial negative amplitude anomaly to the south of the Chirag mud volcano system.

Figure API1 30 Acoustic amplitude map of the Intra2-Apsheron horizon interval showing radial negative amplitude anomaly to the south of the Chirag mud volcano system.

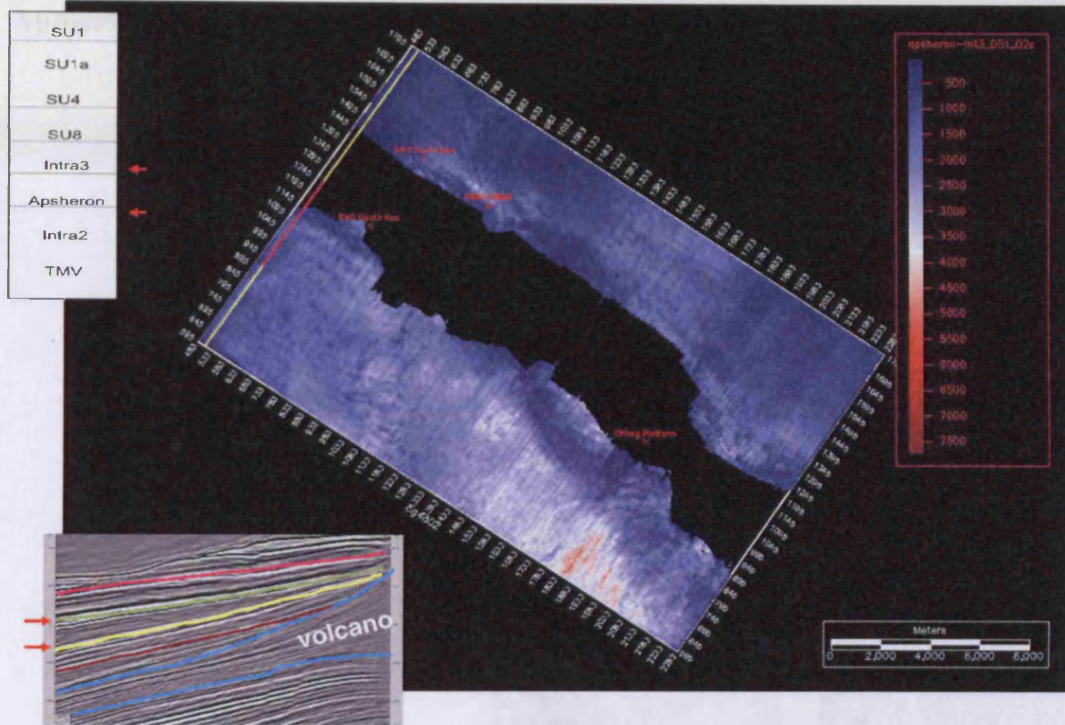


Figure API1 29 Acoustic amplitude map of the Apsheron-Intra3 horizon interval showing radial negative amplitude anomaly to the south of the Chirag mud volcano system. Note the presence of the anomaly immediately to the west of the volcano centre, a feature which rules out the possibility that the anomaly may be of a non-mud volcanic origin.

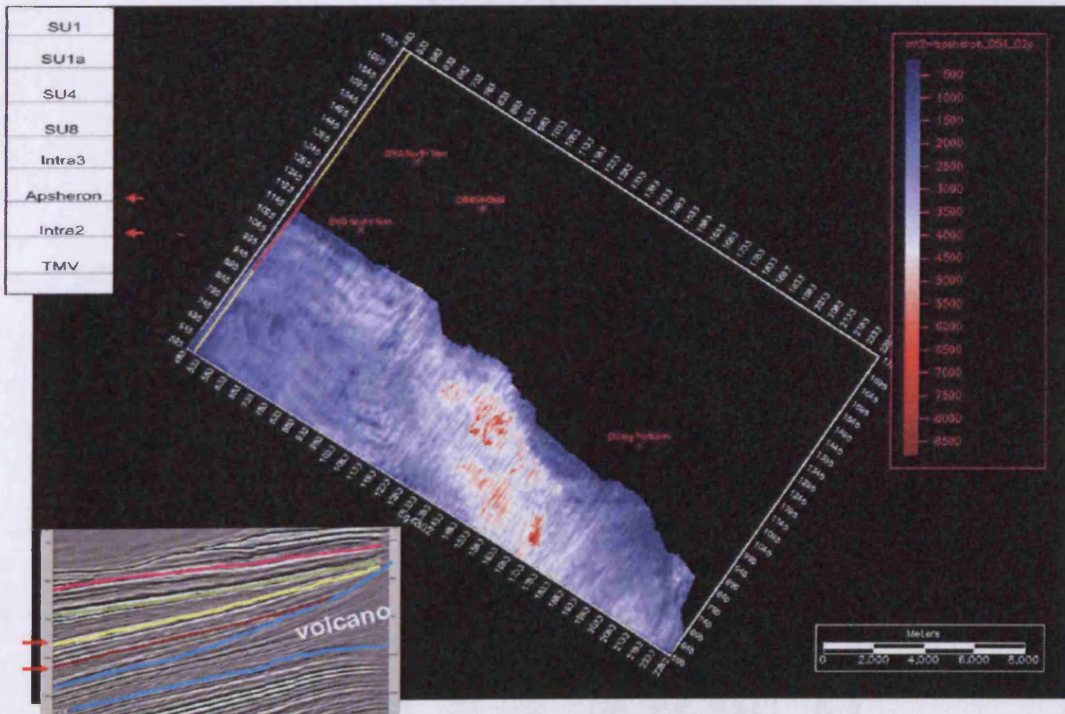


Figure API1 30 Acoustic amplitude map of the Intra2-Apsheron horizon interval showing radial negative amplitude anomaly to the south of the Chirag mud volcano system.

Appendix III: Supplementary Figures to support the conclusions of Chapter 4

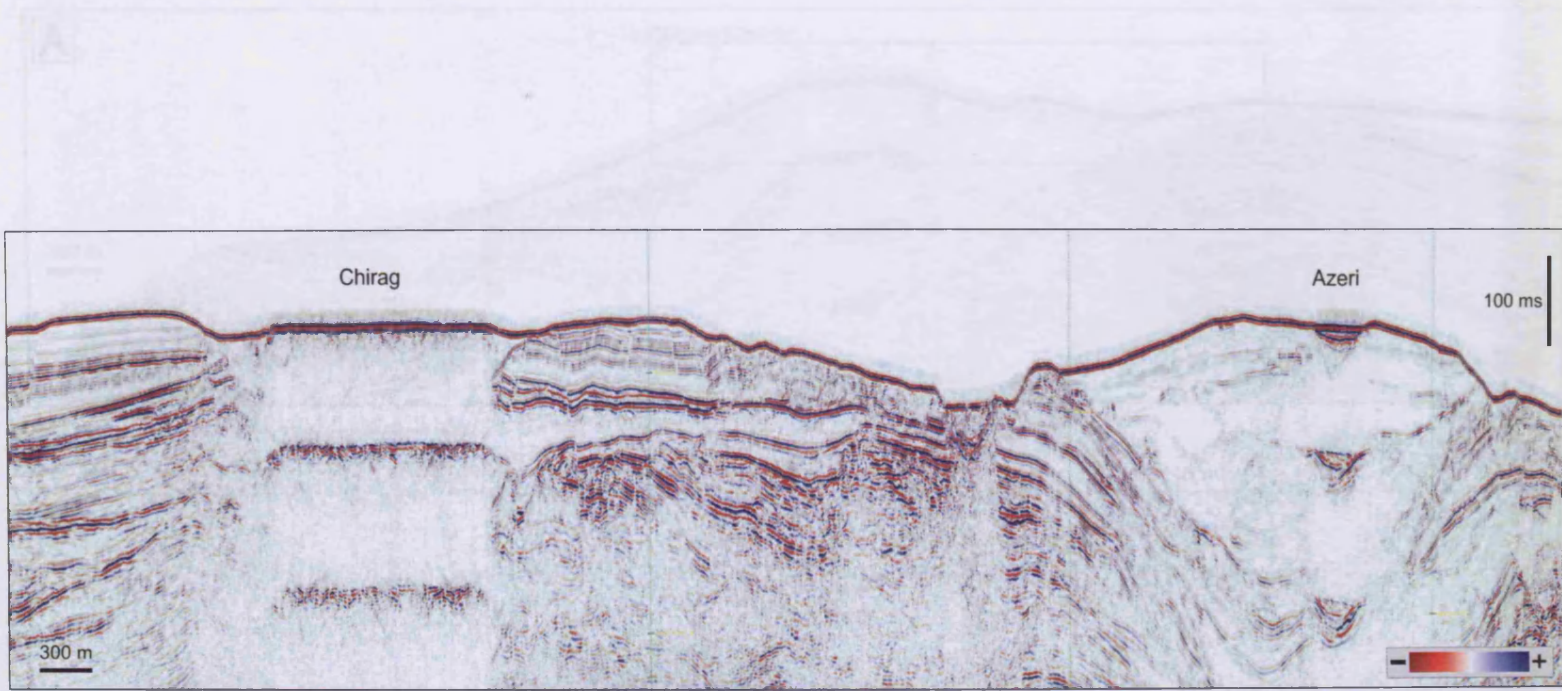


Figure APIII 1 “Hi-resolution” seismic profile through the Chirag and Azeri mud volcanoes showing the phase-reversed sections of seafloor investigated in Chapter 4. Note the ringing multiples beneath each phase-reversed area.

Figure APIII 2 (A) “Hi-resolution” seismic profile through the Azeri mud volcano showing the phase-reversed sections of seafloor investigated in Chapter 4. (B) Zoom in of the resolution analysis section showing the character of the phase-reversed sections of seafloor. The phase-reversed sections are more difficult to identify as their edges are not marked by sharp phase shifts as seen in conventional 1D data. The phase-reversed sections are marked by the red arrows.

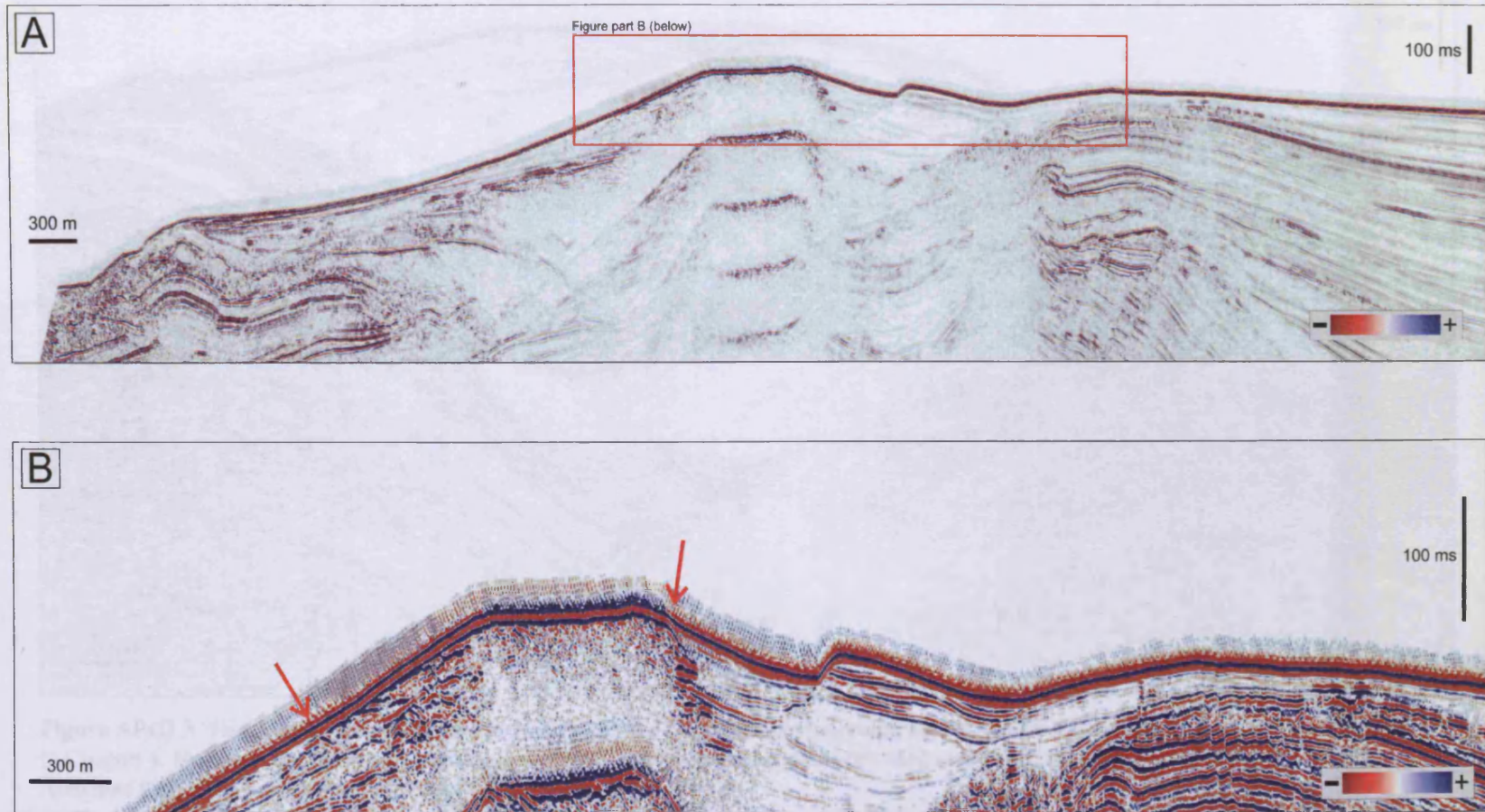


Figure APIII 2 (A) “Hi-resolution” seismic profile through the Azeri mud volcano showing the phase-reversed section of seafloor investigated in Chapter 3. (B) Zoom in of hi-resolution seismic section showing the character of the phase-reversed area of seafloor. It is noted that phase reversals in hi-resolution seismic data are more difficult to identify as their edges are not marked by abrupt phase shifts as seen in conventional 3D data. Limits of phase reversal are marked by the red arrows.

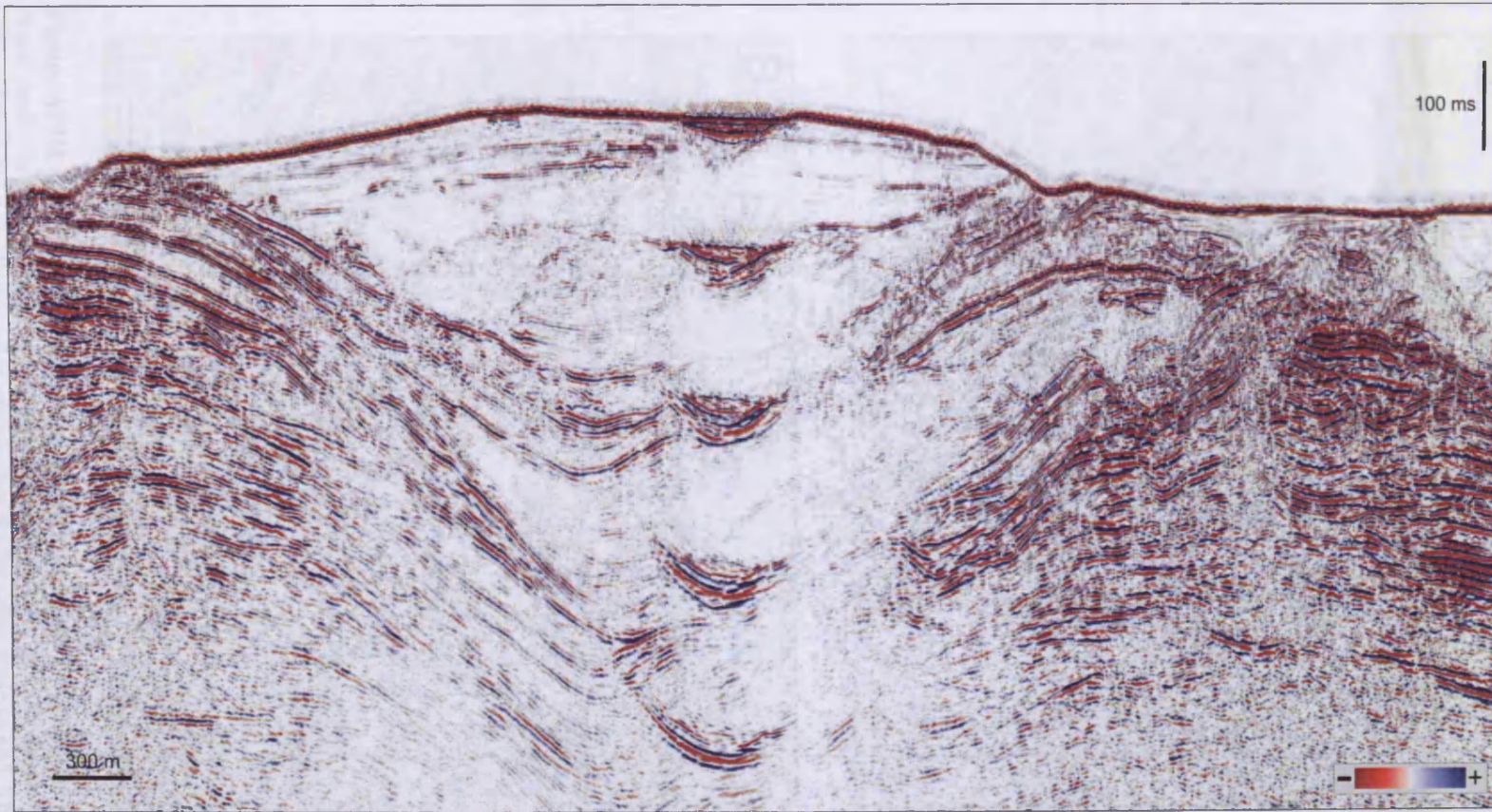


Figure APIII 3 “Hi-resolution” seismic profile through the Azeri mud volcano showing the phase-reversed section of seafloor investigated in Chapter 4. Note the convex-down positive polarity reflection beneath the phase-reversed area interpreted as the base of a seafloor salse. Also note the clear acoustic ringing multiples.

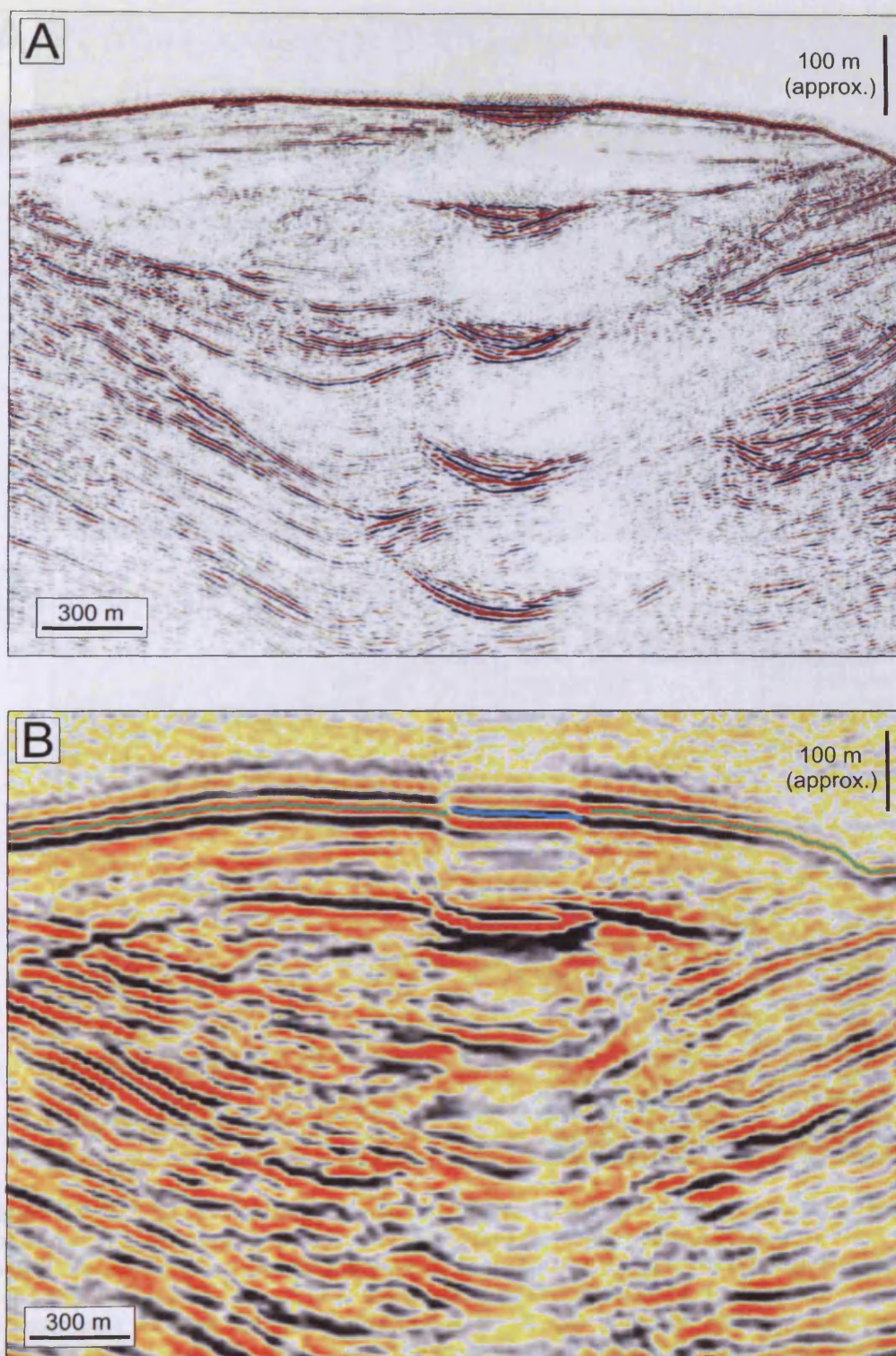


Figure APIII 4 2D-3D data comparison. (A) “Hi-resolution” 2D seismic profile through the Azeri mud volcano showing the phase-reversed area. (B) For comparison the same line on the conventional 3D data displayed at approximately the same scale as (A). The higher frequency of the 2D seismic data is clear as is the presence of the convex-down base-salse reflection which is not imaged in the 3D data.

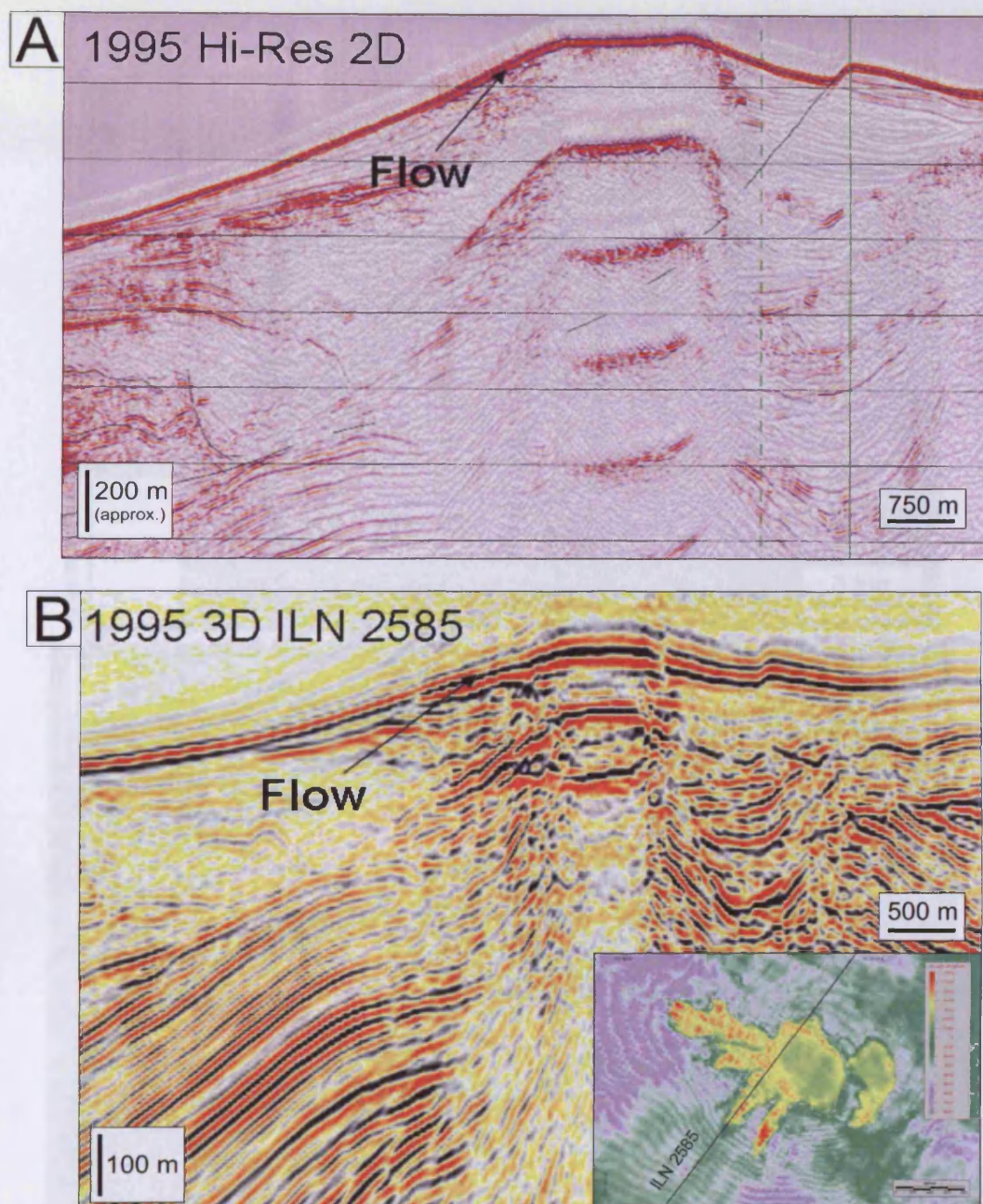


Figure APIII 5 2D-3D data comparison. (A) "Hi-resolution" 2D seismic profile through the Azeri mud volcano showing the phase-reversed area including a large mud flow. (B) For comparison the same line (inline 2585) on the conventional 3D data. The different character of the phase-reversed area is clear. It has clearer edges on the 3D data. The flow has approximately the same length in both sections. Depth scale in metres. This comparison was intended to test whether the phase-reversed was present in multiple surveys. It was also aimed at determining a minimum gas residence time in the seabed sediment. The fact that the flow is phase-reversed in both surveys indicates gas was present at the time of both survey's acquisition and was therefore retained in the seafloor sediment for a minimum of three months.

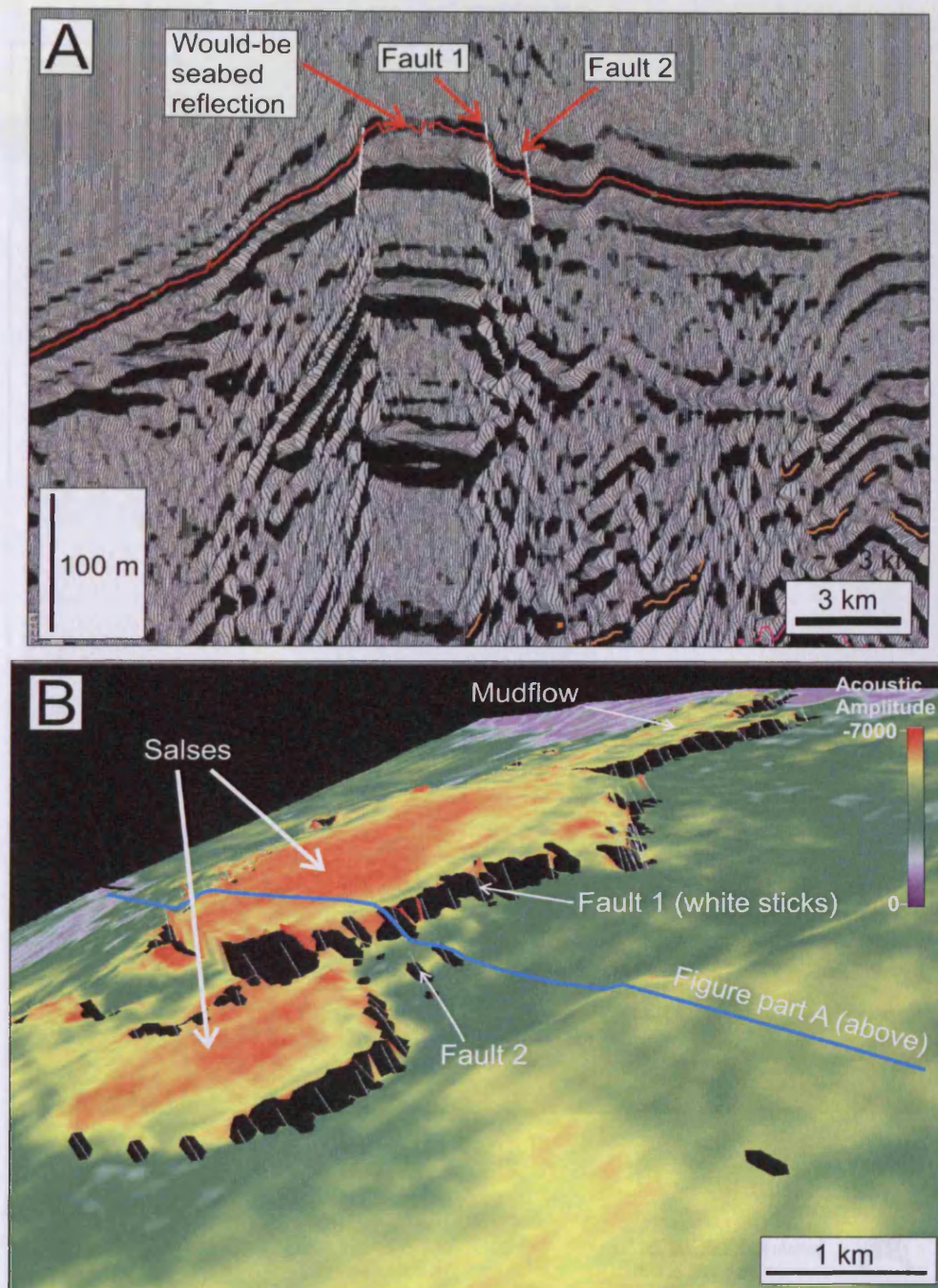


Figure APIII 6 Testing the phase-reversal interpretation: (A) 3D seismic section through the Azeri mud volcano showing the result of a fault-related interpretation created deliberately to test its validity. Faults were interpreted at the margins of the phase-reversal. (B) 3D bathymetric map of the Azeri seabed showing the results of the fault-related interpretation shown in (A). The most plausible interpretation was considered to involve outward dipping extensional faults meaning that the phase-reversed area was raised relative to the surrounding seabed. This does not appear geologically reasonable and does not fit with any non-seismic bathymetry data.

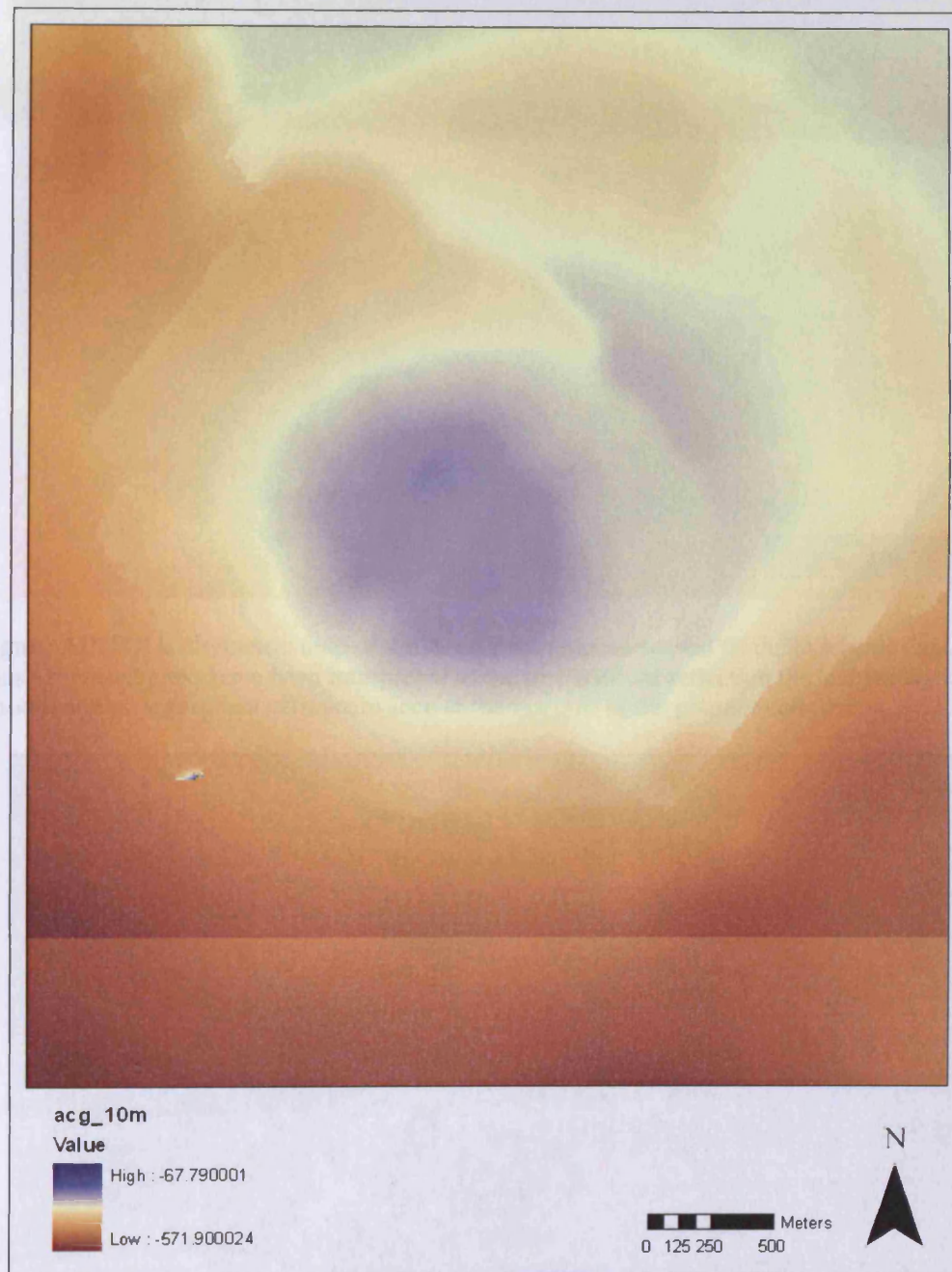


Figure APIII 7 Multibeam bathymetric map of the Azeri mud volcano seabed showing the geomorphology of the phase-reversed area at the conical edifice summit. Note the absence of any abrupt changes in seafloor elevation near the summit area that would indicate the presence of an extensional fault surrounding the phase-reversed area. The fact that this is a non-seismic map supports the interpretation of the seabed amplitude anomalies as true phase reversals and not related to faulting.

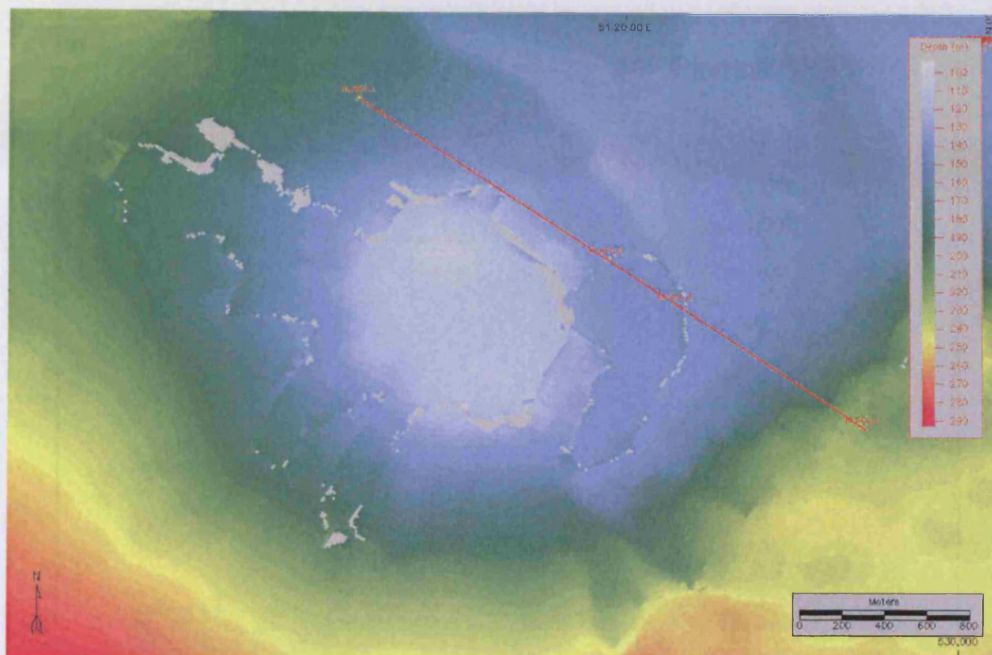


Figure APIII 8 Bathymetric map of the Azeri mud volcano seabed from 3D seismic data. As phase-reversed areas have been interpreted as the true seafloor reflection the bathymetry is smooth and no significant offsets are seen at the margins of the phase reversed area.

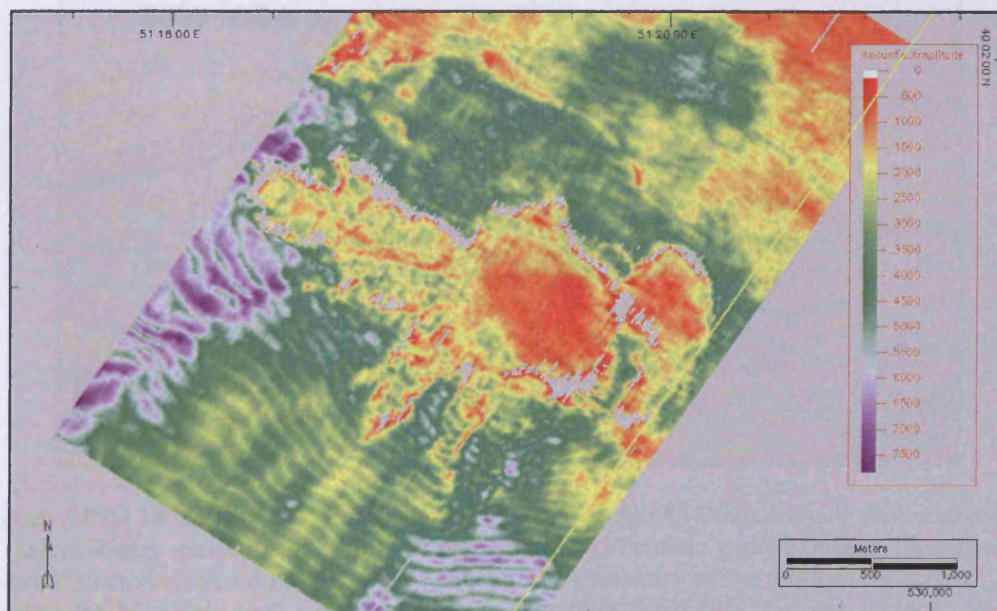


Figure APIII 9 Acoustic amplitude map of the Azeri mud volcano seabed. Seafloor reflection pick has been chosen according to the fault-related interpretation shown in Fig. APIII 5A. Therefore all areas of seafloor are positive polarity. The presence of the same amplitude anomaly in this reflection demonstrates that the leading loop of the true negative polarity reflection mimics the amplitude response of the underlying zero-phase peak.

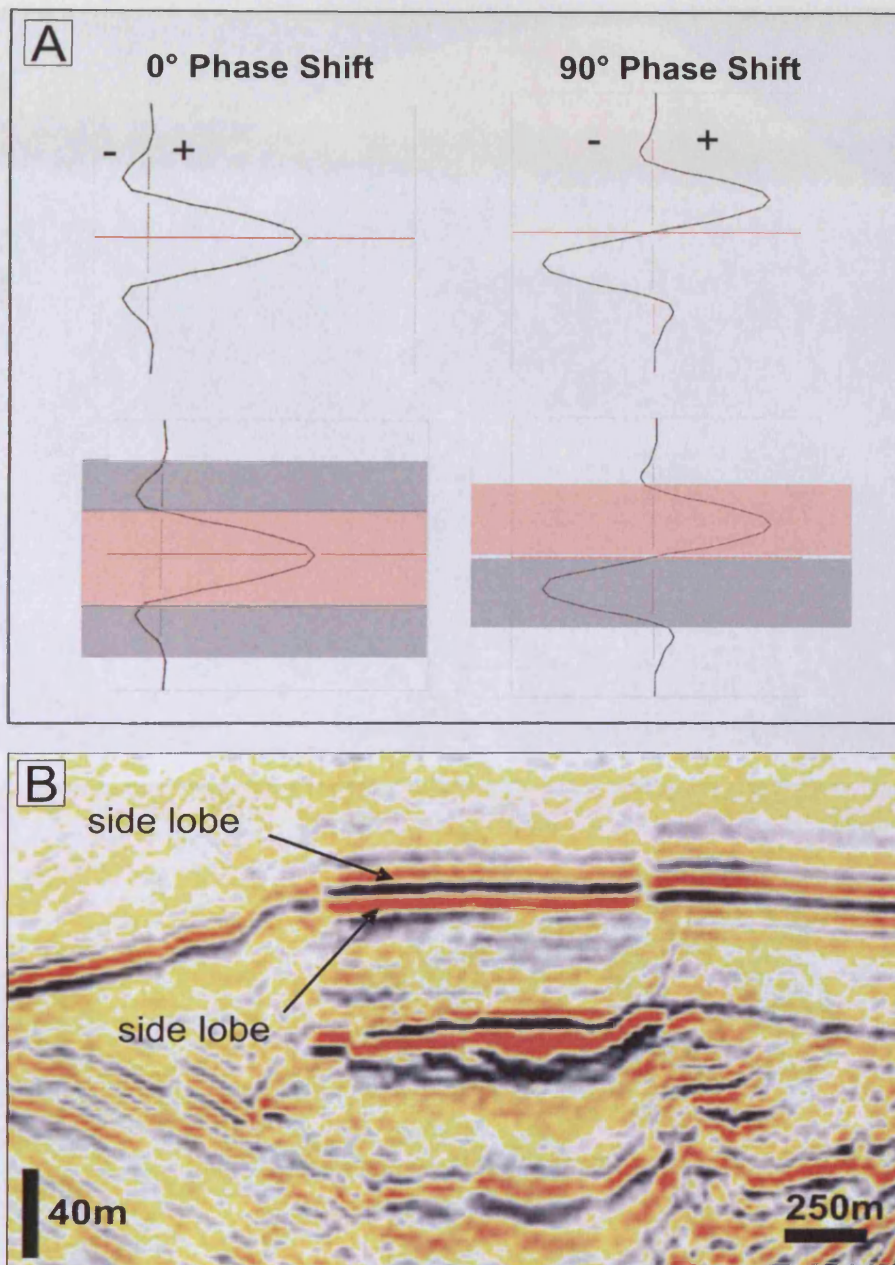


Figure APIII 10 Testing the phase reversal interpretation: (A) Diagrammatic representation of typical Ricker wavelets at 0° and 90° phase shift. (B) Seismic profile through the phase-reversed seabed area of the Azeri mud volcano. The symmetry of the seafloor reflection wavelet can be clearly seen with two clear red side lobes either side of a central black trough. This demonstrates that the seafloor reflection is near zero-phase and therefore the seafloor phase reversals cannot be accounted for by smaller degree phase shifts.

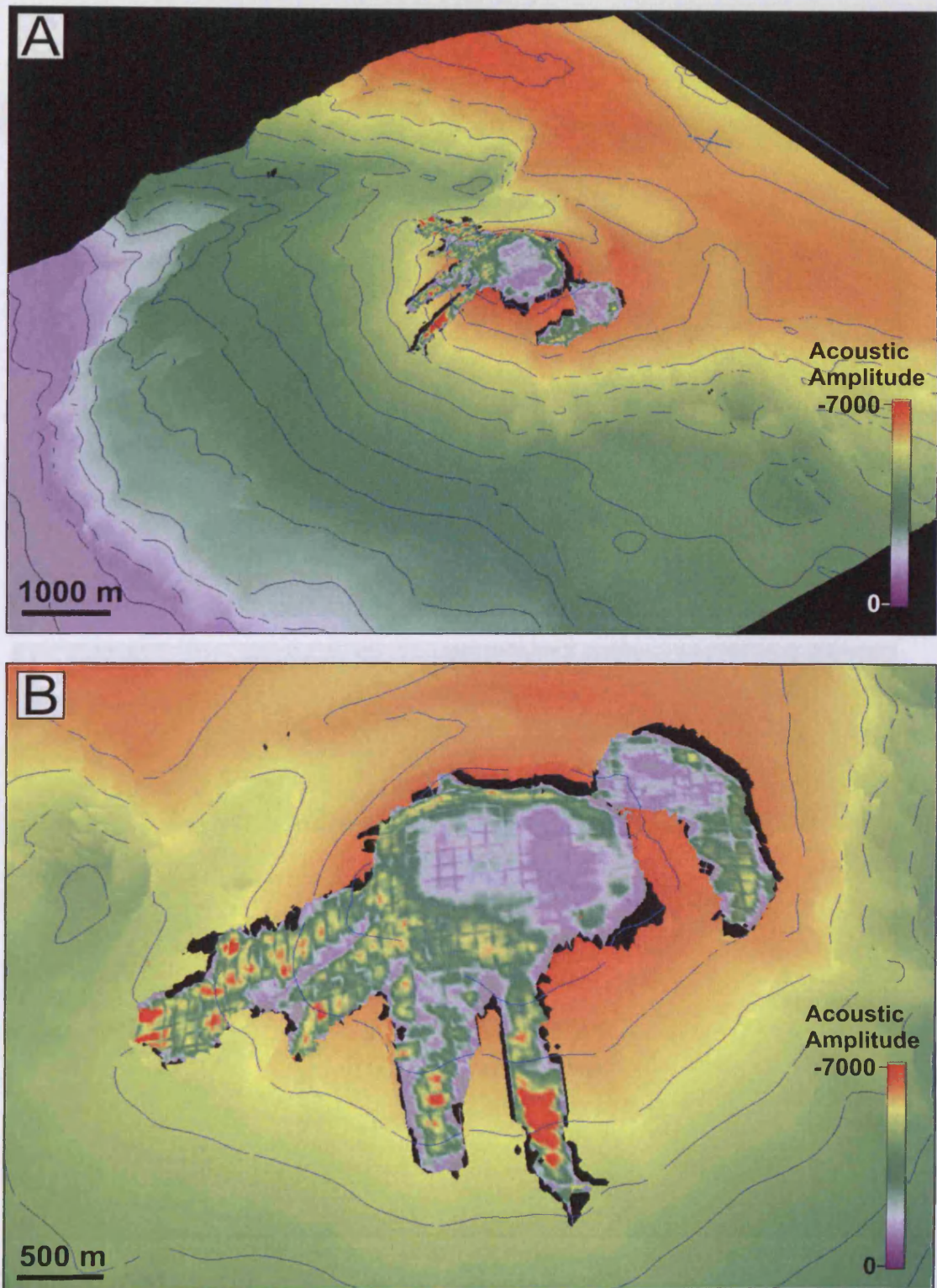


Figure APIII 11 (A-H) Various 3D bathymetric images showing the morphology and position of the phase-reversed seabed area at the Azeri mud volcano edifice. Note the flat nature of the seafloor salses, particularly the largest. Phase-reversed area coloured according to acoustic amplitude. Figure part E shows the map intersected with a seismic profile. The flatness of the seafloor is clear. Phase reversal edges are marked by the red arrows.

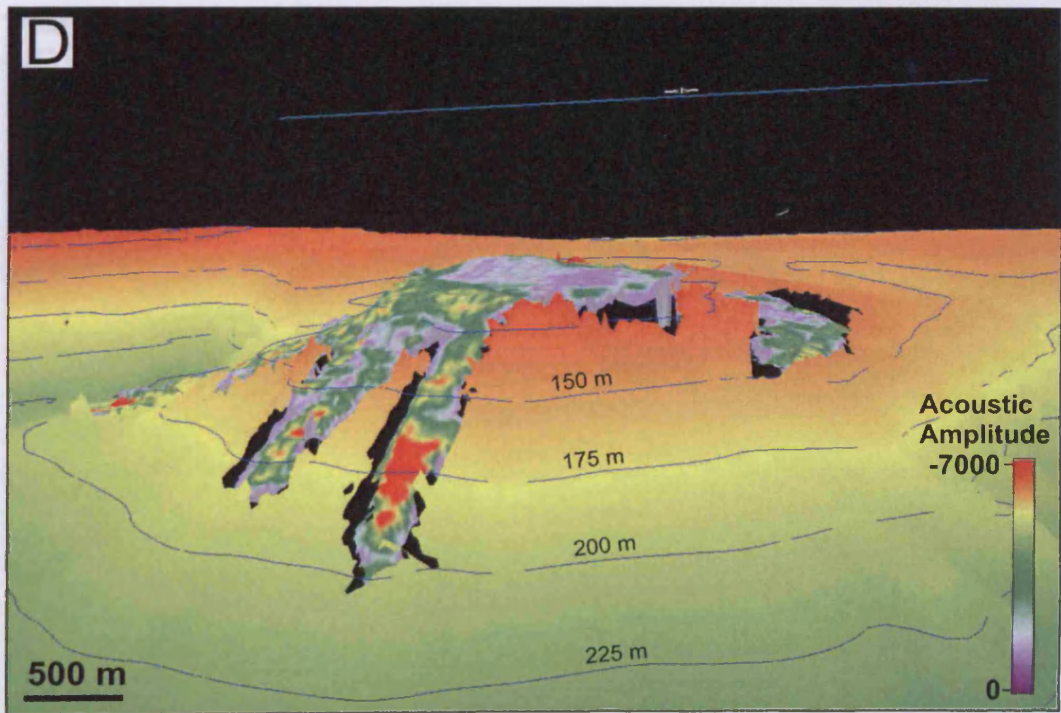
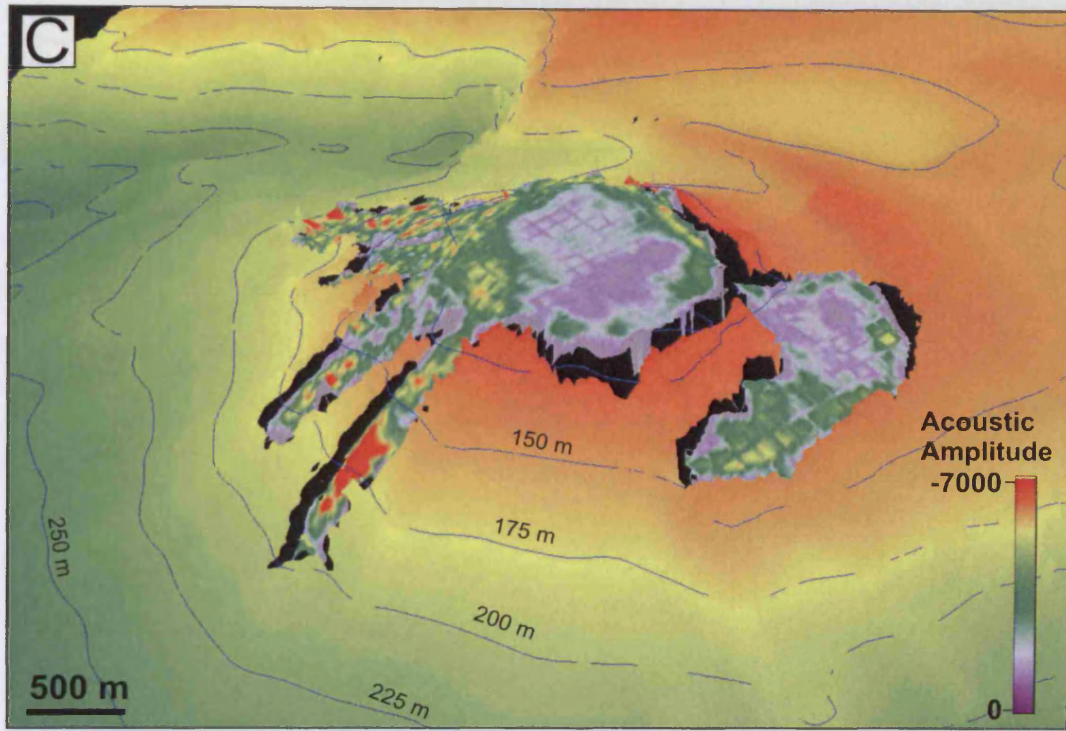


Figure APIII 11 (cont'd)

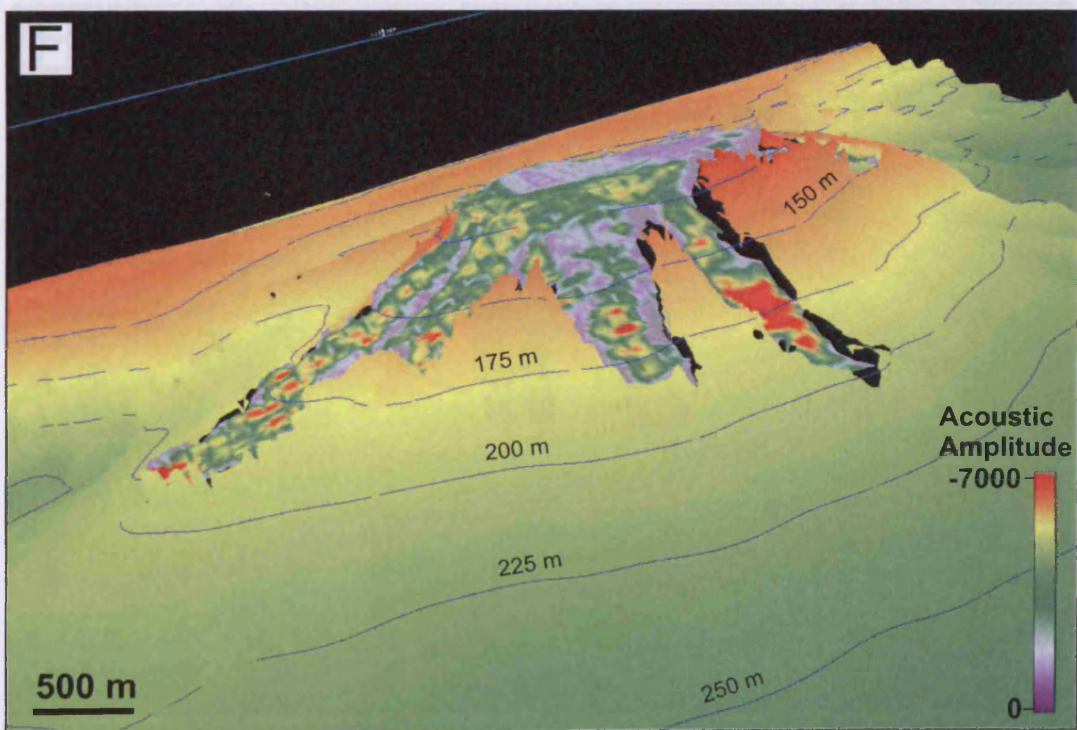
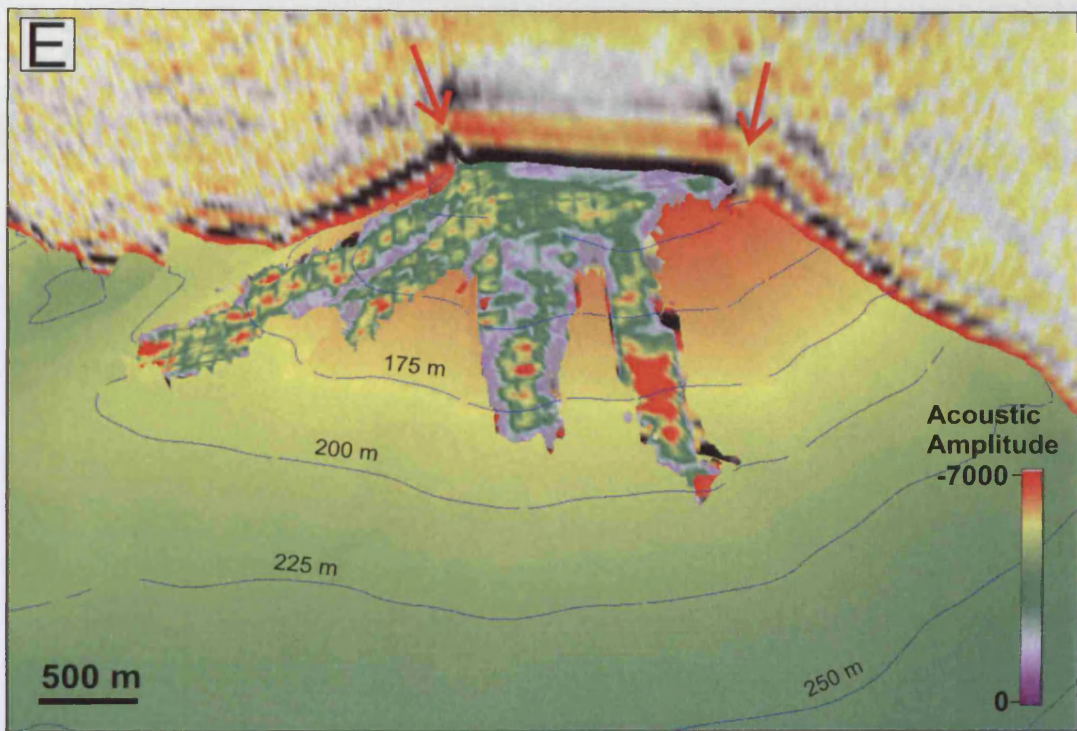


Figure APIII 11 (cont'd)

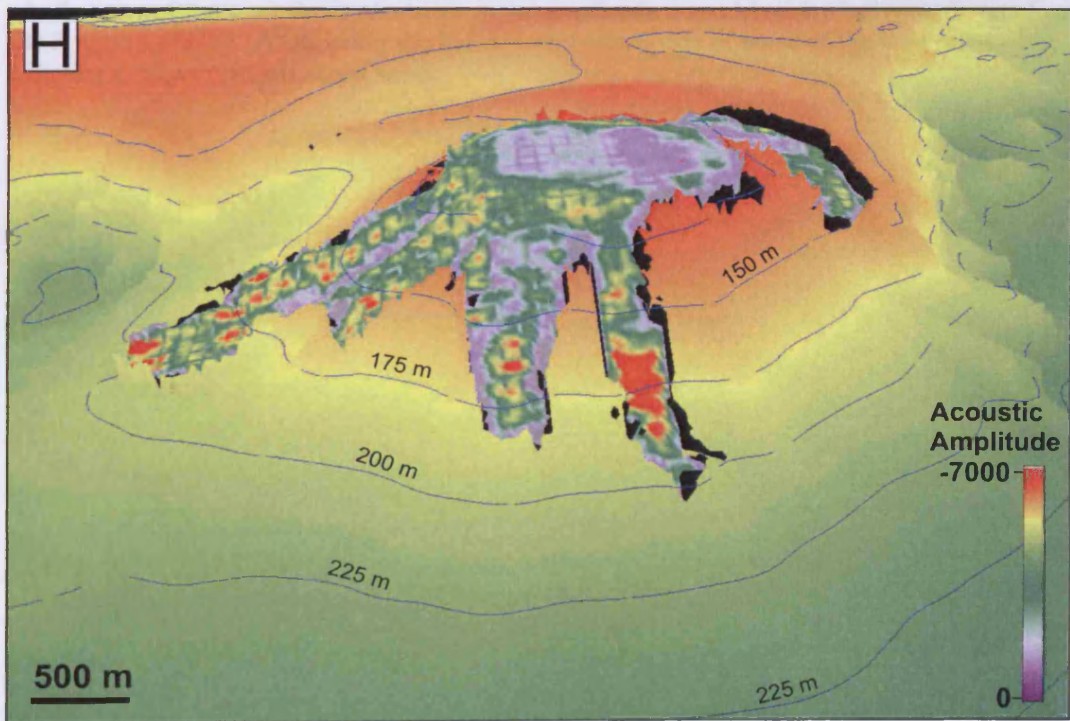
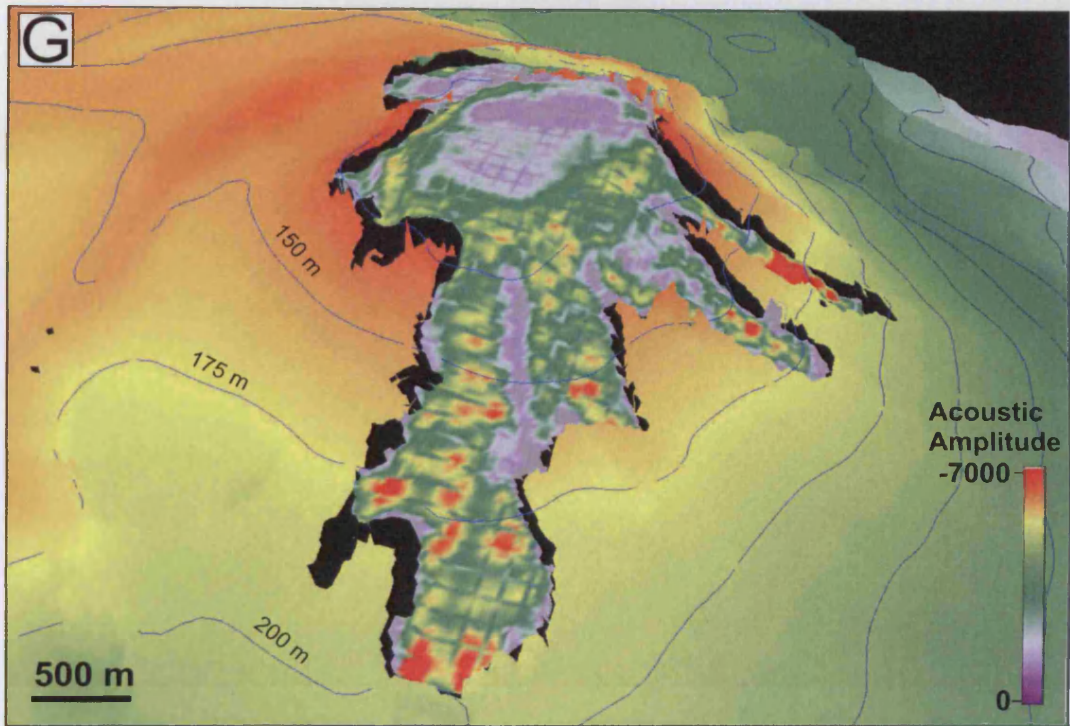


Figure APIII 11 (cont'd)

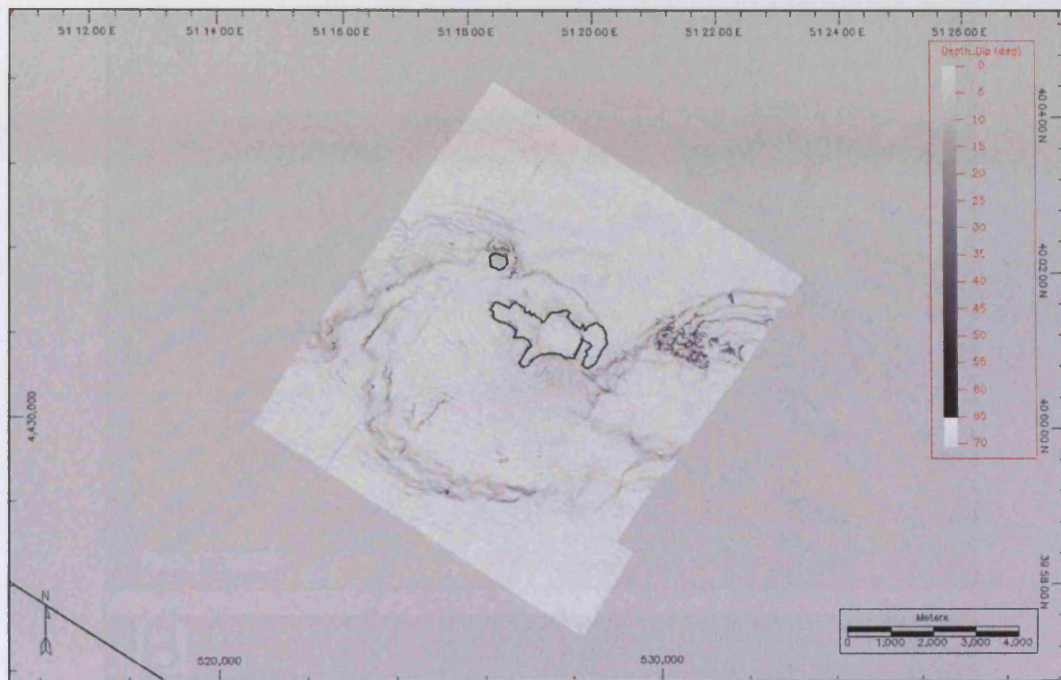


Figure APIII 12 (A) Seafloor dip map of the Azeri mud volcano seabed made to assess whether any of the mud flows identified in the amplitude maps have any bathymetric relief. (B) Zoom in of map (A) showing the bathymetric expression of some of the mud flows radiating from the largest Azeri salt.

Figure APIII 13 (A) 3D seismic profile through the Chirig anticline showing reverse faults in cross-section. (B) The same section as (A) displayed in vertical time (single trace). Profile was created to examine the detailed character of the faulted zone, structural and structural, the two faults, distance from which they have reversed.

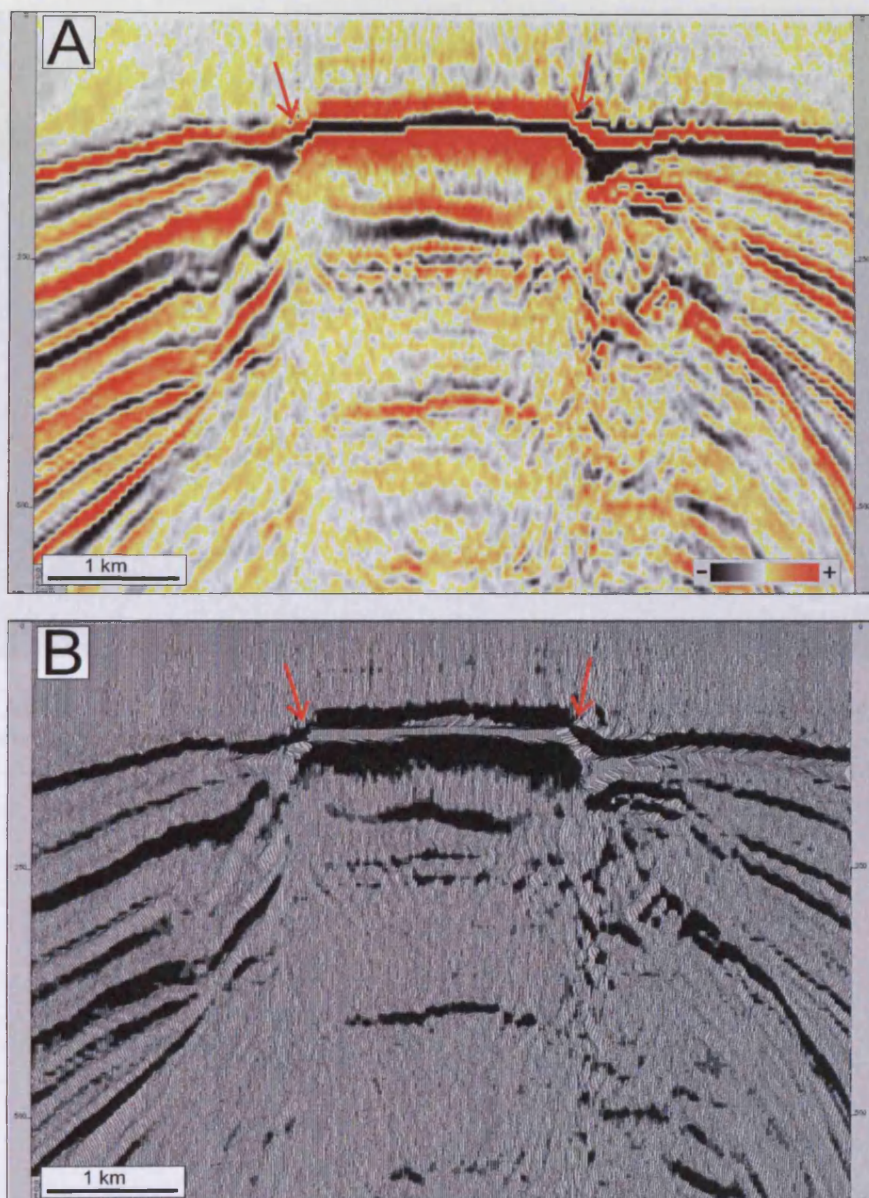


Figure APIII 13 (A) 3D seismic profile through the Chirag seafloor phase reversal taken to examine its character in the 3D seismic data. (B) The same section as (A) displayed in variable area (wiggle trace). Profile was created to examine the detailed character of the seabed phase reversal and determine the horizontal distance over which total phase reversal occurs.

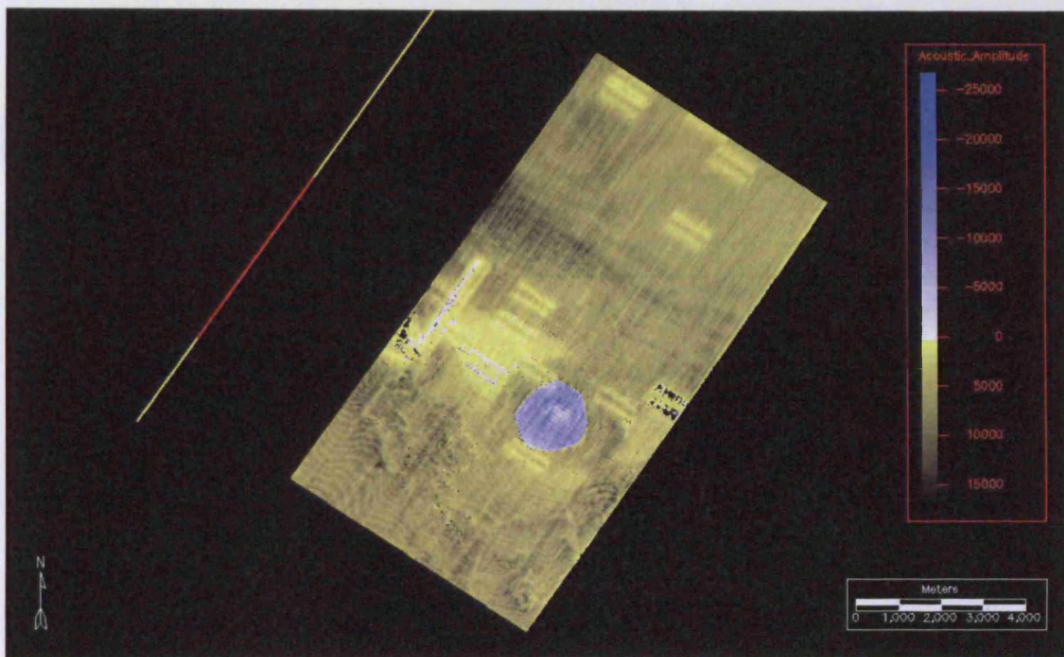


Figure APIII 14 Acoustic amplitude map of the Chirag mud volcano seabed showing circular phase-reversed area. Blue colours indicate negative polarity reflection.

Acoustic Impedance and Reflection Coefficient Calculator			
	Density (g/m ³)	Velocity (m/s)	
Layer 1	1028	1453	Seawater
Layer 2	1480	1459	Seabed Silt
Z Layer 1	1493684		
Z Layer 2	2159320		
RC (1-2)	0.18		

Acoustic Impedance and Reflection Coefficient Calculator			
	Density (g/m ³)	Velocity (m/s)	
Layer 1	1028	1453	Seawater
Layer 2	1200	984	Gassy seabed Silt
Z Layer 1	1493684		
Z Layer 2	1180800		
RC (1-2)	-0.12		

Table APIII 1 Acoustic impedance and reflection coefficient calculators made to compute the reflection coefficient values for various combinations of seabed sediment density and seismic velocity measurements. (A) Sediment properties for normal non-gassy seabed conditions. (B) Sediment properties for gassy seabed conditions. The equation used to calculate the reflection coefficient (RC) is shown below.

$$RC = \frac{(AI_2 - AI_1)}{(AI_2 + AI_1)}$$

Where AI_1 = acoustic impedance of layer 1, AI_2 = acoustic impedance of layer 2.

Figure APIII 15 (A & B): Field photographs from the surface of a sand flow at the Condeep well volcano in Azerbaijan. (A) Under water photos with the surface of the flow appearing 1-2 m in diameter are interpreted as vesicle-like gas expansion sources that suggest the flow is the gas bearing when entrained and deposited.

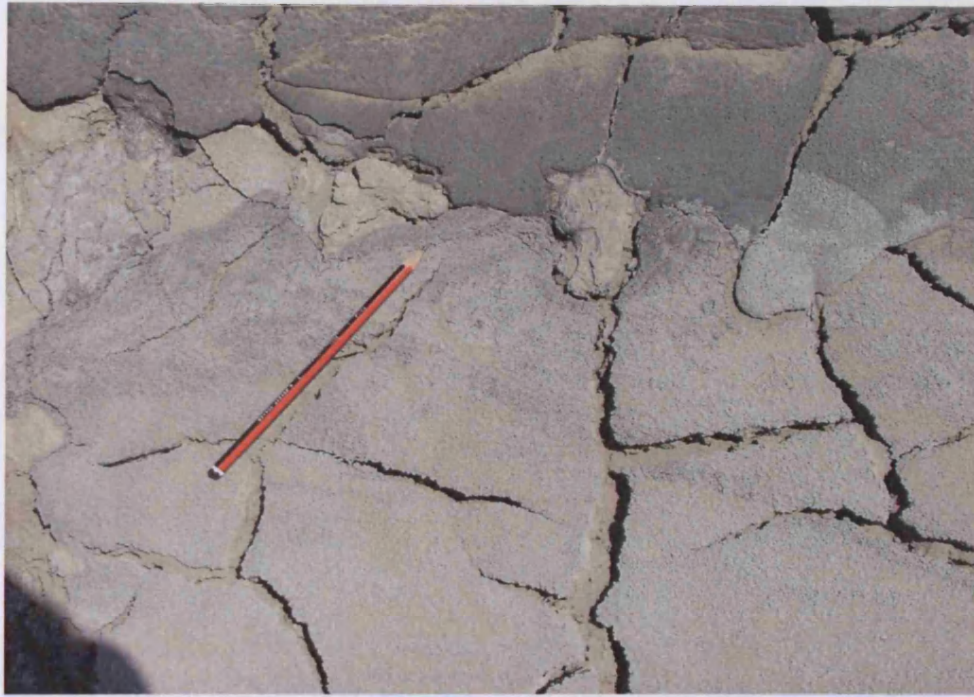


Figure APIII 15 (A & B): Field photographs from the surface of a mud flow at the Doruvdag mud volcano in Azerbaijan. Circular voids present within the surface of the flow measuring 1-3 mm in diameter are interpreted as vesicle-like gas expulsion features that suggest the flow to be gas bearing when extruded and deposited.



Figure APIII 16 Field photograph of a salse at the Dashgil mud volcano near Gobustan in Azerbaijan. A number of salses were examined to assess their similarity to the Azeri seafloor salses imaged by the seabed data.



Figure APIII 17 Bursting mud bubble within a gryphon in a mud volcano near Lokbatan in Azerbaijan. Most gryphons in Azerbaijan display some evidence for gas expulsion including bubbling and hissing.



Figure APIII 18 Additional field photographs showing the salse pictured in Figure 4.5b of Chapter 4.

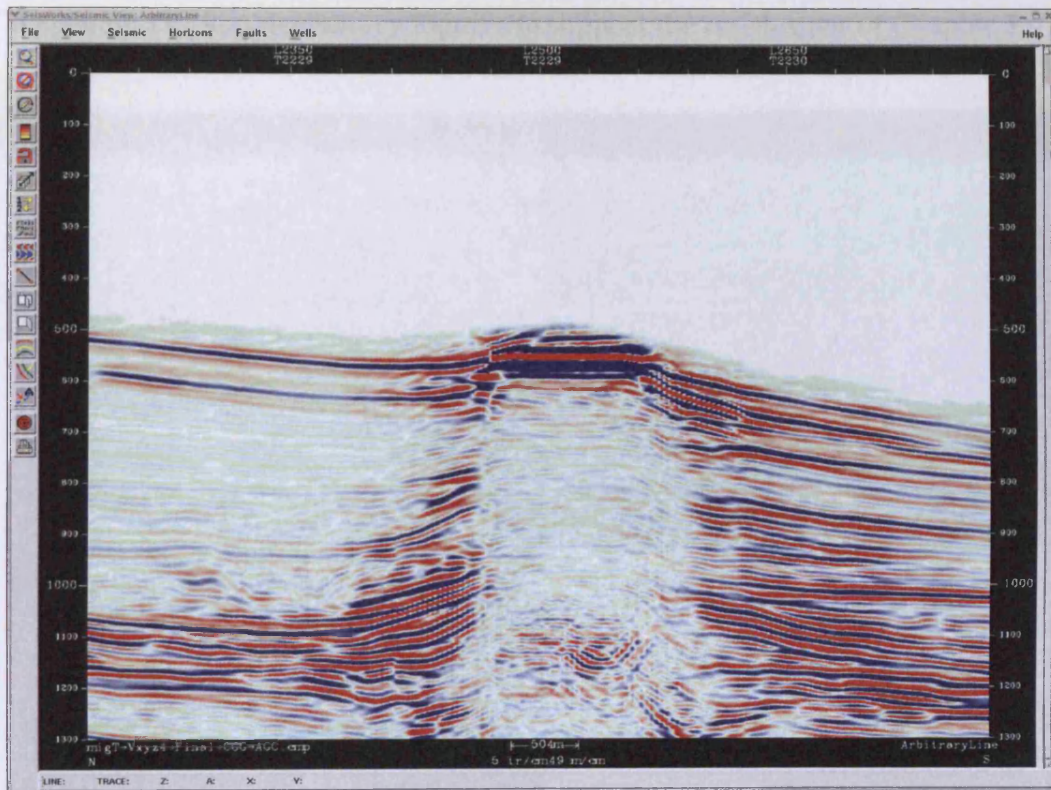


Figure APIII 19 3D seismic profile through a mud volcano from with the Shaz Deniz area of the South Caspian Sea. A clear phase reversal can be seen at the upper termination of a central blanked area. Phase-reversed area appears to be raised in a similar way to Chirag. This example was not investigated in detail and was not included in Chapter 4. It demonstrates that mud volcano-related seabed phase reversals are not unique features found only in the Chapter 4 study area. Other examples are known to exist in the Nile Delta offshore Egypt.

Appendix IV: Supplementary Figures to support the conclusions of Chapter 5



Figure APIV 1 Topographic map showing the locations of the Gora Kagniza-Dag (GKD) and Qaraqus Dagi (QD) mud volcanoes mapped in Chapter 5. Each grid square measures 1 x 1 km. This map was used to determine the height of the two onshore examples in Chapter 5.

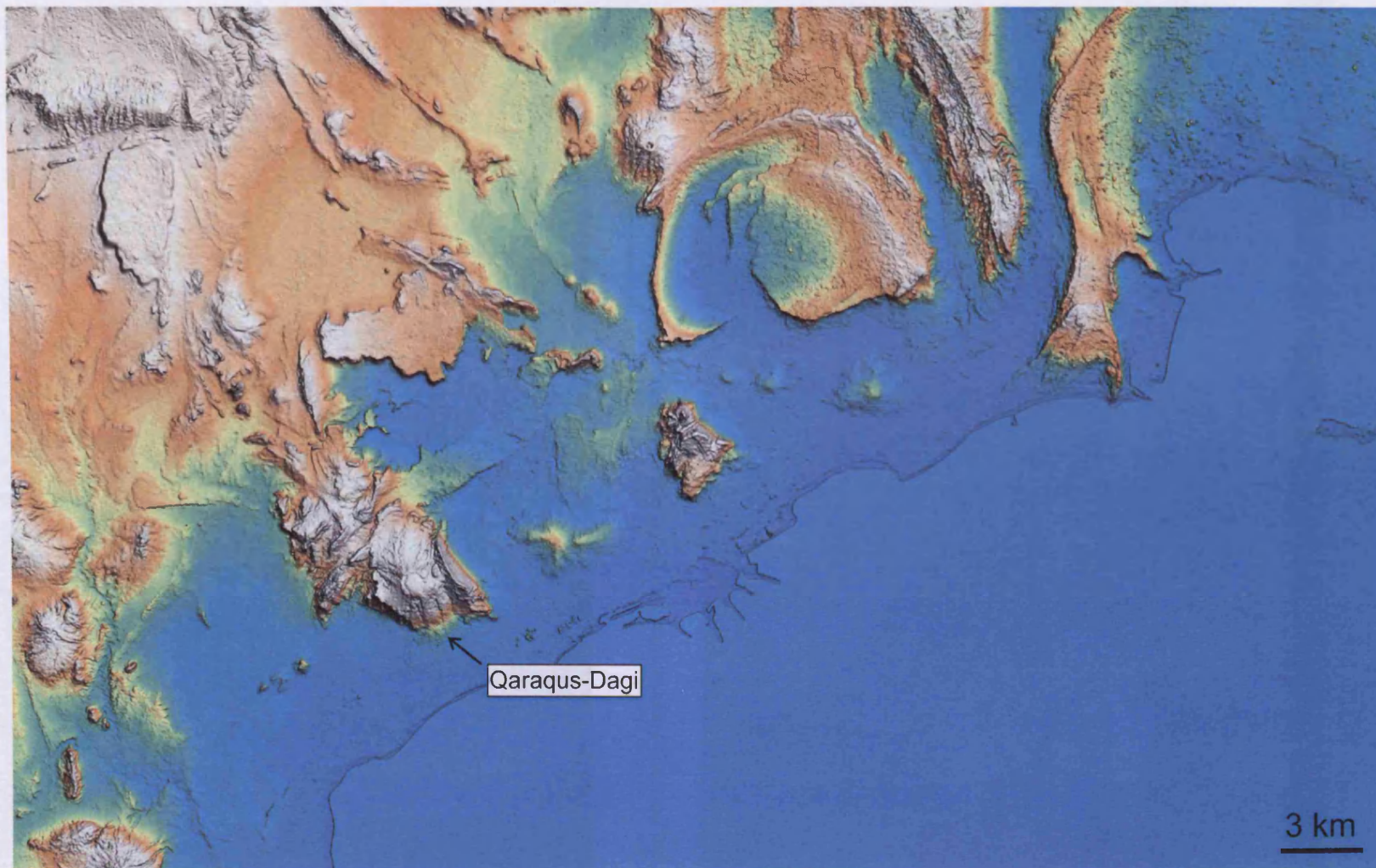


Figure APIV 2 Regional-scale digital elevation model of eastern Azerbaijan showing the QD mud volcano edifice. The “moat and pedestal” crater structure can be seen at the edifice summit.

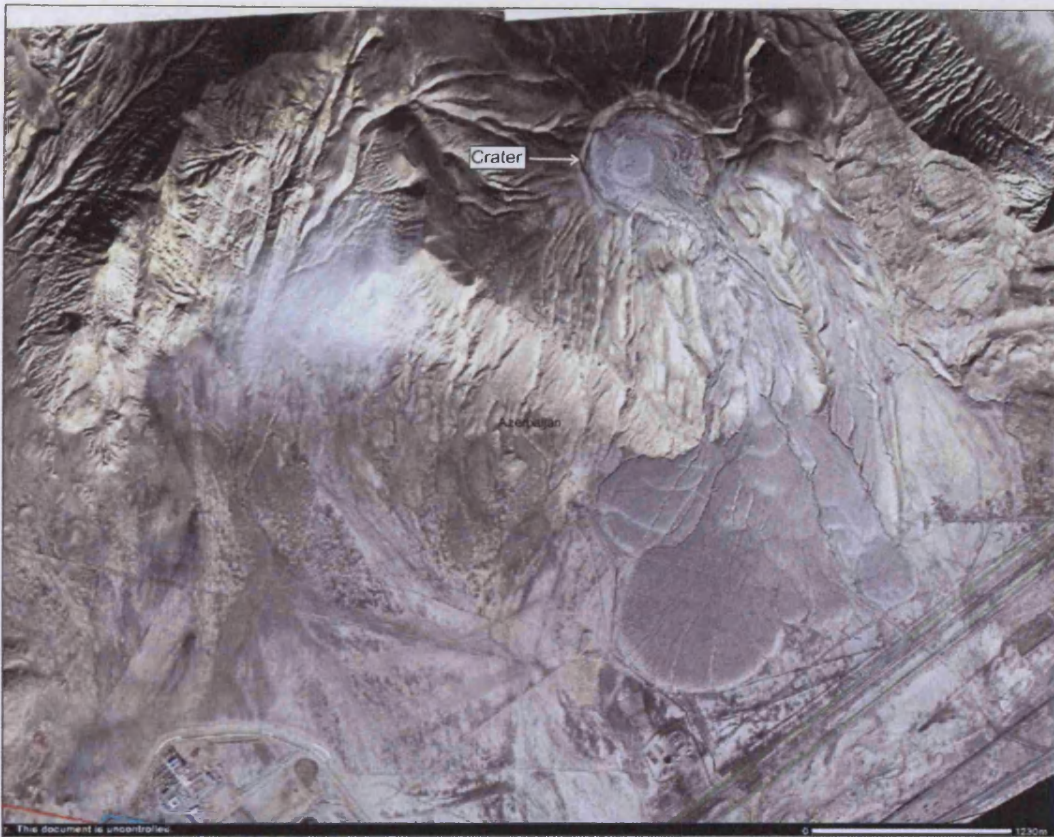


Figure APIV 3 IKONOS satellite image of the Qaraqus-Dagi mud volcano showing the summit crater and large mud flows.

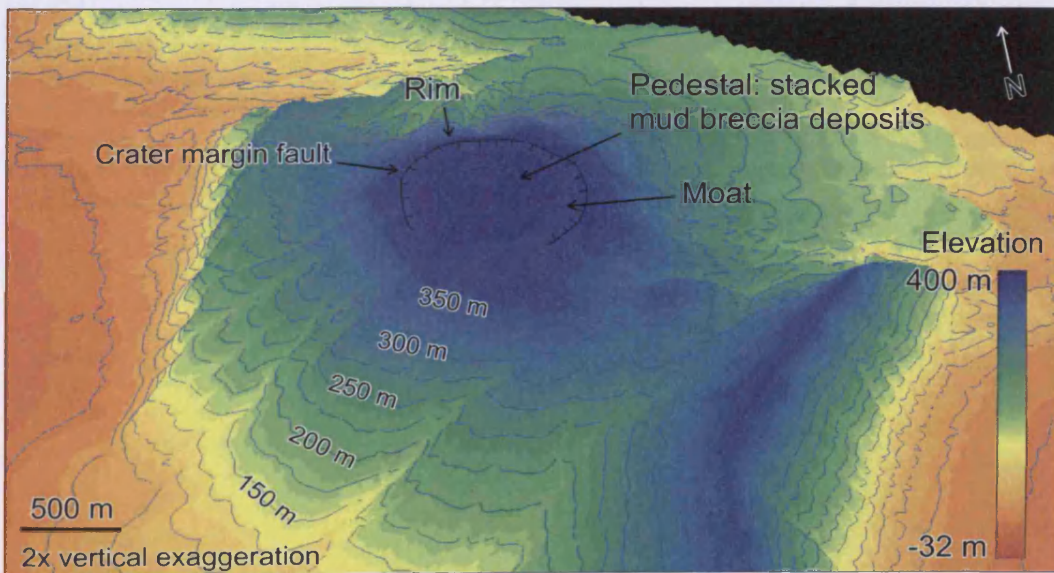


Figure APIV 4 Digital elevation model of the Qaraqus-Dagi mud volcano showing the structure of the edifice, bounding ridges and summit crater.

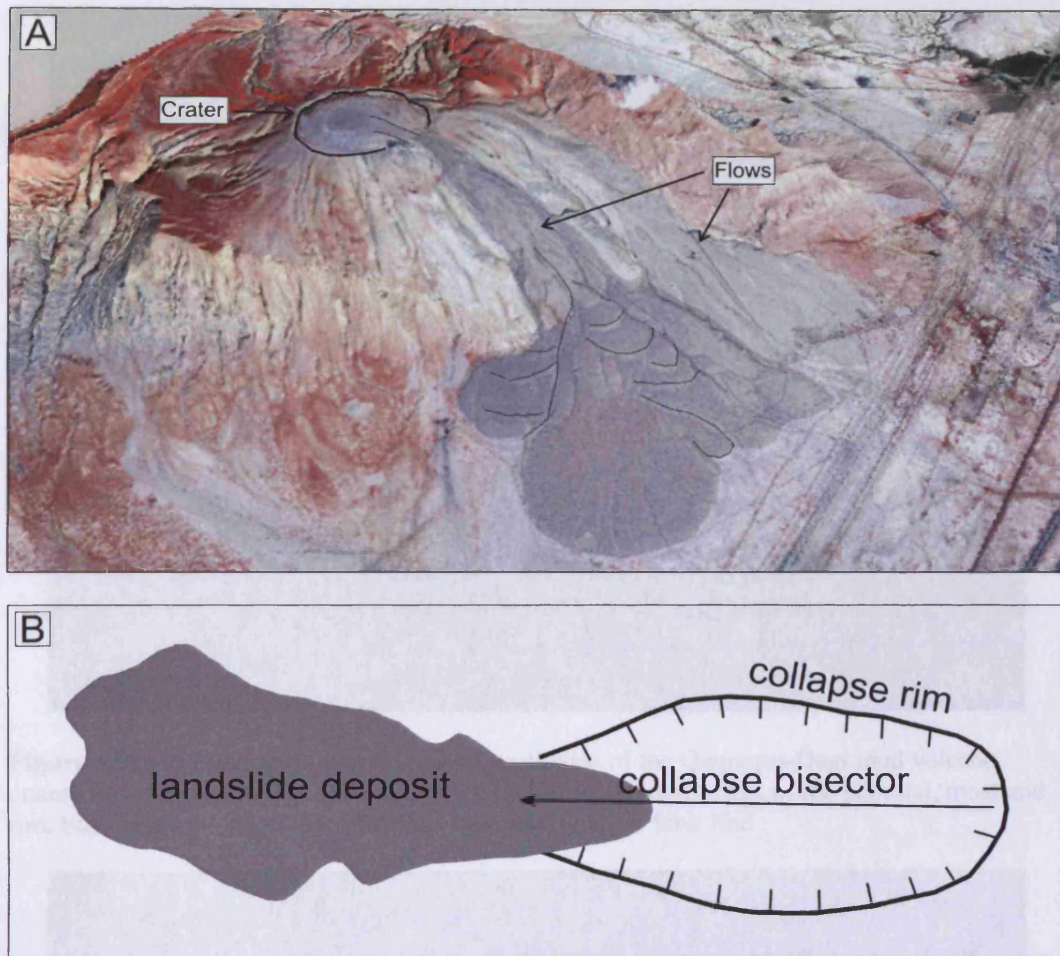


Figure APIV 5 (a) IKONOS satellite image of the Qaraqus-Dagi (QD) mud volcano edifice. Summit crater and large flows are highlighted. (b) For a comparison a simplified geological map of an elongate sector collapse from the Stromboli volcano edifice. The structure of the collapse sector is more elongate and less circular than the crater seen at QD which suggests that simple sector collapse is unlikely to account for the crater structure. Modified from Tibaldi (2001).

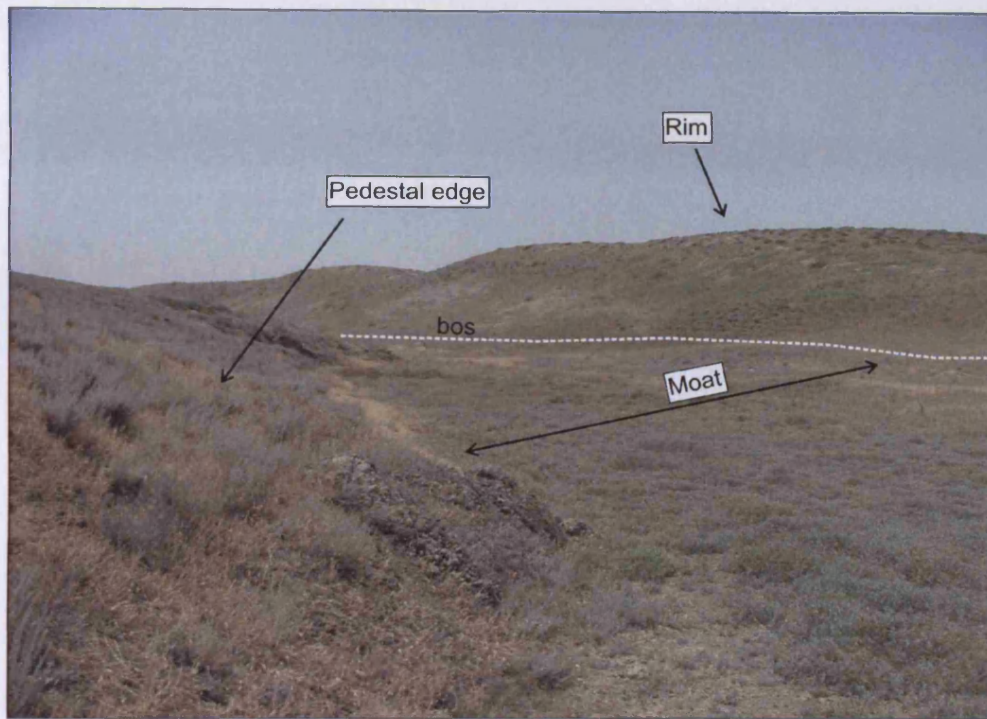


Figure APIV 6 Field photograph looking southwest of the Qaqraqus-Dagi mud volcano crater showing structure of the crater edge including the outer edge of the pedestal, moat and rim. bos= break of slope interpreted as the crater margin fault line.

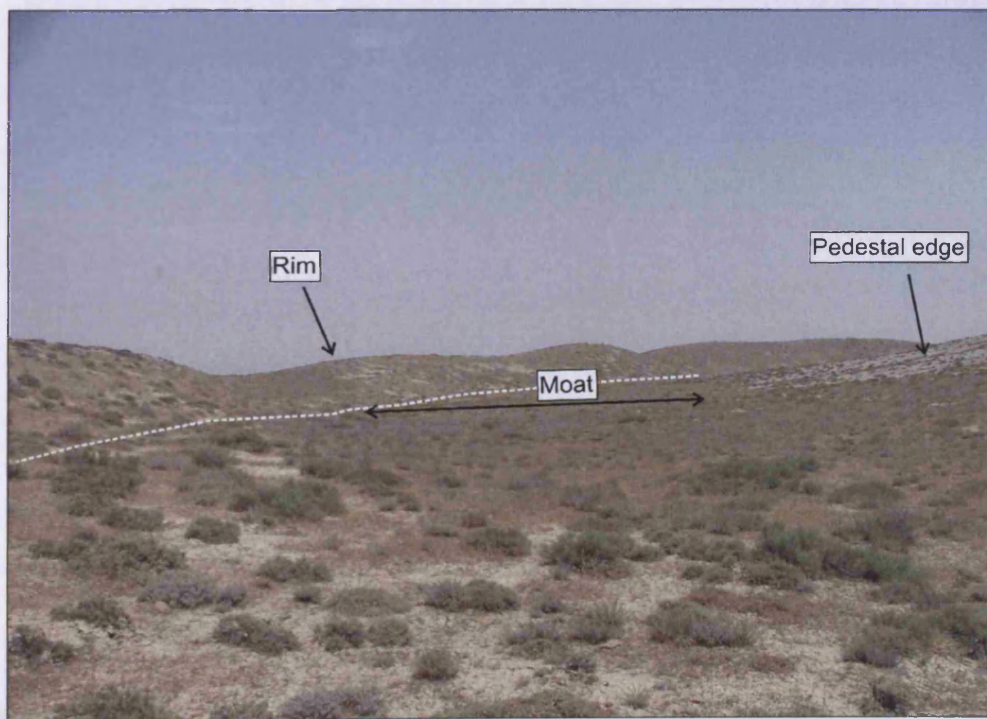


Figure APIV 7 As Fig APIV 6 above looking northeast.

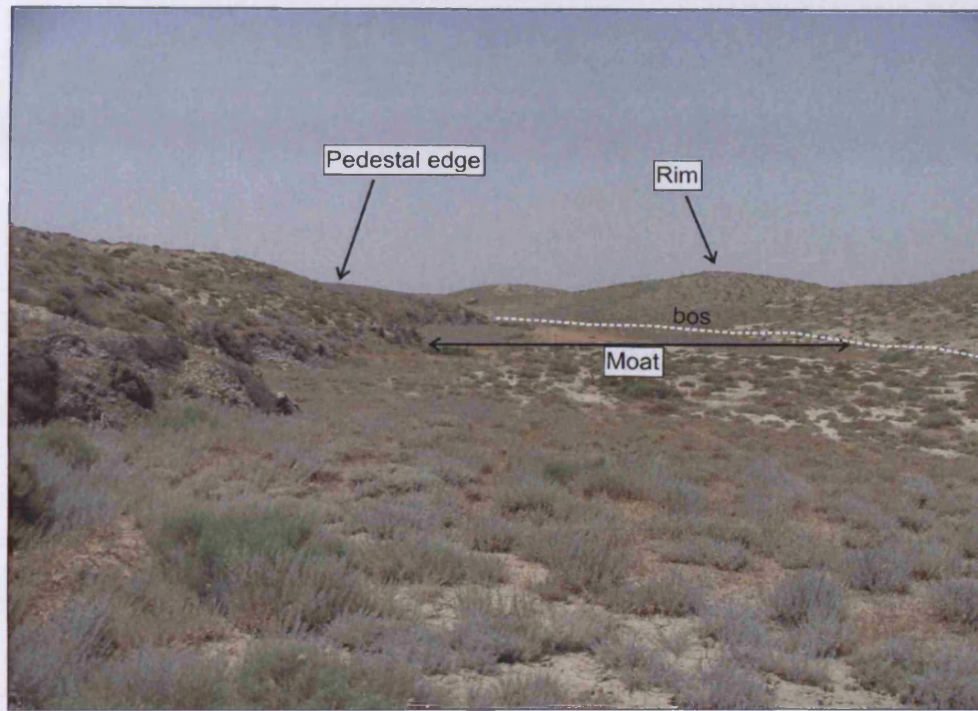


Figure APIV 8 As Fig. APIV 6 above looking west.

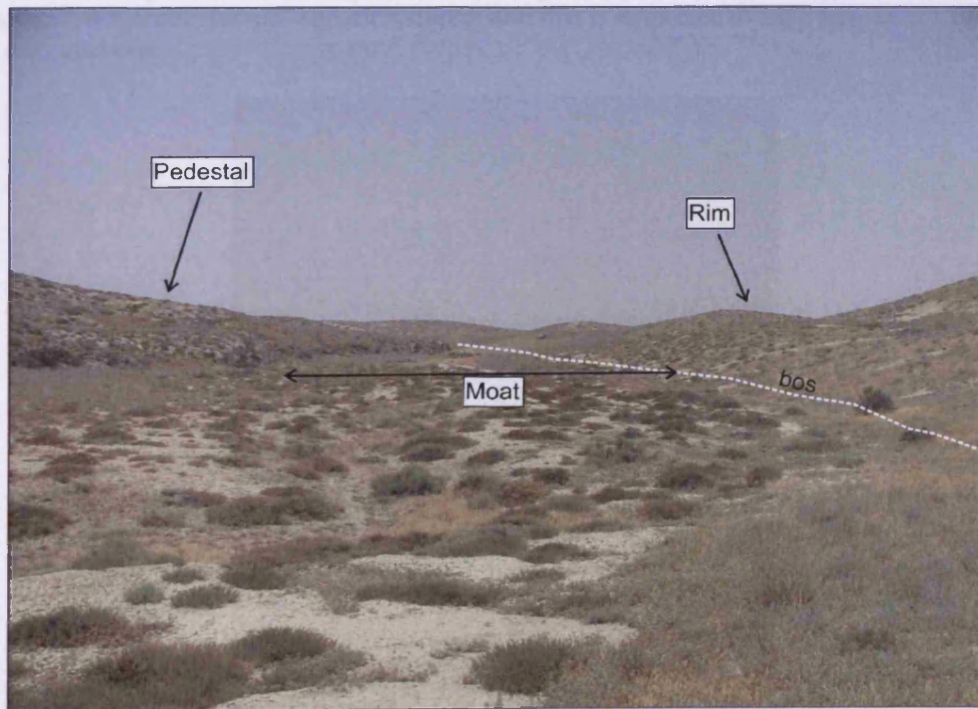


Figure APIV 9 As Fig. APIV 6 above looking south.



Figure APIV 11 Field photograph of the QD crater pedestal mud breccia. The texture of the sediment is rough and it is not vegetated indicating its recent deposition. At the centre of the photograph is a circular half-spherical depression that is suspected to have formed as a result of gas expulsion.

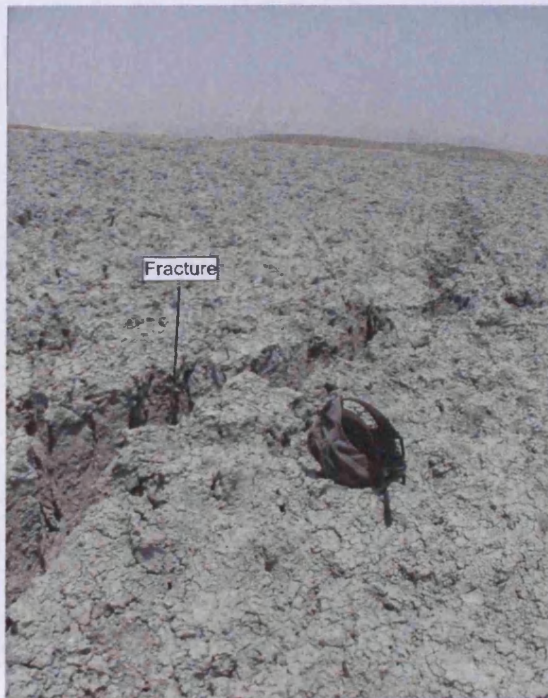


Figure APIV 12 Field photograph of the QD crater pedestal showing the subcircular dilational fracture located at the centre of the pedestal. Rucksack for scale. Looking north.

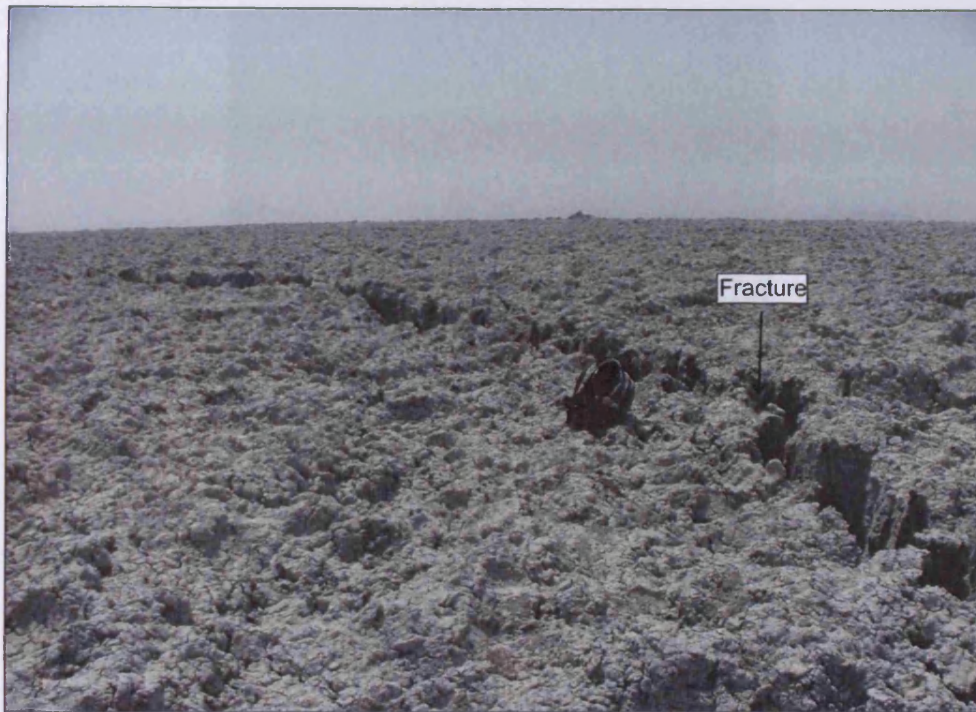


Figure APIV 13 Field photograph of the QD crater pedestal showing the subcircular dilational fracture located at the centre of the pedestal. Rucksack for scale. Looking south.

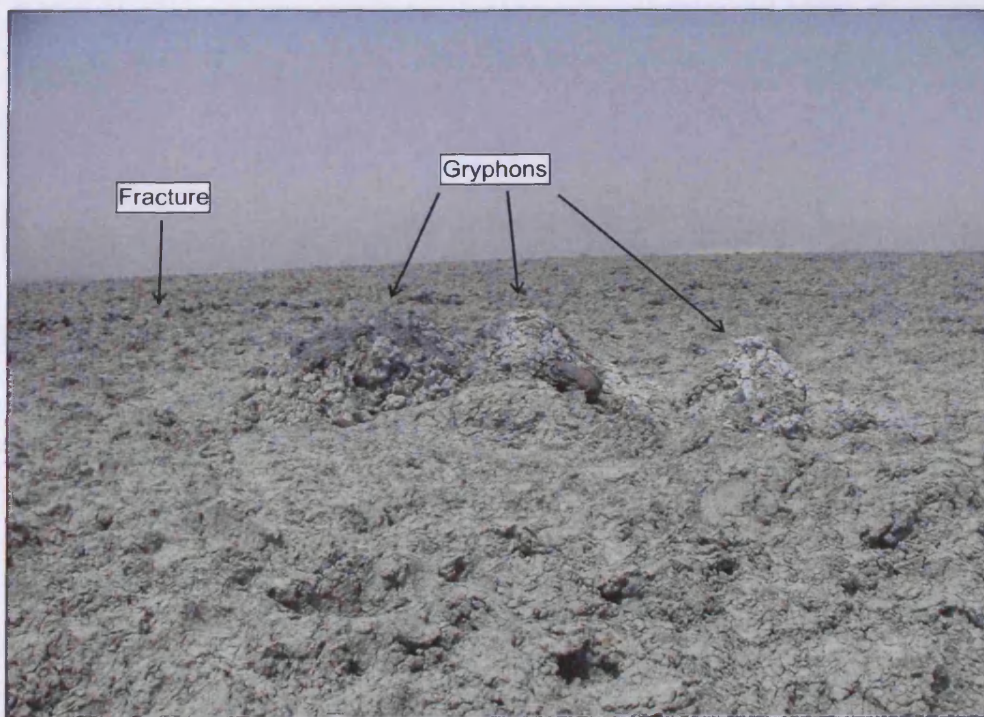


Figure APIV 14 Field photograph of the QD crater pedestal showing the gryphons located at the centre of the pedestal. The subcircular fracture that surrounds the gryphons can be seen in the background. Rucksack for scale, looking north.



Figure APIV 15 Close up field photograph of a gryphon at the centre of the QD crater pedestal. Notebook is 30 cm long.

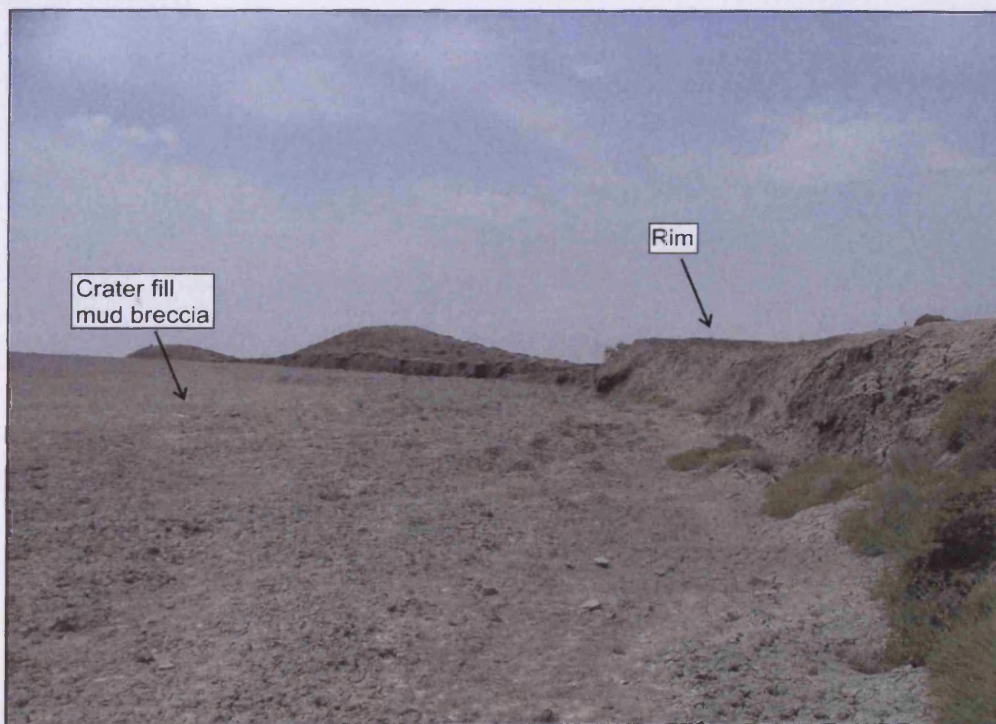


Figure APIV 16 Field photograph of the Gora Kagniza-Dag (GKD) mud volcano crater showing the crater fill mud breccia, the rim and inward dipping crater margin fault scarp. Maximum scarp height is approximately 2 m. Looking northwest.



Figure APIV 17 Field photograph of the Gora Kagniza-Dag (GKD) mud volcano crater showing the crater fill mud breccia, the rim and inward dipping crater margin fault scarp. Looking southwest.



Figure APIV 18 Field photograph from the GKD crater showing the circular fault found near the centre of the crater fill mud breccia. Notebook is 30 cm long. Looking west.



Figure APIV 19 Filed photograph showing a mud flow originating from the GKD crater that has become channelled into a fluvial gully on the edifice flank. Looking northeast.

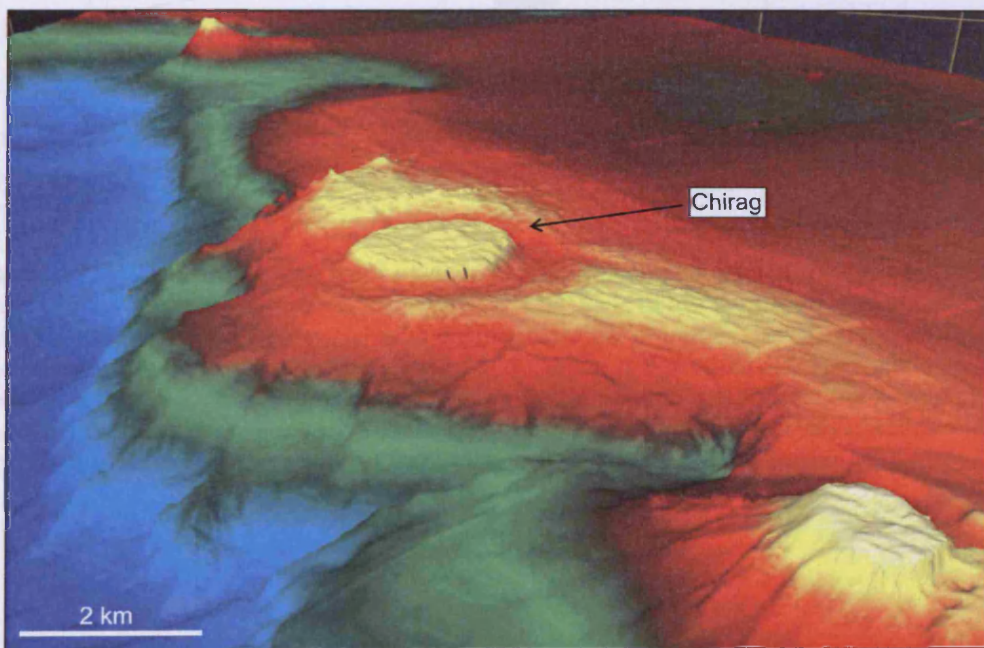


Figure APIV 20 3D visualization of the seabed at the Chirag mud volcano showing the structure of its seabed crater.

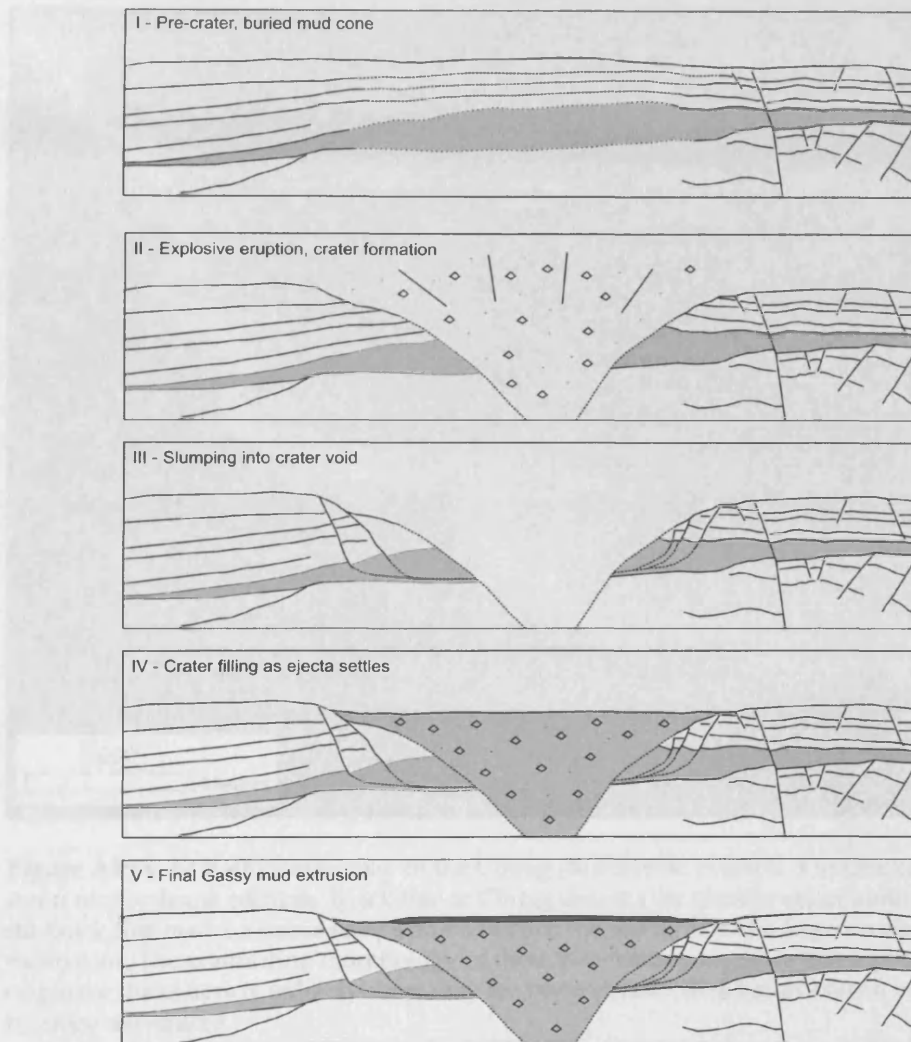


Figure APIV 21 Line drawing from a seismic line of the cross sectional subsurface structure of the Chirag mud volcano crater. This drawing was made to test the idea that mud volcano craters could be produced by excavation during explosive eruptions. It was revealed that a void of over 250 m depth would be required if the crater margin faults to “daylight” in the margins of the void, as would be required by any collapse model of this nature. A void of this size is many times larger than any other explosive craters known in Azerbaijan which suggests that an explosive origin for the craters is highly unlikely.

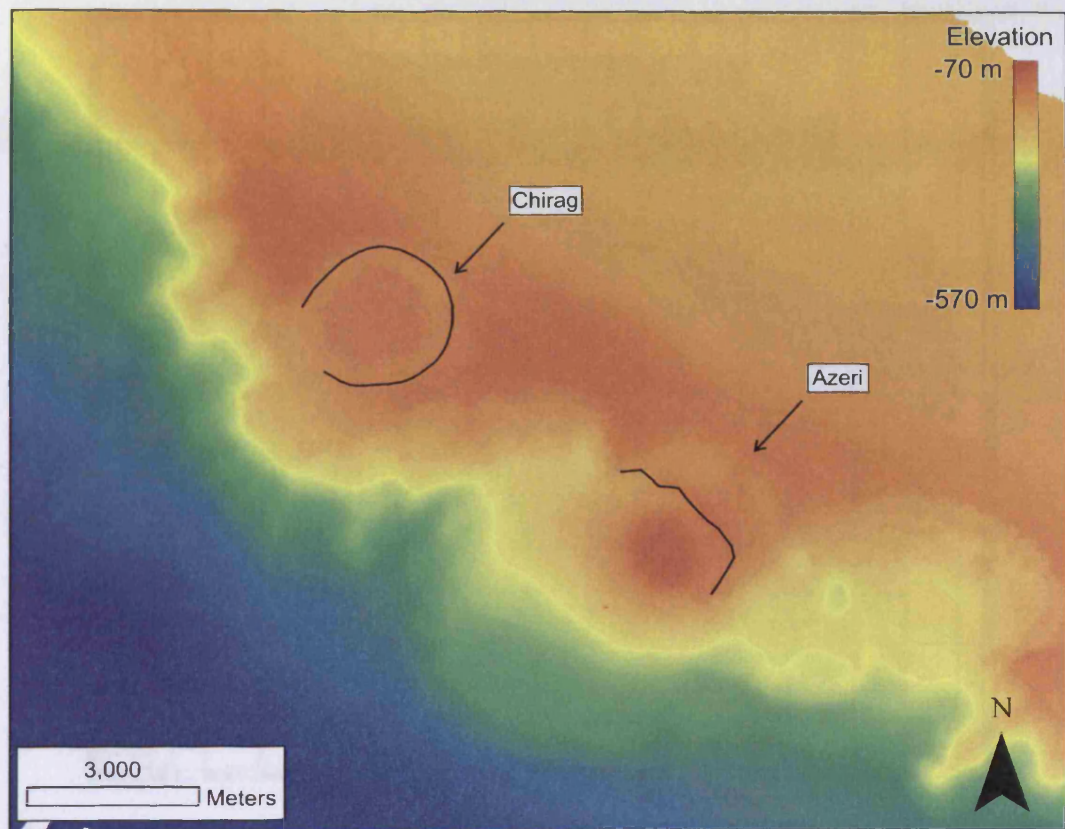


Figure APIV 22 Bathymetric map of the Chirag (Submarine example 1 in Chapter 5) and Azeri mud volcano edifices. Black line at Chirag denotes the circular crater outline. At Azeri the black line marks a linear scarp known to have formed as part of a large rotational slope movement. The contrasting morphology of these two features suggests that a slope movement origin for the craters is unlikely since they are more circular than scarps known to be formed by slope movement.

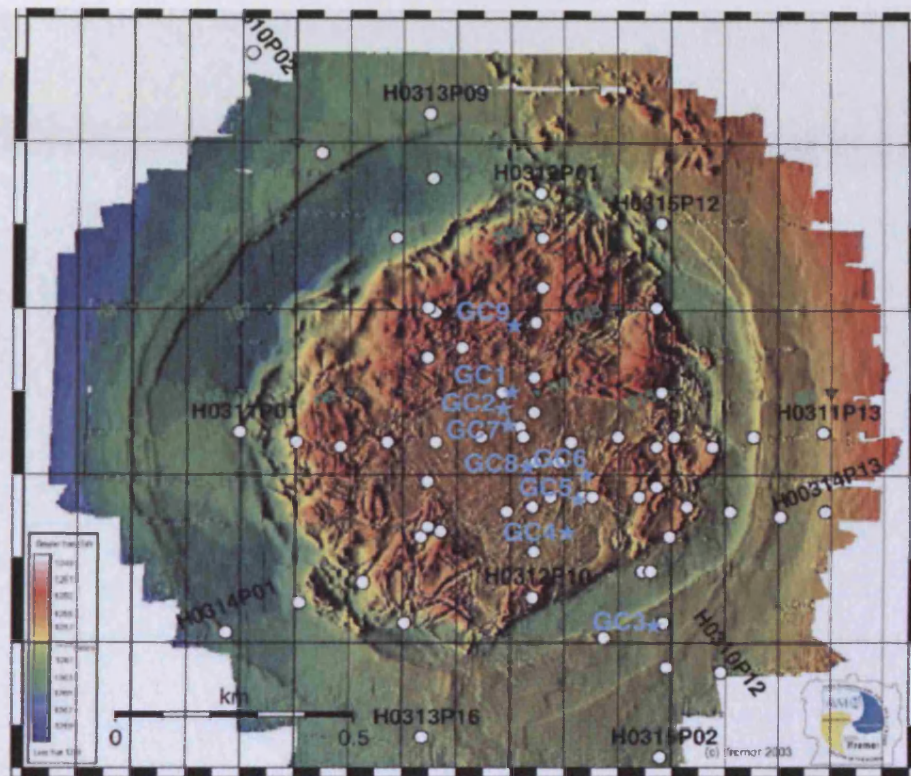


Figure APIV 23 Multibeam bathymetric image of the Håkon Mosby mud volcano from the Barent Sea. This example bears a striking resemblance to the craters described in Chapter 5 and may have a similar origin. In particular the crater margin faults are very well imaged at this example which adds weight to the interpretation of the craters as fault-bound collapse structures. From Kaul et al. (2006).

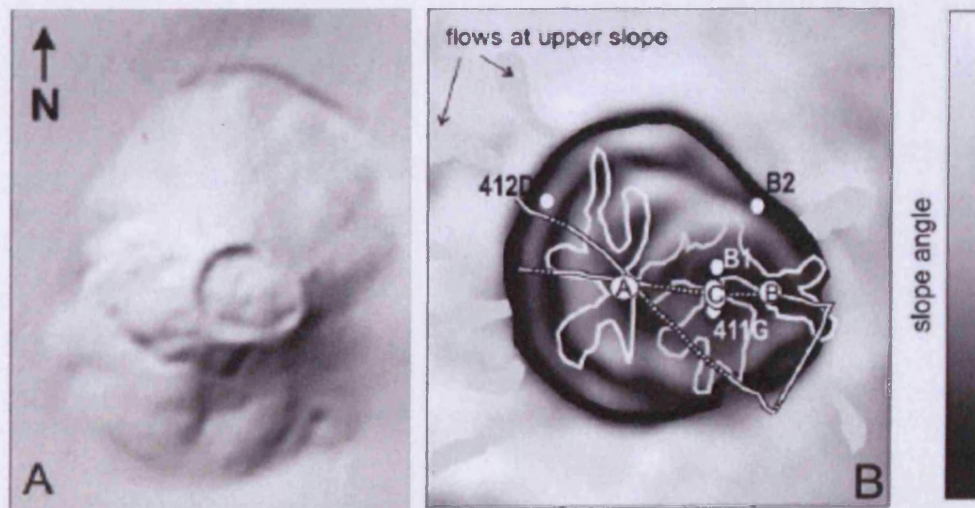


Figure APIV 24 (a) Shaded relief map of the Al Idrissi mud volcano from the Gulf of Cadiz showing the edifice's cone-like morphology and circular summit crater. (b) Close up slope map of the crater of the Al Idrissi mud volcano edifice. This example is similar to the examples described in Chapter 5 and displays similar features such as a rim, moat and pedestal. White lines denote sediment flow boundaries.

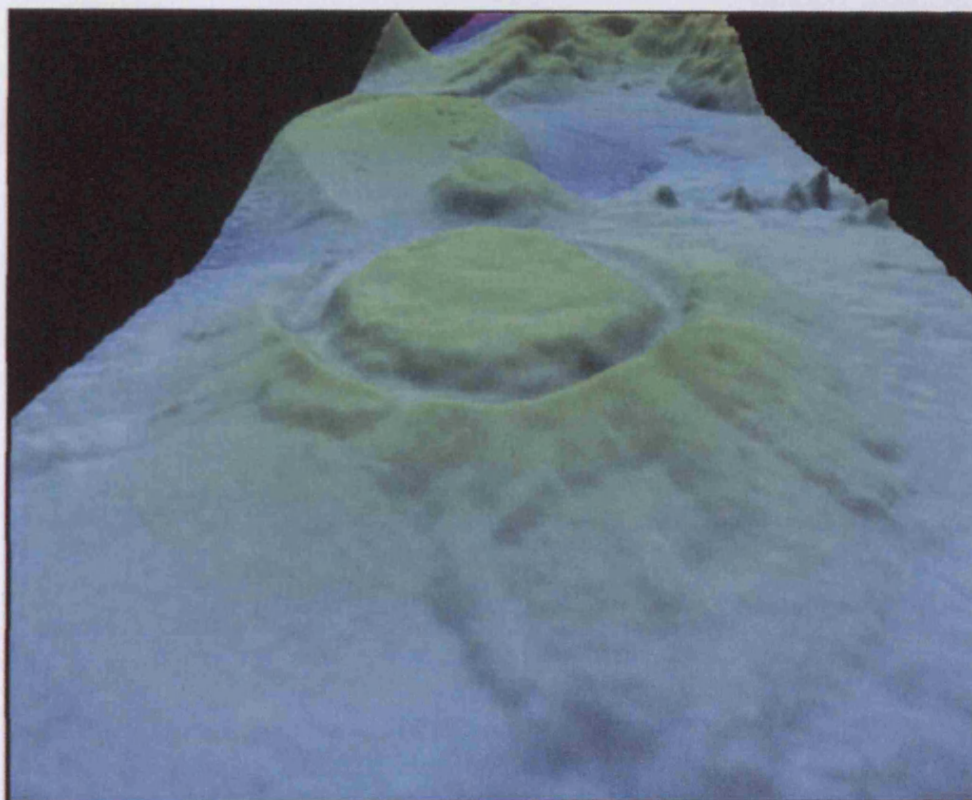


Figure APIV 25 3D bathymetric image of a 220 m wide “fluid expulsion feature” from the Gulf of Mexico. This example shows a strong similarity to the “moat and pedestal” craters described in Chapter 5. From George (2006).

